Role of SF3B1 Mutations in Uveal Melanoma Oncogenesis

Raquel Vivet Noguer

PSL UNIVERSITÉ PARIS

THÈSE DE DOCTORAT
DE L'UNIVERSITÉ PSL

Préparée à l'Institut Curie

Role of *SF3B1* Mutations in Uveal Melanoma Oncogenesis

Rôle des mutations de *SF3B1* dans l'oncogenèse du mélanome de l'uvée

Soutenue par

Raquel VIVET-NOGUER

Le 28 Septembre 2021

Ecole doctorale n° 582

Cancérologie, Biologie, Médecine, Santé (CBMS)

Spécialité

Recherche clinique, innovation technologique, santé publique

Composition du jury :

Corine, BERTOLOTTO DR, Université Côté d'Azur	*Présidente*
Marie-Dominique GALIBERT-ANNE PR, Université de Rennes 1	*Rapporteur*
Cyril BOURGEOIS CR, ENS Lyon	*Rapporteur*
Martin DUTERTRE CR, Institut Curie	*Examinateur*
Sergio ROMAN-ROMAN HDR, Institut Curie	*Directeur de thèse*
Samar ALSAFADI CR, Institut Curie	*Co-directrice de thèse*

institut Curie | PSL

“**Nothing great was ever achieved without enthusiasm**” – Ralph Waldo Emerson

“**Era molt senzill, però s’havia de saber**”– Mercè Rodoreda i Gurgui

Aquesta tesi és fruit del sacrifici i esforç que he après dels meus avis,

a la passió per la ciència que he vist en els ulls del meu pare,

a l'amor per la literatura que m'ha encomanat la meva mare,

a l'evolució constant que he admirat en la meva germana,

i al meu propulsor i brúixola incondicional.

I la seva raó de ser és el vostre estímul que em permet saber-me sempre aprenent.

Quan els referents venen de casa teva, l'únic que pots fer és emprendre el vol.

Acknowledgements

The PhD journey has been thrilling, to say the least. There have obviously been ups and downs, it would be unfair not to admit how tough it has been. It has indeed been thanks to its toughness that I have grown so much, both professionally and most importantly, personally. Even though we tend to think of researchers as people who are rather ergophile and reserved, I would not have achieved this without all my colleagues, friends and family who have supported me all the way. I have learnt that science is rather a team effort. I was very lucky to be surrounded by inspiring scientists and great human beings.

Working next to the lab and garden of Marie Skłodowska-Curie has been highly inspiring. Having female role models is utterly important and I believe the Institut Curie makes a good job in keeping the Curie spirit. It is in fact after her meritorious work that I got the funding for my thesis, for which I would also like to express my gratitude towards the European Commission and the Training Unit.

First of all, I would like to thank my two supervisors Samar Alsafadi and Sergio Roman-Roman. Samar, thank you for being so familiar with troubleshooting as well as being patient with my beginner mistakes while reassuring me that it was part of the learning process. Sergio, moltes gràcies por animarme y dar la talla cuando más lo necesitaba y por ser una fuente contagiosa de optimismo. Thank you both for trusting me to be part of this adventure.

Dominique, ma chère prof, merci beaucoup. Quand quelqu'un t'apprende une langue, il te donne les clés d'un nouvel univers.

Je tiens à remercier les rapporteurs de ma thèse Marie-Dominique Galibert-Anne et Cyril Bourgeois pour votre temps, conseils et vos mots d'encouragement. C'était grâce à votre contribution que mon manuscrit s'est considérablement amélioré. Je voudrais aussi remercier les examinateurs de ma thèse Salem Chouaib, Corine Bertolotto, Sabine Colnot et Martin Dutertre d'avoir accepté faire partie de mon jury. Je remercie aussi les membres de mon comité de thèse Sebastien Apcher, Virginie Mieulet, Géraldine Gentric, Stephan Vagner et Marc-Henri Stern pour m'avoir guidé dans cette aventure. Merci Marc-Henri for making me think outside the box et merci aussi à tous les membres passés et présents qui m'ont fait sentir que je faisais partie de l'équipe. Je remercie aussi mon école doctorale CBMS pour le soutien.

To all lab members, past and present: Malcy, Stéphane, Benjamin, Lisseth, Christine, and Estelle. Malcy, partager le bureau avec toi a fait une énorme différence, travailler à côté d'une personne sportive et motivée m'a apporté beaucoup. J'espère avoir appris quelque chose de ton efficacité. Stéphane, my working buddy, thank you for always thinking beyond the technique while trying to understand the rationale behind it. But most importantly, thank you for playing good music which made cell culture hours fly. Ben, we fell in love with a stimulating project together, and next to you, falling out of love with that same project was sweeter than it would have been if done all alone. Thank you for that exciting ride. Lisseth, nobody said it would be easy to begin with but you proved to be up to the task. Mentoring you has taught me a lot more than I could have imagined plus it has been rewarding. Your presence in the lab coupled with your captivating scientific inquiries and our running adventures cheered me up during a time that would have been otherwise quite lonesome. Christine, you have learnt so much since you arrived in the lab. Keep it up and continue to share your doubts, for that is the only way to improve. Thank you for always encouraging me with French and for understanding my situation as an international newcomer.

Je remercie également Thierry Dubois pour avoir toujours été ouvert à la collaboration entre nos équipes et pour des discussions enrichissantes. Les Trois Mousquetaires, learning and failing together at French lessons was a lot of fun. Ramón, gracias por darnos la bienvenida y por ser un ejemplo de pasión y sentido del humor. Siempre recordaré tu mantra de que al final, nuestro objetivo es ayudar a los pacientes de cáncer y hay que tenerlo presente. Samyuktha, my comrade. There is no way I could conceive having taken this ride without you. Your company, empathy and our harmony were vital, both in and outside the lab. Merci également à tous les membres de l'équipe LIP et BCBG, Fariba, Ranya, Virginie, Mathilde, Olivier, Clarisse, Amélie, Marilou, Rayan et Solène, pour votre soutien scientifique et vos conseils, ainsi que pour tous les pique-niques et repas pris ensemble. Merci aussi à tous les membres du département translationnel de DePiC, Biophenics, Oumou et RTOP. Zhiyan et Celine, je n'oublierai pas nos running aventures et votre patience quand j'avais du mal à parler français. À mes collègues de bureau Alice et Aurelie pour m'avoir accueillie dès le premier jour et pour les moments agréables que nous avons passés ensemble.

To all my previous stimulating mentors: Montse, Ignasi, Toni, Feda, Steve, Mark, and John for believing in my willingness to learn and helping me build my self-confidence.

Special thanks to my IC3i supporting team. Anna, Daniel, Darine, Deep, Maciej, Özge, Ram, Sam, Silvia, Tommaso and Sandra. Hanging out with you was fun and often great therapy. Anna, we got on since the beginning and I am positive you will achieve great heights, I just hope I will be there to witness them! Darine, your multicultural origins have given you a precious ability; you can grasp so much from others' cultures! By your side, I always feel you appreciate the best qualities in your close ones. Deep, philosophizing with you could be considered a hobby hard to find. Silvia, siendo pura y noble cómo eres es tal y como vas a seguir triunfando por la vida. Durante estos años, te he visto superarte y crecer, ¡no dejes que decaiga! Sandra, el entusiasmo que pones en las cosas que te hacen ilusión es un bien escaso que te va a hacer despegar. Tommaso, se sei bravo in laboratorio cosi como lo sei in cucina, non hai nulla di cui preoccuparti!

I shall finish in Catalan to thank my *ohana*. Júlia, he conegut a poques persones tot compartint una habitació d'hotel; vas entrar per la porta gran i durant moments clau has estat un exemple de llum. La teva vitalitat és i serà un bon combustible. Laura i el teu misteri dels senzills, ja fa temps que tinc sort de gaudir de la teva amistat i espero ser-ne sempre mereixedora. Ariadna, abans de conèixer-te no pensava que pogués trobar mai algú com tu, tan noble, directa i assertiva. Espero que la casa portàtil que vam construir amb la Berta ens acompanyi sempre. I que tu Berta sempre ens amaneixis.

I acabaré amb els de casa, que al cap i a la fi és on tot comença. Blanca, sé que moltes vegades has pensat que m'agrada complicar-me la vida, però sempre has acceptat les meves decisions i reflexionar juntes m'ha fet créixer. Mama, gràcies per estar sempre disposada a ser-hi, fos amb una trucada telefònica o un cap de setmana terapèutic d'escapada i nutrició. Papa, gràcies per les teràpies esportives i xerrades de desconnexió que tan necessàries eren per esbravar-me. A tots dos, gràcies per asfaltar el camí i nodrir-me d'estímuls i evidentment per la inversió econòmica que la meva carrera us ha suposat. Que jo sigui aquí en el dia d'avui és causa directa de les facilitats i sacrificis que heu fet per mi, per no mencionar la confiança en mi mateixa que sempre m'heu transmès. Avui ens doctorem junts.

Ivan, sento que em falten recursos per plasmar la gratitud i veracitat que sento. Tant alces les meves ales com em fas tocar de peus a terra i m'aportes una certesa que em calibra. Em pregunto si jo hagués tingut la mateixa talla en una situació invertida. No cal dir que és exclusivament amb tu que concebo la realització exitosa d'aquesta etapa.
Gràcies de tot cor, doctor.

INDEX

List of abbreviations

AML	Acute Myeloid Leukemia
ATP	Adenosine Triphosphate
ATP5A	ATP synthase F1 Subunit Alpha
BAP1	BRCA1 Associated Protein 1
CDK1	Cyclin-dependent Kinase 1
CDK2	Cyclin-dependent Kinase 2
CHCHD7	Coiled-Coil-Helix-Coiled-Coil-Helix Domain Containing 7
CLL	Chronic Lymphocytic Leukemia
CMML	Chronic Myelomonocytic Leukemia
CTL4	Cytotoxic T-Lymphocyte-associated protein-4
CTNNB1	Catenin Beta 1
CYSLTR2	Cysteinyl Leukotriene Receptor 2
DNMT3B	DNA Methyltransferase 3 Beta
DYRK1A	Dual Specificity Tyrosine Phosphorylation Regulated Kinase 1A
EIF1AX	Eukaryotic translation initiation factor 1A, X-chromosomal
eIF2α	Eukaryotic Initiation Factor 2
ESE	Exonic Splicing Enhancer
ETC	Electron Transport Chain
FANCA	Fanconi Anemia Complementation Group A
FASN	Fatty Acid Synthase
FDG	Fluorodeoxyglucose
F6P	Fructose-6-Phosphate
GLDC	Glycine Decarboxylase
GNAQ	Guanine Nucleotide-Binding Protein G(Q) Subunit Alpha
GNA11	Guanine Nucleotide-Binding Protein Subunit Alpha-11
gp100	Glycoprotein 100
GSH	Glutathione Synthesis
GSK-3	Glycogen Synthase Kinase 3β
G3P	Glyceraldehyde-3-Phosphate
G6P	Glucose-6-Phosphate
HAC	Hepatic Artery Chemoembolization
HEAT	Huntingtin, Elongation factor 3, protein phosphatase 2A, Targets of rapamycin 1

HK2	Hexokinase II
HIF-1	Hypoxia-Inducible Factor-1
H2AFY	H2A Histone Family Member Y
IAC	Intra-arterial Liver Chemotherapy
IHP	Isolated Liver Perfusion
IL8	Interleukin 8
MAPK1	Mitogen-Activated Protein Kinase 1
MAPK3	Mitogen-Activated Protein Kinase 3
MBD4	Methyl-CpG Binding Domain 4
MCT	Monocarboxylate Transporters
MDS	Myelodysplastic Syndromes
MTCO2	Cytochrome C Oxidase Subunit 2
NDUFB8	NADH dehydrogenase [ubiquinone] 1 beta subcomplex subunit 8
NMD	Nonsense-Mediated mRNA Decay
OS	Overall Survival
OXPHOS	Oxidative Phosphorylation
PDGF	Platelet-Derived Growth Factor
PDH	Pyruvate Dehydrogenase
PDK	Pyruvate Dehydrogenase Kinase
PDX	Ppatient-derived xenograft
PEP	Phosphoenolpyruvate
PET	Positron Emission Tomography
PFKFB2	Fructose 2,6-biphosphatase
PFK-1	Phosphofructokinase-1
PHGDH	Phosphoglycerate Dehydrogenase
PI3K/Akt	Phosphatidylinositol- 4,5 –biphosphate 3-kinase/ protein kinase B
PKM	Pyruvate Kinase
PLCβ4	1-phosphatidylinositol 4,5-bisphosphate phosphodiesterase beta-4
PPP	Pentose Phosphate Pathway
P-pyr	Phosphohydroxypyruvate
PRAME	Preferentially Expressed Antigen In Melanoma
PSAT1	Phosphoserine Aminotransferase 1
PTBP1	Polypyrimidine Tract Binding Protein 1
PTEN	Phosphatase And Tensin Homolog

PSPH	Phosphoserine Phosphatase
Q	Ubiquinone
QH_2	Reduced Ubiquinone
RARS/RCMD-RS	Refractory anemia with ringed sideroblasts/ Refractory cytopenia with multilineage dysplasia-ringed sideroblasts
RFA	Radiofrequency Ablation
ROS	Reactive Oxygen Species
Ru-5-P	Ribulose-5-Phosphate
R5P	Ribose-5-Phosphate
SDBH	Succinate Dehydrogenase [ubiquinone] Iron-sulfur Subunit
SCD1	Stearoyl-CoA Desaturase 1
SF3A1	Splicing Factor 3a Subunit 1
SF3B1	Splicing Factor 3b Subunit 1
SHMT	Serine Hydroxymethyltransferase
snRNA	Small nuclear RNA
snRNP	Small Nuclear Ribonucleoprotein
SNV	Single-Nucleotide Variant
STAT	Signal Transducer and Activator of Transcription
SUGP1	SURP and G-patch domain containing 1
SR	Serine/arginine rich
SRSF2	Serine/arginine-rich splicing factor 2
STRAP	Serine/Threonine Kinase Receptor Associated Protein
TCA	Tricarboxylic Acid
TIGAR	TP53-Inducible Glycolysis and Apoptosis Regulator)
TRP-1	Tyrosinase-Related Protein 1
ULM	U2AF-ligand motif
UM	Uveal Melanoma
UQCC1	Ubiquinol-Cytochrome C Reductase Complex Assembly Factor 1
UQCC2	Ubiquinol-Cytochrome C Reductase Complex Assembly Factor 2
U2AF	Splicing Factor U2 Small Nuclear RNA Auxiliary Factor
U2AF1	Splicing Factor U2 Small Nuclear RNA Auxiliary Factor 1
U2AF2	Splicing Factor U2 Small Nuclear RNA Auxiliary Factor 2
WT	Wild-Type
ZRSR2	Zinc finger RNA-binding motif and serine/arginine rich 2
3-PG	3-Phosphoglycerate

Research questions

The discovery of introns in the eukaryotic genome started as a mystery that has been and continues to be decrypted nowadays. Our understanding has been extended as a result of the advances made in next generation sequencing technologies and genome-wide analysis. Such advances have helped us appreciate how alternative splicing allows the formation of multiple forms of mature mRNA and protein isoforms from a single gene thus becoming a major actor in generating eukaryotic diversity.

Hence, alternative splicing is a dynamic process that requires tight regulation to control its cascade effect. In this context, this drop-wise mechanism involves multiple regulators which comprise the splicing machinery. Importantly, the correct functioning of splicing is known to be compromised in cancer and recurrent mutations in genes encoding RNA splicing factors have been identified in different types of cancer.

The most frequent mutations in cancer are found in the genes splicing factor 3B, subunit 1 (SF3B1), serine/arginine-rich splicing factor 2 (SRSF2), U2 small nuclear RNA auxiliary factor 1 (U2AF1) and zinc finger, RNA-binding motif and serine/arginine-rich 2 (ZRSR2) (Yoshida *et al.*, 2011; Dvinge *et al.*, 2016). These splicing factor gene mutations display certain features that highlight their importance in oncogenesis. First, these mutations occur in a mutually exclusive manner and all mutated genes code for proteins that play a role in the early steps of splicing (3' splice site recognition). Second, *SF3B1*, *SRSF2* and *U2AF1* mutations trigger a change of function and *ZRSR2* mutations result in a loss of function (Yoshida *et al.*, 2011).

Hence, to further exploit their oncogenic involvement, many studies have addressed the splicing mechanistic carried out by these mutant splicing factors. We now know that mutant splicing factors exhibit an altered splice initiation site or exon recognition which leads to the formation of aberrantly-spliced transcripts. However, there is a knowledge gap in the comprehension of how these abnormalities participate in oncogenesis. The challenge remains to elucidate the fate of the resulting aberrant transcripts and their functional role.

In recent years, growing efforts are being made to determine the fate of several aberrantly-spliced targets that can result in human diseases. It is known that splicing aberrations and their consequences can be cancer-specific thus hampering its study. Another major issue is whether miss-splicing can constitute a target for therapy. Given

that splicing is an essential process in cells, splicing inhibitors could presumably display cytotoxic side effects. Consequently, there has been a drive towards the development of splicing regulators rather than splicing inhibitors, which remains very challenging.

Further understanding of the fate of aberrantly-spliced targets is thus crucial to better comprehend the oncogenic consequences of aberrant splicing and develop targeted therapies. The most frequently mutated splicing factor gene in cancer is *SF3B1* with a high recurrence (23%) in uveal melanoma. The main goal of this thesis is to elucidate the fate of the transcripts that are aberrantly-spliced in *SF3B1*-mutated uveal melanoma cases.

INTRODUCTION

Chapter I – Once upon a time...

Uveal Melanoma at a glance

Uveal melanoma (UM) is the most common primary tumour in the eye of adults and there are around 4.3 cases of UM per million worldwide. UM represents 5% of melanomas and although it shares the melanocytic origin with skin melanoma, they differ widely in terms of etiology, genetic landscape and clinical progression (Singh, Turell and Topham, 2011; Mahendraraj *et al.*, 2016).

The first record of UM dates back from 1809-1812 when described by the Scottish surgeons Allan Burns and James Wardrop. At the time, Allan Burns invited James Wardrop to assist the enucleation (removal of the eye globe) of a female patient whom we know now, had UM. Wardrop had previously detected the presence of intraocular tumours in young children which he reported to arise from the retina and foresought enucleation as a curative treatment (Wardrop, 1809). Different from those white retinoblastoma tumours, the eye tumour of the female patient was black – later known to be due to the pigmentation from the choroid. The colour of the tumor was observed upon enucleation, which was done a year and a half after the appearance of the first symptoms. First, the patient experienced a progressive vision loss, leading to complete blindness 4 months before the operation. A year after the intervention, the patient died due to liver metastasis, the most common metastatic site in UM (Burns, 1811).

UM arises due to the overproliferation of melanocytes from the uveal tract which comprises the iris, ciliary body and choroid (Figure 1). Most UM cases have their origin at the choroid (85%), while fewer cases arise from the ciliary body (5-8%) or the iris (3-5%) (Singh, Turell and Topham, 2011; Mahendraraj *et al.*, 2016).

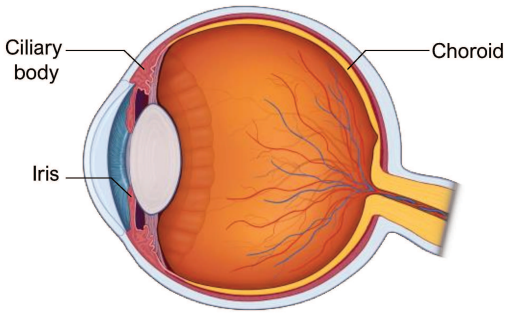

Figure 1. Anatomy of the eye highlighting the layers composing the uveal tract (ciliary body, iris and choroid). Adapted from Blum *et al.*, 2016.

The genetic landscape of uveal melanoma

There are two main types of mutations in UM. The first event consists of activating mutations in G-protein coupled receptors. More than 90% of UMs harbour mutations in *GNAQ* (Guanine nucleotide-binding protein G(q) subunit alpha) or *GNA11* (Guanine nucleotide-binding protein subunit alpha-11) while lesser cases harbour mutations in *CYSLTR2* (Cysteinyl leukotriene receptor 2) and *PLCβ4* (1-phosphatidylinositol 4,5-bisphosphate phosphodiesterase beta-4), accounting for 4 and 2.5% cases, respectively (Van Raamsdonk *et al.*, 2009; Chua *et al.*, 2017; Robertson *et al.*, 2018). These mutations occur in a mutually exclusive manner and lead to the constitutive activation of Gαq signaling, which triggers a dysregulation of downstream pathways like Akt/mTOR, Wnt/β-catenin, Rac/Rho, MAPK, and PI3K pathways (Bakalian *et al.*, 2008). A detailed figure of the dysregulated pathways in UM is provided subsequently (Figure 2 Vivet-Noguer *et al.*, 2019).

The second event comprises mutations in *BAP1* (BRCA1 Associated Protein 1), *SF3B1* (Splicing Factor 3b Subunit 1), *SRSF2* (Serine/arginine-rich splicing factor 2) and *EIF1AX* (Eukaryotic translation initiation factor 1A, X-chromosomal). These mutations (called BSE) are also mutually exclusive in most of UMs and correlate with distinct prognoses. On one hand, *BAP1*-mutated tumours are linked with chromosome 3 monosomy and an early metastatic risk. On the other hand, *SF3B1* and *SRSF2* mutations are mostly linked with chromosome 3 disomy and a late-onset metastatic risk, while *EIF1AX* mutations are associated with chromosome 3 disomy and low metastatic risk (Figure 1A Vivet-Noguer *et al.*, 2019).

SF3B1 mutations in uveal melanoma

The splicing factor gene *SF3B1* codes for the U2 small nuclear riboprotein complex (U2 snRNP) which plays an essential role in recognition of the intron in splicing. *SF3B1* is mutated in 23% of UMs (Alsafadi *et al.*, 2016). Several hotspot mutations have been described including R625, K666 and K700, with a distinctive prevalence of R625 and K666 in UM (Papaemmanuil *et al.*, 2011; Quesada *et al.*, 2011). Provided that *SF3B1* is the splicing factor gene most frequently mutated in cancer and the recurrence of mutations in splicing factor genes in cancer (Dvinge *et al.*, 2016), *SF3B1* mutations have been thoroughly studied in the last decades. In a nutshell, *SF3B1* mutations generate change-of-function mutants which cause aberrant splicing of less than 1% of all splice junctions because mutant SF3B1 recognizes a cryptic branchpoint of the intron which is

located 11-4 nts upstream the canonical site (Alsafadi *et al.*, 2016). While this small section aims to serve as a highlight of the 23% of UM cases harbouring *SF3B1* mutations, a full chapter is dedicated to describing splicing as an emerging hallmark of cancer with a particular focus on *SF3B1* (Chapter II).

Management of primary uveal melanoma (surgery, radiation, and photodynamic therapy)

Under primary settings of the disease, effective treatments include surgical resection, enucleation, radiation, or photodynamic therapy; either alone or in combination. In fact, enucleation was one of the first treatments used for primary UM. Nowadays, other types of surgery include partial resections. Additionally, brachytherapy, a form of site-directed radiotherapy, has proven to be equally beneficial for patients. The most common form of brachytherapy consists of the insertion of a plaque that releases doses of radiation. If the tumour size is too large to allow plaque insertion, charged-particle radiotherapy is used instead (Wang *et al.*, 2013; Barker and Salama, 2018; Mathis *et al.*, 2018; Yang *et al.*, 2018). Charged-particle radiotherapy utilizes charged particles like protons, helium, carbon, or other ions to provide localized peaks of dose targeting the tumour (Wang *et al.*, 2013). Finally, another option is photodynamic therapy (PDT). PDT is a combination of a photosensitizer compound with an infrared laser that will then activate the compound to induce damage in a site-specific manner. The development of successful therapies has diverted the guidelines from enucleation to prioritizing the preservation of vision whenever possible (Barker and Salama, 2018; Mathis *et al.*, 2018; Yang *et al.*, 2018). Altogether, current therapies provide effective control of primary UM. However, retinopathies and vision loss occur in a significant number of patients, thus improvement of these therapies is needed (Table 1).

Adjuvant therapy and novel approaches

Despite good control of local disease, there is still a high metastatic risk in the long term. Precisely, between 20 to 50% of patients develop metastases and the 5-year survival rate has remained unchanged for the last forty years (Diener-West, M. *et al.*, 2005; Aronow, Topham and Singh, 2018). Hence, several adjuvant therapies used for the treatment of skin melanoma have been tested in primary UM.

Treatment with the alkylating agent dacarbazine showed no benefits in UM patients (Desjardins, 1997). No beneficial effects were either observed upon treatment with

interferon (Richtig, Langmann and Schlemmer, 2006; Lane, Egan and Harmon, 2009). Dacarbazine and interferon tested in combination did not result in any benefit in UM patients (NCT01100528) (Binkley *et al.*, 2020) (Table 1). The alkylating agent fotemustine was also tested in clinical trials for UM but had to be stopped for futility (NCT02843386) (Piperno-Neumann *et al.*, 2017) (Table 1).

c-Met and c-Kit are overexpressed in UM (All-Ericsson *et al.*, 2004; Mallikarjuna *et al.*, 2007). Therefore, the tyrosine kinase inhibitor crizotinib (inhibitor of c-Met phosphorylation) has been evaluated in clinical trials but it showed adverse and discontinued effects (NCT02223819) (Khan *et al.*, 2020) (Table 1). On the other hand, the effect of the tyrosinase kinase inhibitor sunitinib (inhibitor of c-Kit) is being assessed on clinical trials (NCT02068586) (Sato *et al.*, 2020) (Table 1).

As aforementioned, *BAP1* inactivating mutations are associated with a higher risk of metastasis in UM. Some clinical trials are based on targeting BAP1-related processes like inhibiting histone deacetylases which are deubiquitinated by BAP1 (Scheuerman *et al.*, 2010; Sahtoe *et al.*, 2016). In line with this, a clinical trial is running to test vorinostat in UM (NCT03022565) (Table 1).

The eye is an immune-privileged environment but contains immune cells like T cells and dendritic cells (Char, Char and Kaleta-Michaels, 1992; De Waard-Siebinga *et al.*, 1996; Polak *et al.*, 2007). Dendritic cells present antigens in order to induce the immune response through activation of T cells and immunotherapy targeting dendritic cells has shown promising results in skin melanoma (Aarntzen *et al.*, 2012). Although skin melanoma and UM differ in terms of etiology, genetics and progression, they share the expression of antigens like tyrosinase-related protein 1 (TRP-1) and glycoprotein 100 (gp100) (Steuhl *et al.*, 1993; De Vries *et al.*, 1998), which are frequent targets of dendritic cells immunotherapy (Aarntzen *et al.*, 2012). First clinical trials of dendritic cell vaccination showed a response for UM patients (Bol *et al.*, 2014), thereby progressing to phase III which is currently running (NCT01983748) (Table 1).

A novel approach for laser therapy is based on AU-011, a compound composed of viral nanoparticles conjugated with a photosensitizer which is injected intravitreal and triggers necrosis upon infrared laser (NCT03052127) (Yang *et al.*, 2018) (Table 1). Additionally, tissue factor (TF) is overexpressed in UM cell lines (Walker *et al.*, 2002) and recently, a fusion protein named ICON-1 was developed to selectively target TF-overexpressing UM cells. ICON-1 a fusion protein of human coagulation factor VII that upon binding to TF will

trigger a decrease in neovascularization. ICON-1 is currently in clinical trials (NCT02771340) (Yang *et al.*, 2018) (Table 1).

Some of the adjuvant therapies used for UM prevent metastasis in skin melanoma but show minimal effect in UM. In fact, no improvement in the patient overall survival (OS) of UM patients has been observed yet (Aronow, Topham and Singh, 2018; Yang *et al.*, 2018). Altogether, the results from clinical trials with adjuvant therapies highlight the need to further investigate them. Accordingly, novel approaches are being investigated as well, like testing dendritic cells immunotherapy, AU-011 and ICON-1, which shed light on the progress needed to improve adjuvant therapy in UM.

Management of metastatic uveal melanoma

Between 20 to 50% of patients develop metastases, mainly in the liver (89%), and less commonly in the lungs (29%), bone (17%), skin (12%) and lymph node (11%) (Diener-West, M. *et al.*, 2005). Despite the existence of effective treatments for primary UM, there is still no treatment of reference for the metastatic setting. The overall survival of UM metastatic patients is 6 to 12 months (Kujala, Mäkitie and Kivelä, 2003; Lane, Kim and Gragoudas, 2018). The lack of established guidelines makes the management of metastatic UM rather experimental and diverse. Current treatments include liver resection, radiotherapy, chemotherapy, targeted therapy and immunotherapy. The latter is sometimes used in combination with chemotherapy or targeted therapy (Yang *et al.*, 2018; Rodriguez-Vidal *et al.*, 2020).

Liver-directed approaches (chemotherapy and surgery)

Given that the liver is the most common site of metastasis (Diener-West, M. *et al.*, 2005), several approaches are aimed at targeting the liver. For instance, intra-arterial liver chemotherapy (IAC) consists of releasing the doses of chemotherapy agents to the liver artery through a catheter. This approach can be combined with chemoembolization (hepatic artery chemoembolization or HAC). The goal of these therapies is to provide site-specific chemotherapy to reduce off-target toxicity. Another liver-directed approach is isolated liver perfusion (IHP), based on vascular isolation of the liver to reduce systemic toxicity (Yang *et al.*, 2018; Rodriguez-Vidal *et al.*, 2020). These approaches have been largely tested in metastatic UM, but no improvement in OS has yet been reported and the lack of established guidelines introduces a lot of bias between treatments which

challenges comparison and outcome analysis (Yang *et al.*, 2018; Rodriguez-Vidal *et al.*, 2020).

Radiofrequency ablation (RFA) has also been assessed alone or in combination with surgery. RFA consists of the transmission of heat, in this case, at the liver site. RFA alone leads to the same OS as surgery in liver metastatic UM (Mariani *et al.*, 2016). Upon relapse after treatment of the initial metastasis, RFA in combination with surgery is also beneficial for patients (Servois *et al.*, 2019). It is important to take into account the fact that the groups of study were small and highly filtered, thus these studies may not represent or be conclusive for all UM cases. Moreover, the combination of RFA and surgery is an aggressive treatment and additional studies are needed to assess the choice of treatment according to the genomic profile of each patient.

On the other hand, surgical resection of the liver is performed for resectable tumours and often combined with chemotherapy. A modest increase in the OS has been observed for some patients undergoing liver resection (Rietschel *et al.*, 2005; Rivoire *et al.*, 2005; Akyuz *et al.*, 2016). However, increased survival may depend on the stage of the tumour and patient selection (Yang *et al.*, 2018; Rodriguez-Vidal *et al.*, 2020).

Chemotherapy

Provided the shared embryonic origin of UM and skin melanoma, chemotherapy treatments used for skin melanoma have been tested in metastatic UM (cisplatin, temozolomide, dacarbazine, temozolomide, cisplatin, carboplatin, and combined treatments) (Schmittel *et al.*, 2006; Homsi *et al.*, 2009; Spagnolo *et al.*, 2013; Khan and Carvajal, 2020; Sussman, Funchain and Singh, 2020). However, as previously mentioned, the etiology, genetic profile and progression of UM and cutaneous melanoma diverge significantly. UM is chemoresistant and yields very low response rates (0-15%) to skin melanoma standard treatments. Hence, novel treatments are being explored like immunotherapy and therapy targeting the dysregulated pathways in UM (Khan and Carvajal, 2020; Sussman, Funchain and Singh, 2020) (Table 1).

Immunotherapy

Cancer cells are known to evade the immune system and in recent years, emerging immune checkpoint inhibitors are aimed at boosting the immune response of patients (Hanahan and Weinberg, 2011). The checkpoint inhibitors targeting T-lymphocyte-associated protein 4 (CTLA-4) and programmed cell death protein 1 (PD-1) have shown

successful results in several types of cancer including skin melanoma (Yu *et al.*, 2019). As previously mentioned, skin melanoma and UM share the expression of antigens like TRP-1 and gp100 (Steuhl *et al.*, 1993; De Vries *et al.*, 1998). Additionally, UM tumours also display infiltration of T-cells and dendritic cells (Char, Char and Kaleta-Michaels, 1992; De Waard-Siebinga *et al.*, 1996; Polak *et al.*, 2007). Consequently, checkpoint inhibitors of CTLA-4 and PD-1 have been tested in clinical trials for patients with metastatic UM (Table 1). Unfortunately, clinical trials testing inhibitors of PD1 and CTLA4 in UM have shown limited clinical benefit and low response rates (Hofmann *et al.*, 2009; Guenterberg *et al.*, 2011; Patel *et al.*, 2011; Heppt *et al.*, 2017) (Table 1). UM display a low mutational burden of a single-nucleotide variant (SNV) mutation of <1 per Mb (Furney *et al.*, 2013). A high mutational burden is known to correlate with the response to checkpoint inhibitors (Cooper and Schneidau, 2015). The low mutational burden may lead to a low neoantigen generation in UM and thus explain why UMs are frequently resistant to immunotherapy. Much attention has been drawn to further comprehend such phenomenon in recent years.

A very interesting finding was seen on two outlier patients with metastatic UM that showed a significant response to anti-PD1 treatment. Strikingly, both patients harboured germline loss-of-function mutations in methyl-CpG binding domain 4 (*MBD4*) (Rodrigues *et al.*, 2018; Johansson *et al.*, 2019), a protein involved in the repair of DNA mismatches (Bellacosa, 2001). MBD4 inhibition results in a hypermutated tumour most probably explaining the sensitivity to checkpoint inhibitors (Rodrigues *et al.*, 2018; Johansson *et al.*, 2019).

Another recent study explored if the transcripts aberrantly spliced by mutant SF3B1 will code for neo-epitopes. Interestingly, *SF3B1* mutations have been shown to trigger the formation of tumor neo-epitopes that are recognized by $CD8^+$ T cells in *SF3B1*-mutated UM metastatic patients. The same study showed that UM cell lines harbouring *SF3B1* mutations were targeted and killed by $CD8^+$ cells (Bigot *et al.*, 2021).

Another study also reported the presence of tumor-infiltrating lymphocytes expressing the marker LAG3 in UM cells (Durante *et al.*, 2020). This opens the possibility of testing checkpoint inhibitors targeting LAG3 in UM, which is currently in clinical trials combined with PD1 inhibitors (NCT04552223) (Table 1).

Finally, a recent clinical study with tebentafusp was conducted in patients with advanced UM. Tebentafusp is a fusion protein specific for gp100 that contains a T-cell receptor

binding domain and an antiCD3 T-cell domain so that it will specifically kill gp100-expressing UM cells. After a follow-up of 14 months, the risk of dying decreased by half and the median overall survival was approximately 22 months, compared with 16 months for other treatments and the 1-year survival rate was 73.2 % versus 58.5% in patients with other treatments (pembrolizumab, ipilimumab or dacarbazine) (NCT03070392) (Table 1). Conclusively, the treatment of UM metastatic patients with tebentafusp resulted in a significant increase of OS in metastatic UM patients.

Overall, immunotherapy based on checkpoints shows poor response rates in metastatic UM (Hofmann *et al.*, 2009; Guenterberg *et al.*, 2011; Patel *et al.*, 2011; Heppt *et al.*, 2017). However, the success of checkpoint inhibitors in UM patients harbouring *MBD4* mutations highlights the importance of personalized medicine. In line with this, the recent discovery of neoepitope formation in SF3B1-mutated UM cells and the expression of LAG3 emphasize the importance of further characterizing the immune profile of UM tumours (Robertson *et al.*, 2018). Last but not least, treatment of patients with metastatic UM by targeting the antigen gp100 offers the first experimental approach to improve OS in advanced UM (NCT03070392) (Table 1).

Table 1. Table of clinical trials in UM over the last 12 years, adapted from clinical trials.gov

Tumor staging	Therapy type*	Drug/ molecule	Target	Pathway / Process	Phase	Patient number	Start year	Clinicaltrials ID
Primary	Chemo/Targeted	Fotemustine	Cytotoxic alkylating agent	DNA	III	302	2009	NCT02843386
		ICON-1	Tissue Factor	Immuno	I	10	2016	NCT02771340
		Crizotinib	Ras	MAPK	II	34	2015	NCT02223819
		Vorinostat	HDAC	BAP1	I	10	2019	NCT03022565
	Targeted + Adj	Sunitinib	VEGF-R2, PDGF-Rβ tyr kinase	Angiogenesis	II	150	2014	NCT02068586
	Laser	Light-activated AU-011	HSPGs		I	52	2017	NCT03052127
					II	31	2020	NCT04417530
	Immuno + Adj	Recombinant interferon α-2b + Dacarbazine	Interferonα + alkylating agent	Cell growth	II	38	2009	NCT01100528
		Dendritic cells vaccine		Dendritic cells	III	200	2018	NCT01983748

Metastatic	Radio	Yttrium-90 microspheres	-	Cell proliferation	II	48	2011	NCT01473004
	Radio + Chemo	Yttrium-90 microspheres + Cisplatin (hepatic application)	-	Cell proliferation + DNA replication	II	108	2016	NCT02936388
	Chemo/Targeted	Bevacizumb + Temozolomide	VEGF + alkylating agent	Angiogenesis	II	35	2009	NCT01217398
		AEB071	PKC	PKC	I	153	2009	NCT01430416
		Carboplatin + Paclitaxel	PDGFR + Microtubules	Cell growth	II	7	2010	NCT01200342
		Everolimus + Pasireotide	mTOR + IGF1-R	mTOR	II	14	2010	NCT01252251
		Sunitinib + Dacarbazine	RTK + alkylating agent	Ras	II	124	2010	NCT01551459
		Selumetinib / Temozolomide	MEK + cell proliferation	MAPK + cell proliferation	II	120	2010	NCT01143402
		Sorafenib	RAF + VEGFR	MAPK + angiogenesis	II	200	2011	NCT01377025
		Sorafenib, Paclitaxel + Carboplatin	RAF + VEGFR and PDGFR and microtubules	MAPK + cell growth	II	25	2011	NCT00329641
		Cixutumumab	IGF-1R	Cell growth	II	18	2011	NCT01413191
		ADI-PEG 2 + Cisplatin	Arginine deiminase + cell cycle	Metabolism + cell growth	I	8	2012	NCT01665183
		Vorinostat	HDAC	BAP1	II	23	2012	NCT01587352
		Sorafenib	RAF + VEGFR	MAPK + angiogenesis	II	32	2012	NCT02517736
		AEB071 + MEK162	PKC + MEK	PKC + MAPK	I	38	2013	NCT01801358
		Cabozantinib, Dacarbazine + Temozolomide	MET, VEGFR2 + alkylating agents	MAPK	II	47	2013	NCT01835145
		Trametinib+/- GSK2141795	MEK + Akt	MAPK + Akt-mTOR	II	44	2013	NCT01979523
		Selumetinib + Dacarbazine	MEK1 + alkylating agent	MAPK	III	152	2014	NCT01974752
		AEB071 + BYL719	PKC + PI3K	PKC + PI3K	I	30	2014	NCT02273219
		LXS196 + HDM201	PKC + MDM2	PKC + p53	I	112	2016	NCT02601378
		Selumetinib	MEK	MAPK	I	28	2017	NCT02768766

		Niraparib	PARP	BAP1	II	47	2018	NCT03207347
		BVD-523	ERK	MAPK	II	27	2018	NCT03417739
		FHD-286	ATPases BRG1 + BRM	BAF chromatin remodeling	I	100	2021	NCT04879017
		Defactinib Hydrochloride + VS-6766	FAK + Raf/MEK	YAP + MAPK	II	18	2021	NCT04720417
		PAC-1 + Entrectinib	Procaspase + ROS1 and ALK	Caspase activation + tyrosine kinase	I and II	38	2021	NCT04589832
	Immuno + Radio	Ipilimumab, Nivolumab + Radioactive Microspheres	CTLA-4 + PD-1	Immuno	I/II	18	2016	NCT02913417
	Immuno	AntiCTLA4	CTLA-4	T cell activation	II	11	2009	NCT01034787
		Nivolumab + Ipilimumab	PD-1 + CTLA-4	Immuno	II	67	2012	NCT01585194
		Pembrolizumab +/- Nivolumab	PD-1	Immuno	II	5	2015	NCT02359851
		IMCgp100	CD3	Pigmentation	I/II	150	2016	NCT02570308
		IMCgp100	CD3	Pigmentation	III	378	2017	NCT03070392
		Ipilimumab + Nivolumab	CTLA-4 + PD-1	Immuno	II	48	2016	NCT02626962
		BPX-701 + Rimiducid	PRAME + FK506-binding protein A	Immuno	I/II	116	2017	NCT02743611
		CVA21 + Ipilimumab	ICAM-1, DAF + CTLA-4	Immuno	I	10	2017	NCT03408587
		Nivolumab + Relatlimab	PD1 + LAG-3	Immuno	II	27	2020	NCT04552223
		mRNA (gp100+tyrosinase) dendritic cells vaccine		Dendritic	I/II	23	2009	NCT00929019
		INCB024360 + MELITAC 12.1	IDO1 inhibitor + vaccine		II	11	2013	NCT01961115
	Immuno + Chemo/Targeted	Paclitaxel + Bevacizumab + Ipilimumab	Microtubules+ VEGF + CTLA-4	Cell division + angiogenesis + immuno	II	112	2013	NCT02158520
		Glembatumumab vedotin	GPNMB	Immuno	II	37	2015	NCT02363283

		ADV/HSV-tk + Valacyclovir + Nivolumab	DNA replication + PD-1	Immuno	II	25	2017	NCT02831933
		Specific T lymphocytes + Cyclophosphamide + Aldesleukin + Ipilimumab	CD8 + cell growth+alkylating agent + IL-2 +Ctla4	Immuno	I	30	2017	NCT03068624
		Pembrolizumab + Entinostat	PD-1 + HDAC	Immuno+ BAP1	II	29	2018	NCT02697630
		Fludarabine + Cyclophosphamide + TIL	DNA synthesis + alkylating agent	DNA replication	II	59	2018	NCT03467516
		IKKb matured Dendritic Cells	Antigens	Dendritic	I	12	2020	NCT04335890
		IKKb matured Dendritic Cells	Antigens	Dendritic	I	12	2020	NCT04335890

Targeted therapy and epigenetic approaches

Emerging therapeutic approaches targeting the signaling pathways dysregulated in UM are discussed in the following review. Additionally, novel therapies aimed at targeting BAP1-downstream processes in BAP1-mutated tumours are further explained.

cancers

MDPI

Review

Emerging Therapeutic Opportunities Based on Current Knowledge of Uveal Melanoma Biology

Raquel Vivet-Noguer, Malcy Tarin, Sergio Roman-Roman and Samar Alsafadi *

Uveal Melanoma Translational Group, Department of Translational Research, Institut Curie, PSL Research University, 75248 Paris, France

* Correspondence: samar.alsafadi@curie.fr; Tel.: +33-1-5624-6275

Received: 24 May 2019; Accepted: 17 July 2019; Published: 20 July 2019

Abstract: Uveal Melanoma (UM) is a rare and malignant intraocular tumor with dismal prognosis. Despite the efficient control of the primary tumor by radiation or surgery, up to 50% of patients subsequently develop metastasis, mainly in the liver. Once the tumor has spread from the eye, the treatment is challenging and the median survival is only nine months. UM represents an intriguing model of oncogenesis that is characterized by a relatively homogeneous histopathological architecture and a low burden of genetic alterations, in contrast to other melanomas. UM is driven by recurrent activating mutations in Gαq pathway, which are associated with a second mutation in BRCA1 associated protein 1 (*BAP1*), splicing factor 3b subunit 1 (*SF3B1*), or eukaryotic translation initiation factor 1A X-linked (*EIF1AX*), occurring in an almost mutually exclusive manner. The monosomy of chromosome 3 is also a recurrent feature that is associated with high metastatic risk. These events driving UM oncogenesis have been thoroughly investigated over the last decade. However, no efficient related therapeutic strategies are yet available and the metastatic disease remains mostly incurable. Here, we review current knowledge regarding the molecular biology and the genetics of uveal melanoma and highlight the related therapeutic applications and perspectives.

Keywords: uveal melanoma; metastasis; targeted therapy; oncogenesis; Gαq pathway; BAP1; SF3B1; EIF1AX

1. Introduction

Uveal melanoma (UM) is the most frequent eye cancer in adults, representing 5% of all types of melanoma [1]. UM mainly arises from melanocytes within the choroid (85%), but it can also originate from the ciliary body (5–8%) or the iris (3–5%), to a lesser extent. The incidence of UM worldwide is estimated at 4.3 cases per million and it has remained stable for the last thirty years [1,2]. Uveal and cutaneous melanomas display major differences in the etiology, mutational profile, and clinical progression, despite sharing cell type and embryonic origin [3].

Uveal melanoma primary tumor can be effectively treated with radiation or surgical removal (enucleation) [4–6]. The prognosis of this cancer remains poor due to the development of metastases in 20–50% of patients, despite good local control [7]. These metastases mainly appear in the liver (89%) and they are particularly resistant to treatment, leading to an overall survival of six to twelve months. Current therapeutic approaches, including chemotherapies or targeted therapies, yield very low response rates (0–15%) in clinical trials, which highlights the need for more effective therapeutic strategies by identifying new targets or combined approaches [8,9].

2. Uveal Melanoma Risk and Prognostic Factors

Uveal melanoma risk factors consist of light skin and eye color (low pigmentation) [3]. UM mutation spectrum does not correlate with ultraviolet radiation (UVR) exposure [10–12], although

UVR-induced mutational patterns (C-to-T transitions) have been described in rare cases (5.6%) [13]. Germline inactivating mutations in *BAP1* (BRCA1 associated protein 1) also represent a genetic risk factor in rare familial and bilateral UM cases, accounting for 2–5% of cases [14–17]. Recently, two UM cases have been reported to harbor germline loss-of-function mutations in *MBD4* (methyl-CpG binding domain 4) [18,19]. MBD4 plays a role in repairing DNA mismatches and its inactivation leads to a hypermutated tumor profile that is sensitive to immune checkpoint inhibitors [19,20].

The UM prognostic features include the age of the patient, tumor size, cell origin and heterogeneity, cytogenetic aberrations, and genetic profile [21–24]. No improvement in overall survival has been observed during the last 30 years, even though prognostication has improved due to the advances in understanding the genomic and genetic status of UM [25,26].

3. Biology-Based Therapeutic Strategies in Uveal Melanoma

3.1. Dysregulated Signaling Pathways

UM exhibits a dysregulation of a set of genes and pathways, most of which have been elucidated in the last two decades and that have been considered as candidates for therapeutic targeting. Here, we describe the potential therapeutic opportunities that are based on the main UM altered signaling pathways and related processes.

3.1.1. Apoptosis and Cell Cycle

BCL2 and *MDM2* are the first genes reported to be highly expressed in UM [27–29]. *TP53* is very rarely mutated, but is frequently inactivated by *MDM2* overexpression in UM. Consequently, Bcl2 and Mdm2 are described as potential targets for therapeutic intervention. For instance, treatment with inhibitors of the apoptotic proteins Bcl2/xL coupled with alkylating agents has been shown to trigger tumor growth inhibition in UM PDXs (Patient-Derived Xenografts) [30]. Clinical studies have failed to provide a therapeutic benefit due to strong adverse effects, although preclinical investigations of Bcl2 and Mdm2 inhibitors have confirmed their antitumorigenic effect in UM [30,31]. Evaluation of other strategies to re-activate p53, including inhibitors of Mdm4, a homolog of Mdm2, may offer good alternatives [32,33].

Rb (Retinoblastoma gene) inhibits proliferation and it is frequently inactivated in UM by phosphorylation induced by cyclin D1 (*CD1*) overexpression [34,35]. Precisely, CD1 is overexpressed in approximately 40% of cases [27,28]. In other cases, Rb phosphorylation may be due to $p16^{INK4a}$ promoter methylation [36]. Rb pathway is disrupted in a wide number of cancers and the targeting approaches include CD inhibitors that are being tested in UM in combination with other therapies. HDAC (histone deacetylase) inhibitors are currently being assessed in UM and they have been found to induce CD1 degradation. Cotherapy with HDACi and CDKi has been shown to induce cell death in UM cell lines [32]. Additionally, CD1 activates CDK4/6, the downstream targets of the MEK pathway that is frequently altered in UM, which implies a potential co-targeting of MEK and CDK4/6.

3.1.2. Hypoxia-Induced Response

HIF (Hypoxia Inducible Factor) is the main node for hypoxia response and it triggers a metabolic reprogramming when the growing tumors lack oxygen supply to increase glucose uptake and promote angiogenesis [37]. This hypoxia response occurs through cMET or CXCR4 (C-X-C chemokine receptor type 4). *HIF* is overexpressed in specific subsets of UM and its inhibition has been shown to suppress tumor growth in UM mouse models [10,38].

3.1.3. cMET-PI3K Pathway

cMET encodes the transmembrane tyrosine kinase receptor that is activated through the binding of the hepatocyte growth factor (HGF). HGF is primarily produced in the liver and it is implicated in the growth of various malignancies. *cMET* expression levels are higher in UM metastatic tumors as

compared to primary tumors, an intriguing fact given the presence of high levels of HGF in the liver tumor microenvironment. The HGF-cMET pathway has been described to mediate resistance to MEK inhibitors in metastatic UM [39]. In fact, HGF-cMET activates the PI3K-Akt pathway through PI3Kβ to compensate for the lack of MEK pathway activation. Therefore, blocking HGF-cMET signaling can resensitize the tumor cells to MEK inhibitors. This effect was observed in ex vivo UM metastatic explants [39]. A combination of MEK and cMET inhibitors is a promising approach that remains to be further investigated. On the other hand, the PI3K-Akt pathway is activated upon PTEN (Phosphatase and TENsin homolog) loss [40]. *PTEN* is a tumor suppressor that is underexpressed in 40% of UMs (mainly by LOH of the *PTEN* locus) [40–42]. There is growing evidence that PTEN is downregulated by miRNAs in UM [43,44]. Rescuing PTEN function is challenging but approaches targeting the PI3K/Akt pathway continue to be evaluated as combined therapies in UM.

3.1.4. NF-κB Proinflammatory Signaling

NF-κB (nuclear factor-kappa B) pathway activation has been described to contribute to the mechanism of resistance to BET (Bromodomain and Extra-Terminal motif proteins) inhibitors in the UM cells. Inhibitors of NF-kB signaling synergized with BET inhibition in vitro and in vivo, which suggested that the inhibition of NF-kB signaling may improve the efficacy of BET inhibition in patients with advanced UM [45]. Furthermore, NF-κB signaling pathway contributes to *PRAME* (Preferentially Expressed Antigen in Melanoma) upregulation [46]. *PRAME* expression has been reported to correlate with the metastatic risk of UM [47]. These findings shed light on the potential targeting of this antigen by PRAME-specific HLA-A2 T-cell clones [48]. A recent study showed that 50% of metastatic UM expressed PRAME and HLA class I, which can be recognized by PRAME-specific T cells, implying the applicability of PRAME-TCR therapy on metastatic UM patients [49]. Currently, a PRAME-TCR clinical trial is ongoing for AML (Acute Myeloid Leukemia) and metastatic UM patients (NCT02743611).

3.2. Genomic Aberrations and Mutational Burden

Few genomic and genetic events characterize UM (Figure 1a). In fact, UM presents a low mutational burden, with an SNV mutation rate of <1 per Mb [11]. Additionally, UM displays a near-diploid karyotype with only a few chromosomal changes affecting chromosome 3 or chromosome arms 1p−, 6p+, 6q-, 8p−, 8q+. The cytogenetic alterations are tightly linked with the clinical outcome. The presence of both monosomy 3 and gain of 8q is correlated with high metastatic risk [50,51]. Harboring only one of the latter events correlates with an intermediate risk and the absence of such aberrations corresponds to a low risk of developing metastasis [10,11,50]. Notably, the monosomy of chromosome 3 is reported in up to 50% of primary UMs and it is considered to be a poor prognostic factor (Figure 1a) [17].

UMs are generally resistant to immunotherapy, which is probably due to their low mutational burden and the consequent low neoantigen generation. However, two exceptional UM cases have recently been reported to exhibit a response to PD-1 inhibitor. As previously stated, these cases are characterized by a hypermutated profile due to the presence of a germline loss-of-function mutation in *MBD4* [18,19].

3.3. Mutational Landscape and Related Therapeutic Perspectives

UM malignant transformation relies on two main events. First, a Gαq-pathway activating mutation in either *GNAQ, GNA11, CYSLTR2* (cysteinyl leukotriene receptor 2), or *PLCβ4* (phospholipase C *β*4), [13,52–54]. Second, a mutation in either *BAP1*, *SF3B1* (splicing factor 3b subunit 1), *SRSF2* (serine/arginine-rich splicing factor 2), or *EIF1AX* (eukaryotic translation initiation factor 1A X-linked) (Figure 1a,b) [10,55]. Based on the characterization of these genetic events, there is a growing interest in therapies targeting either Gαq downstream effectors, BAP1-related molecular mechanisms, splicing, or further related biological processes.

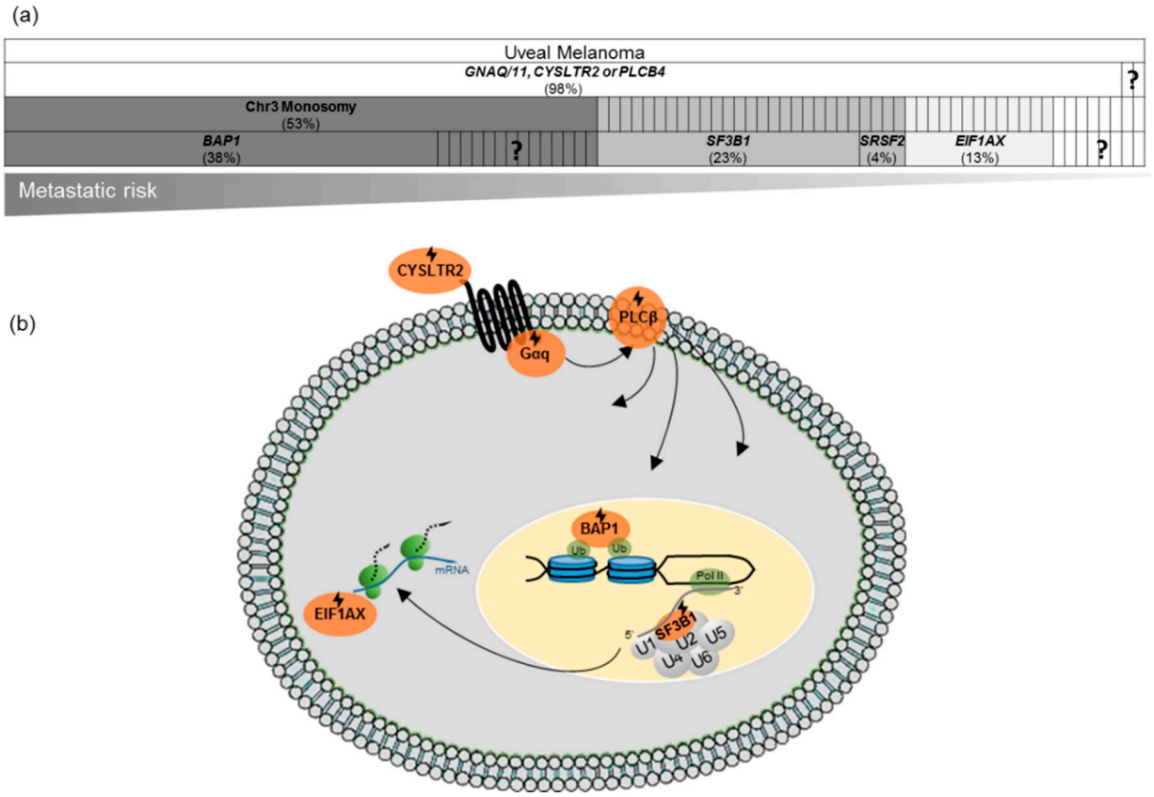

Figure 1. Genomic and genetic alterations in uveal melanoma (UM) and the affected biological processes. (**a**). Frequency of mutations in UM and the associated prognostic value: BRCA1 associated protein 1 (*BAP1)* mutations are mostly associated with chromosome 3 monosomy and an early metastatic risk (~5 years after primary UM diagnosis), splicing factor 3b subunit 1 (*SF3B1*) and serine/arginine-rich splicing factor 2 (*SRSF2*) mutations are mainly associated with chromosome 3 disomy and a late-onset metastatic risk (~8 years after primary UM diagnosis), while eukaryotic translation initiation factor 1A X-linked (*EIF1AX*) mutations are associated with chromosome 3 disomy and a low risk of metastasis. Data is retrieved from The Cancer Genome Atlas (TCGA) UM dataset (cBioportal for Cancer Genomics) [56,57]. (**b**). Main biological processes impacted by the recurrent mutations in UM. Mutations in components of G protein-coupled receptors (GPCRs) lead to the constitutive activation of Gαq signaling and several downstream pathways. Further oncogenic events include mutations in *BAP1*, *SF3B1/SRSF2*, or *EIF1AX*, involved in chromatin modulation, splicing, and translation initiation, respectively. Mutations are indicated by ϟ.

3.3.1. Gαq-Pathway Activating Mutations

The first UM driver event consists of mutations that activate the Gαq pathway [13,52]. *GNAQ/11* mutations are reported in approximately 96% of UM patients, mainly at codon Q209 and less recurrently at R183 or G48 [13,58]. *PLCβ4* and *CYSLTR2* mutations have been recently reported at lesser frequencies (2.5% and 4%, respectively) [10]. *PLCβ4* hotspot mutation is located at p.D630, the region corresponding to the phospholipase C β-4 catalytic domain [53], and *CYSLTR2* mutation encodes an L129 substitution [54]. These mutations are mutually exclusive hotspot mutations that activate the Gαq signaling, thereby stressing the importance of this pathway in UM oncogenesis (Figure 2) [53,54]. Of note, none of these mutations is correlated with differential prognosis or clinical outcome, which suggests an oncogenic rather than metastatic driver effect [10,54,59].

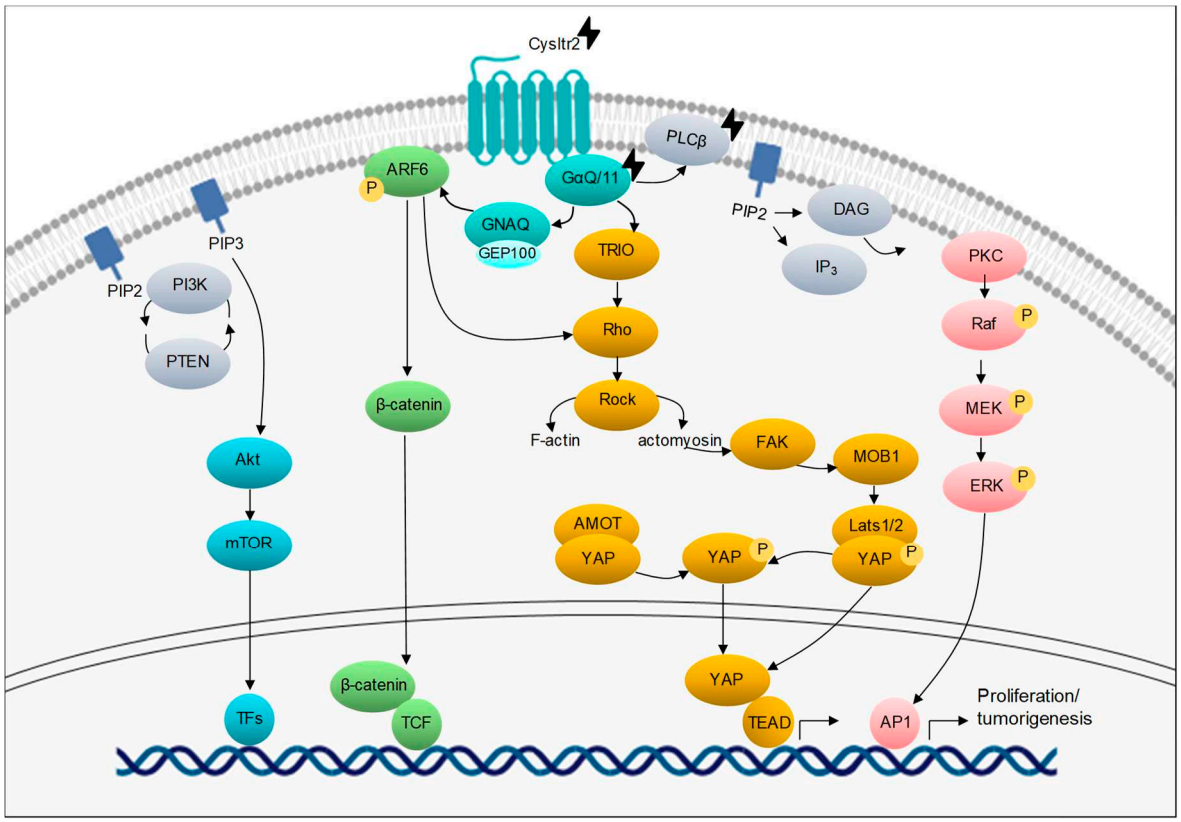

Figure 2. Dysregulated pathways in uveal melanoma. Recurrent mutations in *GNAQ*, *GNA11*, *PLCβ4*, and *CYSLTR2* are mutually exclusive and trigger the activation of Gαq signaling and related pathways (Akt/mTOR, Wnt/β-catenin, Yes-associated protein (YAP), and MAPK pathways) in UM. Mutations are indicated by ϟ.

GNAQ and *GNA11* encode the subunits Gαq and Gα11 that are bound together with β and γ subunits. The resulting heterotrimeric complex is coupled with a GPCR protein (G protein-coupled receptor), which is involved in several signaling transduction pathways, as shown in Figure 2. In the basal state, Gαq/11 is bound to a GDP and it remains inactive. Upon GTP binding, the complex undergoes conformational changes and then targets downstream effectors [52]. *GNAQ/11* mutations lead to a constitutively active α subunit, which results in a dysregulation of several downstream pathways including Akt/mTOR, Wnt/β-catenin, Rac/Rho, MAPK, and PI3K pathways [60].

The importance of Gαq pathways in UM oncogenesis has been described in vitro and in vivo. Accordingly, *GNAQ/11* knockdown inhibits the growth of *GNAQ/11*-mutated UM cell lines, an effect that is not observed in *GNAQ/11* wild-type (WT) cell lines [61]. Moreover, mouse models that harbor *GNAQ/11* mutations develop multiple tumors, which confirms the oncogenic impact of these mutations [13,62,63]. Mice with melanocyte-specific expression of $GNA11^{Q209L}$ recapitulated human Gq-associated melanomas and developed pigmented neoplastic lesions from the melanocytes of the skin and non-cutaneous organs, including the eye and leptomeninges, as well as atypical sites, such as the lymph nodes and lungs [62,63].

Gαq-Corresponding Therapeutic Strategies

Gαq/11 inhibitors development has been a major concern over the last two decades, given the high recurrence of *GNAQ* and *GNA11* mutations in UM. YM-254890 (YM) is a cyclic depsipeptide that is extracted from bacteria that acts as a selective Gαq inhibitor by preventing the GDP release, leading to the blockage of GDP/GTP exchange reaction and Gαq activation [64,65]. Interestingly, YM was shown to inhibit R183 Gαq mutant rather than Q209L Gαq mutant [65,66]. FR900359 (FR) is a

YM analog that was obtained from plants that depicts a similar mode of action. FR has been recently described to trigger differentiation and inhibit the migration of *GNAQ/11*-mutated melanoma cells [67]. FR mainly inhibits Q209L, Q209P, and Q209L Gαq/11 mutants, promoting UM cell cycle arrest and cell death [68]. Despite the promising results of Gαq/11 inhibitors in vitro, such inhibitors have not yet been evaluated for clinical application.

On the other hand, much attention has been drawn on targeting the Gαq downstream effectors Protein Kinase C (PKC) and MEK. The inhibition of each of these pathways has been evaluated, but showed no clinical benefit, which suggested the need for combinatory strategies to abolish different Gαq downstream effectors at once [69,70]. The inhibitors of MEK and PI3K (MEKi, PI3Ki) separately show a modest apoptotic effect on *GNAQ/11*-mutated UM cell lines that is significantly increased upon combination [61,71,72]. Similarly, PI3Ki and mTORi exhibit an apoptotic effect in a wide range of UM cells and tumor growth inhibition in vivo [73]. Another promising strategy is coupling PKC inhibition with p53 activation. Cotreatment with Mdm2i and PKCi decreases the growth rate of the UM cells and promotes cell death that is induced by DNA damage [74]. In vivo studies show that the dual inhibition of PKC and Mdm2 or PKC and mTOR reduces tumor growth in UM PDXs [31]. These results have boosted the assessment of such compounds in clinical trials.

Recent findings pinpointed ARF6 as a downstream effector of Gαq [75]. Interestingly, ARF6 is a GTPase that is known to play a role in proliferation, invasion, and metastasis in some cancers [76,77]. In UM, inhibiting ARF6 induces a decrease in proliferation in vitro and tumorigenesis in vivo [75]. Moreover, activated ARF6 triggers the transport of β-catenin to the nucleus, where it can activate transcription factors, thereby promoting invasion and metastasis [75]. β-catenin is the main node in the canonical Wnt pathway, which plays a vital role in embryonic development and it is known to be mutated in various cancers [78]. β-catenin and its downstream effector Wnt5a were found to be overexpressed in a subset of aggressive UM tumors [79]. Moreover, β-catenin inhibition was shown to induce apoptosis and inhibit cell growth, invasion, and migration in vitro [80].

Hippo pathway, together with the mTOR (Mammalian Target of Rapamycin) pathway, regulate organ size in mammals [81]. YAP (Yes-associated protein) is one of the main effectors of the Hippo pathway, but it can also be activated in a Hippo-independent manner by Gαq through Trio-Rho/Rac or through MOB1 phosphorylation [82,83]. In proliferating cells, YAP is active until a certain cell density is reached. Subsequently, MTS1 and MTS2 (mammalian STE20-like protein kinase 1 and 2) activate LATS1/2 (large tumor suppressor homolog 1 and 2) that phosphorylate YAP, which will stay in the cytoplasm and be further degraded, which leads to growth inhibition [82,84]. On the contrary, dephosphorylated YAP remains in the nucleus, where it can bind to TEAD (transcriptional enhancer activation domain), inducing gene expression and eventually cell proliferation [81]. All the UM cell lines harboring *GNAQ/11* mutations exhibit low YAP phosphorylation and nuclear localization, which indicates YAP activation. The cell growth of *GNAQ/11*-mutated UM cells is significantly decreased upon *YAP* knockdown or inhibition [84,85]. Notably, a recent study identified GPCR-mediated YAP activation and RTK-driven AKT signaling as key pathways that are involved in the escape of UM cells from MEK inhibition [86]. Verteporfin is a drug that is used for the treatment of vascular occlusion of abnormal blood vessels and it has been reported to inhibit TEAD-YAP interaction [85,87]. However, its specificity to YAP has not been confirmed. In UM cells, verteporfin decreased colony formation and proliferation in three-dimensional (3D) cultures. Moreover, verteporfin reduces tumor size and cell proliferation in vivo [82,84]. Recently, FAK has been revealed to activate YAP by MOB1 phosphorylation, resulting in Hippo pathway inhibition. FAK inhibition has been shown to abolish YAP-dependent UM tumor growth in vitro and in vivo [83].

Overall, the successful inhibition of Gαq-signaling-dependent oncogenesis may be achieved by synergistically targeting several downstream effectors. Additional therapeutic strategies have to be pursued for the metastatic settings provided that *GNAQ/11* mutations have no prognostic value in UM.

3.3.2. *BAP1*, *SF3B1*, *SRSF2* or *EIF1AX* Mutations

The second oncogenic event of UM consists of mutations in *BAP1*, *EIF1AX*, *SF3B1*, or *SRSF2*. These mutations are mutually exclusive in almost all UM cases [10,55,88]. *BAP1* mutations are recurrently found to be associated with chromosome 3 monosomy in early metastatic risk cases. Mutations on *SF3B1* and *SRSF2* are mainly associated with chromosome 3 disomy and a late-onset metastatic risk, while *EIF1AX* mutations are associated with chromosome 3 disomy and a low risk of metastasis (Figure 1a) [55,88].

BAP1

BAP1 encodes a deubiquitylase that forms protein complexes that are implicated in several pathways along with cell cycle, cell differentiation, and DNA damage response and it has been described to act as a tumor suppressor in various cancers [17,89,90]. The expression of *BAP1* is lost in up to 84% cases of metastatic UM, due to inactivating mutations. *BAP1* is mutated in 38% of primary UMs, mainly in tumors with monosomy 3, thereby being characteristic of belligerent tumors [10,15,91]. Remarkably, around 84–89% of metastatic tumors harbor somatic mutations in *BAP1*. Hence, *BAP1* alterations are strongly correlated with a higher metastatic risk and reduced survival rate [10,15,59,91,92]. Therefore, targeting BAP1-related processes represents a promising therapeutical strategy for preventing metastatic progression and improving patient survival. BAP1 binds to ASXL1 to form the polycomb complex that deubiquitinates histone 2A [93,94]. Thus, the loss of *BAP1* increases ubiquitinated expression and it may sensitize tumor cells to HDAC (histone deacetylase) inhibitors, like valproic acid, trichostatin A, LBH-589, and syberynalide hydroxamic acid. HDAC inhibition has been shown to stop cell proliferation, induce cell cycle arrest, trigger apoptosis, block migration, promote cell differentiation, and impact the gene expression profile in preclinical UM models [95–97]. A very recent study demonstrated that the combination of MEK and HDAC inhibitors considerably decreased tumor growth in both subcutaneous and liver metastasis xenograft models of UM, which encourages clinical co-targeting of MEK and HDAC in advanced UM [86].

EZH2 (Enhancer of Zeste Homolog 2) forms the polycomb repressive complex 2 (PRC2), which methylates histone H3 lysine 27 (H3K27). BAP1 loss leads to increased H3K27 that, in turn, raises the expression level of EZH2 [98]. However, the UM cells were reported to resist EZH2 inhibition regardless of their *BAP1* status [99].

Additionally, BAP1 forms a complex with BRCA1 and BARD1, which takes part in double-strand break repair through homologous recombination (HR) [100]. BAP1 deficiency results in impaired HR, which may suggest an increased dependency on other DNA repair pathways and a consequent sensitivity to PARP inhibition [100–102]. A clinical trial of a PARP inhibitor (Niraparib) in BAP1-deficient neoplasms including UM is ongoing (NCT03207347).

Overall, targeting BAP1-related processes is a potential therapeutic strategy. Nevertheless, successful approaches to target metastatic malignancies may require combined treatment in order to block all the related processes. A synthetic lethality screen can be a precious tool in revealing vulnerabilities to therapy in BAP1-deficient UM patients.

EIF1AX

EIF1AX missense mutations are recurrent in 13% of UMs. These mutations are mainly associated with disomy 3 and present a low metastatic risk [10,88]. *EIF1AX* encodes eukaryotic translation initiation factor 1A (eIF1A) and it is essential in the recruitment of the ternary complex and for assembling the 43S preinitiation complex (PIC) [103]. Translation initiation is a rate-limited step that is tightly regulated and factors taking part at this stage are known to be misregulated in tumorigenesis [104]. *EIF1AX* overexpression has been documented to boost translation and cell proliferation in bovine mammary epithelial cells [105]. Interestingly, *EIF1AX* was found to harbor heterozygous mutations in papillary carcinomas, the most common thyroid cancer, and in ovarian carcinoma with a worse

prognosis when coupled with mutations of the Ras family [106,107]. Very recently, *EIF1AX* and *RAS* mutations have been shown to cooperate to induce tumorigenesis in isogenic cell lines and mice. EIF1AX-A113splice variants, which are recurrent in advanced thyroid cancer, stabilize the PIC and enable a general increase in protein synthesis through ATF4-induced dephosphorylation of EIF2α. RAS stabilizes c-MYC, which cooperates with ATF4 to sensitize mTOR to amino acid supply. These combined events were shown to generate therapeutic vulnerabilities to MEK, BRD4, and mTOR kinase inhibitors [108]. These findings pinpoint new therapeutic strategies and emphasize the importance of understanding the biological impact of different *EIF1AX* mutations in UM.

SF3B1 and *SRSF2*

The splicing factor (SF) genes *SF3B1, U2AF35*, *ZRSR2*, and *SRSF2* are recurrently mutated in hematological malignancies [109–111] and solid tumors [112–114], which include UM [11,88,115,116]. It is noteworthy that the SF hotspot mutations take place in a mutually exclusive manner and they affect proteins that are involved in the 3′ splice site (3′ss) recognition, an early step of splicing, resulting in specific aberrant splicing patterns. *SF3B1* and *SRSF2* mutations are recurrent in UMs and they lead to a change of function of the SF [109]. Such events highlight the involvement of splicing aberrations in oncogenesis and the relevance of SF therapeutic targeting.

SRSF2 belongs to the family of serine/arginine (SR)-rich proteins that aid splicing through binding exonic splicing enhancers (ESEs). SR proteins contain at least an SR rich binding domain and an RNA recognition motif (RRM), where RNA binding proteins (RBPs) attach. On early steps of splicing, SF1 binds to the BP and SRSF2 and ZRSR2 simultaneously bind to ESEs to aid the binding and stability of the U2AF subunits [117]. *SRSF2* is most commonly mutated in chronic myelomonocytic leukemia (CMML) (47%) [118] and myelodysplastic syndromes (MDS) (15%) [119]. Recently, *SRSF2* has also been found to be mutated in 4% of UMs [10,120]. Upon hotspot mutations at P95m which is located downstream the RRM, SRSF2 undergoes a conformational change on the RRM, and consequently acquires more affinity for G-rich versus C-rich ESEs motifs, differently from the WT, which has an equal affinity for these motifs [109,120–122]. The resulting misregulated exon inclusion causes an aberrant splicing pattern of a broad range of genes comprising the tumor suppressor *ARMC10* or *EZH2* [122,123]. The mis-spliced form of *EZH2* is sensitive to nonsense-mediated RNA decay (NMD), which implies a decrease in EZH2 levels which has already been observed in MDS progression [124]. In fact, *EZH2* and *SRSF2* mutations take place in a mutually exclusive manner [122]. Even though the *SRSF2* mutation rate is low in UM [10,120], it may be a significant event, given the cascade effect of misrecognition of ESEs on a large number of target genes.

SF3B1 encodes the U2 small nuclear riboprotein complex (U2-snRNP) that is responsible for branchpoint (BP) recognition and it is mutated in 23% of UMs [116]. U2-snRNP binds to the BP of the intron in an incomplete manner. Further interactions are required to enhance BP identification and stabilize the interaction, including base-pairing that is mediated by SF3B1 and U2AF35/65 binding. SF3B1 structure consists of a hydrophilic N-terminal harboring a U2AF-binding motif and a C-terminal with 22 different HEAT (Huntingtin, Elongation factor 3, protein phosphatase 2A, Targets of rapamycin 1) repeats [125,126], whose function remains to be elucidated [120]. Hotspot mutations target the HEAT repeats at codons R625, K666, and K700 [125,126]. Hotspot mutation K700 prevails in hematological malignancies, whereas the R625 and K666 mutations prevail in UM and they are frequently associated with disomy 3 and a late metastatic risk [11,55,88,115]. *SF3B1* mutations have been thoroughly investigated and were reported to induce an aberrant splicing pattern by an alternative 3′ss usage upstream the canonical 3′ss in breast cancer, CLL, and UM [116,127]. *SF3B1* mutations generate change-of-function mutants, leading to aberrant splicing of less than 1% of all splice junctions by recognizing an alternative BP localized at 11-14 nts upstream the canonical site [116]. SF3B1 has been reported to be involved in the splicing of key apoptotic genes, like MCL1 and BCL2/xL, which are appealing cancer targets [128]. Yet, further studies are required to link the splicing aberrations to oncogenesis. These findings have resulted in a growing interest in splicing

modulators as therapeutic agents. Microbial and natural metabolites that inhibit splicing were the first candidates, including FR901464 and derivatives. The FR9014 series was isolated from Pseudomonas sp. Number 2663 and constitutes the first antiproliferative molecules that are associated with splicing inhibition. Spliceostatin A is a methylated derivative of FR901464. Spliceostatin B was also isolated from Pseudomonas sp. Number 2663. Spliceostatin E was isolated from Burkholderia sp. FERM BP3421. Thailanstatins were recovered from Burkholderia thailandensis MSMB43. Meayamycin and Sudemycins are synthetic derivatives from the depicted natural products [129,130]. These splicing inhibitors have been shown to regulate Mcl-1 splicing and inhibit cell proliferation in a dose-dependent manner [131,132]. Other compounds that were isolated from bacteria include Pladienolides A-G, E7107, FD-895, and herboxidiene. E7107 has been tested on clinical trials in various solid tumors. No significant response was observed, even though the mRNA levels were altered in a dose-dependent manner [133]. An additional natural compound that is extracted from plants, isogingketin, was also described as a general splicing inhibitor with anti-tumor activity [134]. Nevertheless, inhibiting an essential biological process, like splicing, confers high cytotoxic effects, thereby limiting the therapeutic window [135,136]. Specific compounds are then needed to restore the normal splicing level, rather than inhibiting the whole process of splicing.

Recently, encouraging results were obtained with H3B-8800, a small molecule that is derived from pladienolide that targets SF3B1 complex. Cells harboring *SF3B1* mutations presented higher sensitivity to this inhibitor than cells with WT *SF3B1*, a feature that may overcome the high cytotoxicity of splicing inhibition. The preferential inhibition is associated with an enrichment of alternative 3'ss in SF3B1 mutant cells as compared to WT cells [137]. Further studies are ongoing to confirm the specificity of H3B-8800 in vivo and in a clinical trial in patients with advanced myeloid malignancies, including MDS, AML, and CMML (NCT02841540).

New perspectives also emerged from the studies of neopeptides that were generated by the aberrant transcripts in *SF3B1*-mutant cells. In fact, the splicing-derived putative neoepitopes have a high degree of recurrence, which is suggestive of potential interest for immunotherapeutic intervention. Moreover, these neopeptides are considered for prospective personalized cancer vaccine development [138].

4. Conclusions

UM is a rare cancer in adults, with very stereotyped oncogenic events that have been mostly decrypted over the last 10 years. The epidemiological, genetic, and transcriptional specificity of UM highlight the importance of UM as a model of oncogenesis. The understanding of the molecular mechanisms that underlie UM has considerably progressed over the last decade. However, these advances have not yet been translated into therapeutic progress, and the prognosis of the metastatic form of UM remains somber.

Conclusively, targeted therapies remain to be improved by combinatory strategies in light of a better understanding of the UM-underlying molecular mechanisms. Recently-reported exceptional immune responses in UM patients harboring *MBD4* mutations point up the importance of deciphering cancer mechanisms in order to determine the oncogenic actors and develop the appropriate therapeutic strategies. Moreover, the development of preclinical models that recapitulate the different routes of UM malignant transformation is essential for validating novel therapeutic strategies.

Author Contributions: R.V.-N. and S.A. wrote the manuscript. R.V.-N., M.T., S.R.-R. and S.A. edited and reviewed the text. S.R.-R. and S.A. conceived the review.

Funding: This research was funded by the European Union's Horizon 2020 research and innovation programme (Marie Skłodowska-Curie grant agreement No 666003), the European Union's Horizon 2020 project "UM Cure 2020" (Grant No. 667787) and SIRIC Curie (Grant INCa-DGOS-Inserm_12554).

Conflicts of Interest: The authors declare no conflict of interest.

References

1. Mahendraraj, K.; Lau, C.S.M.; Lee, I.; Chamberlain, R.S. Trends in Incidence, Survival, and Management of Uveal Melanoma: A Population-Based Study of 7516 Patients from the Surveillance, Epidemiology, and End Results Database (1973–2012). *Clin. Ophthalmol.* **2016**, *10*, 2113–2119. [CrossRef] [PubMed]
2. Singh, A.D.; Turell, M.E.; Topham, A.K. Uveal Melanoma: Trends in Incidence, Treatment, and Survival. *Ophthalmology* **2011**, *118*, 1881–1885. [CrossRef] [PubMed]
3. Pandiani, C.; Béranger, G.E.; Leclerc, J.; Ballotti, R.; Bertolotto, C. Focus on Cutaneous and Uveal Melanoma Specificities. *Genes Dev.* **2017**, *31*, 724–743. [CrossRef] [PubMed]
4. Mathis, T.; Cassoux, N.; Tardy, M.; Piperno, S.; Gastaud, L.; Dendale, R.; Maschi, C.; Nguyen, A.; Meyer, L.; Bonnin, N.; et al. Management of Uveal Melanomas, Guidelines for Oncologists. *Bull. Cancer* **2018**, *105*, 967–980. [CrossRef] [PubMed]
5. Yang, J.; Manson, D.K.; Marr, B.P.; Carvajal, R.D. Treatment of Uveal Melanoma: Where Are We Now? *Ther. Adv. Med. Oncol.* **2018**, *10*, 1–17. [CrossRef] [PubMed]
6. Barker, C.A.; Salama, A.K. New NCCN Guidelines for Uveal Melanoma and Treatment of Recurrent or Progressive Distant Metastatic Melanoma. *JNCCN J. Natl. Compr. Cancer Netw.* **2018**, *16*, 646–650. [CrossRef]
7. Kujala, E.; Mäkitie, T.; Kivelä, T. Very Long-Term Prognosis of Patients with Malignant Uveal Melanoma. *Investig. Ophtalmol. Vis. Sci.* **2003**, *44*, 4651–4659. [CrossRef]
8. Amirouchene-Angelozzi, N.; Schoumacher, M.; Stern, M.-H.; Cassoux, N.; Desjardins, L.; Piperno-Neumann, S.; Lantz, O.; Roman-Roman, S. Upcoming Translational Challenges for Uveal Melanoma. *Br. J. Cancer* **2015**, *113*, 1249–1253. [CrossRef]
9. Patel, M.; Smyth, E.; Chapman, P.B.; Wolchok, J.D.; Schwartz, G.K.; Abramson, D.H.; Carvajal, R.D. Therapeutic Implications of the Emerging Molecular Biology of Uveal Melanoma. *Clin. Cancer Res.* **2011**, *17*, 2087–2100. [CrossRef]
10. Robertson, A.G.; Shih, J.; Yau, C.; Gibb, E.A.; Oba, J.; Mungall, K.L.; Hess, J.M.; Uzunangelov, V.; Walter, V.; Danilova, L.; et al. Integrative Analysis Identifies Four Molecular and Clinical Subsets in Uveal Melanoma. *Cancer Cell* **2018**, *32*, 204–220. [CrossRef]
11. Furney, S.J.; Pedersen, M.; Gentien, D.; Dumont, A.G.; Rapinat, A.; Desjardins, L.; Turajlic, S.; Piperno-Neumann, S.; de la Grange, P.; Roman-Roman, S.; et al. SF3B1 Mutations Are Associated with Alternative Splicing in Uveal Melanoma. *Cancer Discov.* **2013**, *3*, 1122–1129. [CrossRef] [PubMed]
12. Royer-bertrand, B.; Torsello, M.; Rimoldi, D.; Zaoui, I.E.; Cisarova, K.; Pescini-gobert, R.; Raynaud, F.; Zografos, L.; Schalenbourg, A.; Speiser, D.; et al. Comprehensive Genetic Landscape of Uveal Melanoma by Whole-Genome Sequencing. *Am. J. Hum. Genet.* **2016**, 1190–1198. [CrossRef] [PubMed]
13. Van Raamsdonk, C.D.; Griewank, K.G.; Crosby, M.B.; Garrido, M.C.; Vemula, S.; Wiesner, T.; Obenauf, A.C.; Wackernagel, W.; Green, G.; Bouvier, N.; et al. Mutations in GNA11 in Uveal Melanoma. *N. Engl. J. Med.* **2010**, *363*, 2191–2199. [CrossRef] [PubMed]
14. Wiesner, T.; Obenauf, A.C.; Murali, R.; Fried, I.; Klaus, G.; Ulz, P.; Windpassinger, C.; Wackernagel, W.; Loy, S.; Wolf, I. Germline Mutations in BAP1 Predispose to Melanocytic Tumors. *Nat. Genet.* **2012**, *43*, 1018–1021. [CrossRef] [PubMed]
15. Ewens, K.G.; Lalonde, E.; Shields, C.L.; Ganguly, A. Comparison of Germline versus Somatic BAP1 Mutations for Risk of Metastasis in Uveal Melanoma. *BMC Cancer* **2018**, *18*, 1–12. [CrossRef] [PubMed]
16. Njauw, C.N.J.; Kim, I.; Piris, A.; Gabree, M.; Taylor, M.; Lane, A.M.; DeAngelis, M.M.; Gragoudas, E.; Duncan, L.M.; Tsao, H. Germline BAP1 Inactivation Is Preferentially Associated with Metastatic Ocular Melanoma and Cutaneous-Ocular Melanoma Families. *PLoS ONE* **2012**, *7*. [CrossRef]
17. Abdel-Rahman, M.H.; Pilarski, R.; Cebulla, C.M.; Massengill, J.B.; Christopher, B.N.; Boru, G.; Hovland, P.; Davidorf, F.H. Germline BAP1 Mutation Predisposes to Uveal Melanoma, Lung Adenocarcinoma, Meningioma, and Other Cancers. *J. Med. Genet.* **2011**, *48*. [CrossRef] [PubMed]
18. Rodrigues, M.; Mobuchon, L.; Houy, A.; Fiévet, A.; Gardrat, S.; Barnhill, R.L.; Popova, T.; Servois, V.; Rampanou, A.; Mouton, A.; et al. Outlier Response to Anti-PD1 in Uveal Melanoma Reveals Germline MBD4 Mutations in Hypermutated Tumors. *Nat. Commun.* **2018**, *9*, 1–6. [CrossRef]
19. Johansson, P.A.; Stark, A.; Palmer, J.M.; Bigby, K.; Brooks, K.; Rolfe, O.; Pritchard, A.L.; Whitehead, K.; Warrier, S.; Glasson, W.; et al. Prolonged Stable Disease in a Uveal Melanoma Patient with Germline MBD4 Nonsense Mutation Treated with Pembrolizumab and Ipilimumab. *Immunogenetics* **2019**, *4*, 1–4. [CrossRef]

20. Bellacosa, A. Role of MED1 (MBD4) Gene in DNA Repair and Human Cancer. *J. Cell. Physiol.* **2001**, *187*, 137–144. [CrossRef]
21. Prescher, G.; Bornfeld, N.; Hirche, H.; Horsthemke, B.; Jöckel, K.; Becher, R. Prognostic Implications of Monosomy 3 in Uveal Melanoma. *Lancet* **1996**, *347*, 1222–1225. [CrossRef]
22. White, V.A.; Chambers, J.D.; Courtright, P.D.; Chang, W.Y.; Horsman, D.E. Correlation of Cytogenetic Abnormalities with the Outcome of Patients with Uveal Melanoma. *Cancer* **1998**, *83*, 354–359. [CrossRef]
23. Onken, M.D.; Worley, L.A.; Char, D.H.; Augsburger, J.J.; Correa, Z.M.; Nudleman, E.; Aaberg, T.M., Jr.; Altaweel, M.M.; Bardenstein, D.S.; Finger, P.T.; et al. Collaborative Ocular Oncology Group Report No. 1: Prospective Validation of a Multi-Gene Prognostic Assay in Uveal Melanoma. *Ophtalmology* **2012**, *119*, 1596–1603. [CrossRef]
24. Worley, L.A.; Onken, M.D.; Person, E.; Robirds, D.; Branson, J.; Char, D.H.; Perry, A.; Harbour, J.W. Transcriptomic versus Chromosomal Prognostic Markers and Clinical Outcome in Uveal Melanoma. *Clin. Cancer Res.* **2007**, *13*, 1466–1471. [CrossRef]
25. Bove, R.; Char, D.H. Nondiagnosed Uveal Melanomas. *Ophthalmology* **2004**, *111*, 554–557. [CrossRef]
26. Shields, C.L.; Kaliki, S.; Rojanaporn, D.; Ferenczy, S.R.; Shields, J.A. Enhanced Depth Imaging Optical Coherence Tomography of Small Choroidal Melanoma. *Arch. Ophthalmol.* **2012**, *130*, 850–856. [CrossRef]
27. Coupland, S.E.; Bechrakis, N.; Schüler, A.; Anagnostopoulos, I.; Hummel, M.; Bornfeld, N.; Stein, H. Expression Patterns of Cyclin D1 and Related Proteins Regulating G1-S Phase Transition in Uveal Melanoma and Retinoblastoma. *Br. J. Ophthalmol.* **1998**, *82*, 961–970. [CrossRef]
28. Brantley, M.A.; Harbour, J.W. Deregulation of the Rb and P53 Pathways in Uveal Melanoma. *Nat. Cell Biol.* **2000**, *157*, 1795–1801. [CrossRef]
29. Helgadottir, H.; Höiom, V. The Genetics of Uveal Melanoma: Current Insights. *Appl. Clin. Genet.* **2016**, *9*, 147–155. [CrossRef]
30. Némati, F.; de Montrion, C.; Lang, G.; Kraus-Berthier, L.; Carita, G.; Sastre-Garau, X.; Berniard, A.; Vallerand, D.; Geneste, O.; de Plater, L.; et al. Targeting Bcl Bcl-X L Induces Antitumor Activity in Uveal Melanoma Patient-Derived Xenografts. *PLoS ONE* **2014**, *9*. [CrossRef]
31. Carita, G.; Frisch-Dit-Leitz, E.; Dahmani, A.; Raymondie, C.; Cassoux, N.; Piperno-Neumann, S.; Némati, F.; Laurent, C.; De Koning, L.; Halilovic, E.; et al. Dual Inhibition of Protein Kinase C and P53-MDM2 or PKC and MTORC1 Are Novel Efficient Therapeutic Approaches for Uveal Melanoma. *Oncotarget* **2016**, *7*. [CrossRef]
32. Heijkants, R.; Willekens, K.; Schoonderwoerd, M.; Teunisse, A.; Nieveen, M.; Radaelli, E.; Hawinkels, L.; Marine, J.-C.; Jochemsen, A. Combined Inhibition of CDK and HDAC as a Promising Therapeutic Strategy for Both Cutaneous and Uveal Metastatic Melanoma. *Oncotarget* **2018**, *9*, 6174–6187. [CrossRef]
33. Marine, J.C.; Jochemsen, A.G. MDMX (MDM4), a Promising Target for P53 Reactivation Therapy and Beyond. *Cold Spring Harb. Perspect. Med.* **2016**, *6*, 1–15. [CrossRef]
34. Brantley, M.A.; Harbour, J.W. Inactivation of Retinoblastoma Protein in Uveal Melanoma by Phosphorylation of Sites in the COOH-Terminal Region. *Cancer Res.* **2000**, *60*, 4320–4323.
35. An, J.; Wan, H.; Zhou, X.; Hu, D.N.; Wang, L.; Hao, L.; Yan, D.; Shi, F.; Zhou, Z.; Wang, J.; et al. A Comparative Transcriptomic Analysis of Uveal Melanoma and Normal Uveal Melanocyte. *PLoS ONE* **2011**, *6*. [CrossRef]
36. Van der Veiden, P.A.; Metzelaar-Blok, J.A.W.; Bergman, W.; Hurks, H.M.H.; Frants, R.R.; Gruis, N.A.; Jager, M.J. Promoter Hypermethylation: A Common Cause of Reduced P16(INK4a) Expression in Uveal Melanoma. *Cancer Res.* **2001**, *61*, 5303–5306.
37. Semenza, G.L. HIF-1: Upstream and Downstream of Cancer Metabolism. *Curr. Opin. Genet. Dev.* **2010**, *20*, 51–56. [CrossRef]
38. Dong, L.; You, S.; Zhang, Q.; Osuka, S.; Devi, N.S.; Kaluz, S.; Ferguson, J.H.; Yang, H.; Chen, G.; Wang, B.; et al. Arylsulfonamide 64B Inhibits Hypoxia/HIF-Induced Expression of c-Met and CXCR4 and Reduces Primary Tumor Growth and Metastasis of Uveal Melanoma. *Clin. Cancer Res.* **2018**, *25*, 2206–2219. [CrossRef]
39. Cheng, H.; Chua, V.; Liao, C.; Purwin, T.J.; Terai, M.; Kageyama, K.; Davies, M.A.; Sato, T.; Aplin, A.E. Co-Targeting HGF-CMET Signaling with MEK Inhibitors in Metastatic Uveal Melanoma. *Mol. Cancer Ther.* **2017**, *118*, 6072–6078. [CrossRef]
40. Triozzi, P.L.; Eng, C.; Singh, A.D. Targeted Therapy for Uveal Melanoma. *Cancer Treat. Rev.* **2008**, *34*, 247–258. [CrossRef]
41. Simpson, L.; Parsons, R. PTEN: Life as a Tumor Suppressor. *Exp. Cell Res.* **2001**, *264*, 29–41. [CrossRef]

42. Abdel-Rahman, M.H.; Yang, Y.; Zhou, X.P.; Craig, E.L.; Davidorf, F.H.; Eng, C. High Frequency of Submicroscopic Hemizygous Deletion Is a Major Mechanism of Loss of Expression of PTEN in Uveal Melanoma. *J. Clin. Oncol.* **2006**, *24*, 288–295. [CrossRef]
43. Ling, J.; Lu, P.; Zhang, Y.; Jiang, S.; Zhang, Z. MiR-367 Promotes Uveal Melanoma Cell Proliferation and Migration by Regulating PTEN. *Genet. Mol. Res.* **2017**, *16*. [CrossRef]
44. Sun, L.; Wang, Q.; Gao, X.; Shi, D.; Mi, S.; Han, Q. MicroRNA-454 Functions as an Oncogene by Regulating PTEN in Uveal Melanoma. *FEBS Lett.* **2015**, *589*, 2791–2796. [CrossRef]
45. Ambrosini, G.; Do, C.; Tycko, B.; Realubit, R.B.; Karan, C.; Musi, E.; Carvajal, R.D.; Chua, V.; Aplin, A.E.; Schwartz, G.K. Inhibition of NF-KB-Dependent Signaling Enhances Sensitivity and Overcomes Resistance to BET Inhibition in Uveal Melanoma. *Cancer Res.* **2019**. [CrossRef]
46. Wadelin, F.R.; Fulton, J.; Collins, H.M.; Tertipis, N.; Bottley, A.; Spriggs, K.A.; Falcone, F.H.; Heery, D.M. PRAME Is a Golgi-Targeted Protein That Associates with the Elongin BC Complex and Is Upregulated by Interferon-Gamma and Bacterial PAMPs. *PLoS ONE* **2013**, *8*. [CrossRef]
47. Field, M.G.; Decatur, C.L.; Kurtenbach, S.; Gezgin, G.; Van Der Velden, P.A.; Jager, M.J.; Kozak, K.N.; Harbour, J.W. PRAME as an Independent Biomarker for Metastasis in Uveal Melanoma. *Clin. Cancer Res.* **2016**, *22*, 1234–1242. [CrossRef]
48. Griffioen, M.; Heemskerk, M.H.M.; van Loenen, M.M.; de Boer, R.; van Kooten, C.; Lugthart, G.-J.; van Veelen, P.A.; van der Steen, D.M.; Falkenburg, J.H.F.; Amir, A.L.; et al. PRAME-Specific Allo-HLA-Restricted T Cells with Potent Antitumor Reactivity Useful for Therapeutic T-Cell Receptor Gene Transfer. *Clin. Cancer Res.* **2011**, *17*, 5615–5625. [CrossRef]
49. Gezgin, G.; Luk, S.J.; Cao, J.; Dogrusöz, M.; Van Der Steen, D.M.; Hagedoorn, R.S.; Krijgsman, D.; Van Der Velden, P.A.; Field, M.G.; Luyten, G.P.M.; et al. PRAME as a Potential Target for Immunotherapy in Metastatic Uveal Melanoma. *JAMA Ophthalmol.* **2017**, *135*, 541–549. [CrossRef]
50. van den Bosch, T.; van Beek, J.G.M.; Vaarwater, J.; Verdijk, R.M.; Naus, N.C.; Paridaens, D.; de Klein, A.; Kiliç, E. Higher Percentage of FISH-Determined Monosomy 3 and 8q Amplification in Uveal Melanoma Cells Relate to Poor Patient Prognosis. *Investig. Ophthalmol. Vis. Sci.* **2012**, *53*, 2668–2674. [CrossRef]
51. Cassoux, N.; Rodrigues, M.J.; Plancher, C.; Asselain, B.; Levy-Gabriel, C.; Lumbroso-Le Rouic, L.; Piperno-Neumann, S.; Dendale, R.; Sastre, X.; Desjardins, L.; et al. Genome-Wide Profiling Is a Clinically Relevant and Affordable Prognostic Test in Posterior Uveal Melanoma. *Br. J. Ophthalmol.* **2014**, *98*, 769–774. [CrossRef]
52. Van Raamsdonk, C.D.; Bezrookove, V.; Green, G.; Bauer, J.; Gaugler, L.; O'Brien, J.M.; Simpson, E.M.; Barsh, G.S.; Bastian, B.C. Frequent Somatic Mutations of GNAQ in Uveal Melanoma and Blue Naevi. *Nature* **2009**, *457*, 599–602. [CrossRef]
53. Johansson, P.; Aoude, L.G.; Wadt, K.; Glasson, W.J.; Warrier, S.K.; Hewitt, A.W.; Kiilgaard, J.F.; Heegaard, S.; Isaacs, T.; Franchina, M.; et al. Deep Sequencing of Uveal Melanoma Identifies a Recurrent Mutation in PLCB4. *Oncotarget* **2016**, *7*, 4624–4631. [CrossRef]
54. Moore, A.R.; Ceraudo, E.; Sher, J.J.; Guan, Y.; Chang, M.T.; Zhang, J.Q.; Walczak, E.G.; Taylor, B.S.; Huber, T.; Chi, P.; et al. Recurrent Activating Mutations of G-Protein-Coupled Receptor CYSLTR2 in Uveal Melanoma. *Nat. Genet.* **2016**, *48*, 675–680. [CrossRef]
55. Yavuzyigitoglu, S.; Koopmans, A.E.; Verdijk, R.M.; Vaarwater, J.; Eussen, B.; Van Bodegom, A.; Paridaens, D.; Kiliç, E.; De Klein, A. Uveal Melanomas with SF3B1 Mutations: A Distinct Subclass Associated with Late-Onset Metastases. *Ophthalmology* **2016**, *123*, 1118–1128. [CrossRef]
56. Gao, J.; Arman Aksoy, B.; Dogrusoz, U.; Dresdner, G.; Gross, B.; Sumer, S.O.; Sun, Y.; Jacobsen, A.; Sinha, R.; Larsson, E.; et al. Integrative Analysis of Complex Cancer Genomics and Clinical Profiles Using the CBioPortal. *Sci. Signal.* **2014**, *6*, 1–34. [CrossRef]
57. Cerami, E.; Gao, J.; Dogrusoz, U.; Gross, B.E.; Sumer, S.O.; Aksoy, B.A.; Jacobsen, A.; Byrne, C.J.; Heuer, M.L.; Larsson, E.; et al. The CBio Cancer Genomics Portal: An Open Platform for Exploring Multidimensional Cancer Genomics Data. *Cancer Discov.* **2012**, *2*, 401–404. [CrossRef]
58. Chua, V.; Lapadula, D.; Randolph, C.; Benovic, J.L.; Wedegaertner, P.B.; Aplin, A.E. Dysregulated GPCR Signaling and Therapeutic Options in Uveal Melanoma. *Mol. Cancer Res.* **2017**, *15*, 501–506. [CrossRef]
59. Koopmans, A.E.; Vaarwater, J.; Paridaens, D.; Naus, N.C.; Kilic, E.; De Klein, A. Patient Survival in Uveal Melanoma Is Not Affected by Oncogenic Mutations in GNAQ and GNA11. *Br. J. Cancer* **2013**, *109*, 493–496. [CrossRef]

60. Bakalian, S.; Marshall, J.C.; Logan, P.; Faingold, D.; Maloney, S.; Di Cesare, S.; Martins, C.; Fernandes, B.F.; Burnier, M.N. Molecular Pathways Mediating Liver Metastasis in Patients with Uveal Melanoma. *Clin. Cancer Res.* **2008**, *14*, 951–956. [CrossRef]
61. Khalili, J.S.; Yu, X.; Wang, J.; Hayes, B.C.; Davies, M.A.; Lizee, G.; Esmaeli, B.; Woodman, S.E. Combination Small Molecule MEK and PI3K Inhibition Enhances Uveal Melanoma Cell Death in a Mutant GNAQ- and GNA11-Dependent Manner. *Clin. Cancer Res.* **2012**, *18*, 4345–4355. [CrossRef]
62. Huang, J.L.; Urtatiz, O.; Van Raamsdonk, C.D. Oncogenic G Protein GNAQ Induces Uveal Melanoma and Intravasation in Mice. *Cancer Res.* **2015**, *75*, 3384–3398. [CrossRef]
63. Moore, A.R.; Ran, L.; Guan, Y.; Sher, J.J.; Hitchman, T.D.; Zhang, J.Q.; Hwang, C.; Walzak, E.G.; Shoushtari, A.N.; Monette, S.; et al. GNA11 Q209L Mouse Model Reveals RasGRP3 as an Essential Signaling Node in Uveal Melanoma. *Cell Rep.* **2018**, *22*, 2455–2468. [CrossRef]
64. Taniguchi, M.; Suzumura, K.; Nagai, K.; Kawasaki, T.; Takasaki, J.; Sekiguchi, M.; Moritani, Y.; Saito, T.; Hayashi, K.; Fujita, S.; et al. YM-254890 Analogues, Novel Cyclic Depsipeptides with Gαq/11 Inhibitory Activity from Chromobacterium Sp. QS3666. *Bioorg. Med. Chem.* **2004**, *12*, 3125–3133. [CrossRef]
65. Nishimura, A.; Kitano, K.; Takasaki, J.; Taniguchi, M.; Mizuno, N.; Tago, K.; Hakoshima, T.; Itoh, H. Structural Basis for the Specific Inhibition of Heterotrimeric Gq Protein by a Small Molecule. *Proc. Natl. Acad. Sci. USA* **2010**, *107*, 13666–13671. [CrossRef]
66. Takasaki, J.; Saito, T.; Taniguchi, M.; Kawasaki, T.; Moritani, Y.; Hayashi, K.; Kobori, M. A Novel Gαq/11-Selective Inhibitor. *J. Biol. Chem.* **2004**, *279*, 47438–47445. [CrossRef]
67. Schrage, R.; Schmitz, A.-L.; Gaffal, E.; Annala, S.; Kehraus, S.; Wenzel, D.; Büllesbach, K.M.; Bald, T.; Inoue, A.; Shinjo, Y.; et al. The Experimental Power of FR900359 to Study Gq-Regulated Biological Processes. *Nature* **2015**, *6*, 1–7. [CrossRef]
68. Lapadula, D.; Farias, E.; Randolph, C.; Purwin, T.; McGrath, D.; Charpentier, T. Effects of Oncogenic Gαq and Gα11 Inhibition by FR900359 in Uveal Melanoma. *Mol. Cancer Res.* **2018**, *17*, 963–973. [CrossRef]
69. Carvajal, R.D.; Sosman, J.A.; Quevedo, J.F.; Milhem, M.M.; Joshua, A.M.; Kudchadkar, R.R.; Linette, G.P.; Gajewski, T.F.; Lutzky, J.; Lawson, D.H.; et al. Effect of Selumetinib vs Chemotherapy on Progression-Free Survival in Uveal Melanoma: A Randomized Clinical Trial. *JAMA* **2014**, *311*, 2397–2405. [CrossRef]
70. Piperno-Neumann, S.; Kapitejin, E.; Larkin, J.M.G.; Carvajal, R.D.; Luke, J.J.; SeifertInge Roozen, H.; Zoubir, M.; Yang, L.; Choudhury, S.; Yerramilli-Rao, P.; et al. Phase I Dose-Escalation Study of the Protein Kinase C (PKC) Inhibitor AEB071 in Patients with Metastatic Uveal Melanoma. *J. Clin. Oncol.* **2014**, *32*. [CrossRef]
71. Wu, X.; Zhu, M.; Fletcher, J.A.; Giobbie-Hurder, A.; Hodi, F.S. The Protein Kinase C Inhibitor Enzastaurin Exhibits Antitumor Activity against Uveal Melanoma. *PLoS ONE* **2012**, *7*. [CrossRef]
72. Nelson, E.E.; Guyer, A.E. The Phosphoinositide 3-Kinaseα Selective Inhibitor, BYL719, Enhances the Effect of the Protein Kinase C Inhibitor, AEB071, in GNAQ/GNA11 Mutant Uveal Melanoma Cells. *Mol. Cancer Ther.* **2015**, *13*, 1044–1053. [CrossRef]
73. Amirouchene-Angelozzi, N.; Frisch-Dit-Leitz, E.; Carita, G.; Dahmani, A.; Raymondie, C.; Liot, G.; Gentien, D.; Némati, F.; Decaudin, D.; Roman-Roman, S.; et al. The MTOR Inhibitor Everolimus Synergizes with the PI3K Inhibitor GDC0941 to Enhance Anti-Tumor Efficacy in Uveal Melanoma. *Oncotarget* **2016**, *7*, 23633–23646. [CrossRef]
74. Heijkants, R.C.; Nieveen, M.; Hart, K.C.T.; Teunisse, A.F.A.S.; Jochemsen, A.G. Targeting MDMX and PKCδ to Improve Current Uveal Melanoma Therapeutic Strategies. *Oncogenesis* **2018**, *7*. [CrossRef]
75. Yoo, J.H.; Shi, D.S.; Grossmann, A.H.; Sorensen, L.K.; Tong, Z.; Mleynek, T.M.; Rogers, A.; Zhu, W.; Richards, J.R.; Winter, J.M.; et al. ARF6 Is an Actionable Node That Orchestrates Oncogenic GNAQ Signaling in Uveal Melanoma. *Cancer Cell* **2017**, *29*, 889–904. [CrossRef]
76. Otsuka, Y.; Oikawa, T.; Yoshino, H.; Hashimoto, S.; Handa, H.; Yamamoto, H.; Hashimoto, A.; Sabe, H. Frequent Overexpression of AMAP1, an Arf6 Effector in Cell Invasion, Is Characteristic of the MMTV-PyMT Rather than the MMTV-Neu Human Breast Cancer Model. *Cell Commun. Signal.* **2018**, *16*, 1–9. [CrossRef]
77. Morishige, M.; Hashimoto, S.; Ogawa, E.; Toda, Y.; Kotani, H.; Hirose, M.; Wei, S.; Hashimoto, A.; Yamada, A.; Yano, H.; et al. GEP100 Links Epidermal Growth Factor Receptor Signalling to Arf6 Activation to Induce Breast Cancer Invasion. *Nat. Cell Biol.* **2008**, *10*, 85–92. [CrossRef]
78. Zhan, T.; Rindtorff, N.; Boutros, M. Wnt Signaling in Cancer. *Oncogene* **2017**, *36*, 1461–1473. [CrossRef]

79. Zuidervaart, W.; Pavey, S.; Van Nieuwpoort, F.A.; Packer, L.; Out, C.; Maat, W.; Jager, M.J.; Gruis, N.A.; Hayward, N.K. Expression of Wnt5a and Its Downstream Effector β-Catenin in Uveal Melanoma. *Melanoma Res.* **2007**, *17*, 380–386. [CrossRef]
80. Zheng, L.; Liu, Y.; Pan, J. Inhibitory Effect of Pyrvinium Pamoate on Uveal Melanoma Cells Involves Blocking of Wnt/β-Catenin Pathway. *Acta Biochim. Biophys. Sin. (Shanghai)* **2017**, *49*, 890–898. [CrossRef]
81. Yu, F.X.; Zhao, B.; Guan, K.L. Hippo Pathway in Organ Size Control, Tissue Homeostasis, and Cancer. *Cell* **2015**, *163*, 811–828. [CrossRef]
82. Feng, X.; Degese, M.S.; Iglesias-bartolome, R.; Vaque, J.P.; Molinolo, A.; Rodrigues, M.; Zaidi, M.R.; Ksander, B.R.; Merlino, G.; Chen, Q.; et al. Hippo-Independent Activation of YAP by the GNAQ Uveal Melanoma Oncogene through a Trio-Regulated Rho GTPase Signaling Circuitry. *Cancer Cell* **2014**, *25*, 831–845. [CrossRef]
83. Feng, X.; Arang, N.; Cosimo Rigiracciolo, D.; Lee, J.S.; Yeerna, H.; Wang, Z.; Lubrano, S.; Kishore, A.; Pachter, J.A.; König, G.M.; et al. A Platform of Synthetic Lethal Gene Interaction Networks Reveals That the GNAQ Uveal Melanoma Oncogene Controls the Hippo Pathway through FAK. *Cancer Cell* **2019**, *35*, 457–472. [CrossRef]
84. Yu, F.-X.; Luo, J.; Mo, J.-S.; Liu, G.; Chul Kim, Y.; Meng, Z.; Zhao, L.; Peyman, G.; Ouyang, H.; Jiang, W.; et al. Mutant Gq/11 Promote Uveal Melanoma Tumorigenesis by Activating YAP. *Cancer Cell* **2014**, *25*, 822–830. [CrossRef]
85. Liu-chittenden, Y.; Huang, B.; Shim, J.S.; Chen, Q.; Lee, S.; Anders, R.A.; Liu, J.O.; Pan, D. Genetic and Pharmacological Disruption of the TEAD–YAP Complex Suppresses the Oncogenic Activity of YAP. *Genes Dev.* **2012**, *26*, 1300–1305. [CrossRef]
86. Faião-Flores, F.; Emmons, M.F.; Durante, M.A.; Kinose, F.; Saha, B.; Fang, B.; Koomen, J.M.; Chellappan, S.P.; Maria-Engler, S.S.; Rix, U.; et al. HDAC Inhibition Enhances the in Vivo Efficacy of MEK Inhibitor Therapy in Uveal Melanoma. *Clin. Cancer Res.* **2019**. [CrossRef]
87. Bressler, N.M.; Bressler, S.B. Photodynamic Therapy with Verteporfin (Visudyne): Impact on Ophthalmology and Visual Sciences. *IOVS* **2000**, *41*, 624–628.
88. Martin, M.; Mabhöfer, L.; Temming, P.; Rahmann, S.; Metz, C.; Bornfeld, N.; Maßhöfer, L.; Temming, P.; Rahmann, S.; Metz, C.; et al. Exome Sequencing Identifies Recurrent Somatic Mutations in EIF1AX and SF3B1 in Uveal Melanoma with Disomy 3. *Nat. Genet.* **2013**, *45*, 933–936. [CrossRef]
89. Aoude, L.G.; Wadt, K.; Bojesen, A.; Crüger, D.; Borg, A.; Trent, J.M.; Brown, K.M.; Gerdes, A.M.; Jönsson, G.; Hayward, N.K. A BAP1 Mutation in a Danish Family Predisposes to Uveal Melanoma and Other Cancers. *PLoS ONE* **2013**, *8*. [CrossRef]
90. Ismail, I.H.; Davidson, R.; Gagné, J.P.; Xu, Z.Z.; Poirier, G.G.; Hendzel, M.J. Germline Mutations in BAP1 Impair Its Function in DNA Double-Strand Break Repair. *Cancer Res.* **2014**, *74*, 4282–4294. [CrossRef]
91. Harbour, J.W.; Onken, M.D.; Roberson, E.D.O.; Duan, S.; Worley, L.A.; Council, M.L.; Matatall, K.A.; Helms, C.; Bowcock, A.M. Frequent Mutation of BAP1 in Metastasizing Uveal Melanomas. *Science* **2011**, *330*, 1410–1413. [CrossRef]
92. Van De Nes, J.A.P.; Nelles, J.; Kreis, S.; Metz, C.H.D.; Hager, T.; Lohmann, D.R.; Zeschnigk, M. Comparing the Prognostic Value of BAP1 Mutation Immunohistochemistry in Uveal Melanoma. *Am. J. Pathol.* **2016**, *40*, 796–805. [CrossRef]
93. Sahtoe, D.D.; Van Dijk, W.J.; Ekkebus, R.; Ovaa, H.; Sixma, T.K. BAP1/ASXL1 Recruitment and Activation for H2A Deubiquitination. *Nat. Commun.* **2016**, *7*, 1–13. [CrossRef]
94. Scheuerman, J.; Gaytán de Ayala Alonso, A.; Oktaba, K.; Ly-Hartig, N.; McGinty, R.K.; Fraterman, S. Histone H2A Deubiquitinase Activity of the Polycomb Repressive Complex PR-DUB. *Nature* **2010**, *465*, 243–247. [CrossRef]
95. Wang, Y.; Liu, M.; Jin, Y.; Jiang, S.; Pan, J. In Vitro and in Vivo Anti-Uveal Melanoma Activity of JSL-1, a Novel HDAC Inhibitor. *Cancer Lett.* **2017**, *400*, 47–60. [CrossRef]
96. Landreville, S.; Agapova, O.A.; Matatall, K.A.; Kneass, Z.T.; Onken, M.D.; Lee, R.S.; Bowcock, A.M.; Harbour, J.W. Histone Deacetylase Inhibitors Induce Growth Arrest and Differentiation in Uveal Melanoma. *Clin. Cancer Res.* **2012**, *18*, 408–416. [CrossRef]
97. Tan, J.; Cang, S.; Ma, Y.; Petrillo, R.L.; Liu, D. Novel Histone Deacetylase Inhibitors in Clinical Trials as Anti-Cancer Agents. *J. Hematol. Oncol.* **2010**, *3*, 1–13. [CrossRef]

98. Lafave, L.M.; Béguelin, W.; Koche, R.; Teater, M.; Spitzer, B.; Chramiec, A.; Papalexi, E.; Keller, M.D.; Hricik, T.; Micol, J.; et al. Loss of BAP1 Function Leads to EZH2-Dependent Transformation. *Nat. Med.* **2016**, *21*, 1344–1349. [CrossRef]
99. Schoumacher, M.; Le Corre, S.; Houy, A.; Mulugeta, E.; Stern, M.H.; Roman-Roman, S.; Margueron, R. Uveal Melanoma Cells Are Resistant to EZH2 Inhibition Regardless of BAP1 Status. *Nat. Med.* **2016**, *22*, 577–578. [CrossRef]
100. Yu, H.; Pak, H.; Hammond-Martel, I.; Ghram, M.; Rodrigue, A.; Daou, S.; Barbour, H.; Corbeil, L.; Hebert, J.; Drobetsky, E.; et al. Tumor Suppressor and Deubiquitinase BAP1 Promotes DNA Double-Strand Break Repair. *Proc. Natl. Acad. Sci. USA* **2014**, *111*, 285–290. [CrossRef]
101. Parrotta, R.; Okonska, A.; Ronner, M.; Weder, W.; Stahel, R.; Penengo, L.; Felley-Bosco, E. A Novel BRCA1-Associated Protein-1 Isoform Affects Response of Mesothelioma Cells to Drugs Impairing BRCA1-Mediated DNA Repair. *J. Thorac. Oncol.* **2017**, *12*, 1309–1319. [CrossRef]
102. de Koning, L.; Decaudin, D.; Botty, R.E.; Nicolas, A.; Carita, G.; Schuller, M.; Naguez, A.; Fleury, J.; Cooke, V.; Wylie, A.; et al. PARP Inhibition Increases the Response to Chemotherapy in Uveal Melanoma. *Cancers* **2019**, *11*, 751. [CrossRef]
103. Pestova, T.V.; Borukhov, S.I.; Hellen, C.U.T. Eukaryotic Ribosomes Require Initiation Factors 1 and 1A to Locate Initiation Codons. *Nature* **1998**, *394*, 854–859. [CrossRef]
104. Ali, M.U.; Ur Rahman, M.S.; Jia, Z.; Jiang, C. Eukaryotic Translation Initiation Factors and Cancer. *Tumor Biol.* **2017**, *39*. [CrossRef]
105. Yu, C.; Luo, C.; Qu, B.; Khudhair, N.; Gu, X.; Zang, Y.; Wang, C.; Zhang, N.; Li, Q.; Gao, X. Molecular Network Including EIF1AX, RPS7, and 14-3-3γ Regulates Protein Translation and Cell Proliferation in Bovine Mammary Epithelial Cells. *Arch. Biochem. Biophys.* **2014**, *564*, 142–155. [CrossRef]
106. Grawal, N.; Akbani, R.; Aksoy, B.A.; Ally, A.; Arachchi, H.; Asa, S.L.; Auman, J.T.; Balasundaram, M.; Balu, S.; Baylin, S.B.; et al. Integrated Genomic Characterization of Papillary Thyroid Carcinoma. *Cell* **2015**, *159*, 184–199. [CrossRef]
107. Etemadmoghadam, D.; Azar, W.J.; Lei, Y.; Moujaber, T.; Garsed, D.W.; Kennedy, C.J.; Fereday, S.; Mitchell, C.; Chiew, Y.E.; Hendley, J.; et al. EIF1AX and NRAS Mutations Co-Occur and Cooperate in Low-Grade Serous Ovarian Carcinomas. *Cancer Res.* **2017**, *77*, 4268–4278. [CrossRef]
108. Krishnamoorthy, G.P.; Davidson, N.R.; Leach, S.D.; Zhao, Z.; Lowe, S.W.; Lee, G.; Landa, I.; Nagarajah, J.; Saqcena, M.; Singh, K.; et al. EIF1AX and RAS Mutations Cooperate to Drive Thyroid Tumorigenesis through ATF4 and C-MYC. *Cancer Discov.* **2019**, *9*, 264–281. [CrossRef]
109. Yoshida, K.; Sanada, M.; Shiraishi, Y.; Nowak, D.; Nagata, Y.; Yamamoto, R.; Sato, Y. Frequent Pathway Mutations of Splicing Machinery in Myelodysplasia. *Nature* **2011**, *478*, 64–69. [CrossRef]
110. Wang, L.; Lawrence, M.S.; Wan, Y.; Stojanov, P.; Sougnez, C.; Stevenson, K.; Werner, L.; Sivachenko, A.; DeLuca, D.S.; Zhang, L.; et al. SF3B1 and Other Novel Cancer Genes in Chronic Lymphocytic Leukemia. *N. Engl. J. Med.* **2011**, *365*, 2497–2506. [CrossRef]
111. Graubert, T.A.; Shen, D.; Ding, L.; Okeyo-Owuor, T.; Cara, L.; Shao, J.; Krysiak, K.; Harris, C.C.; Koboldt, D.C.; David, E.; et al. Recurrent Mutations in the U2AF1 Splicing Factor in Myelodysplastic Syndromes. *Nat. Genet.* **2012**, *44*, 53–57. [CrossRef]
112. Biankin, A.V.; Waddell, N.; Kassahn, K.S.; Gingras, M.; Muthuswamy, L.B.; Johns, A.L.; Miller, D.K.; Wilson, P.J.; Wu, J.; Chang, D.K.; et al. Pancreatic Cancer Genomes Reveal Aberrations in Axon Guidance Pathway Genes. *Nature* **2012**, *491*, 399–405. [CrossRef]
113. Maguire, S.L.; Leonidou, A.; Wai, P.; Marchiò, C.; Ng, C.K.Y.; Sapino, A.; Salomon, A.V.; Reis-Filho, J.S.; Weigelt, B.; Natrajan, R.C. SF3B1 Mutations Constitute a Novel Therapeutic Target in Breast Cancer. *J. Pathol.* **2015**, *235*, 571–580. [CrossRef]
114. Stephens, P.J.; Tarpey, P.S.; Davies, H.; Loo, P.V.; Wedge, D.C.; Nik-zainal, S.; Martin, S.; Varela, I.; Bignell, G.R.; Yates, L.R.; et al. The Landscape of Cancer Genes and Mutational Processes in Breast Cancer. *Nature* **2012**, *486*, 400–404. [CrossRef]
115. Harbour, J.W.; Roberson, E.D.O.; Anbunathan, H.; Onken, M.D.; Worley, L.A.; Bowcock, A.M. Recurrent Mutations at Codon 625 of the Splicing Factor SF3B1 in Uveal Melanoma. *Nat. Genet.* **2013**, *45*, 133–135. [CrossRef]

116. Alsafadi, S.; Houy, A.; Battistella, A.; Popova, T.; Wassef, M.; Henry, E.; Tirode, F.; Constantinou, A.; Piperno-neumann, S.; Roman-Roman, S.; et al. Cancer-Associated SF3B1 Mutations Affect Alternative Splicing by Promoting Alternative Branchpoint Usage. *Nat. Commun.* **2016**, *7*, 1–12. [CrossRef]
117. Pandit, S.; Zhou, Y.; Shiue, L.; Coutinho-Mansfield, G.; Li, H.; Qiu, J.; Huang, J.; Yeo, G.W.; Ares, M., Jr.; Fu, X.-D. Genome-Wide Analysis Reveals SR Protein Cooperation and Competition in Regulated Splicing. *Mol. Cell* **2013**, *50*, 223–225. [CrossRef]
118. Meggendorfer, M.; Roller, A.; Haferlach, T.; Eder, C.; Dicker, F.; Grossman, V.; Kohlmann, A.; Alpermann, T.; Yoshida, K.; Ogawa, S.; et al. SRSF2 Mutations in 275 Cases with Chronic Myelomonocytic Leukemia (CMML). *Blood* **2012**, *120*, 3080–3088. [CrossRef]
119. Haferlach, T.; Nagata, Y.; Grossmann, V.; Okuno, Y.; Bacher, U.; Nagae, G.; Schnittger, S.; Sanada, M.; Kon, A.; Alpermann, T.; et al. Landscape of Genetic Lesions in 944 Patients with Myelodysplastic Syndromes. *Leukemia* **2014**, *28*, 241–247. [CrossRef]
120. Dvinge, H.; Kim, E.; Abdel-wahab, O.; Bradley, R.K. RNA Splicing Factors as Oncoproteins and Tumor Suppressors. *Nat. Rev. Cancer* **2016**, *16*, 413–430. [CrossRef]
121. Gentien, D.; Kosmider, O.; Nguyen-Khac, F.; Albaud, B.; Rapinat, A.; Dumont, A.G.; Damm, F.; Popova, T.; Marais, R.; Fontenay, M.; et al. A Common Alternative Splicing Signature Is Associated with SF3B1 Mutations in Malignancies from Different Cell Lineages. *Leukemia* **2014**, *28*, 1355–1357. [CrossRef]
122. Kim, E.; Ilagan, J.O.; Liang, Y.; Daubner, G.M.; Stanley, C.; Ramakrishnan, A.; Li, Y.; Chung, Y.R.; Micol, J.; Murphy, M.; et al. SRSF2 Mutations Contribute to Myelodysplasia Through Mutant-Specific Effects on Exon Recognition. *Cancer Cell* **2016**, *27*, 617–630. [CrossRef]
123. Zhang, J.; Lieu, Y.K.; Ali, A.M.; Penson, A.; Reggio, K.S.; Rabadan, R.; Raza, A.; Mukherjee, S.; Manley, J.L. Disease-Associated Mutation in *SRSF2* Misregulates Splicing by Altering RNA-Binding Affinities. *Proc. Natl. Acad. Sci. USA* **2015**, *112*, E4726–E4734. [CrossRef]
124. Muto, T.; Sashida, G.; Oshima, M.; Wendt, G.R.; Mochizuki-Kashio, M.; Nagata, Y.; Sanada, M.; Miyagi, S.; Saraya, A.; Kamio, A.; et al. Concurrent Loss of *Ezh2* and *Tet2* Cooperates in the Pathogenesis of Myelodysplastic Disorders. *J. Exp. Med.* **2013**, *210*, 2627–2639. [CrossRef]
125. Quesada, V.; Conde, L.; Villamor, N.; Ordóñez, G.R.; Jares, P.; Bassaganyas, L.; Ramsay, A.J.; Beà, S.; Pinyol, M.; Martínez-trillos, A.; et al. Exome Sequencing Identifies Recurrent Mutations of the Splicing Factor SF3B1 Gene in Chronic Lymphocytic Leukemia. *Nat. Genet.* **2011**, *44*, 47–52. [CrossRef]
126. Papaemmanuil, E.; Cazzola, M.; Boultwood, J.; Malcovati, L.; Vyas, P.; Bowen, D.; Pellagatti, A.; Wainscoat, J.S.; Hellstrom-Lindberg, E.; Gambacorti-Passerini, C.; et al. Somatic *SF3B1* Mutation in Myelodysplasia with Ring Sideroblasts. *N. Engl. J. Med.* **2011**, *365*, 1384–1395. [CrossRef]
127. DeBoever, C.; Ghia, E.M.; Shepard, P.J.; Rassenti, L.; Barrett, C.L.; Jepsen, K.; Jamieson, C.H.M.; Carson, D.; Kipps, T.J.; Frazer, K.A. Transcriptome Sequencing Reveals Potential Mechanism of Cryptic 3′ Splice Site Selection in SF3B1-Mutated Cancers. *PLoS Comput. Biol.* **2015**, *11*, 1–19. [CrossRef]
128. Moore, M.J.; Wang, Q.; Kennedy, C.J.; Silver, P.A. An Alternative Splicing Network Links Cell Cycle Control to Apoptosis. *Cell* **2010**, *142*, 625–636. [CrossRef]
129. Larrayoz, M.; Blakemore, S.J.; Dobson, R.C.; Blunt, M.D.; Rose-Zerilli, M.J.J.; Walewska, R.; Duncombe, A.; Oscier, D.; Koide, K.; Forconi, F.; et al. The SF3B1 Inhibitor Spliceostatin A (SSA) Elicits Apoptosis in Chronic Lymphocytic Leukaemia Cells through Downregulation of Mcl-1. *Leukemia* **2016**, *30*, 351–360. [CrossRef]
130. Kaida, D.; Motoyoshi, H.; Tashiro, E.; Nojima, T.; Hagiwara, M.; Ishigami, K.; Watanabe, H.; Kitahara, T.; Yoshida, T.; Nakajima, H.; et al. Spliceostatin A Targets SF3b and Inhibits Both Splicing and Nuclear Retention of Pre-MRNA. *Nat. Chem. Biol.* **2007**, *3*, 576–583. [CrossRef]
131. Gao, Y.; Koide, K. Chemical Perturbation of Mcl-1 Pre-MRNA Splicing to Induce Apoptosis in Cancer Cells. *ACS Chem. Biol.* **2014**, *8*, 895–900. [CrossRef]
132. Gao, Y.; Trivedi, S.; Ferris, R.L.; Koide, K. Regulation of HPV16 E6 and MCL1 by SF3B1 Inhibitor in Head and Neck Cancer Cells. *Sci. Rep.* **2014**, *4*, 1–10. [CrossRef]
133. Eskens, F.A.L.M.; Ramos, F.J.; Burger, H.; O'Brien, J.P.; Piera, A.; De Jonge, M.J.A.; Mizui, Y.; Wiemer, E.A.C.; Carreras, M.J.; Baselga, J.; et al. Phase I Pharmacokinetic and Pharmacodynamic Study of the First-in-Class Spliceosome Inhibitor E7107 in Patients with Advanced Solid Tumors. *Clin. Cancer Res.* **2013**, *19*, 6296–6304. [CrossRef]
134. Salton, M.; Misteli, T. Small Molecule Modulators of Pre-MRNA Splicing in Cancer Therapy. *Trends Mol. Med.* **2016**, *22*, 28–37. [CrossRef]

135. Xargay-Torrent, S.; López-Guerra, M.; Rosich, L.; Montraveta, A.; Roldán, J.; Rodríguez, V.; Villamor, N.; Aymerich, M.; Lagisetti, C.; Webb, T.R.; et al. The Splicing Modulator Sudemycin Induces a Specific Antitumor Response and Cooperates with Ibrutinib in Chronic Lymphocytic Leukemia. *Oncotarget* **2015**, *6*, 22734–22749. [CrossRef]
136. Pawellek, A.; McElroy, S.; Samatov, T.; Mitchell, L.; Woodland, A.; Ryder, U.; Gray, D.; Lührmann, R.; Lamond, A.I. Identification of Small Molecule Inhibitors of Pre-MRNA Splicing. *J. Biol. Chem.* **2014**, *289*, 34683–34698. [CrossRef]
137. Seiler, M.; Yoshimi, A.; Darman, R.; Chan, B.; Keaney, G.; Thomas, M.; Agrawal, A.A.; Caleb, B.; Csibi, A.; Sean, E.; et al. H3B-8800, an Orally Available Small-Molecule Splicing Modulator, Induces Lethality in Spliceosome-Mutant Cancers. *Nat. Med.* **2018**, *24*, 497–504. [CrossRef]
138. Kahles, A.; Lehmann, K. Van; Toussaint, N.C.; Hüser, M.; Stark, S.G.; Sachsenberg, T.; Stegle, O.; Kohlbacher, O.; Sander, C.; Caesar-Johnson, S.J.; et al. Comprehensive Analysis of Alternative Splicing Across Tumors from 8705 Patients. *Cancer Cell* **2018**, *34*, 211–224. [CrossRef]

As discussed in the review, there is still an urgent need to find an effective treatment for metastatic UM and thus improve the OS (Kujala, Mäkitie and Kivelä, 2003; Lane, Kim and Gragoudas, 2018). Many treatments aimed at targeting dysregulated signaling pathways have been evaluated in trials but the response rates were very low. Growing evidence is thus arguing for targeting several pathways simultaneously.

In line with the current trend of targeting UM dysregulated pathways simultaneously, we recently described concurrent inhibition of Bcl-2/XL/W and MDM2 as a promising therapy for UM. In this study we carried out an *in vitro* screen of 30 combinations of inhibitors targeting dysregulated pathways in 8 UM cell lines and their effect was assessed by cell viability, cell cycle, and apoptosis. Precisely, we assessed inhibitors targeting BCL2/XL, MEK, MDM2-p53 and mTOR pathways. The most synergistic combinations were selected to be then tested in patient-derived xenografts (PDX).

The top 8 synergistic combinations in UM cell lines included BCL2/XL inhibitors (ABT263 and ABT199) combined with either mTOR (AZD8055, RAD001), MEK (Trametinib), or MDM2 (RG7112, HDM201, Nutlin3, CGM097). These combinations resulted in an increase of caspase 3/7 activation corresponding with an increase of sub-G1 phase and a decrease of cells in S phase. Our *in vitro* data suggest that BCL2/XL inhibitors sensitize cells to the inhibition of mTOR, MEK and MDM2 and therefore we tested the combinations in PDXs. Precisely, the tested inhibitor combinations included BCL-2/XL/W alone or combined with MEK1/2 (ABT263 and trametinib), mTOR (ABT263 and RAD001) or MDM2 inhibitor (ABT263 and HDM201).

While trametinib and RAD001 showed a significant antitumour response when administered alone, no additive effect was seen upon combination. However, we observed a synergistic effect upon combined treatment with ABT263 and HDM201. This synergistic effect coupled with the high expression of BCL2 and MDM2 in UM (Coupland *et al.*, 1998; Brantley and Harbour, 2000; Helgadottir and Höiom, 2016) points out the interest for testing this combination in clinics. Conclusively, inhibiting Bcl-2/XL/W and MDM2 is a promising therapy for UM patients. Consistent with our findings, several inhibitor combinations are currently being tested in clinical trials for UM patients (Table 1). The corresponding manuscript is attached as an annex (Annex I).

Chapter II – Splicing as an emerging hallmark of cancer

What is splicing?

The mRNA is transcribed in the nucleus as an immature form named pre-mRNA. The pre-mRNA undergoes three maturation processes: 5' capping, splicing and addition of a 3' polyadenylation tail. The mRNA processing is tightly coupled with transcription and once the pre-mRNA is processed, the mRNA is exported to the cytoplasm to undergo translation (Wahl, Will and Lührmann, 2009).

This chapter is focused on splicing which consists of the removal of the introns (non-coding sequences) and ligation of the exons (coding sequences) of the pre-mRNA. The machinery in charge of carrying out splicing is the spliceosome and it recognizes four consensus regions of the introns: the 5' splice site (5' ss), the 3' splice site (3' ss), the branch point (BP) and the polypyrimidine tract. The 5' ss contains a GU dinucleotide and the 3' ss harbours an AG dinucleotide. The 3' ss is also characterized by the presence of a sequence rich in pyrimidines, namely the polypyrimidine tract, found upstream the 3' ss and downstream the BP. The BP contains a conserved adenosine that is essential for the first splicing reaction (Figure 2) (Yoshimi and Abdel-Wahab, 2017). Further details are provided in the following section about how the different components of the spliceosome will recognize these consensus sequences and trigger splicing reactions.

Figure 2. Schema of a pre-mRNA including two exons linked by an intron with its consensus sequences; donor 5' ss: 5' splice site, 3' ss: 3' splice site, BP: branch point, Py: polypyrimidine tract. Dinucleotide residues (GU at the 5' ss and AG at the 3' ss) and the BP sequence are also displayed.

Discovery of splicing

The discovery of splicing took place later than we may think. In 1977, two independent teams led by Phillip Sharp and Richard Roberts described this phenomenon for the first time in adenovirus. They isolated the DNA from adenovirus and formed R-loops with mRNA isolated from cells infected with the virus. They detected some RNA untailed fragments of approximately 100-200 nucleotides at the 5' and 3'end. The single-stranded

RNA fragments at the 3' end belonged to the polyA tail which is added as a post-transcriptional modification. Regarding the single-stranded 5' fragments, they concluded the RNA sequence next to the polyA is processed or spliced into a shorter RNA. Hence, these fragments corresponded to what we now call introns (Berget, Moore and Sharp, 1977; Chow *et al.*, 1977).

Discovering that genes are comprised of coding sequences (exons) which are separated by long non-coding sequences (introns) was puzzling at the time. This discovery and following advances in molecular cloning furthered our understanding of the complexity of gene expression and evolution of multicellular organisms. Splicing serves as an excellent example of efficiency as several combinations (protein isoforms) can be obtained from the same genetic sequence by combining different fragments (exons/introns).

Constitutive and alternative splicing

In mammals, approximately 95% of the genes are alternatively spliced. In fact, alternative splicing prevails in higher eukaryotes, thereby enabling the production of multiple mRNA variants from a single gene. Several splicing events can take place and lead to several mRNA products (Figure 3) (Pan *et al.*, 2008; Barash *et al.*, 2010).

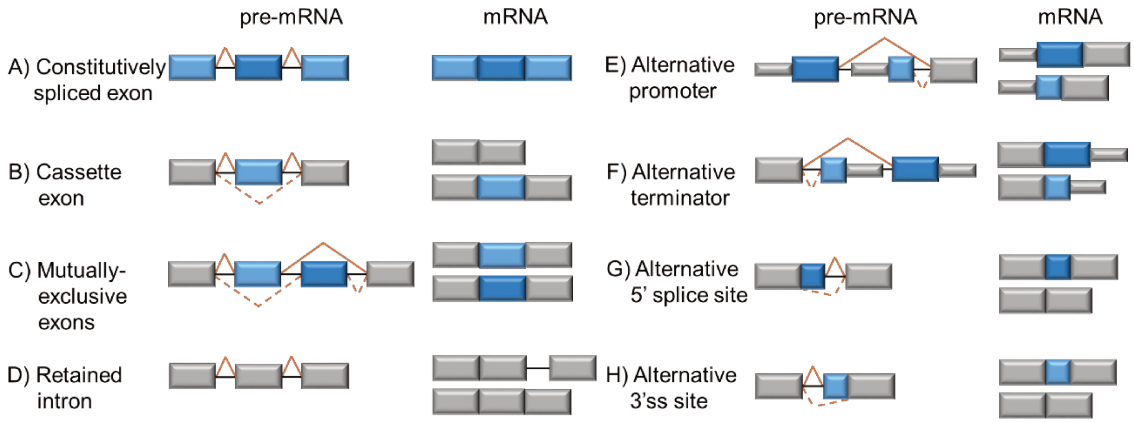

Figure 3. Schema of constitutive (A) and alternative (B-H) splicing events. The first column displays the sequence of pre-mRNA and the second column exhibits the potential mRNA products for each event. Introns are coloured in grey and exons in blue. Adapted from Dvinge et al., 2016.

Spliceosome and splicing process

Before detailing the splicing mechanisms, a description of the spliceosome components is needed. The spliceosome is a large complex of RNAs and proteins and there exist two types: the major and the minor spliceosome. The major spliceosome carries out splicing

for approximately more than 95% of all introns and is comprised of the small nuclear ribonucleoproteins or “snurps” (snRNPs) U1, U2, U4/U6 and U5 which contain a small nuclear RNA and a large number of associated proteins (Yoshimi and Abdel-Wahab, 2017). On the other hand, while the minor spliceosome shares a similar mechanism of splicing with the major spliceosome and most proteins, it recognizes different consensus sequences of a rare type of introns and consists of snRNPs U11, U12, U4atac, U6atac and U5 which is used by both spliceosomes (Hall and Padgett, 1994, 1996; Will *et al.*, 1999). Notably, the minor spliceosome is approximately 100 times less abundant than the major spliceosome (Montzka and Steitz, 1988; Tarn and Steitz, 1996).

The splicing process consists of two consecutive transesterification reactions that will allow intron removal and exons ligation to occur. First, the 2’ hydroxyl group of the conserved adenosine located at the BP (Figure 2) performs a nucleophilic attack on the phosphate at the 5’ ss (Figure 4 complex B*). This leads to the cleavage of the 3’-5’ phosphodiester bond at the 5’ ss and the formation of a 2’-5’ phosphodiester bond between the first nucleotide of the intron and the adenosine of the BP, which prompts the lariat formation (intronic loop) (Figure 4 complex C). Second, upon the new conformation, the 3’ hydroxyl at the 5’ of the free exon carries out a nucleophilic attack on the phosphate at the 3’ ss. This triggers the removal of the lariat and the ligation of the exons through a 3’-5’ phosphodiester bond (Figure 4 complex C and final product) (Wahl, Will and Lührmann, 2009; Yoshimi and Abdel-Wahab, 2017). These subsequent reactions are mediated by the spliceosome through the base-pairing of small nuclear RNAs (snRNAs) to the consensus sequences of the pre-mRNA and the binding of additional proteins. Overall, RNA-RNA, protein-RNA and protein-protein interactions are crucial to identify and remove the intronic sequences and ligate the exons (Yoshimi and Abdel-Wahab, 2017).

High-resolution structures obtained by cryo-electron microscopy have brought light to the different steps that take place during splicing and the involvement of the distinct spliceosome components at each step (Yan *et al.*, 2015; Cretu *et al.*, 2016; Nguyen *et al.*, 2016; Wan, *et al.*, 2016). The first step consists of the complex E formation by the binding of the snRNP U1 to the 5’ ss, the splicing factor to the BP and U2AF2 and U2AF1 (splicing factor U2 Small Nuclear RNA Auxiliary Factor (U2AF) heterodimer composed of 65 (U2AF2) and 35 kDa subunits (U2AF1)) to the polypyrimidine tract and 3’ ss, respectively. Once bound to the 3’ ss, U2AF1 allows the replacement of SF1 for the snRNP U2 to the BP, which results in the formation of complex A. The BP-U2 interaction requires further

stabilization by binding of additional factors including SF3A1 and SF3B1 (Splicing Factor Subunit 3a and 3b subunit 1) as well as the splicing factors SRSF2 and ZRSR2 (Serine/Arginine Rich Splicing Factor 2 and Zinc finger RNA-binding motif and serine/arginine-rich 2) (Wahl, Will and Lührmann, 2009). SF3B is a core component of U2 snRNP and is composed of several subunits, including the p14/SF3b14a which binds to the BP and SF3B1 (Zhang *et al.*, 2018). SF3B1 mediates the binding of snRNP U2 to the BP by interacting with the intronic sequencing and binding to the C-terminus of U2AF2 (Gozani, Potashkin and Reed, 1998).

Next, the pre-assembled U4/U6-U5 complex binds to constitute complex B. Complex B gets activated (Complex B*) when U1/U4 is released. As previously explained, the first transesterification reaction occurs driving conformational rearrangements that lead to complex C. Last, complex C catalyzes the second transesterification reaction that results in the formation of mature mRNA. The spliceosome components are finally detached and reused for the following reactions (Wahl, Will and Lührmann, 2009) (Figure 4).

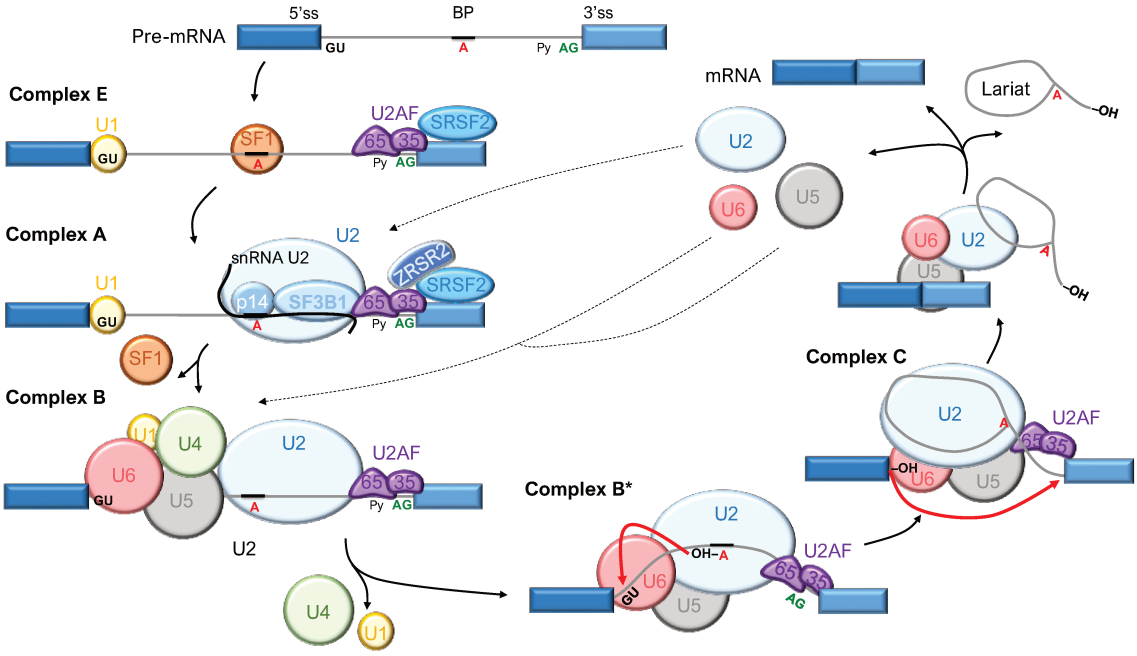

Figure 4. Splicing is a dynamic and tightly regulated process that consists of successive binding of the snRNPs U1, U2, U4/U6 and U5 to the pre-mRNA. These interactions are reinforced by additional binding of splicing factors (SF3B1, U2AF1, U2AF2, SRSF2 and ZRSR2). SF3B1 mediates the binding of U2 snRNP to the BP. U2AF2 binds to the polypyrimidine tract and U2AF1 binds to the 3' ss. SRSF2 recognizes exonic splicing enhancer (ESE) sequences. ZRSR2 interacts with U2AF2 and SRSF2. Adapted from Yoshimi and Abdel-Wahab, 2017 and Dvinge *et al.*, 2016.

Where is the spliceosome stored?

The spliceosome is stored in nuclear bodies. Precisely, snRNAs are transcribed in the nucleus, exported to the cytoplasm and assembled into complexes with the 7 conserved Sm proteins and hypermethylated at the 5' end. Once assembled, snRNPs are transported back to the nucleus where they congregate as Cajal bodies (Matera, Terns and Terns, 2007), named after Santiago Ramón y Cajal who described them in 1910 for the first time (Ramón y Cajal, 1910).

On the other hand, splicing factors including SF3B1, U2AF, SRSF2 and ZRSR2, are located in nuclear speckles (Lerner *et al.*, 1981; Cáceres, Screaton and Krainer, 1998). Nuclear speckles are found in the interchromatin of the nucleosomes where DNA is scarce. Nuclear speckles are frequently close to active transcription sites, supporting the hypothesis that nuclear speckles are involved in the regulation of suppliance of pre-mRNA processing machinery. In fact, nuclear speckles also contain transcription factors, translation initiation factors and structural proteins (Lamond and Spector, 2003) which can be explained by the fact that most splicing events take place co-transcriptionally (Girard *et al.*, 2012).

Nuclear speckles are dynamic compartments whose density is variable according to the levels of gene expression and signal response needed for each cell line. When transcription is inactive, splicing factors are assembled in bigger and round nuclear speckles. Upon active transcription levels, speckles become smaller because fewer splicing factors are present (Lamond and Spector, 2003; Spector and Lamond, 2011).

The suppliance rate of splicing factors from speckles could be regulated by kinases that colocalize in nuclear speckles. Phosphorylation of the serine/arginine-rich (SR) splicing factors is required for their recruitment and binding with the spliceosome (Cáceres, Screaton and Krainer, 1998; Spector and Lamond, 2011). For example, the phosphorylation of the SR protein SRSF1 triggers the assembly of the spliceosome while its dephosphorylation is required for the first splicing reaction to occur (Tacke, Chen and Manley, 1997). Other than SR proteins, the only phosphorylated splicing element is SF3B1. SF3B1 phosphorylation occurs at the first splicing reaction and remains phosphorylated during the two transesterification reactions (Figure 4 Complex B*) (Wang *et al.*, 1998; Bessonov *et al.*, 2010). The threonine-proline dipeptide motifs at the N-terminal of SF3B1 are phosphorylated by CDK2 (cyclin-dependent kinase 2) (Seghezzi

et al., 1998; Boudrez *et al.*, 2002), CDK1 (cyclin-dependent kinase 1) (Boudrez *et al.*, 2002) and DYRK1A (Dual Specificity Tyrosine Phosphorylation Regulated Kinase 1A) (De Graaf *et al.*, 2006). Precisely, threonine residues T211, T235, T313 and T328 as well as the serines 129 and 322 have been reported to be phosphorylated (Girard *et al.*, 2012).

All about the protein SF3B1

SF3b is a core component of the U2 snRNP together with SF3a and the 12s RNA unit (Will *et al.*, 2001). SF3b plays a key role in pre-mRNA splicing in 3' ss recognition by mediating the binding of the U2 snRNP to the BP and reinforcing this bond by interacting with U2AF2 (Gozani, Potashkin and Reed, 1998; Will *et al.*, 2001; Darman *et al.*, 2015; Alsafadi *et al.*, 2016). SF3b is a 450 kDa multiprotein complex holding seven subunits: SF3b155, SF3b130, SF3b145, SF3b49, p14/SF3b14a and SF3b10 (Will *et al.*, 2002). SF3B1/SF3b155 is the largest subunit and contains an N-terminal with the and p14 (Spadaccini *et al.*, 2006) and U2AF2 binding domains respectively (ULM; U2AF-ligand motif) (Figure 5) (Cass and Berglund, 2006; Spadaccini *et al.*, 2006; Thickman *et al.*, 2006). The C-terminus of SF3B1 (residues 1-459) displays a HEAT (Huntington, Elongation factor 3, protein phosphatase 2A, Targets of rapamycin 1) domain (Wang *et al.*, 1998; Golas *et al.*, 2003; Spadaccini *et al.*, 2006), which includes 20 tandem repeats organized as a superhelix (Figure 5) (Wang *et al.*, 1998; Cretu *et al.*, 2016).

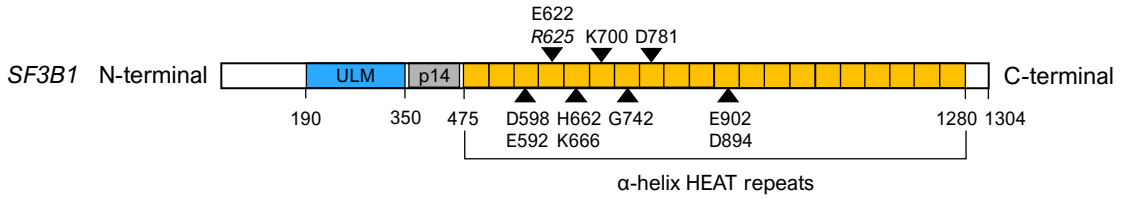

Figure 5. Structure of the human protein SF3B1. N-terminal and C-terminal are highlighted with their corresponding domains (ULM; U2AF ligand motifs and 20 HEAT repeats). Adapted from Liu *et al.*, 2020; Canbezdi *et al.*, 2021.

Mutations of the splicing factors genes *SF3B1*, *U2AF1*, *ZRSR2* and *SRSF2* in cancer

In 2011, whole-exome sequencing pinpointed for the first time the presence of *U2AF*, *ZRSR2*, *SRSF2* and *SF3B1* mutations in myelodysplastic syndromes (MDS) (Yoshida *et al.*, 2011). Contemporary studies reported *SF3B1* mutations in chronic lymphocytic leukemia (CLL) (Quesada *et al.*, 2011; Wang *et al.*, 2011), in myelodysplasia with ring sideroblasts (Papaemmanuil *et al.*, 2011) and *U2AF1* mutations in MDS (Graubert *et al.*,

2012). Later, *SF3B1* mutations were also described in breast cancer (Stephens *et al.*, 2012), pancreatic cancer (Biankin *et al.*, 2012) and uveal melanoma (UM) (Furney *et al.*, 2013; Harbour *et al.*, 2013; Martin *et al.*, 2013). Gradually, mutations in spliceosomal genes have been characterized in both hematologic malignancies and solid tumours, thereby emerging as a hallmark of cancer. Notably, the splice factor genes *U2AF1*, *ZRSR2*, *SRSF2* and *SF3B1* mutations are the most frequently mutated in cancer (Dvinge *et al.*, 2016).

Interestingly, as explained earlier in this chapter, the splicing factors U2AF1, ZRSR2, SRSF2 and SF3B1 participate at the initial step of splicing which consists of the 3' ss recognition. The fact that these mutations take place in a mutually exclusive manner suggests that either the splicing factors bear redundant functions or that loss of more than one may trigger synthetic lethality. These mutations are also heterozygous with at least one copy of the wild-type allele preserved, implying that further alterations in splicing are not tolerated for survival. Splicing factor gene mutations confer a gain or a change of function, except for *ZRSR2* mutations, which lead to a loss of function. Altogether, the high frequency of *U2AF1*, *ZRSR2*, *SRSF2* and *SF3B1* mutations in cancer suggests they could drive tumorigenesis (Dvinge *et al.*, 2016).

Despite sharing the role of 3' ss recognition as splicing factors, the splicing factors U2AF1, ZRSR2, SRSF2 and SF3B1 recognize and bind to distinct sites. Furthermore, they harbour different hotspot mutations that prevail in different cancer types. Given the emerging role of splicing factor mutations in cancer, growing efforts have been made to understand the underlying mechanism. Mutant splicing factors carry out abnormal or aberrant splicing that will lead to the formation of aberrant mRNA transcripts. Precisely, each mutant splicing factor will cause aberrant splicing of a specific set of genes, a phenomenon known as the splicing signature (Yoshida *et al.*, 2011). In this section, the role of each splicing factor will be delineated together with the functional impact upon the presence of mutations in cancer.

Splicing factor U2AF1

U2AF2 binds to the polypyrimidine tract and U2AF1 binds to the 3' ss (Zamore, Patton and Green, 1992; Wu *et al.*, 1999) and interacts with SRSF2 (Cho *et al.*, 2011). *U2AF1* mutations usually target the S34 and Q157 residues at the conserved two zinc-finger domains. S34 and Q157 hotspot mutations are both found in hematologic malignancies (5-12% of MDS, 9-16% secondary acute myeloid leukemia (AML), 8-17% CMML, 2-7%

AML, 16% RARS/RCMD-RS) (Yoshida *et al.*, 2011; Graubert *et al.*, 2012; Saez, Walter and Graubert, 2017) and S34 are also found in lung cancer (3%) (Imielinski *et al.*, 2012; Esfahani *et al.*, 2019). S34 and Q157 mutations trigger exon skipping and contribute to disease progression (Ilagan *et al.*, 2015; Okeyo-Owuor *et al.*, 2015; Shirai *et al.*, 2015; Fei *et al.*, 2018). While WT (wild-type) U2AF1 recognizes the conserved y**AG**r (y=pyrimidine, r=purine) motifs at the 3' ss of the intron, S34F mutant U2AF1 preferably recognizes C**AG**r>T**AG**r motifs and Q157 mutant U2AF1 has more affinity for y**AG**G>y**AG**A motifs (Brooks *et al.*, 2014; Dvinge *et al.*, 2016).

Mutant U2AF1 mis-splices genes involved in MDS pathogenesis through epigenetic regulation and response to DNA damage (Ilagan *et al.*, 2015; Shirai *et al.*, 2015). Precisely, mis-splicing of *BCOR* by mutant U2AF1 results in a BCOR isoform which lacks a domain that interacts with the transcription factor *MLL-AF9* (fusion target in AML), thereby repressing *AF9*-induced transcription (Shirai *et al.*, 2015). The targets *DNMT3B* (DNA Methyltransferase 3 Beta) and *FANCA* (Fanconi Anemia Complementation Group A), involved in hematologic malignancies progression, are also mis-spliced by mutant U2AF1 (Ilagan *et al.*, 2015). *CTNNB1* (Catenin Beta 1), *CHCHD7* (Coiled-Coil-Helix-Coiled-Coil-Helix Domain Containing 7) and *PTBP1* (Polypyrimidine Tract Binding Protein 1) targets, which play a role in oncogenic pathways are also mis-spliced by mutant U2AF1 (Brooks *et al.*, 2014). Another study explored the functional link of the mis-spliced targets by U2AF1^{S34F}: *H2AFY* (H2A Histone Family Member Y) and *STRAP* (Serine/Threonine Kinase Receptor Associated Protein). Interestingly, mis-splicing of these targets leads to different phenotypes of myeloid lineages in MDS (Yip *et al.*, 2017).

Overall, many studies pinpoint that mutant U2AF1 leads to mis-splicing of targets that play a role in pathogenesis, yet additional studies are needed to exploit this functional link with oncogenesis. To this end, some studies have suggested that *U2AF1*^{S34F} impairs RNA processing through defects in 3' UTRs (Park *et al.*, 2017) or the formation of R-loops (Chen *et al.*, 2018; Nguyen *et al.*, 2019). Other mis-spliced targets include genes involved in ribosome processes and translation (Shirai *et al.*, 2015). Another study further described the emerging role of U2AF1 as a translational repressor through mRNA binding. In contrast, upon the presence of S34F mutation, U2AF1 no longer binds the mRNA of its targets. For instance, mutant U2AF1 does not bind *IL8* (Interleukin 8) mRNA that results in increased secretion of IL8 which is linked with a worse prognosis (Palangat *et al.*, 2019). A study also reported that mutant U2AF1 mis-splices *IRAK4* leading to exon 4 retention, encoding a longer protein that activates MAPK *(*Mitogen-Activated Protein

Kinase) and NF-Kb pathway, a driver of MDS/AML malignant transformation (Smith *et al.*, 2019). Although the oncogenic link of mutant U2AF1 is not clearly established yet, increasing evidence is showing a direct role of mutant U2AF1 in oncogenesis through cancer-specific targets.

Splicing factor ZRSR2

ZRSR2 recognizes both U1 (spliced by the major spliceosome) and U12 introns (spliced by the minor spliceosome) but it is mainly involved in the splicing of the latter (Tronchère, Wang and Fu, 1997; Madan *et al.*, 2015). *ZRSR2* mutations are found in hematologic malignancies (1-11% of MDS, 0.8-8% of CMML, 2-8% of secondary AML, 5-6% of AML, 1.4% of RARS/RCMD-RS) (Anczukow and Krainer, 2016; Saez, Walter and Graubert, 2017) and bladder cancer. Differently from mutations of *U2AF1, SRSF2* and *SF3B1* that consist of missense mutations, *ZRSR2* mutations are found along the gene which is located on the chromosome X and trigger the appearance of stop codons. This, coupled with the higher recurrence of ZRSR2 mutations in males, confirms a loss-of-function, in contrast with *U2AF1, SRSF2* and *SF3B1* mutations that consist of either change-of-function or gain-of-function (Yoshida *et al.*, 2011; Anczukow and Krainer, 2016). *ZRSR2* mutations trigger retention of U12-type introns, affecting oncogenic targets like *PTEN* (Phosphatase And Tensin Homolog)*, MAPK1, MAPK3, BRAF* and *E2F2* (Madan *et al.*, 2015). Elucidating the mechanisms impaired upon mis-splicing of these targets remains crucial to establish a link between mutant ZRSR2 and oncogenesis.

Splicing factor SRSF2

SRSF2 recognizes exonic splicing enhancer (ESE) sequences at the exon of the 3' ss (Graveley and Maniatis, 1998; Schaal and Maniatis, 1999; Liu *et al.*, 2000). *SRSF2* is mutated in chronic myelomonocytic leukemia (CMML) (47%) (Meggendorfer *et al.*, 2012), MDS (15%), (Haferlach *et al.*, 2014) RARS/RCMD-RS (5%) (Saez, Walter and Graubert, 2017) and UM (4%) (Dvinge *et al.*, 2016; Robertson *et al.*, 2018). SRSF2 belongs to the SR family of proteins which play an essential role in splicing. Hotspot mutations target the residue P95 at the N-terminal RNA recognition motif and the C-terminal RS domain (Papaemmanuil *et al.*, 2011; Yoshida *et al.*, 2011). Although SRSF2 has an equal affinity for G/C-rich motifs, upon P95 hotspot mutations, mutant SRSF2 acquires more affinity for G-rich ESEs motifs, thereby promoting exon exclusion (Yoshida *et al.*, 2011; Gentien *et al.*, 2014; Dvinge *et al.*, 2016; Kim *et al.*, 2016).

The tumour suppressors *ARMC10* and *EZH2* have been described to be aberrantly-spliced by mutant SRSF2 (Muto *et al.*, 2013; Kim *et al.*, 2016). Mutant SRSF2 induces the formation of an aberrantly-spliced transcript of *EZH2* which is sensitive to NMD (Nonsense-Mediated mRNA Decay) degradation. The resulting decreased EZH2 levels have been previously linked with MDS progression (Muto *et al.*, 2013). Further studies are needed to fill the gap between *SRSF2* mutations and the resulting oncogenic functional impact.

Splicing factor SF3B1

The main actor of this thesis is *SF3B1*, the most frequently mutated splicing gene in cancer (Vivet-Noguer *et al.*, 2019). SF3B1 guides the binding of U2 to the BP while interacting with U2AF2 (Gozani, Potashkin and Reed, 1998). Hence, the following sections will focus on *SF3B1* models, the type of *SF3B1* hotspot mutations and the corresponding underlying mechanism, a phenomenon that has been thoroughly characterized in recent years (Darman *et al.*, 2015; DeBoever *et al.*, 2015; Alsafadi *et al.*, 2016).

SF3B1 hotspot mutations are found in hematologic malignancies (48-79% RARS/RCMD-RS, 6-26% CLL, 4-7% MDS, 4-5% CMML, 3-7% AML), (Papaemmanuil *et al.*, 2011; Wang *et al.*, 2011; Yoshida *et al.*, 2011; Quesada, Ramsay and Lopez-Otin, 2012; Anczukow and Krainer, 2016), pancreatic ductal adenocarcinomas (3%) (Biankin *et al.*, 2012), breast cancer (1.8%) (Stephens *et al.*, 2012), skin cancer (Kong, Krauthammer and Halaban, 2014), bladder cancer (Dvinge *et al.*, 2016), skin melanoma (1%) (Anczukow and Krainer, 2016) and UM (~23%) (Furney *et al.*, 2013; Harbour *et al.*, 2013; Martin *et al.*, 2013). Although *SF3B1* is mutated at a low percentage in most solid tumors (Kong, Krauthammer and Halaban, 2014), *SF3B1* is mutated in a significant number of UM (~23%) (Furney *et al.*, 2013; Harbour *et al.*, 2013; Martin *et al.*, 2013; Alsafadi *et al.*, 2016). Reported hotspot mutations commonly target the HEAT repeats in a cancer lineage-specific fashion. Precisely, R625 hotspot mutations are more common in UM (Furney *et al.*, 2013; Harbour *et al.*, 2013; Martin *et al.*, 2013), whereas K700 hotspot mutations prevail in hematologic malignancies and skin cancer (Figure 5) (Dvinge *et al.*, 2016).

SF3B1^{mut} underlying mechanism

During the last years, our group and others have contributed to the characterization of the mechanistic consequences of *SF3B1* mutations (Darman *et al.*, 2015; DeBoever *et al.*, 2015; Alsafadi *et al.*, 2016).

DeBoever and colleagues first showed that mutant SF3B1 recognizes a cryptic 3' ss located upstream of the canonical 3' ss. Mutant SF3B1 mediates this aberrant splicing of a specific set of genes with a sequence requirement comprising the dinucleotide AG located ~13-17 bp downstream the BP and >10 bp upstream the canonical 3' ss. Hence, introns, where the BP is ~24 bp far from the 3' ss, are sensitive to aberrant splicing induced by mutant SF3B1. However, not all genes meeting these requirements showed the usage of a cryptic 3' ss, suggesting that further criteria are taking place. To investigate whether the resulting aberrant transcripts are sensitive to NMD pathway degradation, they performed a gene enrichment analysis of the NMD reactome. They found that indeed, the NMD reactome was enriched in differentially expressed genes mis-spliced by *SF3B1*^{mut}. Nevertheless, in-frame and out-of-frame cryptic 3' ss transcripts were subject to NMD at similar rates, thus suggesting that aberrant 3' ss selection does not affect gene transcription. They further screened for oncogenic targets amongst the aberrantly-spliced genes by mutant SF3B1. Several genes involved in cancer were spotted (DeBoever *et al.*, 2015) but further studies are essential to bringing light to the oncogenic link.

In extension to this work, Darman and collaborators showed that *SF3B1* mutations result in a neomorphic protein. *SF3B1*^{mut} mediates the selection of a cryptic 3' ss through the usage of a cryptic BP but still requires the canonical polypyrimidine tract. They also predicted that half of the resulting aberrant transcripts were sensitive to NMD. In this study, they analyzed data sets harbouring different *SF3B1* hotspot mutations and highlighted that some aberrant transcripts are shared across cancer types while others are cancer-specific (Darman *et al.*, 2015).

Both studies characterized the splicing pattern of mutant SF3B1 by RNA-sequencing from patients' tumors harbouring different hotspot mutations (DeBoever *et al.* and Darman *et al.* covered CLL, breast cancer and a few UM samples). A third study published in our group further approached the mechanism underlying mutant SF3B1 on primary and metastatic UM samples (Alsafadi *et al.*, 2016). The previously described aberrant splicing pattern was validated; mutant SF3B1 triggers mis-splicing of a limited

set of junctions (~0.5%) (DeBoever *et al.*, 2015; Alsafadi *et al.*, 2016). Furthermore, cellular models harbouring WT/mutant *SF3B1* demonstrated that mutant SF3B1 directly causes aberrant splicing through a gain-of-function. Loss or change of function were excluded because the splicing pattern could not be recapitulated by knockdown either by overexpression of *SF3B1*^{WT}. As already introduced in the other studies, mutant SF3B1 recognizes a cryptic AG and BP located 11-14 nts upstream of the canonical ones (Darman *et al.*, 2015; DeBoever *et al.*, 2015; Alsafadi *et al.*, 2016). To note, WT SF3B1 mediates the binding of U2 snRNP to the BP and to further stabilize this binding, WT SF3B1 binds U2AF2. However, the novel binding of mutant SF3B1 at the cryptic BP is less dependent on U2AF interaction. Conclusively, the recognition and binding to a cryptic 3' ss upstream of the canonical site lead to the inclusion of an intronic fragment (Figure 6) (Alsafadi *et al.*, 2016).

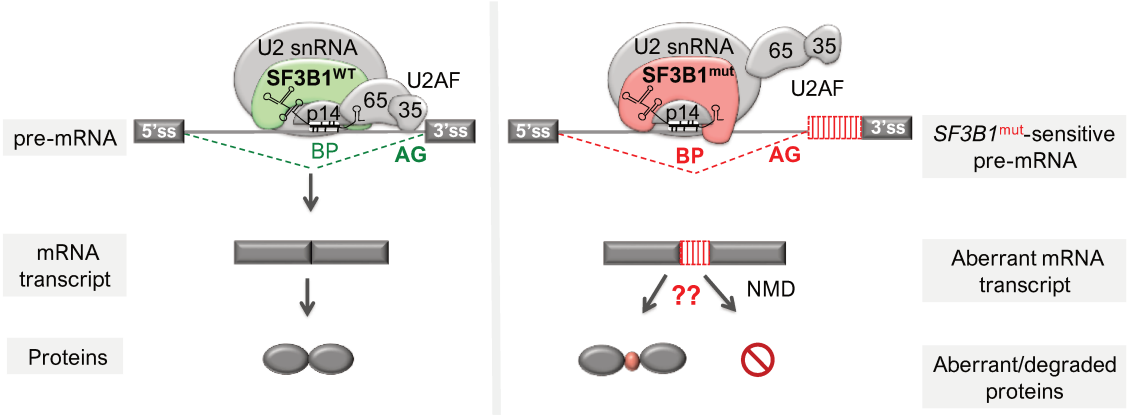

Figure 6. Schema of the mechanism of splicing for SF3B1^{WT} and SF3B1^{mut}. The consensus sequences of the intron (Figure 2) are recognized by the spliceosome. SF3B1^{WT} recognizes the canonical sites that results in the canonical mRNA transcript that will be translated into proteins (left panel). SF3B1^{mut} recognizes cryptic sites located upstream of the canonical ones which leads to the formation of an aberrant mRNA transcript with an additional intronic fragment (red) whose fate remains unknown (right panel). Adapted from Alsafadi et al., 2016.

Two questions arise from these studies: **1)** How do *SF3B1* mutations alter the base-pairing of U2 snRNA? **2)** What is the fate of the resulting aberrant transcripts?

How do *SF3B1* mutations alter the base-pairing of U2 snRNA?

A recent study showed that SF3B1 interacts with another splicing factor named SUGP1 (SURP and G-patch domain containing 1). Upon *SF3B1* mutations, interaction with the splicing factor SUGP1 (SURP and G-patch domain containing 1) is weakened during BP recognition. This loss can be partially rescued by *SUGP1* overexpression. Furthermore,

the knockdown of *SUGP1* recapitulates the aberrant splicing pattern induced by mutant SF3B1. This suggests that the lost interaction of mutant SF3B1 with SUGP1 contributes to aberrant splicing (Zhang *et al.*, 2019). In addition to these findings, Liu *et al*. and our group demonstrated that *SUGP1* mutations coupled with loss-of-heterozygosity trigger the *SF3B1*^{mut} splicing pattern in cell lines and tumours (Z Liu *et al.*, 2020; Alsafadi *et al.*, 2021).

Another explanation may be that mutations at the HEAT repeats of *SF3B1* change the conformational disposition of SF3B1. During 3' ss recognition, the conformation of the HEAT repeats of SF3B1 is supported by interactions with SF3b130, SF3b10 and SF3b14b which form a superhelix. The superhelix and SF3b14b form an RNA-binding pocket (Cretu *et al.*, 2016). The distance between the cryptic and the canonical 3' ss changes for each hotspot mutation (Zhaoqi Liu *et al.*, 2020). The differences between the splicing signatures induced by each hotspot mutation have been poorly studied. Our group recently developed cell models harbouring different *SF3B1* hotspot mutations to compare the functional outcome and predict the tertiary structure *in silico*. The analysis revealed that hotspot mutations may trigger a conformational change at the N-terminal of SF3B1, thereby affecting the binding with other splicing factors. At the same time, hotspot mutations trigger different rates of aberrant splicing. The extent of the conformational change directly correlates with the rate of aberrant splicing that could explain different functional impacts (Canbezdi *et al.*, 2021). Additional studies should explore additional conformational changes at the HEAT repeats that could be further exploited in the clinics in a hotspot-specific trend.

What is the fate of the resulting aberrant transcripts?

These studies have brought light to the mechanism underlying *SF3B1* mutations. However, we still ignore the fate of the resulting aberrant transcripts. Whether these aberrant transcripts will be degraded by NMD or translated into truncated or untruncated proteins remains uncertain. To this end, several studies have disclosed the fate of some of the resulting aberrant transcripts. This section will briefly outline those studies that provide an insight into the oncogenic involvement of the aberrant transcripts.

For example, *SF3B1* mutations lead to the formation of a *MAP3K7* aberrant transcript that contains a premature codon and is thus degraded by NMD. The decrease in MAP3K7 protein levels triggers a hyperactivation of the NF-κB pathway, an MDS driver (Lee *et al.*,

2018; Li *et al.*, 2021). Likewise, *SF3B1*^{K700E} induces aberrant splicing of *PPP2R5A*. This results in downregulation of *PPP2R4A* and an increased MYC stability thus impacting apoptosis (Zhaoqi Liu *et al.*, 2020). *SF3B1* mutations also cause mis-splicing of *DVL2*, which codes for a negative regulator of the Notch pathway (Pozzo *et al.*, 2020; Zhao *et al.*, 2021).

Another study demonstrated that *SF3B1* mutations give rise to the inclusion of a poison exon in the *BRD9* transcript, ultimately repressing *BRD9* (Inoue *et al.*, 2019). BRD9 recruits the non-canonical chromatin remodeling complex (ncBAF) to the gene to regulate transcription. BRD9 contributes to oncogenesis in several types of cancer and targeting BRD9 is being extensively explored (Zhu, Liao and Tang, 2020). An interesting approach was in fact proposed in this study to correct *BRD9* aberrant splicing. Strikingly, tumor growth was repressed by the usage of antisense oligonucleotides or mutagenesis (Inoue *et al.*, 2019).

Overall, growing evidence shows that *SF3B1*^{mut}-induced mis-splicing can play a role in oncogenesis. However, it remains to be determined whether the impact of *SF3B1* mutations is broader.

SF3B1 models

Depletion of *SF3B1* by knockout is lethal in mouse embryos. *SF3B1* haploinsufficiency impairs SF3B1 interaction with proteins of the polycomb group which is involved in gene transcription. This results in dysregulation of the Hox genes which play a key role in embryonic development. Accordingly, *SF3B1* heterozygous mice have defects in the skeleton (Isono *et al.*, 2005).

The development of knockin mice models with *SF3B1* mutations has also been assessed. The fact that hematopoiesis is highly conserved between mice and humans coupled with the high recurrence of *SF3B1* mutations in hematologic malignancies has driven the development of this type of model. Obeng *et al*. generated a conditional knockin mouse model to assess the effects of K700E hotspot mutation, commonly found in MDS. Although the mice developed macrocytic anemia and progressive myelodysplasia, there was no presence of ring sideroblasts. While increased usage of aberrant 3' ss was confirmed, *ABCB7* (a target mis-spliced by mutant SF3B1 and consequently downregulated), was not mis-spliced in the mouse model. This can be explained by the lack of intronic conservation between mice and humans and the fact that *ABCB7* is not mis-spliced across all hematologic malignancies (Obeng *et al.*, 2016). The same findings

were described by a second study (Mupo *et al.*, 2017). A third study established a mouse model with conditional expression of heterozygous *SF3B1*^{K700E} mutation in B cells but CLL was only recapitulated partially (Yin *et al.*, 2019).

On the other hand, the *SF3B1* ortholog is also essential for development in zebrafish (An and Henion, 2013) and *C. elegans* (Serrat *et al.*, 2019). In contrast to cancer cells that harbour *SF3B1* mutations in heterozygosis and require the *SF3B1* WT allele for viability, homozygous *sftb-1* (*SF3B1* ortholog in *C. elegans*) mutations have been observed in *C. elegans* (Serrat *et al.*, 2019). This *sftb-1[K718E] C. elegans* model does not display an aberrant 3' ss usage as the main splicing defect (Serrat *et al.*, 2019), as previously described (Darman *et al.*, 2015; DeBoever *et al.*, 2015; Alsafadi *et al.*, 2016). In contrast, exon skipping was the most frequent event of aberrant splicing (Serrat *et al.*, 2019).

Several reasons may explain the differences observed in the splicing outcome. First, the shorter length of introns, the absence of a BP and the presence of a consensus UUUUCAG/R sequence instead of a polypyrimidine tract in *C. elegans* (Morton and Blumenthal, 2011). Second, the fact that only about 35% of genes are alternatively spliced in *C. elegans* (Tourasse, Millet and Dupuy, 2017), while 95% of genes are alternatively spliced in humans (Pan *et al.*, 2008). Third, it is known that aberrant transcripts are often the under-representated form and thus harder to detect. Last, some transcripts displaying alternative 3' ss usage may be degraded by NMD (Darman *et al.*, 2015).

Overall, these models recapitulate the disease partially and exhibit splicing aberrations that differ from those found in human tumours, which may be explained by the low conservation of intronic sequences across species.

Role of splicing factors in metabolism

Given the shared role in 3' ss recognition of the most frequently mutated splicing genes in cancer (SF3B1, SRSF2, U2AF1 and ZRSR2) and the mutually exclusive fashion of their mutations, perhaps there exists a shared induced perturbation and/or neo-epitopes generation.

An interesting insight is the link of splicing defects with metabolic impairment. Loss of *SRSF3* expression induces aberrant splicing of targets involved in glucose and lipid metabolism, which in turn impairs the maturation of hepatocytes (Sen, Jumaa and Webster, 2013). Similarly, knockdown of *ESRP1* in breast cancer cells impairs

oxidoreductase reactions and lipid metabolism by decreasing the mRNA and protein levels of FASN (fatty acid synthase), SCD1 (stearoyl-CoA desaturase 1) and PHGDH (phosphoglycerate dehydrogenase). Depletion of *ESPR1* increased basal and spare respiration capacity while the extracellular acidification rate (ECAR) remained unchanged (Gökmen-Polar *et al.*, 2019).

Differently from the aforementioned studies showing metabolic defects upon loss of splicing factors, a recent study reported metabolic impairment upon *SF3B1* mutations. Precisely, in breast cancer cells, mutant SF3B1 triggers the aberrant splicing of *UQCC1* (ubiquinol-cytochrome C reductase complex assembly factor 1), a core assembly factor of the mitochondrial electron transport chain. *UQCC1* aberrant transcript is less abundant and results in decreased protein levels as well. In fact, gene ontology analysis showed an enrichment of metabolic pathways amongst the underexpressed proteins by mutant SF3B1. This was linked with a reduced mitochondrial respiration capacity in *SF3B1*^{K700E} cells, although the ECAR was unchanged. A second major metabolic target mis-spliced by mutant SF3B1 is *PHGDH*, which codes for the enzyme catalyzing the first step of the synthesis of serine *de novo*. In consequence, *SF3B1*^{K700E} cells are more sensitive to serine and glycine starvation than *SF3B1*^{WT} cells. Serine and glycine starvation also showed tumor regression in mice injected with *SF3B1*^{K700E} and *SF3B1*^{K666N} cells as compared to *SF3B1*^{WT} cells (Dalton *et al.*, 2019). This is the first study showing that splicing defects induced by mutant SF3B1 impair metabolism thereby triggering oncogenesis.

To further exploit the role of splicing defects in reshaping the metabolic profile of cancer cells and see if this could be the link through which splicing factor gene mutations induce oncogenesis, the next chapter of the introduction will address the metabolic defects in cancer.

Chapter III – Metabolism as a hallmark of cancer: fuel for thought

In aerobic conditions, differentiated cells degrade glucose via glycolysis to obtain pyruvate which is completely oxidized into CO_2 by oxidative phosphorylation (OXPHOS) in the mitochondria. This process generates up to 36 ATP molecules per molecule of glucose, resulting in an efficient energy obtention. OXPHOS requires oxygen as the final electron acceptor to oxidize glucose. However, when oxygen is limiting, differentiated cells transform pyruvate into lactate. This process is called anaerobic glycolysis and provides 2 ATP molecules per molecule of glucose. ATP production is considerably reduced but glycolysis continues to occur by cycling NADH to NAD^+ (Figure 7). Otto Warburg was the first to report metabolic alterations in cancer in 1925. Warburg's pioneering work described that, as opposed to normal differentiated cells which rely on mitochondrial OXPHOS to meet the energetic demands, some cancer cells rely on aerobic glycolysis. Hence, cancer cells degrade glucose into lactate regardless of the presence of oxygen, following "the Warburg effect" (Warburg, 1925) (Figure 7).

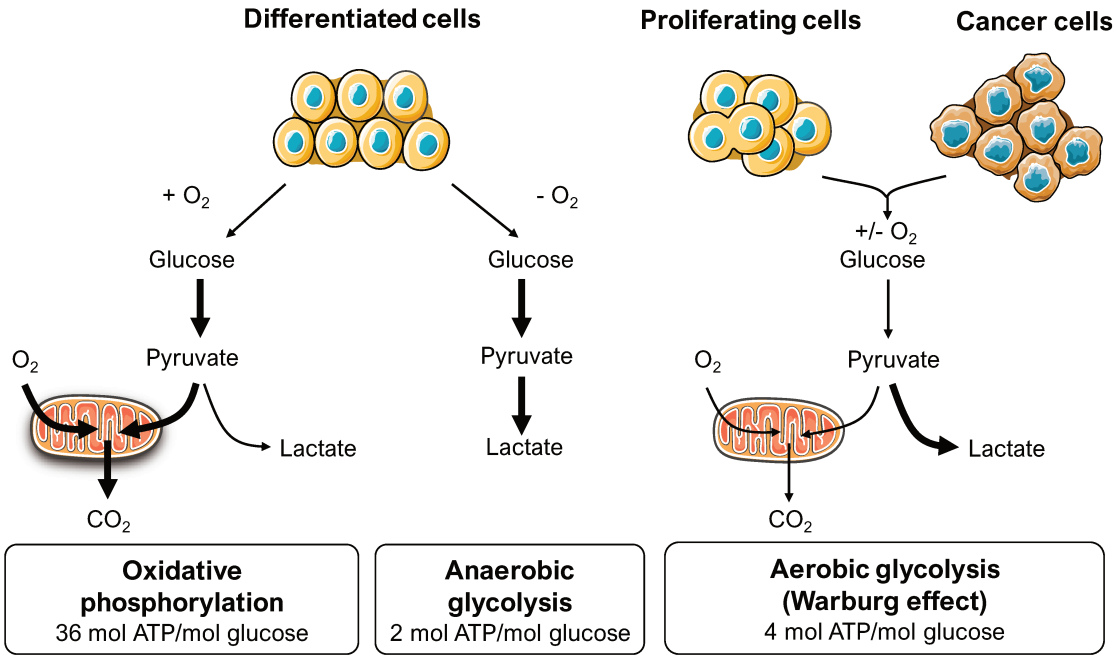

Figure 7. Schema of the glucose metabolism in differentiated, proliferating and cancer cells. In aerobic conditions, differentiated cells degrade glucose via oxidative phosphorylation (36 molecules of ATP per mole of glucose). In anaerobic conditions, differentiated cells ferment glucose to lactate (2 molecules of ATP per molecule of glucose). Regardless of the oxygen levels, proliferating and cancer cells favour lactate obtention (Warburg effect) (4 molecules of ATP per molecule of glucose). Adapted from Vander Heiden, Cantley and Thompson, 2009.

This metabolic switch found in cancer cells towards aerobic glycolysis results in approximately 18-fold lower efficiency of ATP obtention, as compared to mitochondrial OXPHOS. Hence, claiming that cancer cells prefer a less efficient process to generate energy was counter-intuitive at first. Since then, extensive research has been conducted comparing metabolic profiles across tumours, rather than comparing tumours with their normal counterparts. Little by little, evidence has proved that Warburg's effect does not apply to all sorts of cancer cells. In 2011, Hanahan and Weinberg defined "deregulation of cellular bioenergetics" as a hallmark of cancer, which explains that actually, cancer cells can rewire their metabolism in additional ways or directions than the one suggested by Warburg (Hanahan and Weinberg, 2011). Therefore, cancer cells are capable of reprogramming energy metabolism.

This chapter will scope some of the metabolic pathways that are altered in various cancer types. It is relevant to note that not all metabolic switches found in cancer derive towards the same direction in all cancer types; some tumours may promote the usage of certain pathways while other tumours may favour other pathways. Of note, provided that a vast range of metabolic dysregulations have been described in cancer, this chapter will focus exclusively on metabolic defects that were revealed in UM during this thesis (Article attached in chapter IV). Although no major metabolic dysregulations have been described in UM to date, this chapter will encompass studies exploring the metabolic profile of UM tumors.

Glucose metabolism

Strictly speaking, glycolysis consists of the transformation of glucose into pyruvate in the cytoplasm and it renders 2 molecules of ATP per molecule of glucose. Pyruvate will then undergo different biochemical reactions according to the oxygen levels and energetic requirements for ATP generation and the needs of anabolic processes for cell growth (Pfeiffer, Schuster and Bonhoeffer, 2001; De Berardinis and Chandel, 2016). Briefly, in aerobic conditions, pyruvate will be transformed into acetyl-CoA which will go through the tricarboxylic acid (TCA) or Krebs cycle and OXPHOS in the mitochondria. In anaerobic conditions, pyruvate is transformed into lactate which is excreted (De Berardinis and Chandel, 2016) (Figure 8). The next sections describe the different fates of pyruvate and describe assays to measure mitochondrial and glycolytic functions in cells.

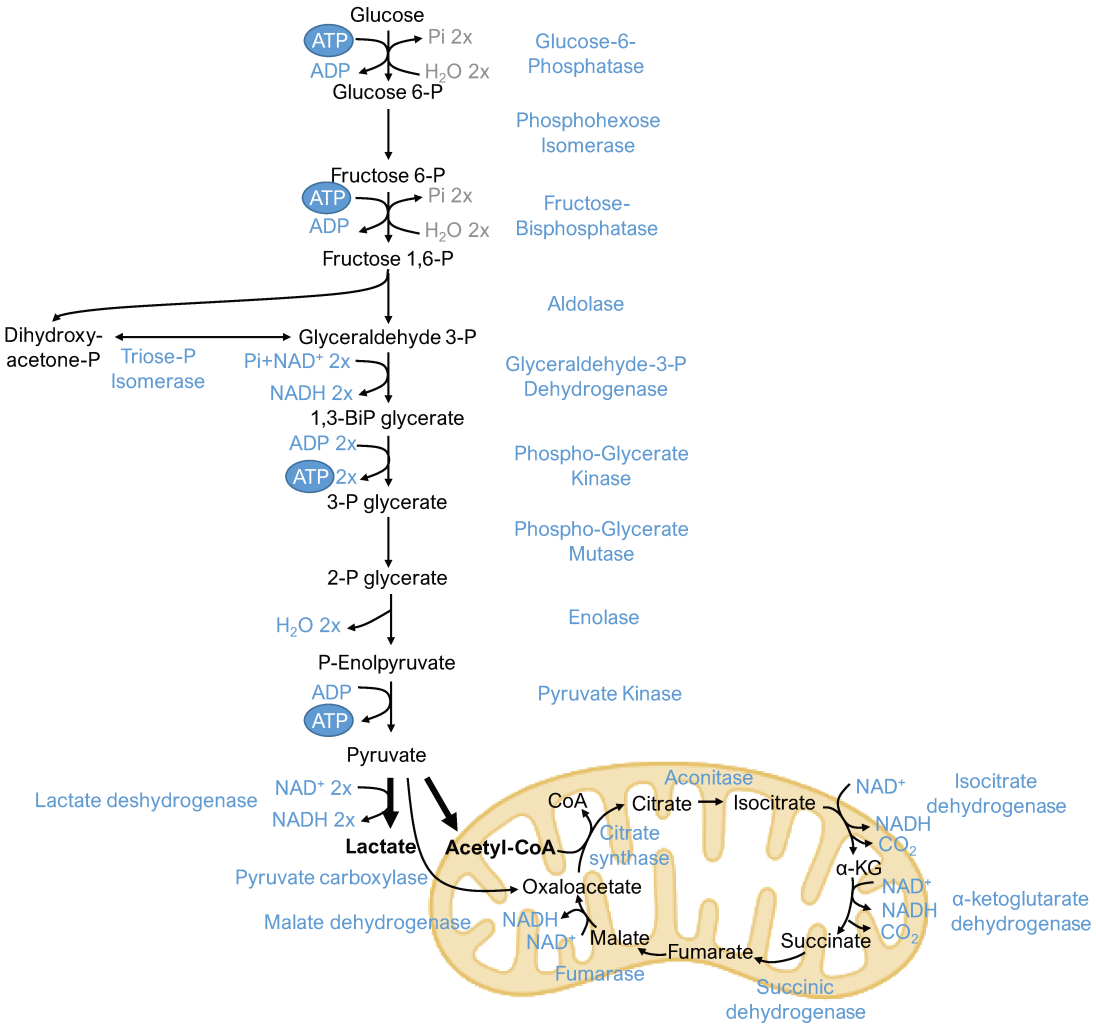

Figure 8. Schema of glycolysis. In the first stage, glucose is degraded to pyruvate. In the second stage, pyruvate can have different fates according to the current conditions; it can be converted to lactate which is then secreted out of the cell or further oxidized via the oxidative phosphorylation in the mitochondria. Adapted from Levine and Puzio-Kuter, 2010.

Oxidative phosphorylation

In the presence of oxygen, pyruvate enters the mitochondria where it is first oxidized into acetyl-CoA by the pyruvate dehydrogenase. Acetyl-CoA undergoes the TCA or Krebs cycle in the matrix of the mitochondria. The TCA is a closed loop that consists of eight steps that produce 4 CO_2, 6 H^+, 2 ATP, 6 NADH and 2 $FADH_2$ molecules (Figure 8). The electrons from the coenzymes NADH and $FADH_2$ are then transferred to the electron transport chain (ETC), where OXPHOS takes place (Figure 9). Glycolysis and OXPHOS are tightly coupled as one of the major products of glycolysis is pyruvate, which is a substrate for OXPHOS (De Berardinis and Chandel, 2016) (Figure 8).

The ETC is the last component of aerobic glycolysis and is formed of 5 transmembrane protein complexes (complexes I-V) which are anchored at the inner membrane of the mitochondria. NADH, $FADH_2$ and succinate provide the electrons which are transferred through the ETC complexes I-IV in a series of redox reactions. During the transfer of electrons, the energy obtained is used to pump hydrogen ions through the membrane into the intermembrane space, resulting in an uneven accumulation of hydrogen ions in one side of the membrane, thus establishing an electrochemical gradient. The resulting proton gradient drives the generation of ATP from ADP by the ATP synthase through diffusion of the hydrogen ions back to the mitochondrial matrix. Oxygen acts as the last electron acceptor and water is generated (Figure 9). OXPHOS renders a total of 34 molecules of ATP per molecule of glucose (De Berardinis and Chandel, 2016). Conclusively, in aerobic conditions, glycolysis followed by OXPHOS produces a total of 38 molecules of ATP per molecule of glucose (2 ATP from glycolysis and 2 ATP from TCA plus 34 ATP from OXPHOS) (De Berardinis and Chandel, 2016). Notably, the ETC leads to reactive oxygen species (ROS) production (Zhao *et al.*, 2019).

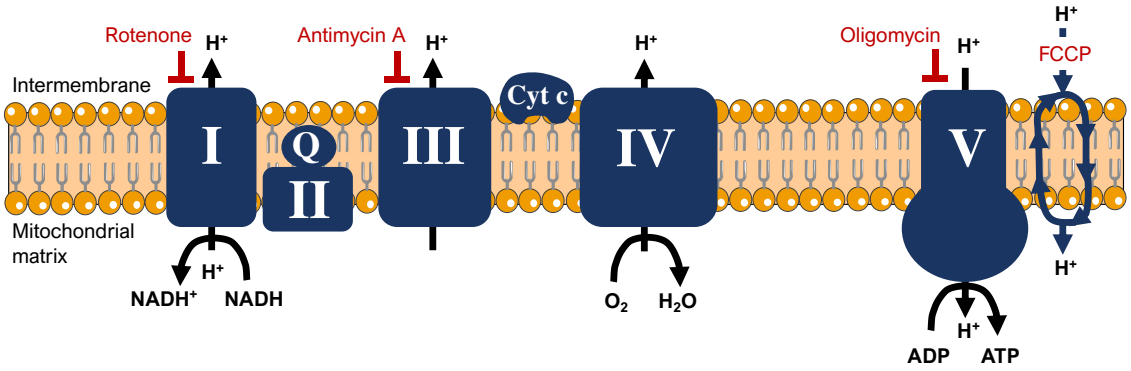

Figure 9. Electron transport chain of the mitochondria. Complex I: NADH-ubiquinone oxidoreductase transfers electrons from matrix NADH to ubiquinone (Q), complex II: succinate dehydrogenase catalyzes the oxidation of succinate to fumarate, complex III: CoQ-cytochrome c reductase transfers the electrons carried by QH_2 (reduced ubiquinone (Q)), complex IV: cytochrome c oxidase transfer electrons from cytochrome c to the final acceptor O_2 to obtain H_2O, complex V: ATP synthase synthesizes ATP from ADP and inorganic phosphate with the energy derived from the proton gradient which moves from the inner membrane of the mitochondria to the intermembrane space. Complex inhibitors used to assess mitochondrial function by measuring the OCR (Oxygen Consumption Rate) are shown in red. Oligomycin inhibits complex V, FCCP (carbonyl cyanide-4 trifluoromethoxy phenylhydrazone) collapses the proton gradient, rotenone inhibits complex I and antimycin inhibits complex III. Adapted from Zhao *et al.*, 2019.

Oxidative phosphorylation in cancer

As previously mentioned, OXPHOS can be either upregulated or downregulated in cancer. While there is a significant branch of research focusing on the development and treatment with OXPHOS inhibitors for cancer types with upregulated OXPHOS, this chapter will only cover those cases displaying downregulated OXPHOS. The main reason is that our findings reveal an underexpression of OXPHOS upon *SF3B1* mutations in UM (Article in chapter IV), susceptible to constitute a therapeutic opportunity.

Downregulation of OXPHOS is linked with worse clinical progression and is usually found in invasive tumours (Gaude and Frezza, 2016). This downregulation may be due to decreased mitochondrial DNA content, as reported in breast cancer, gastric cancer, hepatocellular carcinoma and non-small cell lung cancer (Cavalli, Varella-Garcia and Liang, 1997; Viale, Corti and Draetta, 2015). Precisely, analysis of the mitochondrial genome across cancer types from The Cancer Genome Atlas (TCGA) dataset showed that deleterious mitochondrial DNA mutations were present in rectal adenocarcinomas, colon adenocarcinomas, ovarian serous cyst adenocarcinomas and acute myeloid leukemias (Larman *et al.*, 2012). Interestingly, a study tested metformin, an inhibitor of complex I used to treat diabetes, in cancer cells with mitochondrial DNA mutations in complex I. These cells had an increased sensitivity in comparison with cells lacking complex I mutations (Birsoy *et al.*, 2014). Similar effects were observed upon treatment with another complex I inhibitor, phenformin, in xenografts derived from cells with complex I mutations (Wallace, 2012). These studies reflect the relevance of therapeutic approaches aiming to correct mitochondrial defects.

Assessing mitochondrial function

Dysregulated OXPHOS found in cancer can be due to defective mitochondrial metabolism. Mitochondrial defects can consist of decreased respiration, increased ROS production, impaired citrate synthase activity or a reduced mitochondrial content (Weinhouse, 1976; Fantin, St-Pierre and Leder, 2006; Weinberg *et al.*, 2010; De Berardinis and Chandel, 2016). This section summarizes some approaches used to assess mitochondrial content and function.

A common approach consists of isolating the mitochondria by centrifugation. However, organelles of similar density may precipitate together with mitochondria, thereby yielding

low purification rates (Glancy and Balaban, 2011; Kappler *et al.*, 2016; van der Walt and Louw, 2020). To this end, several approaches have been developed in recent years.

Citrate synthase is the enzyme that catalyzes the entry of metabolites into the TCA cycle. Previous studies reported a correlation between citrate synthase activity and mitochondrial content in different types of cells (Larsen *et al.*, 2012; McLaughlin *et al.*, 2020). However, citrate synthase can be found in other organelles like the peroxisome so prior high quality purification steps are required (McLaughlin *et al.*, 2020).

Another approach consists of labelling mitochondria with fluorescent probes in live cells to either assess mitochondrial potential or content under the microscope. These probes are cationic fluorophores (rhodamine 123 and tetramethylrodamine methylester) that acummulate in the mitochondria by attraction to the negative mitochondrial membrane potential and dettach when mitochondria undergo a loss in membrane potential. MitoTracker dyes are a type of cationic fluorophers that contain a chloromethyl group that binds covalently with thiols on proteins and peptides so that the dye is retained in the mitochondria (Kholmukhamedov, Schwartz and Lemasters, 2013).

Mitochondrial respiration can be directly studied by measuring the oxygen consumption rate in cells. Oxygen electrode chambers were first used to measure oxygen in cells, isolated mitochondria or tissue in suspension. These can be replaced by respirometes which allow the perfusion of buffers (Brand and Nicholls, 2011).

A broadly used device is a cell multi-well plate reader that measures the oxygen consumption rate (OCR) (Seahorse XF Flux Analyser). The Seahorse device contains sensor cartridges that allow the injection of respiration modulators to the live cells. These respiration modulators inhibit different complexes of the ETC so that respiration can be modulated and analyzed. A first OCR measurement is done to obtain the basal respiration which corresponds to the oxygen consumption to meet the ATP demand in order to compensate for the proton leak in the ETC. In other words, the energetic demand of the cell under baseline conditions is obtained. Second, oligomycin is injected to inhibit complex V or ATP synthase. ATP synthase inhibition results in a decreased electron flow through the ETC which reduces the OCR. The decrease observed compared to the levels of basal respiration reflects how much OCR is linked to ATP production. Third, FCCP (carbonyl cyanide-4 trifluoromethoxy phenylhydrazone) is injected. FCCP is an uncoupling agent that collapses the proton gradient and disrupts the mitochondrial membrane potential. As a consequence of the collapsed proton gradient, electrons flow

uninhibitedly. The OCR readings after FCCP injection correspond to the maximal respiration capacity of the cells. Spare respiration capacity can be obtained by subtracting the basal respiration to the maximal respiration. This feature tells us about the response of cells under stressful or highly demanding conditions. Fourth, rotenone and antimycin A are injected to inhibit complex I and complex III, respectively. These inhibitions result in the ETC shut down, thus the OCR levels obtained reflect oxygen consumption via non-mitochondrial processes (Figures 9 and 10) (Divakaruni *et al.*, 2014).

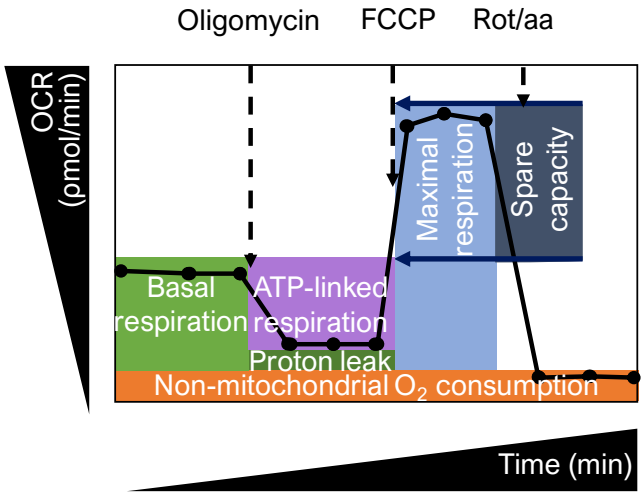

Figure 10. Schematic example of the assessment of oxygen consumption rate (OCR) in cells with respiration modulators. The oxygen consumption values (ρmol) are obtained over time (min), resulting in OCR (ρmol/min). Basal respiration, proton leak, ATP-linked respiration, maximal respiration and spare respiration capacity are highlighted, as well as OCR corresponding to non-mitochondrial oxygen consumption. These values are obtained by modulating the ETC with injections of oligomycin (inhibitor of complex V or ATP synthase), FCCP (carbonyl cyanide-4 trifluoromethoxy phenylhydrazone uncoupling agent) and a mix of rotenone and antimycin A (Rot/aa inhibitors of complexes I and III, respectively) over time. The assay is simulated on a Seahorse XF Flux Analyzer. Adapted from Divakaruni *et al.*, 2014.

Aerobic glycolysis

In the absence of oxygen, pyruvate is degraded into lactate. Lactate is then secreted to the extracellular membrane. The obtention process of lactate under low concentrations of oxygen is known as fermentation or anaerobic glycolysis (Pasteur, 1857). In another scenario, cancer cells have the capacity to promote lactate production despite the presence of oxygen, by aerobic glycolysis or the Warburg effect (Warburg, 1925). Although aerobic glycolysis is less efficient in terms of energy obtention (4 ATP molecules per molecule of glucose versus 36 in OXPHOS), the rate of energy obtention is faster. In line with this, when aerobic glycolysis is favoured in cells, OXPHOS is less

promoted thereby increasing the rate of glycolysis which additionally enhances the increase of glucose uptake (Yang *et al.*, 2016). In addition, ROS, which can be harmful for cells, are generated. Altogether, these modulated features help cancer cells sustain tumoral growth (Pfeiffer, Schuster and Bonhoeffer, 2001; De Berardinis and Chandel, 2016). The Warburg effect assumed that cancer cells rewired metabolism to compensate for metabolic defects or decreased OXPHOS (Warburg, 1925), which had previously been described in cancer (Seyfried, 2015). Nowadays we know that while some cancer types display an impaired mitochondrial metabolism, other cancer types do not have defective mitochondria (leukemias, lymphomas, pancreatic cancer, a subtype of melanoma and endometrial carcinoma) (Weinberg and Chandel, 2015). Therefore, aerobic glycolysis can be promoted despite the absence of metabolic defects (Weinhouse, 1976; Fantin, St-Pierre and Leder, 2006; Weinberg *et al.*, 2010; De Berardinis and Chandel, 2016).

Assessing the rate of glycolysis

Assessing the rate of glycolysis can be informative about the metabolic profile of cancer cells. Glycolytic flux can be measured by quantifying glucose uptake. A labeled isoform of glucose can be introduced into the cell media and traced in cells for a certain period of time. The glucose analogs can be labeled to become radioactive (^{18}FDG) or fluorescent (2-NBDG) or carried out with bioluminescent substrates to ease tracing. Another option is to measure the activity of rate-limiting glycolytic enzymes (hexokinase, phosphofructokinase or pyruvate kinase). Metabolic profiling can be used to detect and quantify metabolites. Unlabeled or 13C-labeled metabolites can be quantified by mass spectrometry or nuclear magnetic resonance spectrometry.

Given the broad number of available approaches, this section focuses on measuring the glycolytic flux by quantifying lactate excretion. The main reason is that we conducted this approach and can ease comprehension and interpretation of the results displayed in the following chapter (Article in chapter IV). The transformation of glucose to pyruvate and eventually lactate implies an extrusion of protons to the extracellular medium which in turn acidifies the media. This extracellular acidification rate (ECAR) can be thus quantified in multi-well plates of cells (Seahorse XF Flux Analyzer). Cells are first incubated in a media deprived of glucose and pyruvate, followed by ECAR readings which correspond to the basal acidification levels. Second, glucose is injected at saturation levels so that cells undergo glycolysis and ECAR is read, obtaining the rate of glycolysis under basal

conditions. Third, oligomycin is injected to inhibit complex V ATP synthase from the ETC which stops the mitochondrial ATP production. Hence, obtained ECAR levels inform us about the maximum capacity of glycolysis performance in cells. Fourth, the analog of glucose 2-deoxy-glucose (2-DG) is injected. 2-DG competes with glucose to bind hexokinase, the enzyme that catalyzes the first step of glycolysis. The ECAR levels decrease and subtracting this from the maximum capacity of glycolysis, we obtain the glycolytic reserve or the acidification not produced by glycolysis (Figures 9 and 11) (Divakaruni *et al.*, 2014).

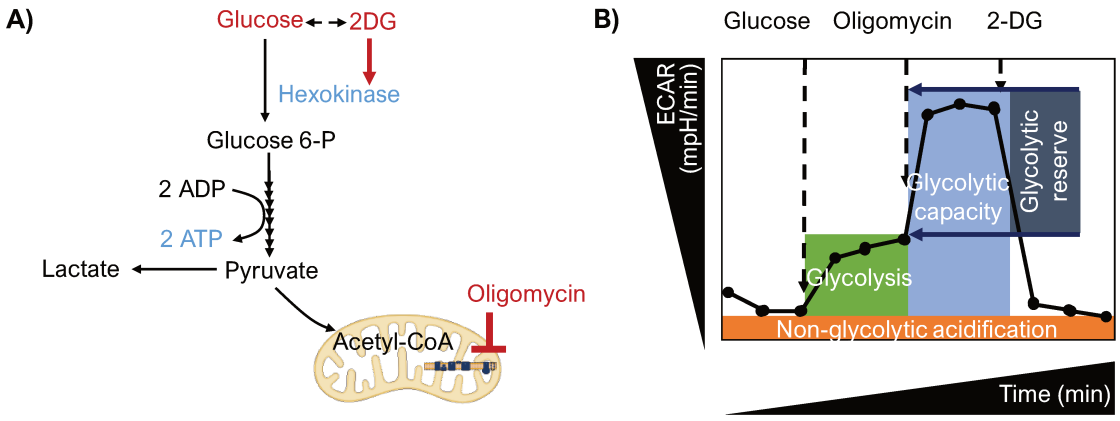

Figure 11. Schematic examples of the assessment of extracellular acidification rate (ECAR) in cells with glycolysis modulators. A) Glucose is degraded into glucose 6-phosphate by the enzyme hexokinase. Further steps of glycolysis follow which lead to the production of pyruvate which is further degraded into lactate. The whole process of glycolysis generates 2 molecules of ATP per molecule of glucose. Glycolysis modulators are highlighted: saturating levels of glucose stimulate glycolysis, 2-deoxy-glucose (2-DG) competes with glucose to bind to hexokinase thus inhibiting glycolysis and oligomycin inhibits complex V or ATP synthase, thereby inhibiting mitochondrial ATP production. **B)** The extracellular acidification values (mpH) are obtained over time (min), resulting in ECAR (mpH/min). The ECAR values directly correlate with the amount of lactate excreted by the cells due to the associated extrusion of protons. Glycolysis, glycolytic capacity, glycolytic reserve are highlighted, as well as ECAR corresponding to non-glycolytic acidification. These values are obtained by modulating the ETC with the insertion of glycolysis modulators mentioned in A). The simulated assay is done on a Seahorse XF Flux Analyzer. Adapted from Divakaruni *et al.*, 2014.

Glycolysis and oncogenic events

Several events can take place in the cell and promote aerobic glycolysis. For instance, PI3K/Akt (phosphatidylinositol- 4,5 –biphosphate 3-kinase/ protein kinase B) is a signaling pathway involved in cellular proliferation and apoptosis which is frequently dysregulated

in cancer. In fact, inhibition of PI3K/Akt suppresses tumor growth and induces apoptosis *in vitro* and *in vivo*. Several PI3K/Akt inhibitors are being tested in clinical trials (Alzahrani, 2019). PI3K/Akt activation consists of activation of PI3K that phosphorylates and activates Akt, a serine/threonine kinase that can then trigger the activation of mTOR and upregulate transcription factors to regulate glucose metabolism, apoptosis, cell proliferation, transcription and cell migration. At the same time, activated mTORC2 phosphorylates and activates Akt (Fedele *et al.*, 2010). GSK-3 (Glycogen synthase kinase 3β) is one of the downstream targets activated by Akt. GSK-3 is a serine/threonine kinase that phosphorylates several substrates including metabolic targets and transcription factors. Briefly, insulin and growth factors activate PI3K-dependent Akt that phosphorylates the serine at the N terminal of GSK-3 that results in its inactivation. GSK-3 inactivation leads to an accumulation of cyclin D1 that triggers the progression of the cell cycle and proliferation (Diehl *et al.*, 1998; Alt *et al.*, 2000).

Notably, when the proliferation rate of tumor cells surpasses the rate of blood vessel formation, the environment becomes hypoxic with oxygen levels ranging from 0 to 2% (Jain, Munn and Fukumura, 2002). HIF-1 (Hypoxia-Inducible Factor-1) is downstream PI3K/Akt and HIF-1 levels vary according to the oxygen concentration in the environment; increasing under hypoxic conditions (Zeng *et al.*, 2016; Lv *et al.*, 2017). Provided that HIF-1α is regulated via the PI3K/Akt/mTOR pathway, it can activate the expression of glycolytic enzymes (Lv *et al.*, 2017), including GLUT1, hexokinase II, phosphofructokinase 2 and lactate dehydrogenase A. Activation of these enzymes leads to increased lactate secretion (Zeng *et al.*, 2016). Of note, hypoxia leads to high levels of HIF-1α that is then activated in a PI3K/Akt/mTOR independent manner (Arsham *et al.*, 2002). A growth factor that activates HIF-1α and c-Myc is PDGF (Platelet-Derived Growth Factor). Activation of HIF-1α and c-Myc triggers a decrease in the activity of the mitochondrial complex IV and activates PI3K/Akt pathway *in vitro*. In addition, the effect of treatment with GLUT1 inhibitors can be reversed by PDGF stimulation by inverting the decrease in glucose uptake and lactate production. Hence, PDGF is linked with both mitochondrial activity and activated glycolysis (Moench *et al.*, 2016).

PI3K/Akt also regulates the expression of PFKFB2 (fructose 2,6-biphosphatase) and boosts glycolysis. The activation of PFKFB2 is controlled through phosphorylation of the residues Ser466 and Ser483 at the C-terminal (Kitamura *et al.*, 1988; Depre *et al.*, 1993; Bertrand *et al.*, 1999).

Another alteration frequent in cancer is the gain of function of MYC which triggers the expression of genes that favour anabolic growth such as enzymes and transporters playing a role in glycolysis, fatty acid synthesis, glutaminolysis, serine metabolism and mitochondrial metabolism (Stine *et al.*, 2015).

Pyruvate dehydrogenase (PDH) is the enzyme catalyzing the conversion of pyruvate to acetyl-coA, a critical transition step between glycolysis and OXPHOS. PDH is inactivated upon phosphorylation by PDK (pyruvate dehydrogenase kinase), another target upregulated by MYC and/or HIF-1α (Kim *et al.*, 2006).

The *TP53* gene, encoding p53, is mutated or deleted in half of human cancers (Hollstein *et al.*, 1991). Loss of p53 triggers an increase in the glycolytic flux to favour anabolism and redox balance, essential for tumorigenesis (Kruiswijk, Labuschagne and Vousden, 2015). Precisely, the tumor suppressors p53 slows down the glycolytic flux via TIGAR (TP53-inducible glycolysis and apoptosis regulator) and upon mutation, p53 results in the accumulation of fructose 2,6-biphosphate that activates PFK-1 (phosphofructokinase-1) to sustain glycolysis (Hay, 2016).

The expression of the STATs (Signal Transducer and Activator of Transcription) also plays a role in regulating aerobic glycolysis (Poli and Camporeale, 2015). For instance, higher expression of STAT3 triggers upregulation of HK II and PKM2, and vice-versa (Li *et al.*, 2017).

Allosteric regulation

There are additional phenomena that can alter the rate of glycolysis; the availability of substrates and products of glycolysis can affect the glycolytic flux. G6P (Glucose-6-Phosphate) is the product resulting from the first step of glycolysis and high levels of G6P act as a negative feedback loop on the enzyme HK. The downstream glycolytic target F-2,6-BP activates PFK1 that can speed up the flux of glycolysis. 3-PG (3-phosphoglycerate) inhibits 6-phosphogluconate dehydrogenase which results in the dysregulation of PPP whereas 2-PG activates the PHGDH (phosphoglycerate dehydrogenase) which catalyzes the first step of serine synthesis. Additionally, PEP (phosphoenolpyruvate) and lactate accumulation inactivate PFK (Hay, 2016). Conclusively, activation loops take place between substrates and products of the different steps of glycolysis which also affects the rate of the whole process.

Pentose phosphate pathway and cancer

The pentose phosphate pathway (PPP) branches from glycolysis at the first step of G6P (obtained from glucose by HK). In the oxidative phase, G6P is oxidized into ribulose-5-phosphate (Ru-5-P) that is isomerized into ribose-5-phosphate (R5P). R5P can be used as a nucleotide precursor or further metabolized via the non-oxidative PPP phase to obtain fructose-6-phosphate (F6P) and glyceraldehyde-3-phosphate (G3P), which are also produced during glycolysis (Figure 12). NADPH is produced at two steps of the PPP (Figure 12) and is key for highly proliferating cells to remove the reactive oxygen species (ROS), mostly produced by OXPHOS. Cancer cells also rely on PPP to produce R5P and further obtain nucleotides (Riganti *et al.*, 2012). The fact that products of the PPP can be transformed into glycolytic substrates, results in a tight connection between glycolysis and PPP, thereby implying that the flux can be adapted to the energetic requirements of the cell at a given situation.

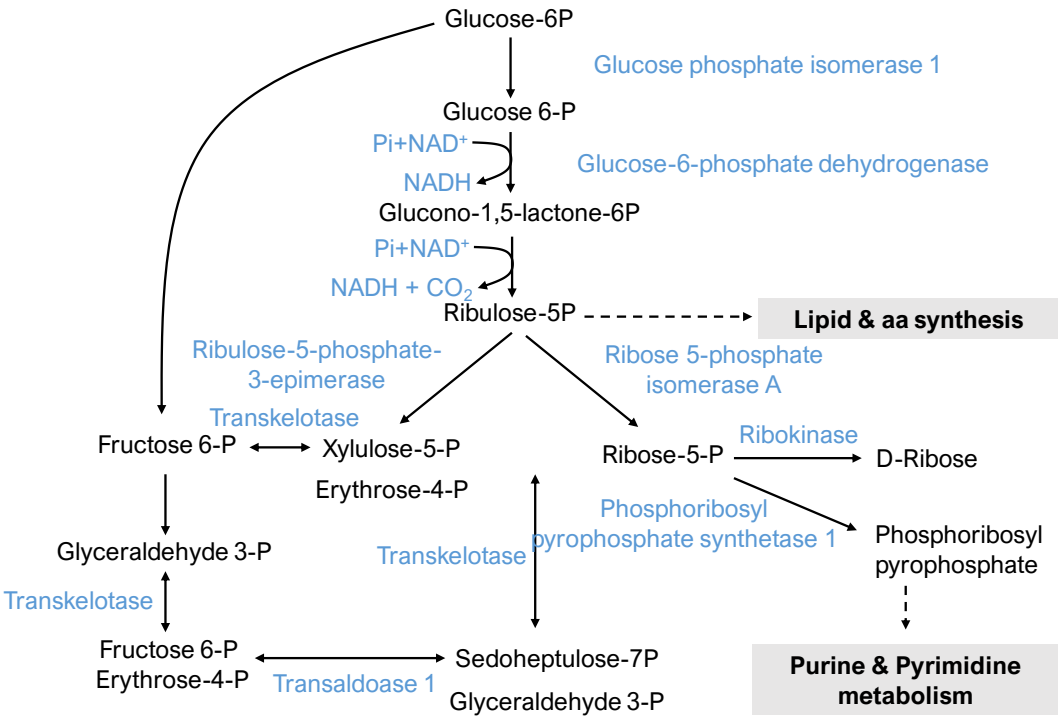

Figure 12. Schema of the pentose phosphate pathway. In parallel with glycolysis, the pentose phosphate pathway takes place in two stages, starting from glucose-6-phosphate. The first stage generates NADH and the second stage generates pentoses including ribulose 5-phosphate and phosphoribosyl pyrophosphate, contributing thus to lipid and amino acid synthesis as well as purine and pyrimidine metabolism, respectively. Adapted from Levine and Puzio-Kuter, 2010.

Cancer cells may promote R5P production rather than NADPH or ATP obtention in order to synthesize nucleotide precursors to sustain a fast proliferation. In this context, the glycolytic products F6P and G3P undergo the PPP and R5P is obtained (5 moles of G6P result in 2 moles of NADPH and 1 of R5P). However, if cells require ATP to meet the energy demand and NADPH to scavenge ROS, the flux goes through the same step but starting from a bigger amount of G6P (6 moles of G6P lead to 12 moles of NADPH and 6 moles of R5P). The R5P obtained is transformed into F6P and G3P (by TKT and TALDO1) which allow the obtention of G6P via the gluconeogenic pathway. If more NADPH is needed, G6P can be fully oxidized to CO_2 (Bouzier-Sore and Bolaños, 2015).

Amino acids metabolism

Early metabolic studies were mainly focused on glycolysis and OXPHOS. However, growing evidence has highlighted the importance of amino acids in fueling cancer metabolism.

Serine and Glycine

PHGDH is the enzyme that catalyzes the first rate-limiting step of the *de novo* serine synthesis, from the glycolytic compound 3-phosphoglycerate to 3-phospho hydroxypyruvate (P-pyr) with NAD^+ reduction to NADH. *PHGDH* is overexpressed in a breast cancer subset and skin melanoma (Locasale *et al.*, 2011; Possemato *et al.*, 2012). Next, PSAT1 (phosphoserine aminotransferase 1) catalyzes the reaction in which the amino group from glutamate is accepted resulting in phospho-serine and α-ketoglutarate. α-ketoglutarate will go to the TCA cycle and phospho-serine is dephosphorylated by PSPH (phosphoserine phosphatase). Serine is a non-essential amino acid that can be converted into ceramide for lipid synthesis or into glycine by SHMT (serine hydroxymethyltransferase). Glycine can result in methylene-THF, a one-carbon compound that feeds the folate cycle for nucleotide synthesis. Glycine can be cleaved in the mitochondria to transfer a one-carbon unit to methylene-THF. Inhibition of GLDC (glycine decarboxylase) impairs cell proliferation and tumorigenesis (Zhang *et al.*, 2012). Glycine is critical for GSH (glutathione synthesis) obtention, an essential antioxidant. Thus, serine also has an antioxidative role through glycine production. Additionally, reducing agents like NADPH can be obtained in the reaction from GSH to GSSG. Under hypoxia or mitochondrial defects, cells upregulate the serine pathway and SHMT2

expression, most likely to promote an antioxidant effect (Figure 13) (Bao *et al.*, 2016; Samanta *et al.*, 2016).

Serine can contribute to the modification of lipids, nucleic acids and proteins by providing methyl groups. Other than in the cytosol, methylene-THF can also be produced in the mitochondria. Folate metabolism or one-carbon metabolism is a process needed to transfer one-carbon units for the synthesis of purine and thymidine as well as homocysteine remethylation. Given its role in the nucleic acid synthesis, inhibition of folate metabolism may suppress cell proliferation (Andersona, Quintero and Stovera, 2011). Precisely, cleavage of serine to glycine and one-carbon units in the folate metabolism favours the synthesis of porphyrin, thymidylate, purine, glutathione and S-adenosyl methionine synthesis. One-carbon metabolism also contributes to the formation of ATP and NADPH (Figure 13) (Pan *et al.*, 2020).

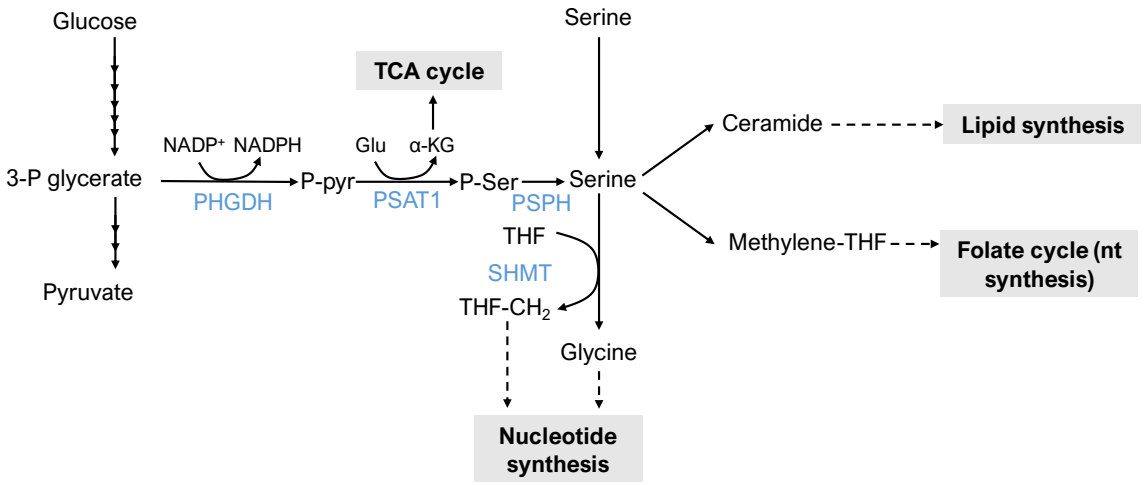

Figure 13. Schema of the serine synthesis pathway. In parallel with glycolysis, the serine synthesis pathway takes place in three steps starting from the glycolytic intermediate 3-phosphoglycerate. The first step consists of the conversion of the 3-phosphoglycerate hydroxyl group to a ketone rendering 3-phosphohydroxypyruvate. Transamination of 3-phosphohydroxypyruvate results in phosphoserine which can be hydrolyzed to form serine. Serine can then be transformed into glycine and contribute to nucleotide synthesis, into ceramide to take part in lipid synthesis or into methylene-THF into the folate cycle for nucleotide synthesis. Adapted from Levine and Puzio-Kuter, 2010.

Serine is also an allosteric activator of PKM2, an isoform of the enzyme PKM (pyruvate kinase) which catalyzes the step which converts phosphoenolpyruvate to pyruvate. Precisely, serine starvation reduces the activity of PKM2 which results in an accumulation of 3-P glycerate, the substrate of *de novo* serine synthesis. Given that cells expressing

PKM2 show higher proliferation rates as compared to cells expressing PKM1, serine synthesis seems to play a key role in regulating cell growth (Christofk *et al.*, 2008; Chaneton *et al.*, 2012; Ye *et al.*, 2012).

Some transcription factors regulate the three enzymes of the serine pathway (PHGDH, PSAT1 and SHMT), including eIF2α (eukaryotic initiation factor 2) which, upon activation activates the translation of several mRNAs such as ATF4. Under amino acid starvation, PHGDH, PSAT1 and PSPH are induced by ATF4. Hence, if ATF4 is repressed, cell proliferation is suppressed under serine depletion (Ye *et al.*, 2012).

Other amino acids

Tryptophan, histidine and choline can also be sources of one-carbon units. Although serine is the main contributor to one-carbon metabolism, both essential and non-essential amino acids can be one-carbon carriers (Reina-Campos, Diaz-Meco and Moscat, 2020).

Metabolic dysregulations in uveal melanoma

After having described common metabolic dysregulations in cancer, it is of utter importance to detail the status of such dysregulations in UM in general and upon *SF3B1* mutations in particular. Nevertheless, unlike other cancer types, no major switch in the metabolic profile has been characterized in UM. However, several studies pinpoint specific metabolic dysregulations.

Glucose uptake rate in uveal melanoma

PET scan (Positron Emission Tomography) is a diagnostic tool widely used for the detection of solid tumours and metastases. Cancer cells display an increased glucose uptake rate so they incorporate radiolabeled FDG (Fluorodeoxyglucose) at higher rates. PET scan coupled with FDG was tested in UM early on to assess glucose consumption in patients. FDG is a type of glucose used as a tracer that indicates the rate of glucose uptake thus providing information about the metabolism of the tumour. First FDG-PET scans done in patients showed a minority of positive cases (2/2, 7/20, 3/12 were detected in three studies), implying that this tool was not sensitive enough to diagnose primary UM (Lucignani *et al.*, 1992; Modorati *et al.*, 1996; Spraul, Lang and Lang, 2001). Later studies showed that FDG-PET scans may be more sensitive to detect large UM tumors and metastatic UMs, given that a higher proportion of FDG-PET scans was positive for a majority of patients with liver metastasis, yet not all cases could be confirmed. This suggests that although this tool is sensitive enough to detect UM, the signal varies widely according to the size of the tumour (Francken *et al.*, 2006). Nowadays, PET scans can be combined with CT (computer tomography) which provides the anatomic positioning combined with PET metabolic findings. PET-CT may be more useful to examine the whole body and detect remote metastatic lesions (Papastefanou *et al.*, 2014). Additionally, the lack of consistency in the detection of positive PET scans may not only be explained by the size of the tumour but also by the genetic differences across tumour types found in patients. To this end, PET scans should be revisited taking into account the genomic profile of each UM tumour.

Metabolic features in *BAP1^{mut}* uveal melanoma tumours

Another study explored the metabolic profiles of *BAP1^{mut}* UM tumours. Previous studies have reported that BAP1 plays a role in the control of ROS levels, mitochondrial function,

or lipid and glucose metabolism in mouse liver (Baughman *et al.*, 2017; Hebert *et al.*, 2017). Han and colleagues found that UM cell lines and tumours harbouring *BAP1* mutations displayed an upregulation of OXPHOS genes ($OXPHOS^{high}$), as compared to $BAP1^{WT}$ ($OXPHOS^{low}$). $OXPHOS^{high}$ subset displayed an increased nucleotide synthesis and glucose metabolism while $OXPHOS^{low}$ group favoured fatty acid metabolism. Furthermore, $OXPHOS^{high}$ cells were more sensitive to inhibitors targeting nucleotide synthesis and glycolysis, and $OXPHOS^{low}$ cells were more sensitive to inhibitors targeting fatty acid metabolic pathways (Han *et al.*, 2021). Overall, this study opens a new therapeutic window based on metabolic adapted treatment for UM patients with distinct genetic profiles and consequent metabolic defects.

Glycolysis alterations in *SF3B1*^{mut} cells

A recent study found an enrichment of aerobic glycolysis metabolites upon *SF3B1* mutations in pancreatic ductal adenocarcinoma cells. In fact, $SF3B1^{K700E}$ cells showed increased glucose consumption, lactate release and increased ECAR, demonstrative of increased glycolysis (Yang *et al.*, 2021). Studies revealing a role of mutant SF3B1 in metabolic dysregulation are highly interesting and shed light on new roles of SF3B1 beyond splicing.

Serine and glycine dependency in cancer and induced by *SF3B1*^{mut}

Given that PHGDH is overexpressed in several types of cancer, inhibiting PHDGH continues to be explored for cancer therapy purposes. A study on glioblastoma found that treatment with imipridones activates the serine pathway thus they tested imipridones in combination with PHGDH inhibitors (NCT-503 and CBR-5884). Strikingly, combined treatment triggered cell death *in vitro* and *in vivo* (Ishida *et al.*, 2019). Another study on multiple myeloma showed that resistance to bertozomib is associated with overexpression of PHGDH and increased serine synthesis, thereby opening a new therapeutic window by coinhibition of PHGDH (Zaal *et al.*, 2017). It was also shown that, in HIF2α-knockout tumor cells, *PHGDH* was upregulated and the serine pathway was more active. Consistently, treatment with a PHGDH inhibitor (CBR-5884 and NCT-503) on these HIF2α-deficient tumor cells triggered apoptosis *in vitro* and *in vivo* (Yoshino *et al.*, 2018).

However, underexpression of PHGDH has also been reported in two types of kidney carcinoma and liver carcinoma, as detected in the TCGA datasets (Li and Ye, 2020). It was also found that SF3B1 mutations trigger the mis-splicing of *PHGDH* which is then degraded by NMD (Nonsense-Mediated mRNA Decay) pathway, thereby leading to a PHGDH underexpression in breast epithelial cells. Strikingly, deprivation of serine and glycine reduces cell growth *in vitro* and tumor growth *in vivo* (Dalton *et al.*, 2019, 2020). Indeed, certain subsets of breast cancer are dependent on the serine synthesis pathway (Murphy *et al.*, 2018). Moreover, suppression of PHGDH in endothelial cells has been shown to disturb mitochondrial homeostasis and heme synthesis, such could explain the formation of ring sideroblasts, which are iron deposits in the mitochondria and a distinctive feature of MDS, driven by *SF3B1* mutations (Papaemmanuil *et al.*, 2011; Vandekeere *et al.*, 2018).

OXPHOS upregulation as a response to escape treatment

As previously detailed (Chapter I), in UM, *GNAQ* and *GNA11* mutations trigger the activation of the MEK-ERK signaling pathway and MEK inhibitors have long been investigated for UM treatment showing little effect, thus combination with other inhibitors is currently being assessed (Vivet-Noguer *et al.*, 2019). Cyclin D1 is a downstream target of MEK-ERK signaling which is activated by MEK-ERK. Cyclin D1, in turn, activates CDK4/6 which promotes cell cycle progression. Teh *et al*. hypothesized that testing MEK inhibitors in combination with CDK4/6 inhibitors *in vitro* and *in vivo* may increase the response in UM. However, they did not observe a synergistic effect as UM cells and tumors were rather resistant to treatment combination. Surprisingly, they observed an upregulation of OXPHOS upon combined treatment, suggesting that metabolic rewiring is a strategy that cancer cells use to escape treatment (Teh *et al.*, 2020). Further studies are essential to decrypt the underlying mechanism and exploit clinical approaches to target this metabolic switch.

OXPHOS dysregulation by *SF3B1*^{mut}

Dalton *et al*. showed that mutant SF3B1 reprograms mitochondrial metabolism in breast epithelial cells by downregulating proteins that are highly enriched in metabolic pathways. Metabolic reprogramming is a hallmark of cancer that can guide tumorigenesis by redirecting nutrient utilization. The core assembly factors of the mitochondria are the transport chain UQCC1 (ubiquinol-cytochrome C reductase complex assembly factor 1)

and UQCC2 (ubiquinol-cytochrome C reductase complex assembly factor 2), NDUFB8 (NADH dehydrogenase [ubiquinone] 1 beta subcomplex subunit 8), SDBH (Succinate dehydrogenase [ubiquinone] iron-sulfur subunit), MTCO2 (Cytochrome c oxidase subunit 2), and ATP5A (ATP synthase F1 subunit alpha). One notable signal was in the mitochondrial respiratory chain complex III of the ETC, assembled by UQCC1 and UQCC2 factors. In fact, mutant SF3B1 mis-splices *UQCC1*, leading to a decrease in the levels of expression of mitochondrial complex III (Dalton *et al.*, 2019).

Emerging roles of mutant SF3B1 in metabolic dysfunction provide a highly appealing frame of research. Although this chapter may seem less linear than the other two, it is important to note that separate metabolic defects have been described in independent studies of UM and the observed metabolic errors may differ. Further light will be brought into the role of mutant SF3B1 in the metabolism of UM in the following chapter which will wrap up what has been explained in the three chapters of the introduction. Another fascinating point to consider is whether these metabolic features will be present in tumours. This remains to be elucidated because energy obtention patterns are highly heterogeneous in tumours.

RESULTS

Chapter IV – Glycolysis-dependency as the Acheeles' hill of uveal melanoma cells

During my PhD, I have addressed the dynamics, process and downstream outcomes of mis-splicing caused by mutations in the splicing factor gene *SF3B1*. For this, I have undertaken a comprehensive molecular study of the consequences of R625G *SF3B1* mutation, a recurrent mutation in uveal melanoma (UM). The gene expression profile has revealed that the aberrant splicing induced by mutant SF3B1 has a limited effect on the global expression of mRNAs and proteins. I have also shown that newly synthesized proteins and translation efficiency are not significantly affected by *SF3B1*^{R625G}-induced aberrant splicing. On the other hand, I have demonstrated that the mis-splicing induced by mutant SF3B1 directly impacts the translatability of the aberrant transcripts in a target-specific manner. Interestingly, translated aberrant transcripts are highly enriched in metabolic pathways with a decrease on the abundance of metabolic proteins.

After pinpointing the downstream impact of mutant SF3B1 at the levels of translatability and protein abundance of metabolic targets, I examined the metabolic functional consequences. *SF3B1*^{mut} UM cell lines exhibit a decreased mitochondrial respiration which is compensated by glycolysis enhancement. This metabolic dependency can be potentially exploited for therapeutic purposes because *SF3B1*^{mut} cells are more sensitive to glycolysis inhibition than wild-type cells. My research work sheds light on the fate of the aberrant transcripts induced by mutant SF3B1 in UM for the first time. These findings have been reported in a manuscript entitled "Glycolysis dependency as a hallmark of *SF3B1*-mutated cells in uveal melanoma" which is currently under review in Cell Reports.

In addition to revealing glycolysis dependency as a metabolic hallmark induced by mutant SF3B1, I also found that *SF3B1*^{mut} cells exhibit other impaired metabolic pathways including pentose phosphate pathway and serine synthesis *de novo*. These metabolic defects urge further metabolic characterization. To do so, I am currently performing experiments under hypoxic conditions and deprivation of glutamine or essential amino acids.

Questions

To date, we know that *SF3B1* mutations lead to a change of function by which mutant SF3B1 recognizes cryptic AG' and BP sites, located upstream of the canonical sites. This cryptic recognition takes place in a subset of genes and gives rise to the formation of aberrant mRNA transcripts that contain a fragment of the intron (Darman *et al.*, 2015; DeBoever *et al.*, 2015; Alsafadi *et al.*, 2016). However, we still ignore whether these aberrant transcripts will be degraded by NMD or translated into either truncated or non-truncated proteins. Considering that *SF3B1*^{mut}-induced aberrant splicing occurs in a subset of genes, we may question whether some of these genes and the encoded proteins share a functional link or are enriched in a particular biological process. Moreover, we may interrogate whether the aberrantly transcripted genes are enriched in particular oncogenic pathways, thereby potentially explaining the role of mutant SF3B1 in carcinogenesis. To this end, research is crucial to determine the fate of the *SF3B1*^{mut}-induced aberrant transcripts and bringing light to this matter is the goal of my thesis. In the first instance, I aimed to address the following questions:

- Does *SF3B1*^{R625G} trigger a dysregulation (upregulation or downregulation) of the **mRNA expression levels**?
- Does *SF3B1*^{R625G} alter the **nascent protein synthesis**?
- Does *SF3B1*^{R625G} lead to changes in the **translation efficiency** of some proteins?
- Does *SF3B1*^{R625G} induce changes in the **abundance of certain proteins**?

In the second instance, provided we find alterations at any of the levels mentioned above, we wanted to pursue by addressing the following questions:

- What is the **functional impact** of these alterations? Is there any oncogenic link?
- Are these alterations **specific to mutant SF3B1**? Namely, are these alterations induced by other hotspot mutations of *SF3B1* (G742D and K666T)?
- Can we **target or revert** these alterations?

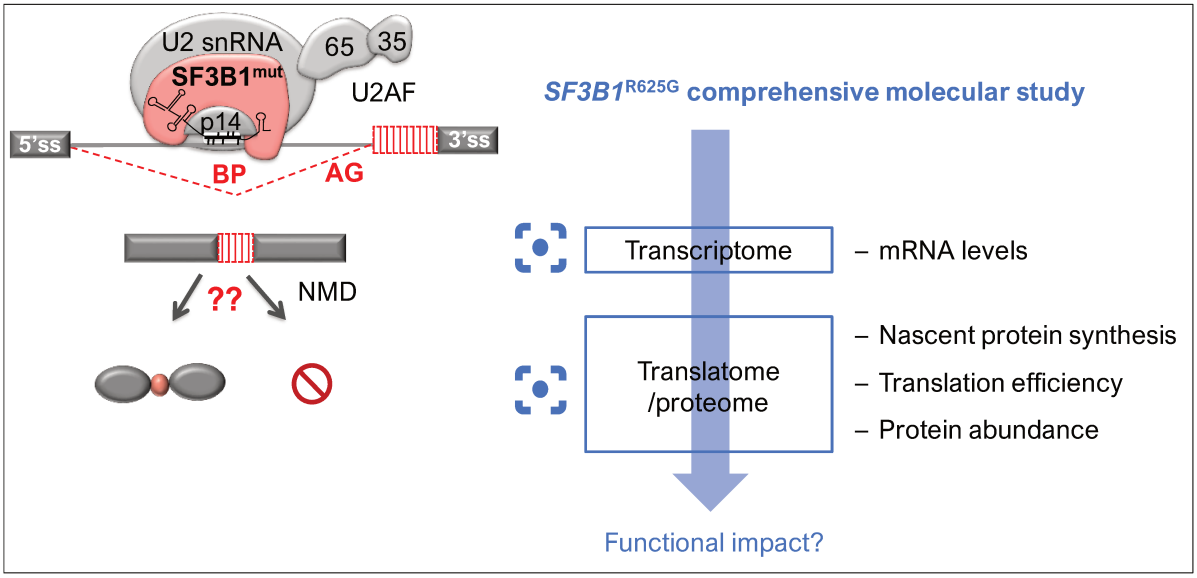

Figure 14. *SF3B1*^{R625G} comprehensive molecular study conducted in the Mel202 UM isogenic model. Mutant SF3B1 triggers the formation of aberrant transcripts with the inclusion of an intronic fragment (red). A comprehensive molecular study to bring light on the fate of these aberrant transcripts was conducted by analyzing the impact of *SF3B1*^{R625G} on different levels: A) transcriptome (mRNA levels), B) translatome/proteome (nascent protein synthesis, translation efficiency and protein abundance).

Strategy and methodology

How can we elucidate the impact of *SF3B1* mutations in uveal melanoma?

Establishment of cell models

First and foremost, we developed an isogenic model of *SF3B1* using the cell line Mel202. This cell line was obtained from a primary UM tumor and displays two *GNAQ* mutations (Q209L and R210K) and an *SF3B1* mutation (R625G). Following the guidelines provided by Zhou *et al.*, 2015, we used CRISPR/Cas9 technology to revert the *SF3B1* mutation and obtain an *SF3B1*^{WT} cell line. Briefly, CRISPR/Cas9 induces double-strand breaks at the N-terminus of the coding region of the endogenous locus. Then, a destabilizing domain or DD tag is inserted by homologous recombination. The DD tag is attached to the mutant SF3B1 protein which is detected and degraded by the proteasome. Hence, this technique allows performing allele-specific degradation (Figure 15).

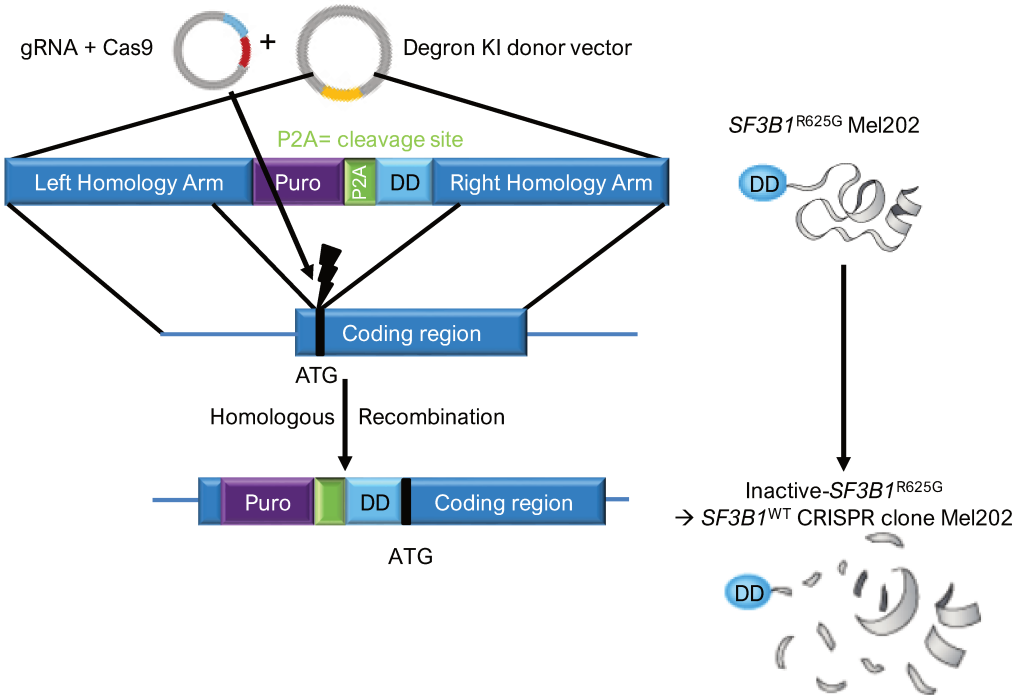

Figure 15. Schema of the depletion of the protein mutant SF3B1-R625G, following the DI-Kegron strategy established by Zhou *et al.* 2015. CRISPR/Cas9 induces double-strand breaks at the N-terminus of the coding region of the endogenous locus which prompts homologous recombination (HR). HR results in the knock-in of the Degron tag (DD) in the presence of the donor vector (Degron KI donor vector). The donor vector contains a cassette of puromycin resistance (Puro), P2A cleavage site (P2A) and DD which are flanked by the left and right homology arms of 1 kb each. After HR, the puromycin resistance gene and DD-tagged *SF3B1* are expressed under the control of the endogenous promoter because P2A is a peptide skipped by the ribosome. Adapted from Zhou *et al.*, 2015.

Once the model was developed, we proceeded to its validation. As a reminder, mutant SF3B1 leads to the formation of aberrant mRNA transcripts that contain an extra fragment of the intron. Our team developed an RT-qPCR tool based on *DPH5*, an mRNA transcript sensitive to mutant SF3B1 (Darman *et al.*, 2015; Alsafadi *et al.*, 2016; Dolatshad *et al.*, 2016; Dalton *et al.*, 2019; Bergot *et al.*, 2020; Canbezdi *et al.*, 2021). This RT-qPCR tool contains two sets of primers; one set amplifies the canonical transcripts of *DPH5* (primers are specific to sequences of the consecutive exons) and the other set amplifies the aberrant transcripts of *DPH5* (primers are specific to the sequences of the first exon and the intronic fragment) (Figure 16) (Alsafadi *et al.*, 2016). This way we can calculate the aberrant splice index (aberrant splice product/canonical splice product) which indicates the proportion of aberrant splicing taking place. As we can see in figure 12, the mother cell line Mel202 (*SF3B1*^{R625G}) displays a high aberrant splice index induced by mutant SF3B1 whereas, upon depletion of mutant SF3B1, the resulting Mel202 CRISPR

clone exhibits an *SF3B1*^{WT} phenotype with residual aberrant splicing. It is important to note that there is always residual aberrant splicing, even when there are no mutations in *SF3B1*. In conclusion, the splicing pattern was validated in the *SF3B1* isogenic model (Figure 16).

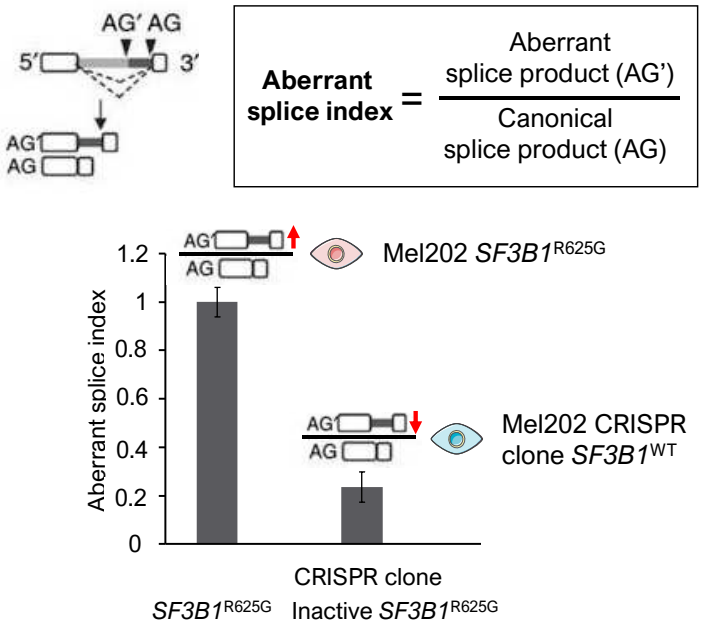

Figure 16. Validation of the *SF3B1* isogenic UM cell model by RT-qPCR in the *SF3B1*^{R625G}-sensitive pre-mRNA transcript *DPH5*. SF3B1^{R625G} induces the recognition of a cryptic AG (AG') on a subset of transcripts, including *DPH5*. The developed RT-qPCR tool includes personalized primers that will amplify the canonical transcripts (where AG is recognized) and the aberrant transcripts (where AG' is recognized) separately. The aberrant splice index results from the division of the expression of the aberrant splice product by the expression of the canonical splice product thus providing information on the percentage of aberrant splicing. The mother cell line Mel202 harbours an R625G mutation on *SF3B1* which results in the recognition of an AG' thus a high aberrant splice index. Upon degradation of mutant R625G SF3B1 protein by CRISPR/Cas9 following the DI-Kegron strategy (Figure 15), due to the absence of mutant SF3B1, the canonical AG is recognized, leading to a decreased aberrant splice index (Mel202 CRISPR clone *SF3B1*^{WT}).

Furthermore, we developed two additional *SF3B1* isogenic models from two cell lines displaying a different origin than UM (HEK293T and HAP1) in order to confirm specificity concerning the *SF3B1* mutational status. HEK293T isogenic cell model harbouring *SF3B1*^{K666T} was generated by CRISPR/Cas9 as previously described (Alsafadi *et al.*, 2016). Briefly, a point mutation in *SF3B1* that leads to K666T amino-acid substitution was introduced by CRISPR/Cas9 double-strand breaks followed by homologous recombination. The donor vector contained a puromycin resistance cassette that was transfected at a 1:1:1 ratio with Cas9 (Addgene 41815) and an *SF3B1*-specific gRNA (built from gRNA cloning vector, Addgene 41824). The selection cassette was removed

by flippase-mediated excision. HAP1 isogenic cell model harboring *SF3B1*^{G742D} was also obtained by CRISPR/Cas9 with the Lipofectamine™ CRISPRMAX™ Cas9 Transfection Reagent (CMAX00008, Invitrogen) following the manufacturer's instructions. Selection of resistant clones, single-cell dilution were undertaken to screen for a cell clone with the intended mutation. The mutational status of all isogenic cell lines was verified by Sanger sequencing and RNA-sequencing.

On the UM isogenic cell model, we conducted the analysis of global RNA expression by RNAseq, analysis of nascent protein synthesis, polysome profiling to evaluate the translation efficiency, LC-MS/MS analysis to evaluate protein abundance, and gene enrichment analysis related to the under-represented proteins in *SF3B1*^{R625G} cells. Having observed metabolic dysregulation in *SF3B1*^{R625G} cells, we proceeded to the characterization of the metabolic profile of these isogenic cell models with a focus on PHGDH (Posphoglycerate Dehydrogenase), PGD (6-phosphogluconate dehydrogenase), PDH (Pyruvate Dehydrogenase), and OXPHOS complexes. We found that *SF3B1*^{mut} triggers a decrease in mitochondrial respiration resulting in a higher glucose uptake in *SF3B1*^{R625G} cells versus *SF3B1*^{WT}cells, suggesting an increased glycolytic rate to promote the obtention of glycolytic intermediates on early glycolysis. Finally, we assessed the therapeutic potential of this metabolic feature by treating the cells with a PFKFB3 (6-phosphofructo-2-kinase/fructose-2,6-biphosphate 3) inhibitor. All the data obtained are exposed in the following manuscript:

Glycolysis dependency as a hallmark of *SF3B1*-mutated cells in uveal melanoma

Raquel Vivet-Noguer[1], Malcy Tarin[1], Christine Canbezdi[1], Stéphane Dayot[2,3], Lisseth Silva[1], Alexandre Houy[2], Sylvain Martineau[4,5], Virginie Mieulet[6], Géraldine Gentric[6], Damarys Loew[7], Bérangère Lombard[7], Fariba Nemati[1], Sophie Richon[8], Lea Guyonnet[9], Vincent Servois[10], Stephan Vagner[4,5], Marc-Henri Stern[2], Sergio Roman-Roman[1], Samar Alsafadi[1,2,*]

[1]Institut Curie, PSL Research University, Translational Research Department, Paris, France.
[2]Institut Curie, PSL Research University, INSERM U830, DNA Repair and Uveal Melanoma (D.R.U.M.), *Equipe labellisée par la Ligue Nationale Contre le Cancer*, Paris, France.
[3]Gustave Roussy Institute, Paris-Saclay University, INSERM U1279, Villejuif, France.
[4]Institut Curie, PSL Research University, CNRS UMR3348, INSERM U1278, Orsay, France.
[5]Université Paris Sud, Université Paris-Saclay, CNRS UMR3348, INSERM U1278, Orsay, France.
[6] Institut Curie, PSL Research University, INSERM U830, Stress and Cancer Laboratory, *Equipe labellisée par la Ligue Nationale Contre le Cancer*, Paris, France.
[7]Institut Curie, PSL Research University, Mass Spectrometry and Proteomics Facility, Paris, France.
[8]Institut Curie, PSL Research University, CNRS UMR 144, Paris, France.
[9]Institut Curie, PSL Research University, Cytometry Core, Paris, France.
[10]Institut Curie, PSL Research University, Department of Radiology, Paris, France.
[*]Correspondence: samar.alsafadi@curie.fr

Summary

SF3B1 mutations are frequent in cancer and result in aberrant transcripts whose fate remains unknown. Here, we provide a comprehensive analysis of the functional consequences of mutant SF3B1 in uveal melanoma. Transcriptional and proteomic analyses showed a minor impact on the global expression of mRNAs and proteins. Polysome profiling revealed that 35% of aberrantly-spliced transcripts are more translated than their corresponding canonically-spliced transcripts. This mostly occurs in genes with enriched metabolic functions. Further proteomic analysis confirmed that mutant SF3B1 specifically impacts abundance of proteins involved in metabolism. Functional metabolic characterization revealed that mutant SF3B1 decreases mitochondrial respiration and promotes glycolysis to compensate for the defective mitochondrial metabolism. Hence, mutant SF3B1 induces glycolysis dependency which sensitizes cells to glycolysis inhibition. Overall, we provide evidence of the oncogenic involvement of mutant SF3B1 in uveal melanoma through a metabolic switch to glycolysis, revealing vulnerability to glycolysis inhibitors as a promising therapeutic strategy.

Keywords

SF3B1, splicing, uveal melanoma, oncogenesis, metabolism, mitochondrial respiration, glycolysis inhibitors

Introduction

Splicing defects are frequent in cancer and are mostly caused by mutations of genes encoding for splicing factors involved in 3' splice site (3'ss) recognition, an early step in pre-mRNA splicing. *SF3B1* (Splicing Factor 3b, Subunit 1) is the most frequently mutated splicing gene in cancer, found recurrently in hematological malignancies (28% in myelodysplastic syndromes (MDS), 15% in chronic lymphocytic leukemia (CLL)) and also in 23% of uveal melanoma (UM) (Furney et al., 2013; Malcovati et al., 2015; Quesada et al., 2012; Vivet-Noguer et al., 2019; Yoshida et al., 2011). Several *SF3B1* hotspot mutations have been described at the C-terminal of the HEAT (Huntingtin, Elongation factor 3, protein phosphatase 2A, Targets of rapamycin 1) repeats with different prevalence according to the cancer type. Notably, mutations targeting the codon R625 predominate in UM (Alsafadi et al., 2016; Furney et al., 2013; Harbour et al., 2013). *SF3B1* mutations are change-of-function missense mutations that lead to the recognition of cryptic 3'ss, and consequently to aberrant splice junctions in a specific set of transcripts. These splicing aberrations have been thoroughly characterized by our group and others in the last years (Alsafadi et al., 2016; Darman et al., 2015; DeBoever et al., 2015). It is now well established that mutant SF3B1 corrupts recognition of the intronic branchpoint sequence by the U2 snRNP complex and promotes the recognition of a cryptic branchpoint located upstream of the canonical site, thereby leading to the inclusion of an intronic sequence in the final mRNA product (Alsafadi et al., 2016; Darman et al., 2015; DeBoever et al., 2015).

Although splicing aberrations induced by *SF3B1* mutations are now well defined, little is known about the fate of the aberrant transcripts. Recent studies have brought to light different functional impacts of these aberrant transcripts. For instance, it has been demonstrated that *SF3B1* mutations lead to the production of an aberrant splicing isoform of the *MAP3K7* pre-mRNA containing a premature codon leading to its degradation by NMD (Nonsense-Mediated mRNA Decay). This defect in MAP3K7 production in turn leads to hyperactivation of the NF-κB pathway that is known to drive MDS (Lee et al., 2018; Li et al., 2021). *SF3B1* mutations have also been reported to induce the inclusion of a poison exon in the *BRD9* mRNA leading to its repression. Interestingly, correcting the *BRD9* missplicing by antisense oligonucleotides or mutagenesis repressed tumor growth (Inoue et al., 2019). Similarly, *SF3B1*^{K700E}-induced missplicing of *PPP2R5A* leads to its downregulation and to a concomitant increase in the stability of the MYC protein thereby altering apoptosis (Liu et al., 2020). More recently, it has been shown that *SF3B1* mutations lead to *DVL2* missplicing, a gene that encodes a negative regulator of the Notch pathway (Pozzo et al., 2020; Zhao et al.,

2021). These missplicing-driven dysregulations of specific targets can then contribute to the oncogenic role of *SF3B1* mutations, yet the impact of *SF3B1* mutations seems to exceed these specific alterations.

Prior studies linked defects in splicing factors with metabolic impairment. For example, loss of expression of *SRSF3* (Serine/arginine-Rich Splicing Factor 3) triggers missplicing of key regulators of glucose and lipid metabolism in hepatocytes (Sen et al., 2013). In breast cancer cells, knock-down of *ESRP1* (Epithelial Splicing Regulatory Protein 1) decreased the expression of fatty acid, lipid metabolism targets and oxidoreductases including *PHGDH* (D-3-phosphoglycerate dehydrogenase). *ESPR1* depletion increased basal and spare respiration capacity while no changes were seen in the ECAR (extracellular acidification rate) (Gökmen-Polar et al., 2019). Furthermore, mutant SF3B1 has been shown to alter the abundance of proteins affecting metabolic pathways in breast cancer cells (Dalton et al., 2019). Proteins enriched in the mitochondrial electron transport chain, including UQCC1 (ubiquinol-cytochrome C reductase complex assembly factor 1) whose pre-mRNA is aberrantly-spliced by mutant SF3B1, showed reduced abundance. *SF3B1*^{K700E} cells were shown to present a reduced mitochondrial respiration capacity while the ECAR was unaltered. *PHGDH,* encoding for an enzyme involved in the *de novo* synthesis of serine, is also aberrantly-spliced by mutant SF3B1. Consequently, *SF3B1*^{K700E} cells are more sensitive to serine and glycine starvation than *SF3B1*^{WT} cells (Dalton et al., 2019). Overall, growing evidence argues for therapeutic targeting of metabolism in cells with splicing defects, providing therapeutic alternatives to splicing inhibitors that lack specificity and confer cytotoxic effects (Vivet-Noguer et al., 2019).

Here, we performed a comprehensive study of the impact of *SF3B1* mutation on RNA levels, nascent protein synthesis, protein abundance and translation efficiency in UM cells. Our work provides evidence that *SF3B1* mutation alters translation of specific transcripts encoding proteins involved in metabolism, which triggers a metabolic switch towards an increased glucose uptake. Consequently, *SF3B1*-mutated cells are more sensitive to glycolysis inhibition than *SF3B1* wild-type cells. Thus, our study sheds light on a new aspect of the oncogenic impact of mutant SF3B1 and provides an appealing therapeutic approach based on glycolysis inhibition, possibly combined with targeting other cancer-related pathways.

Results

SF3B1^{R625G} mutation poorly impacts global gene expression

To functionally characterize the downstream impact of *SF3B1* mutation in UM cells, we performed RNA sequencing (RNA-seq) of Mel202-*SF3B1*^{R625G} and CRISPR/Cas9-generated Mel202-*SF3B1*^{WT} cells. We first validated the aberrant splicing pattern in *SF3B1*^{R625G} cells. In fact, 1,445 aberrant splice junctions of the previously established splice pattern in *SF3B1*-mutated tumors (Alsafadi et al., 2016; Darman et al., 2015) were found to be differentially-expressed in *SF3B1*^{R625G} cells as compared to *SF3B1*^{WT} cells (Figure 1A and Supplementary Table 1). Global gene expression analysis revealed 181 differentially-expressed genes (p-values ≤ 10^{-5}, $\log_2$ fold-change ≥ |1|) in *SF3B1*^{R625G} cells as compared to *SF3B1*^{WT} cells (Figures 1B, 1C and Supplementary Table 2). Gene ontology (GO) enrichment analysis showed that the 181 differentially-expressed genes were poorly enriched in cancer-related processes (Figure 1D and Supplementary Table 3). Hence, only 1.1% of the whole genome expression (with poor functional involvement in oncogenesis) is significantly dysregulated upon *SF3B1* mutation.

To determine whether the *SF3B1*^{R625G}-induced splice aberration of a specific gene affects the expression of the corresponding transcript, we compared the list of differentially-expressed genes with that of aberrant junctions induced by mutated *SF3B1*. Only 8.3% of all differentially-expressed genes were aberrantly-spliced (1.7% downregulated and 6.6% upregulated genes) (Figure 1E). Amongst the differentially-expressed and aberrantly-spliced genes, 12 contained one aberrant junction (5 in-frame and 7 out-of-frame) and 3 contained two aberrant junctions (2 in-frame and 4 out-of-frame) (Figure 1F). Such finding suggests an NMD-independent regulation.

Taken together, our results imply that *SF3B1*^{R625G} triggers a restricted dysregulation of gene expression and that this dysregulation is mostly independent of the splicing aberrations.

Translated *SF3B1*^{R625G}-induced aberrantly-spliced transcripts are enriched in metabolic pathways

We then investigated whether the oncogenic effect of *SF3B1*^{R625G} takes place at the level of the translatome since splicing factors have been suggested to also act as regulators of translation (Aviner et al., 2017; Maslon et al., 2014; Michlewski et al., 2008; Palangat et al., 2018; Sanford et al., 2004). To assess whether *SF3B1*^{R625G} alters nascent protein synthesis, we labeled protein lysates of *SF3B1*^{WT} and *SF3B1*^{R625G}

Mel202 cells with L-azidohomoalanine (AHA) and performed a click reaction with alkyne-biotin. While cycloheximide (CHX) treatment efficiently inhibited protein synthesis, *SF3B1*^{WT} and *SF3B1*^{R625G} cells displayed comparable signals of nascent protein synthesis. This finding implies that *SF3B1*^{R625G} does not impact global protein synthesis (Figure 2A).

To further assess the impact of *SF3B1* mutation on the translatome at a transcript-specific level, we investigated whether *SF3B1*^{R625G}-induced aberrantly-spliced mRNAs are efficiently translated into proteins. We therefore performed polysome profiling followed by RNA-seq in *SF3B1*^{WT} and *SF3B1*^{R625G} cells. We observed comparable polysome profiles of *SF3B1*^{WT} and *SF3B1*^{R625G} cells (Figure 2B), suggesting again that *SF3B1*^{R625G} does not impact global translation efficiency. We investigated the translation efficiency of the aberrantly-spliced transcripts of *DPH5* and *ARMC9*, two genes reported to be aberrantly-spliced by mutant *SF3B1* (Alsafadi et al., 2016; Bergot et al., 2020; Canbezdi et al., 2021; Dalton et al., 2019; Darman et al., 2015; Dolatshad et al., 2015). We performed RT-qPCR analysis in each of the fractions to determine the relative abundance of the aberrant transcript to the canonical transcript, that we called aberrant splice index. As expected, the aberrant splice index increased for both *DPH5* and *ARMC9* in the *SF3B1*^{R625G} cells as compared to the *SF3B1*^{WT} cells. Most notably, in *SF3B1*^{R625G} cells, the *DPH5* aberrant splice index was higher in fractions 3-8 (containing mRNAs that are not engaged in polysomes) than in other fractions (Figure 2C). This suggests that the *DPH5* aberrant transcript is relatively less translated than the canonical *DPH5* transcript in *SF3B1*^{R625G} cells. In contrast, the *ARMC9* aberrant splice index was higher in fractions 9-16 (containing mRNAs that are engaged in polysomes) than in other fractions, indicating that the *ARMC9* aberrant transcript is relatively more translated than the canonical *ARMC9* transcript in *SF3B1*^{R625G} cells. This implies different consequences of *SF3B1*^{R625G}-induced splice aberrations on the translatability of aberrantly-spliced transcripts.

Figure 2D shows the fractional distribution of the *SF3B1*^{R625G}-aberrant transcripts plotted as the logarithmic ratio of each aberrant transcript fold-change in polysomes to its fold-change in monosomes in *SF3B1*^{R625G} cells. Our results indicate that 35% of aberrantly-spliced transcripts in *SF3B1*^{R625G} cells are relatively more translated than their corresponding canonically-spliced transcripts (group A, including *ARMC9*), while 65% are less translated (group B, including *DPH5*) (Figure 2D and Supplementary Table 4). We also investigated whether the 5'ss and 3'ss motifs correlate with the translational fate of the aberrant transcripts. STAR motifs define the two nucleotides after the 5' ss and the two nucleotides preceding the 3' ss. We found that CT/AC and GT/AG were the most

common motifs in the aberrant transcript, while CT/GC and GC/AG motifs were extremely rare. However, the translational fate of the aberrant transcripts was not determined by the motif residues (Figure 2E).

Next, we focused on the subset of genes for which the aberrantly-spliced transcripts in *SF3B1*^{R625G} cells are relatively more translated than their corresponding canonically-spliced transcripts (group A) to search for potential oncogenic functions. Enrichment analysis of KEGG pathways revealed a major involvement of group A in metabolism, including carbon metabolism and metabolic pathways (Figure 2F and Supplementary Table 5).

Conclusively, our findings show that *SF3B1* mutation impacts translation in a transcript-specific manner. While most *SF3B1*^{R625G}-induced aberrantly-spliced transcripts are less translated than their corresponding canonically-spliced transcript (group B, 65%), those that are more translated (group A, 35%) tend to encode proteins involved in metabolism.

SF3B1^{R625G} impacts the abundance of proteins involved in metabolism

To address the impact of *SF3B1* mutation on protein abundance, we performed a quantitative label-free tandem liquid chromatography-mass spectrometry (LC-MS/MS) analysis of *SF3B1*^{WT} and *SF3B1*^{R625G} Mel202 cells. We quantified a total number of 8,573 proteins. As shown in Figure 3A, we found 439 under-represented and 494 over-represented proteins in *SF3B1*^{R625G} cells as compared to *SF3B1*^{WT} cells (with at least 3 detected peptides per protein in all replicates, absolute fold change ≥1.2, p-value ≤0.05) (Figure 3A and Supplementary Table 6). We then explored genes which are both aberrantly-spliced by *SF3B1*^{R625G} and coding for dysregulated proteins according to our quantitative LC-MS/MS findings. Our analysis revealed that only 8.8% of aberrantly-spliced genes are associated with dysregulated protein levels, accounting for 2.7% of the over-represented proteins and 6.1% of the under-represented proteins (Figure 3B). The *SF3B1*^{R625G}-induced splicing aberrations altering protein abundance involved either out-of-frame (n=69) or in-frame junctions (n=44) (Figure 3C). We also compared the differentially-expressed genes with the differentially-abundant proteins and found that 7.2% of differentially-expressed genes encode proteins that are dysregulated by *SF3B1*^{R625G} (5.5% encoding over-represented proteins and 1.7% encoding under-represented proteins) (Figure 3D). Accordingly, the impact of *SF3B1*^{R625G} on the proteome seems to be independent of the mRNA abundance.

We then studied the functional impact of proteins dysregulated by *SF3B1*^{R625G} by GO analysis. Enrichment analysis of biological processes revealed a significant under-representation of metabolic proteins, implying a metabolic alteration induced by mutant SF3B1. Interestingly, 19 under-represented metabolic proteins were encoded by genes that are aberrantly-spliced by *SF3B1*^{R625G} (*UQCC1, DLST, OGDHL, CBS, AMDHD2, PHGDH, FDPS, NADSYN1, MUT, COASY, POLR1E, GALT, NDUFB1, PPOX, UBA1, PRKDC, PPP2R5A, PPP2R3A,* and *SOAT1*). Notably, proteins involved in mitochondrial respiratory chain complex III assembly were significantly under-represented, including the main complex III assembly factors UQCC1 and UQCC2. PHGDH that catalyzes the first step of the L-serine biosynthesis pathway was also aberrantly-spliced and under-represented (Supplementary Figure 1 and Supplementary Table 7).

SF3B1 mutation leads to a decrease in mitochondrial respiration and promotes cell dependency on glycolysis

Considering the *SF3B1*^{R625G}-induced dysregulation of proteins involved in metabolism, we conducted a functional evaluation of the metabolic features in *SF3B1*^{WT} and *SF3B1*^{R625G} Mel202 cells. As shown in Figure 4A, *SF3B1*^{R625G} cells display a low basal protein expression of PHGDH as compared to *SF3B1*^{WT} cells, which validates the LC-MS/MS findings. PHGDH is essential to generate carbon units from serine and glycine (SG). When deprived of SG for 4 days, *SF3B1*^{WT} and *SF3B1*^{R625G} cells display a viability decrease by 37% and 58%, respectively, indicating higher dependency of *SF3B1*^{R625G} cells on SG as compared to *SF3B1*^{WT} cells (Figure 4B).

Additionally, we show that G6PD (Glucose-6-phosphate dehydrogenase), the key enzyme catalyzing the first step in the oxidative branch of the pentose phosphate pathway (PPP), is decreased in *SF3B1*^{R625G} as compared to *SF3B1*^{WT} cells. This finding is consistent with the under-representation of PGD (6-phosphogluconate dehydrogenase) detected by LC-MS/MS. PGD catalyzes the formation of ribulose 5-phosphate that can be converted into ribose 5-phosphate and be used for nucleotide synthesis. Thus, the underexpression of the initial PPP enzyme G6PD together with the under-representation of the enzyme PGD imply a decreased rate of PPP in *SF3B1*^{R625G} cells. Although PPP is one of the main sources of NADPH used to scavenge ROS (Reactive Oxygen Species) (Dubreuil et al., 2020), we found comparable ROS levels in *SF3B1*^{WT} and *SF3B1*^{R625G} cells (Supplementary Figures 2A and 2B). The expression levels of LDHA (lactate dehydrogenase A) which catalyzes the conversion of pyruvate to

lactate on the last step of glycolysis (Ooi and Gomperts, 2015), were also comparable in *SF3B1*^{WT} and *SF3B1*^{R625G} cells (Figure 4A).

PDH (Pyruvate Dehydrogenase) catalyzes the conversion of pyruvate to acetyl CoA thus connecting the citric acid cycle and subsequent oxidative phosphorylation (OXPHOS) to glycolysis, gluconeogenesis and lipid and amino acid metabolism pathways. Our results show that the amount of total PDH is reduced in *SF3B1*^{R625G} cells as compared to *SF3B1*^{WT} cells, suggesting functional impairment of PDH in *SF3B1*^{R625G} cells (Figure 4A).

In line with our findings on *SF3B1*^{R625G}-induced missplicing of UQCC1 and UQCC2 and low abundance of OXPHOS proteins, immunoblotting analysis showed a decreased expression of OXPHOS complexes in *SF3B1*^{R625G} cells as compared to *SF3B1*^{WT} cells. A further decrease in the expression of complexes I, III, IV and V was observed in *SF3B1*^{WT} cells after SG deprivation, while the expression was maintained in *SF3B1*^{R625G} cells (Figure 4A).

Considering these mitochondrial defects in *SF3B1*^{R625G} cells, we investigated whether cell reliance on OXPHOS to generate ATP is increased in *SF3B1*^{R625G} cells. Cells grown in media rich in glucose rely on glycolysis and are less affected by mitochondrial defects. We therefore replaced glucose (Glc) with galactose (Gal) in cell culture media to increase cell reliance on OXPHOS to meet the energy demand. At 4 days, the growth of *SF3B1*^{WT} and *SF3B1*^{R625G} cells decreased by 63% and 77%, respectively, implying that *SF3B1*^{R625G} accentuates the cell reliance on glycolysis (Figure 4B).

To further comprehend the observed glycolysis dependency in *SF3B1*^{R625G} cells, we assessed mitochondrial respiration and glycolysis by measuring the oxygen consumption rate (OCR) and ECAR of *SF3B1*^{WT} and *SF3B1*^{R625G} cells with a Seahorse XF96 Analyzer. We found that both minimal and maximal cellular OCR were significantly decreased in *SF3B1*^{R625G} cells as compared to *SF3B1*^{WT} cells in glucose rich conditions. These results were also confirmed with further isogenic cell models of *SF3B1*^{G742D}-HAP1 and *SF3B1*^{K666T}-HEK293T cell lines (Supplementary Figures 3A and 3B). The decreased respiration can be explained by the underexpression of OXPHOS complexes in *SF3B1*^{R625G} cells (Figures 4A and 5A). Of note, this decrease in OCR was not associated with a decrease of mitochondrial content as comparable levels were observed in *SF3B1*^{WT} and *SF3B1*^{R625G} cells (Supplementary Figures 2A and 2C). On the other hand, we observed no significant alteration in minimal and maximal ECAR, which is in line with the unaltered LDHA expression (Figures 4A and 5B). Taken together, our results indicate

that *SF3B1* mutations trigger a decrease in mitochondrial respiration capacity thus reshaping cell metabolism.

We further investigated whether *SF3B1*^{R625G} cells are more dependent on early glycolysis to compensate for the decreased mitochondrial respiration. Strikingly, glucose uptake assessment revealed that *SF3B1*^{R625G} cells display an increase of 40% of glucose uptake as compared to *SF3B1*^{WT} cells (Figure 6A). This finding suggests that mutant SF3B1 increases glucose uptake to produce glycolytic intermediates needed to compensate for the impaired OXPHOS. To explore this feature, we inhibited early steps of glycolysis in *SF3B1*^{WT} and *SF3B1*^{R625G} Mel202 cells with PFK158, a PFKFB3 (6-phosphofructo-2-kinase/fructose-2,6-biphosphate 3) inhibitor. As shown in Figure 6A, PFK158 induced a decrease of glucose uptake in both *SF3B1*^{WT} and *SF3B1*^{R625G} Mel202 cells (Figure 6A). Interestingly, *SF3B1*^{WT} cells exhibited IC_{50} values of 2.4 and 2.1 µM at 48 and 72 hours of treatment while *SF3B1*^{R625G} cells displayed IC_{50} values of 1.7 and 1.5 µM at 48 and 72 hours of treatment, respectively (Figure 6B). Increased sensitivity to PFK158 was also observed in *SF3B1*^{G742D} and *SF3B1*^{K666T} cells as compared to *SF3B1*^{WT} cells (Supplementary Figures 4A and 4B). These findings denote that cells mutated for *SF3B1* are more sensitive to glycolysis inhibition than *SF3B1*^{WT} cells.

Discussion

SF3B1 missense mutations are recurrent in several cancers including UM. Mutant SF3B1 corrupts the 3' ss recognition leading to the formation of aberrant transcripts. The molecular mechanism by which mutant SF3B1 induces the aberrant splice pattern has been well characterized (Alsafadi et al., 2016; Darman et al., 2015; DeBoever et al., 2015), yet little is known about its consequent downstream impact and functional involvement. Here, we provide a comprehensive study to elucidate the fate of aberrant transcripts induced by mutant SF3B1 in UM cells. We investigated the impact of *SF3B1*^{R625G} in Mel202 isogenic cell model at different molecular levels: transcription, nascent protein synthesis, protein abundance, translation and metabolism.

Our transcriptomic analysis showed that mutant SF3B1 poorly impairs global gene expression. We found that most *SF3B1*^{R625G}-induced splice aberrations do not affect mRNA expression levels. Restricted impact of the aberrant splicing on mRNA expression levels has also been reported in previous studies (Dalton et al., 2019; Shiozawa et al., 2018). Of note, mRNA expression dysregulations associated with splice aberrations can be due to NMD, altered splicing efficiency or impaired export of aberrant transcripts (Dalton et al., 2019; Shiozawa et al., 2018).

At the proteomic level, analysis of nascent protein synthesis did not reveal any major impairment in *SF3B1*^{R625G} cells, implying no impact of mutant SF3B1 on global translation efficiency. However, polysome profiling of *SF3B1*^{R625G} cells revealed target-specific translational alterations. We found that 65% of aberrantly-spliced transcripts induced by mutant SF3B1 were less translated than their corresponding canonically-spliced transcripts, while 35% were more translated. This second group (*i.e.* 35%) corresponded to genes enriched for metabolic functions, including carbon metabolism and metabolic pathways. Moreover, quantitative LC-MS/MS analysis showed an altered abundance of metabolic proteins in *SF3B1*^{R625G} cells. Notably, UQCC1 and UQCC2, needed for the assembly of the complex III of the mitochondrial respiratory chain, were less abundant in *SF3B1*^{R625G} cells as compared to *SF3B1*^{WT} cells. PHGDH, which is involved in the *de novo* synthesis of serine, and OXPHOS were also under-represented. Interestingly, *UQCC1*, *UQCC2* and *PHGDH* are aberrantly-spliced by mutant SF3B1, implying that the splicing aberrations of these genes may be at the origin of the protein reduced expression. To explore the impact of such dysregulation of metabolic proteins, we characterized the related metabolic functions in *SF3B1*^{R625G} as compared to *SF3B1*^{WT} Mel202 cells. Our results reveal a reduced rate of mitochondrial respiration in *SF3B1*^{R625G} cells, which is consistent with the observed low abundance of proteins of the electron transport chain.

Given that PHGDH catalyzes the first step of SG synthesis, we evaluated the cell vulnerability to SG starvation and showed that *SF3B1*^{R625G} cells are more dependent of SG than *SF3B1*^{WT} cells. Of note, SG dependency has been reported in cancer and SG deprivation and PHGDH inhibition have been shown to reduce tumor growth (Reid et al., 2018; Tajan et al., 2021). Moreover, *SF3B1* hotspot mutations on codons K700, K666, H662 have been described to induce dysregulation of metabolic enzymes including PHGDH in acute myeloid leukemia and breast cancer cells, leading to increased dependency on serine (Brian Dalton et al., 2020; Dalton et al., 2019). Our study extends these findings to *SF3B1*^{R625G} hotspot mutation in UM cells. Furthermore, our results reveal an increased glucose dependency of *SF3B1*^{R625G} cells as compared to *SF3B1*^{WT} cells. In fact, cells mutated for *SF3B1* display a higher capacity of glucose uptake and are more sensitive to glucose deprivation than *SF3B1*^{WT} cells. This finding suggests that *SF3B1*^{R625G} cells trigger a metabolic switch towards glycolysis to compensate for their mitochondrial defects, a common feature of tumoral transformation (Warburg, 1925). OXPHOS is the preferable source of ATP for normal cells while cancer cells have the capacity to switch to early glycolysis. These results suggest that cells harboring *SF3B1* mutations tend to be addicted to glucose. Accordingly, our results show that cells mutated for *SF3B1* display an increased sensitivity to PFK158, a glycolysis inhibitor, as compared to *SF3B1*^{WT} cells.

Overall, we provide a comprehensive molecular study of mutant SF3B1 in UM cells. We demonstrate that mutant SF3B1 decreases mitochondrial respiration, promoting dependency on glycolysis and sensitizing cells to glycolysis inhibition. Our study sheds light on the oncogenic involvement of mutant SF3B1 through a metabolic switch towards a highly glycolytic metabolism. These findings offer new therapeutic perspectives to target mutant SF3B1 tumors by glycolysis inhibitors or dietary restrictions.

Acknowledgments:

We thank Dr. Sebastien Apcher (Gustave Roussy Institute) for the helpful discussions and for reviewing the manuscript. We acknowledge the Mass Spectrometry and Proteomics, Cytometry and Genomics Facilities at Institut Curie's Research Centre, and the valuable technical assistance of Valentin Sabatet, David Gentien, Aude Vieillefon and Virginie Raynal. This research was funded by the European Union's Horizon 2020 research and innovation programme (Marie Skłodowska-Curie grant agreement No 666003), the European Union's Horizon 2020 project "UM Cure 2020" (Grant No 667787)

and SIRIC Curie (Grant INCa-DGOS-Inserm_12554). This work benefits also from the financial support of the *Ligue Nationale Contre le Cancer* (Grant No 20117 and group labellisation), "*Région Ile-de-France*" and "*Fondation pour la Recherche Médicale*".

Author Contributions

RVN, MHS, SRR, SA designed the study. RVN, MT, CC, SD, LS, SM, LG, BL conducted the experiments and collected data. RVN, MT, AH, SA analyzed the data. VM, GG, DL, FN, SR, VS, SV reviewed the experiments and contributed to the data interpretation. RVN and SA wrote the manuscript. All authors have reviewed and approved the manuscript.

Competing Interests

Authors declare no competing interests in relation to this work.

Figure legends

Figure 1. *SF3B1*^{R625G}-induced splicing aberrations in *SF3B1*^{WT} *and SF3B1*^{R625G} isogenic Mel202 cells are not associated with a major transcriptional dysregulation.

A) Heatmap validation of the aberrant splice pattern induced by *SF3B1* mutations reported in previous studies (Alsafadi et al., 2016; Darman et al., 2015) in the established isogenic *SF3B1*^{WT} and *SF3B1*^{R625G} Mel202 model. A total of 1,445 splice junctions are differentially-expressed upon *SF3B1*^{R625G} mutation. R1 and R2 are two independent replicates. **B)** Heatmap analysis of the differentially-expressed genes according to *SF3B1* mutational status. A total of 181 genes were differentially-expressed upon *SF3B1*^{R625G} mutation. **C)** Volcano plot of the differential gene expression in *SF3B1*^{R625G} cells as compared to *SF3B1*^{WT} cells. Y-axis represents the adjusted p-value and the x-axis displays the $\log_2$ fold-change ($\log_2$FC). The $\log_2$FC threshold is ±1 and significantly upregulated or downregulated genes are colored in green (p-value $<10^{-4}$). **D)** Functional enrichment analysis of biological processes and KEGG pathways of the differentially-expressed genes. Left-axis corresponds to the bars that represent the gene counts and the right-axis corresponds to the dots that display the p-values. Only significant biological processes and pathways are included ($p<0.05$). **E)** Venn diagram of the differentially-expressed (downregulated and upregulated) and aberrantly-spliced gene counts, indicating an overlap of 8.3% of differentially-expressed genes (n=15/181 in total; n=3 downregulated and n=12 upregulated) with the aberrantly-spliced genes. **F)** mRNA differential expression represented as $\log_2$FC(gene expression in *SF3B1*^{R625G} cells/ gene expression in *SF3B1*^{WT} cells) is plotted on the y-axis according to the splice category of genes on the x-axis; canonically-spliced genes (genes with no splice aberrations), genes with predicted NMD-sensitive aberrant splice junctions, and genes with predicted NMD-insensitive aberrant splice junctions.

Figure 2. Impact of *SF3B1*^{R625G} on nascent protein synthesis and translation fate of the *SF3B1*^{R625G}-induced splicing transcripts.

A) Nascent protein synthesis in *SF3B1*^{WT} and *SF3B1*^{R625G} Mel202 cells by Click-iT L-azidohomoalanine (AHA) labeling. Cells were starved of methionine for 1 hour and incubated with AHA for 3 hours. Lysates underwent a Click-iT reaction in which azide tags reacted with alkyne-biotin and biotin was visualized by immunoblotting. Cycloheximide-treated (CHX) cell lysates were used as a control of protein synthesis inhibition. β-actin was immunoblotted as a control of protein quantity. **B)** Polysome

profiles of the *SF3B1*^{WT} (blue) and *SF3B1*^{R625G} (orange) Mel202 cells. The sequenced samples are highlighted (pooled monosome fractions 2-8; and pooled polysome fractions 9-14). The sucrose gradient 15-50% of sample fractioning is displayed. **C)** The aberrant splice index (aberrantly-spliced transcript/canonical transcript) obtained by RT-qPCR for the *SF3B1*^{R625G}-sensitive genes *DPH5* and *ARMC9* is plotted for each fraction from *SF3B1*^{WT} (blue) and *SF3B1*^{R625G} (orange) Mel202 cells. **D)** The log_2FC(normalized expression in polysome fractions/ normalized expression in monosome fractions) of the SF3B1^{R625G} cells as determined by RNA-seq is plotted for each aberrantly-spliced transcript (p-values ≤ 10^{-5}). The aberrantly-spliced transcripts with positive log_2FC values (group A) are relatively more translated than their corresponding canonically-spliced transcripts, while those with negative log_2FC values (group B) are less translated than their corresponding canonically-spliced transcripts. *ARMC9* and *DPH5* are highlighted. **E)** The log_2FC(normalized expression in polysome fractions/ normalized expression in monosome fractions) of the aberrant splice transcripts is plotted according to the impaired STAR motif (CT/AC, CT/GC, GC/AG and GT/AG). **F)** KEGG pathways enrichment analysis of the translated aberrantly-spliced transcripts (group A) identified by polysome profiling (Figure 2D). Enriched KEGG pathways are represented against the minus log p-value. Only significant splice transcripts are displayed (p-value ≤ 10^{-5}).

Figure 3. *SF3B1*^{R625G} impact on protein abundance.

A) Differential protein abundance analysis obtained by using quantitative label-free LC-MS/MS analysis. The volcano plot illustrates the differentially abundant proteins. The minus log p-value is plotted against the log_2FC of protein expression (*SF3B1*^{R625G} *versus* *SF3B1*^{WT}). Proteins with at least 3 detected peptides in all replicates (n=3) are displayed, absolute fold change ≥1.2 and p-value ≤0.05 are considered as significantly dysregulated. External plots show proteins with peptides identified only in one condition (left in *SF3B1*^{WT} and right in *SF3B1*^{R625G}). **B)** Venn diagram showing a restricted overlap between the differentially-abundant proteins (under-represented and over-represented) and the aberrantly-spliced genes. A total of 8.8% aberrantly-spliced genes (n=128/1,445) display dysregulated protein levels (n=88 under-represented proteins and n=40 over-represented proteins). **C)** Log_2FC of protein expression (*SF3B1*^{R625G} *versus SF3B1*^{WT}) is plotted on the x-axis according to the splice category; canonically-spliced genes (genes with no splice aberrations), genes with predicted NMD-sensitive aberrant splice junctions, and genes with predicted NMD-insensitive aberrant splice junctions. **D)** Overlap between differentially-abundant proteins and differentially-expressed genes

shown by Venn diagram. A total of 7.2% of differentially-abundant proteins are encoded by differentially-expressed genes (n=13/181; n=3 under-represented and n=10 over-represented).

Figure 4. *SF3B1*^{R625G} leads to a decreased expression of metabolic proteins and sensitizes cells to serine, glycine and glucose deprivation.

A) Expression of metabolic targets involved in serine *de novo* synthesis, PPP (pentose phosphate pathway), glycolysis and OXPHOS (oxidative phosphorylation) upon 3 days media deprivation in *SF3B1*^{WT} and *SF3B1*^{R625G} isogenic Mel202 cells by Western Blot. β-actin was immunoblotted as a control of protein quantity. **B)** Cell viability of *SF3B1*^{WT} and *SF3B1*^{R625G} Mel202 cells upon media starvation (Gal: galactose, Glc: glucose, and SG: serine and glycine). Complete media condition was also included (+Glc+SG). Data are represented as the mean of triplicates ± SD.

Figure 5. *SF3B1*^{R625G} triggers a decrease of mitochondrial respiration.

A) Oxygen consumption rate (OCR) of *SF3B1*^{WT} (blue) and *SF3B1*^{R625G} (orange) isogenic Mel202 cells as measured by Seahorse XF96 Analyzer. Minimal and maximal OCR are also displayed. **B)** Extracellular acidification rate (ECAR) of *SF3B1*^{WT} (blue) and *SF3B1*^{R625G} (orange) isogenic Mel202 cells as measured by Seahorse XF96 Analyzer. Minimal and maximal ECAR are also plotted.

Figure 6. *SF3B1*^{R625G} induces an increase of glycolytic rate thus sensitizing cells to glycolysis inhibition.

A) Glucose uptake rate per cell in *SF3B1*^{WT} (blue) *and SF3B1*^{R625G} (orange) isogenic Mel202 cells without or with treatment with PFK158 at 1.6 µM for 3 days. Paired *t*-test was used to generate the *p*-values comparing each condition to the untreated *SF3B1*^{WT} cells; $^{**}p < 0.005$; NS: non-significant. **B)** Cell viability of *SF3B1*^{WT} (blue) *and SF3B1*^{R625G} (orange) Mel202 cells upon treatment with PFK158 at 48 and 72 hours. Data are represented as the mean of triplicates ± SD.

STAR Methods

Cell model development and maintenance. Mel202 cell line was obtained from the European Searchable Tumour Line Database (Tubingen, University, Germany). A destabilizing domain (DD) tag derived from human FKBP12 was inserted by CRISPR/Cas9 at the endogenous R625G-SF3B1 protein in Mel202 following the previously reported Degron-KI system (Zhou et al., 2015). DD insertion leads to the degradation of the endogenous mutant SF3B1 protein resulting in a WT phenotype. Both *SF3B1*^{WT} and *SF3B1*^{R625G} Mel202 cells were cultured with RPMI-1640 supplemented with 10% fetal bovine serum (FBS). A point mutation in *SF3B1* leading to a G742D amino-acid substitution was inserted in HAP1 cell line using the Lipofectamine™ CRISPRMAX™ Cas9 Transfection Reagent (CMAX00008, Invitrogen) following the manufacturer's instructions. Selection of resistant clones, single cell dilution and subsequent Sanger sequencing of the monoclonal cell colonies were carried out to screen for a cell clone with the intended deletion and to obtain the isogenic cell line. Isogenic HEK293T cell model harboring *SF3B1*^{K666T} was generated by CRISPR/Cas9 as previously described (Alsafadi et al., 2016). HAP1 and HEK293T cell lines were cultured with DMEM supplemented with 10% FBS. The mutational status of all cell lines was verified by Sanger sequencing and RNA-seq.

RNA-seq analysis. Differential splice junction and gene expression analysis was carried out as previously described (Alsafadi et al., 2016).

Analysis of nascent protein synthesis. *SF3B1*^{WT} and *SF3B1*^{R625G} Mel202 cells were plated on 6-well plates ($1x10^6$ cells/well) and incubated overnight until a 70-80% confluency was achieved. Before labeling, cells were incubated with a methionine-free RPMI medium supplemented with 2% FBS for 1 hour. Then, 50 µM of Click-IT AHA Reagent (L-Azidohomoalanine from Invitrogen C101102) was added to the cells and incubated for 4 hours. Cells were then washed three times with PBS and lysis buffer (1% SDS in 50 mM Tris-HCl pH 8) was added and incubated for 30 minutes on ice. Cells were sonicated and the protein concentration of the lysates was measured. Equivalent amounts of protein lysates underwent Click-It reaction using the kit (Click-iT™ Protein Reaction Buffer Kit Invitrogen C10276) according to the manufacturer's protocol. Briefly, the Click-iT reaction occurs between the azido-incorporated nascent proteins and the alkyne-biotin (PEG4 carboxamide-propargyl biotin from Invitrogen B10187). Biotinylated nascent proteins were immunoblotted against anti-biotin and β-actin (Cell Signaling #5597 and #3700 respectively) antibodies.

Isolation of polysome fractions, RNA extraction and sequencing. Cells were plated in 15-cm Petri dishes and incubated overnight until a 60-70% confluency was obtained. A total number of 30 million cells were obtained per cell line. Cells were then treated with 100 µg/ml of cycloheximide (CHX) and incubated at 37ºC, 5% CO_2 for 15 minutes. Cells were washed with PBS containing CHX and pelleted down. Cells were lysed with a lysis buffer containing 20 mM Tris pH 7.5, 100 mM NaCl, 3 mM MgCl2 and fresh 1 mM DTT, 100 U/mL RNAsine and 100 µg/ml CHX. Cell lysates were centrifuged and loaded onto a sucrose gradient of 15-50% and ultracentrifuged in a rotor SW41 Ti. The resulting samples were then separated by the fractioning system (Brandel/Teledyne ISCO) equipped with a spectrophotometer to monitor absorbance at 260 nm. RNA was extracted from polysomal fractions with a phenol:guanidine isothiocyanate monophasic solution with TRIZOL LS following standard protocols. For polysome sequencing, two replicates were sequenced for each condition. Monosome-like samples consisted of RNA extracted from fractions 2-8, while polysome-like samples included RNA extracted from fractions 9-14.

Proteomics and quantitative mass spectrometry analysis. *Sample preparation* - *SF3B1*^{WT} and *SF3B1*^{R625G} Mel202 cells were plated on 6 well-plates (500,000 cells/well). Once attached, cells were washed with PBS and pelleted down. Cell pellets were lysed with a cell lysis buffer supplemented with inhibitor phosphatase 1X and protease inhibitor for incubation in ice for 45 minutes. Cell lysates were centrifuged and supernatants were solubilized in 8 M urea and 50 mM NH4HCO3. After dilution to a final concentration of 1M urea, proteins were reduced by incubation with 5 mM dithiothreitol (DTT) at 57 °C for one hour and then alkylated with 9 mM iodoacetamide for 30 min at room temperature in the dark. Trypsin/LysC (Promega) was added at 1:100 (wt:wt) enzyme:substrate. Digestion was allowed to proceed overnight at 37 °C. Samples were then loaded onto a homemade C18 StageTips for desalting. Peptides were eluted from beads by incubation with 40/60 MeCN/H2O + 0.1% formic acid. The peptides were dried in a Speedvac and reconstituted in 2/98 MeCN/H2O + 0.3% trifluoroacetic acid (TFA) prior to liquid chromatography-tandem mass spectrometry (LC-MS/MS) analysis. Samples were added in triplicates. *LC-MS/MS analysis* - Samples were chromatographically separated using an RSLCnano system (Ultimate 3000, Thermo Scientific) coupled online to a Q Exactive HF-X with a Nanosrpay Flex ion source (Thermo Scientific). Peptides were first loaded onto a C18-reversed-phase precolumn (75 µm inner diameter × 2 cm; nanoViper Acclaim PepMapTM 100, Thermo Scientific), with buffer A (2/98 MeCN/H2O + 0.1% formic acid) at a flow rate of 2.5 µL/min over 4 min and then switched for separation to an analytical column (75 µm inner diameter × 50 cm; nanoViper C18, 2 µm, 100Å,

Acclaim PepMap™ RSLC, Thermo Scientific) regulated to a temperature of 50 °C with a linear gradient of 2% to 35% buffer B (100% MeCN and 0.1% formic acid) at a flow rate of 300 nL/min over 211 min. MS full scans were performed in the ultrahigh-field Orbitrap mass analyzer in ranges m/z 375–1500 with a resolution of 120,000 at m/z 200, the maximum injection time (MIT) was 50 ms and the automatic gain control (AGC) was set to 3×10^6. The top 20 intense ions were subjected to Orbitrap for further fragmentation via high energy collision dissociation (HCD) activation and a resolution of 15,000 with the intensity threshold kept at 3.2×10^5. We selected ions with charge state from 2+ to 6+ for screening. Normalized collision energy (NCE) was set at 27. For each scan, the AGC was set at 1×10^5, the MIT was 25 ms and the dynamic exclusion of 40s. *Data analysis* - For identification the data were searched against the human Swiss-Prot database (downloaded on 22/08/2017) using Sequest-HT through proteome discoverer (version 2.0). Enzyme specificity was set to trypsin and a maximum of two missed cleavage sites were allowed. Oxidized methionine, N-terminal acetylation, and carbamidomethyl cysteine were set as variable modifications. Maximum allowed mass deviation was set to 10 ppm for monoisotopic precursor ions and 0.02 Da for MS/MS peaks. The resulting files were further processed using myProMS v3.9.1 (Poullet et al., 2007). FDR calculation used Percolator (The et al., 2016) and was set to 1% at the peptide level for the whole study. The label-free quantification was performed by peptide Extracted Ion Chromatograms (XICs) computed with MassChroQ version 2.2.1 (Valot et al., 2011). For protein quantification, XICs from proteotypic peptides shared between compared conditions (TopN matching) with up to two missed cleavages and carbamidomethyl modifications were used. Median and scale normalization was applied on the total signal to correct the XICs for each biological replicate. To estimate the significance of the change in protein abundance, a linear model (adjusted on peptides and biological replicates) was performed and p-values were adjusted with a Benjamini–Hochberg FDR. Protein with at least three total peptides in all replicates (n=3), an absolute 1.2-fold enrichment and an adjusted p-value ≤ 0.05 were considered as significantly dysregulated in sample comparison. Unique proteins were considered with at least three total peptides in all replicates. Mass spectrometry proteomics data have been deposited to the ProteomeXchange Consortium via the PRIDE (Perez-Riverol et al., 2019) partner repository with the dataset identifier PXD022726. *Reviewer account details: Username: reviewer_pxd022726@ebi.ac.uk and Password: 9EvVx3dn.*

Measurement of respiration rate and extracellular acidification rate. Cells were plated on Seahorse XF96 Analyzer cell culture plates in regular culture media and incubated overnight at 37ºC with 5% CO_2 to assess the extracellular acidification rate

(ECAR) and oxygen consumption rate (OCR). After attachment (24h), the media was removed, cells were washed and media was replaced by unbuffered assay media at pH 7.4 for ECAR analysis, and unbuffered assay media at pH 7.4 containing 25 mM of glucose, 4 mM of glycine and 1 mM of pyruvate for OCR measurement. Cells were then incubated at 37ºC without CO_2 for 1 hour. Cell plates were loaded into the Seahorse machine and pH and oxygen levels were measured. *SF3B1*^{WT} and *SF3B1*^{G742D} HAP1 cells were injected with 1 µM oligomycin, 2 µM carbonyl cyanide-p-trifluoromethoxyphenylhydrazone (FCCP) and 2 µM rotenone/antimycin A. *SF3B1*^{WT} and *SF3B1*^{R625G} Mel202 cells and *SF3B1*^{WT} and *SF3B1*^{K666T} HEK293T cells were injected with 2 µM oligomycin, 2 µM FCCP and 2 µM rotenone/antimycin A. Further analysis was done with the Wave 2.6 software.

Mitochondrial content and ROS levels analysis. The mitochondrial content and ROS levels of *SF3B1*^{WT} and *SF3B1*^{R625G} Mel202 cells were assessed by staining with Mitotracker Red FM (Molecular Probes MM22425) and CellROX Green Reagent (Molecular Probes C10444), respectively. Cells were plated in 24-well plates and incubated overnight. Cells were incubated with either 250 nM of Mitotracker Red FM or 2 µM of CellROX Green Reagent for 30 minutes at 37 ºC. Cells were then washed with PBS, trypsinized and resuspended with a buffer of PBS with 2% FBS and 2mM EDTA for flow cytometric analysis. Flow cytometry data were acquired using a ZE5 cell analyzer (BioRad) and analyzed with FlowJo analysis software (FlowJo, LLC).

Viability assay. *C*ells were plated in 96 well-plates and incubated overnight to allow attachment. Cells were then treated with increasing concentrations of PFK158 (Selleckchem S8807) (0-5 µM) for 48 and 72 hours. Cell viability was assessed by Orangu colorimetric assay according to the manufacturer's instructions (OR01-500, Cell Guidance Systems) and incubated for 3 hours. Absorbance at 450 nm was read using TECAN-Spark microplate reader.

Glucose uptake assay. Glucose uptake was measured in cells following the manufacturer's recommendations (Glucose Uptake-Glo™ Assay Promega J1342). Cells were plated on 96 well-plates and treated with PFK158 for 72 hours. Cells were starved for glucose by preincubation with Krebs-Ringer-Phosphate-HEPES buffer containing 2% BSA for 40 min and washed with PBS. Next, 50 µl of 1 mM 2DG were added and incubated at RT for 20 minutes. After the addition of Stop Buffer and Neutralization Buffer, 2DG6P Detection Reagent was added and incubated for 2 hours. Luminescence was recorded at 0.5-second integration using TECAN-Spark microplate reader.

References

Alsafadi, S., Houy, A., Battistella, A., Popova, T., Wassef, M., Henry, E., Tirode, F., Constantinou, A., Piperno-Neumann, S., Roman-Roman, S., et al. (2016). Cancer-associated SF3B1 mutations affect alternative splicing by promoting alternative branchpoint usage. Nat. Commun. *7*.

Aviner, R., Hofmann, S., Elman, T., Shenoy, A., Geiger, T., Elkon, R., Ehrlich, M., and Elroy-Stein, O. (2017). Proteomic analysis of polyribosomes identifies splicing factors as potential regulators of translation during mitosis. Nucleic Acids Res. *45*, 5945–5957.

Bergot, T., Lippert, E., Douet-Guilbert, N., Commet, S., Corcos, L., and Bernard, D. (2020). Human cancer-associated mutations of SF3B1 lead to a splicing modification of its own RNA. Cancers (Basel). *12*, 1–16.

Brian Dalton, W., Helmenstine, E., Pieterse, L., Li, B., Gocke, C.D., Donaldson, J., Xiao, Z., Gondek, L.P., Ghiaur, G., Gojo, I., et al. (2020). The K666N mutation in SF3B1 is associated with increased progression of MDS and distinct RNA splicing. Blood Adv.

Canbezdi, C., Tarin, M., Houy, A., Bellanger, D., Popova, T., Stern, M.H., Roman-Roman, S., and Alsafadi, S. (2021). Functional and conformational impact of cancer-associated SF3B1 mutations depends on the position and the charge of amino acid substitution. Comput. Struct. Biotechnol. J. *19*, 1361–1370.

Dalton, W.B., Helmenstine, E., Walsh, N., Gondek, L.P., Kelkar, D.S., Read, A., Natrajan, R., Christenson, E.S., Roman, B., Das, S., et al. (2019). Hotspot SF3B1 mutations induce metabolic reprogramming and vulnerability to serine deprivation. J. Clin. Invest. *8*.

Darman, R.B., Seiler, M., Agrawal, A.A., Lim, K.H., Peng, S., Aird, D., Bailey, S.L., Bhavsar, E.B., Chan, B., Colla, S., et al. (2015). Cancer-Associated SF3B1 Hotspot Mutations Induce Cryptic 3' Splice Site Selection through Use of a Different Branch Point. Cell Rep.

DeBoever, C., Ghia, E.M., Shepard, P.J., Rassenti, L., Barrett, C.L., Jepsen, K., Jamieson, C.H.M., Carson, D., Kipps, T.J., and Frazer, K.A. (2015). Transcriptome Sequencing Reveals Potential Mechanism of Cryptic 3' Splice Site Selection in SF3B1-mutated Cancers. PLoS Comput. Biol. *11*, 1–19.

Dolatshad, H., Pellagatti, A., Fernandez-Mercado, M., Yip, B.H., Malcovati, L., Attwood, M., Przychodzen, B., Sahgal, N., Kanapin, A.A., Lockstone, H., et al. (2015). Disruption of SF3B1 results in deregulated expression and splicing of key genes and pathways in myelodysplastic syndrome hematopoietic stem and progenitor cells. Leukemia *29*, 1092–1103.

Dubreuil, M.M., Morgens, D.W., Okumoto, K., Honsho, M., Contrepois, K., Lee-McMullen, B., Traber, G.M.A., Sood, R.S., Dixon, S.J., Snyder, M.P., et al. (2020). Systematic Identification of Regulators of Oxidative Stress Reveals Non-canonical Roles for Peroxisomal Import and the Pentose Phosphate Pathway. Cell Rep. *30*, 1417-1433.e7.

Furney, S.J., Pedersen, M., Gentien, D., Dumont, A.G., Rapinat, A., Desjardins, L., Turajlic, S., Piperno-Neumann, S., de la Grange, P., Roman-Roman, S., et al. (2013). SF3B1 mutations are associated with alternative splicing in uveal melanoma. Cancer Discov.

Gökmen- Polar, Y., Neelamraju, Y., Goswami, C.P., Gu, Y., Gu, X., Nallamothu, G., Vieth, E., Janga, S.C., Ryan, M., and Badve, S.S. (2019). Splicing factor ESRP 1 controls ER - positive breast cancer by altering metabolic pathways . EMBO Rep. *20*, 1–19.

Harbour, J.W., Roberson, E.D.O., Anbunathan, H., Onken, M.D., Worley, L.A., and Bowcock, A.M. (2013). Recurrent mutations at codon 625 of the splicing factor SF3B1 in uveal melanoma. Nat. Genet.

Inoue, D., Chew, G.L., Liu, B., Michel, B.C., Pangallo, J., D'Avino, A.R., Hitchman, T., North, K., Lee, S.C.W., Bitner, L., et al. (2019). Spliceosomal disruption of the non-canonical BAF complex in cancer. Nature *574*, 432–436.

Lee, S.C., North, K., Kim, E., Jang, E., Lu, S.X., Liu, B., Inoue, D., Yoshimi, A., Ki, M., Zhang, X.J., et al. (2018). Synthetic Lethal and Convergent Biological Effects of Cancer-Associated Spliceosomal Gene Mutations. Cancer Cell *34*, 225–241.

Li, Z., Zhao, B., Yueru, S., Liang, Y., Qian, R., and Wan, Y. (2021). Characterization of the aberrant splicing of MAP3K7 induced by cancer-associated SF3B1 mutation. J. Biochem. *mvab023*.

Liu, Z., Yoshimi, A., Wang, J., Cho, H., Lee, S.C.W., Ki, M., Bitner, L., Chu, T., Shah, H., Liu, B., et al. (2020). Mutations in the RNA splicing factor SF3B1 promote tumorigenesis through MYC stabilization. Cancer Discov.

Malcovati, L., Karimi, M., Papaemmanuil, E., Ambaglio, I., Jädersten, M., Jansson, M., Elena, C., Gallì, A., Walldin, G., Della Porta, M.G., et al. (2015). SF3B1 mutation identifies a distinct subset of myelodysplastic syndrome with ring sideroblasts. Blood *126*, 223–241.

Maslon, M.M., Heras, S.R., Bellora, N., Eyras, E., and Cáceres, J.F. (2014). The translational landscape of the splicing factor SRSF1 and its role in mitosis. Elife *2014*, 1–27.

Michlewski, G., Sanford, J.R., and Cáceres, J.F. (2008). The Splicing Factor SF2/ASF Regulates Translation Initiation by Enhancing Phosphorylation of 4E-BP1. Mol. Cell *30*, 179–189.

Ooi, A.T., and Gomperts, B.N. (2015). Molecular Pathways: Targeting Cellular Energy Metabolism in Cancer via Inhibition of SLC2A1 and LDHA. Clin. Cancer Res. *21*, 2440 LP – 2444.

Palangat, M., Anastasakis, D., Liang, F., Lindblad, K.E., Bradley, R., Hourigan, C.S., Hafner, M., and Larson, D.R. (2018). The splicing factor U2AF1 contributes to cancer progression through a non-canonical role in translation regulation. BioRxiv *4*, 482–497.

Perez-Riverol, Y., Csordas, A., Bai, J., Bernal-Llinares, M., Hewapathirana, S., Kundu, D.J., Inuganti, A., Griss, J., Mayer, G., Eisenacher, M., et al. (2019). The PRIDE database and related tools and resources in 2019: improving support for quantification data. Nucleic Acids Res. *47*, D442–D450.

Poullet, P., Carpentier, S., and Barillot, E. (2007). myProMS, a web server for management and validation of mass spectrometry-based proteomic data. Proteomics *7*, 2553–2556.

Pozzo, F., Bittolo, T., Tissino, E., Vit, F., Vendramini, E., Laurenti, L., D'Arena, G., Olivieri, J., Pozzato, G., Zaja, F., et al. (2020). *SF3B1*-mutated chronic lymphocytic leukemia shows evidence of NOTCH1 pathway activation including CD20 downregulation. Haematologica *Online ahe*.

Quesada, V., Conde, L., Villamor, N., Ordóñez, G.R., Jares, P., Bassaganyas, L., Ramsay, A.J., Beà, S., Pinyol, M., Martínez-Trillos, A., et al. (2012). Exome sequencing identifies recurrent mutations of the splicing factor SF3B1 gene in chronic lymphocytic leukemia. Nat. Genet. *44*, 47–52.

Reid, M.A., Allen, A.E., Liu, S., Liberti, M. V., Liu, P., Liu, X., Dai, Z., Gao, X., Wang, Q., Liu, Y., et al. (2018). Serine synthesis through PHGDH coordinates nucleotide levels by maintaining central carbon metabolism. Nat. Commun. *9*, 1–11.

Sanford, J.R., Gray, N.K., Beckmann, K., and Cáceres, J.F. (2004). 2004A novel role for shuttling SR proteins in mRNA translation.Genes&development.pdf. 755–768.

Sen, S., Jumaa, H., and Webster, N.J.G. (2013). Splicing factor SRSF3 is crucial for hepatocyte differentiation and metabolic function. Nat. Commun. *4*.

Shiozawa, Y., Malcovati, L., Gallì, A., Sato-Otsubo, A., Kataoka, K., Sato, Y., Watatani, Y., Suzuki, H., Yoshizato, T., Yoshida, K., et al. (2018). Aberrant splicing and defective mRNA production induced by somatic spliceosome mutations in myelodysplasia. Nat. Commun. *9*.

Tajan, M., Hennequart, M., Cheung, E.C., Zani, F., Hock, A.K., Legrave, N., Maddocks, O.D.K., Ridgway, R.A., Athineos, D., Suárez-Bonnet, A., et al. (2021). Serine synthesis pathway inhibition cooperates with dietary serine and glycine limitation for cancer therapy. Nat. Commun. *12*, 1–16.

The, M., MacCoss, M.J., Noble, W.S., and Käll, L. (2016). Fast and Accurate Protein False Discovery Rates on Large-Scale Proteomics Data Sets with Percolator 3.0. J. Am. Soc. Mass Spectrom. *27*, 1719–1727.

Valot, B., Langella, O., Nano, E., and Zivy, M. (2011). MassChroQ: a versatile tool for mass spectrometry quantification. Proteomics *11*, 3572–3577.

Vivet-Noguer, R., Tarin, M., Roman-Roman, S., and Alsafadi, S. (2019). Emerging therapeutic opportunities based on current knowledge of uveal melanoma biology. Cancers (Basel).

Warburg, O. (1925). The metabolism of carcinoma cells 1. J. Cancer Res. *9*, 148–163.

Yoshida, K., Sanada, M., Shiraishi, Y., Nowak, D., Nagata, Y., Yamamoto, R., Sato, Y., Sato-Otsubo, A., Kon, A., Nagasaki, M., et al. (2011). Frequent pathway mutations of splicing machinery in myelodysplasia. Nature.

Zhao, B., Hu, X., Zhou, Y., Shi, Y., Qian, R., and Wan, Y. (2021). Characterization of the aberrant splicing of DVL2 induced by cancer-associated SF3B1 mutation. Biochem. Biophys. Res. Commun. *546*, 21–28.

Zhou, Q., Derti, A., Ruddy, D., Rakiec, D., Kao, I., Lira, M., Gibaja, V., Chan, H.M., Yang, Y., Min, J., et al. (2015). A chemical genetics approach for the functional assessment of novel cancer genes. Cancer Res. *75*, 1949–1958.

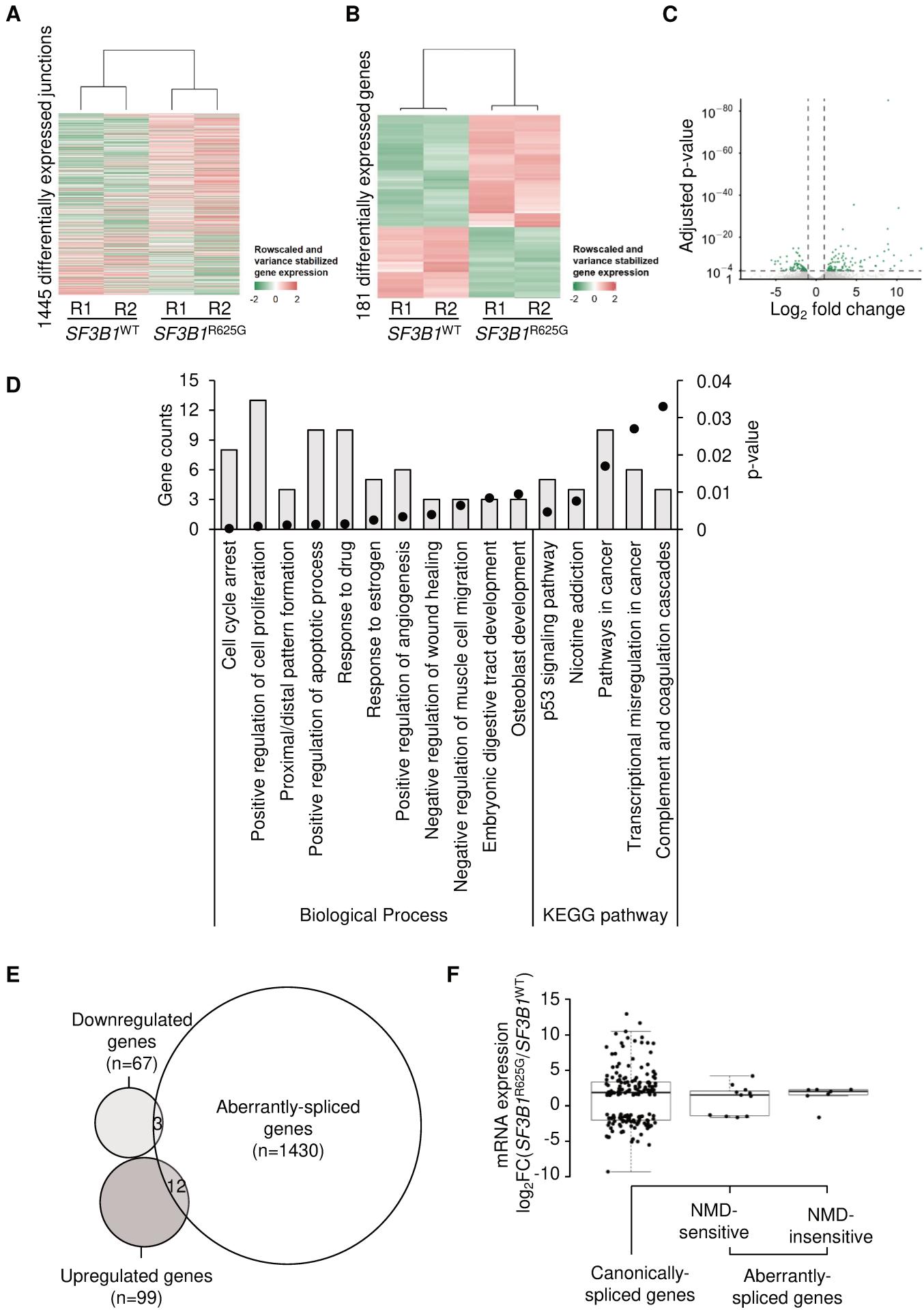
A
1445 differentially expressed junctions
R1
R2
R1
R2
SF3B1WT
SF3B1R625G
Rowscaled and variance stabilized gene expression
-2 0 2
B
181 differentially expressed genes
R1
R2
R1
R2
SF3B1WT
SF3B1R625G
Rowscaled and variance stabilized gene expression
-2 0 2
C
Adjusted p-value
10−80
10−60
10−40
10−20
10−4
1
-5 0 5 10
Log2 fold change
D
Gene counts
15
12
9
6
3
0
0.04
0.03
0.02
0.01
0
p-value
Cell cycle arrest
Positive regulation of cell proliferation
Proximal/distal pattern formation
Positive regulation of apoptotic process
Response to drug
Response to estrogen
Positive regulation of angiogenesis
Negative regulation of wound healing
Negative regulation of muscle cell migration
Embryonic digestive tract development
Osteoblast development
p53 signaling pathway
Nicotine addiction
Pathways in cancer
Transcriptional misregulation in cancer
Complement and coagulation cascades
Biological Process
KEGG pathway
E
Downregulated genes (n=67)
3
12
Aberrantly-spliced genes (n=1430)
Upregulated genes (n=99)
F
mRNA expression log2FC(SF3B1R625G/SF3B1WT)
15
10
5
0
-5
-10
NMD-sensitive
NMD-insensitive
Canonically-spliced genes
Aberrantly-spliced genes

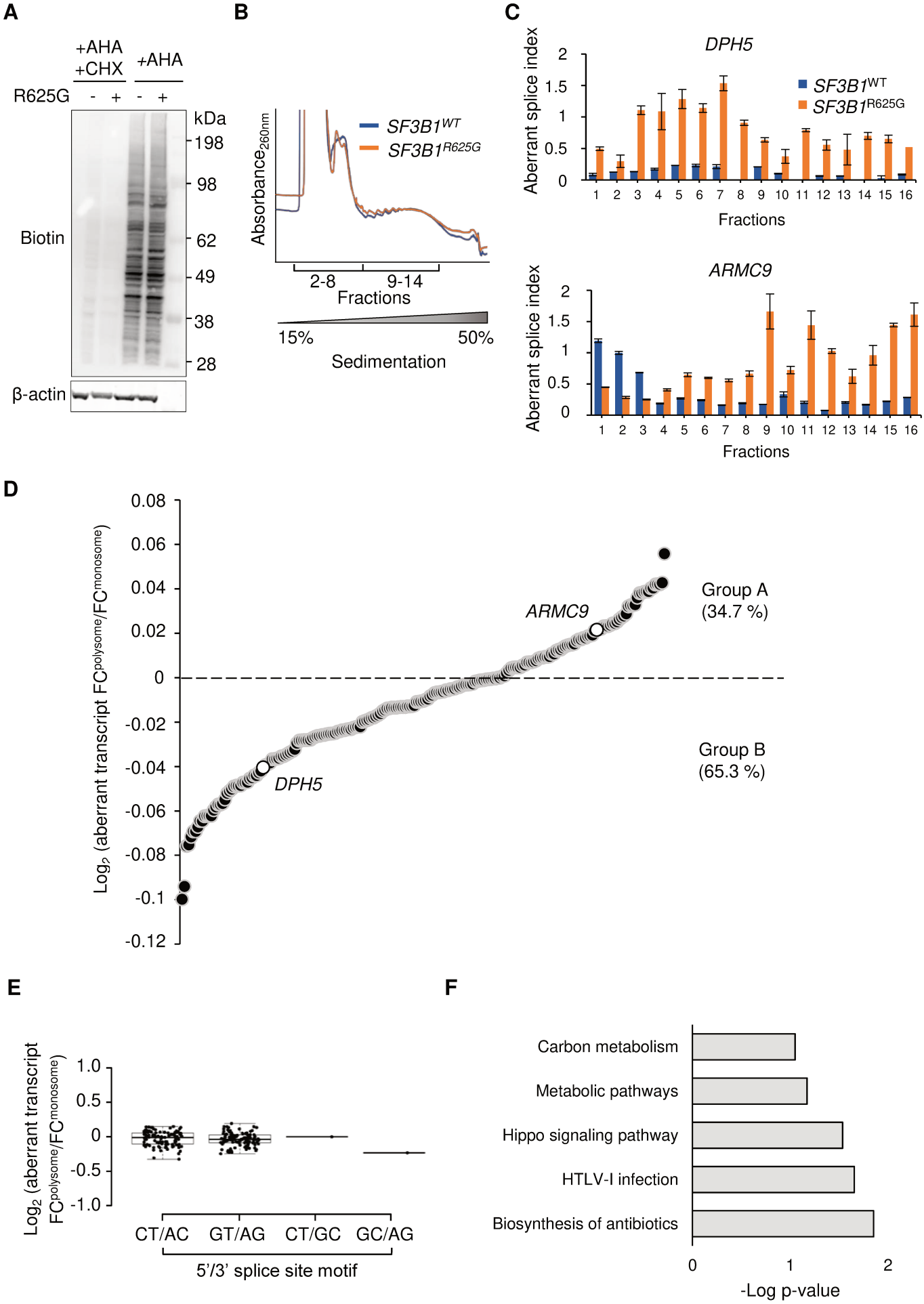
A
+AHA
+CHX
+AHA
R625G - + - +
kDa
198
98
62
49
38
28
Biotin
β-actin
B
Absorbance260nm
SF3B1WT
SF3B1R625G
2-8
9-14
Fractions
15%
50%
Sedimentation
C
DPH5
Aberrant splice index
SF3B1WT
SF3B1R625G
Fractions
ARMC9
Aberrant splice index
Fractions
D
Log2 (aberrant transcript FCpolysome/FCmonosome)
ARMC9
DPH5
Group A
(34.7 %)
Group B
(65.3 %)
E
Log2 (aberrant transcript FCpolysome/FCmonosome)
CT/AC
GT/AG
CT/GC
GC/AG
5'/3' splice site motif
F
Carbon metabolism
Metabolic pathways
Hippo signaling pathway
HTLV-I infection
Biosynthesis of antibiotics
-Log p-value

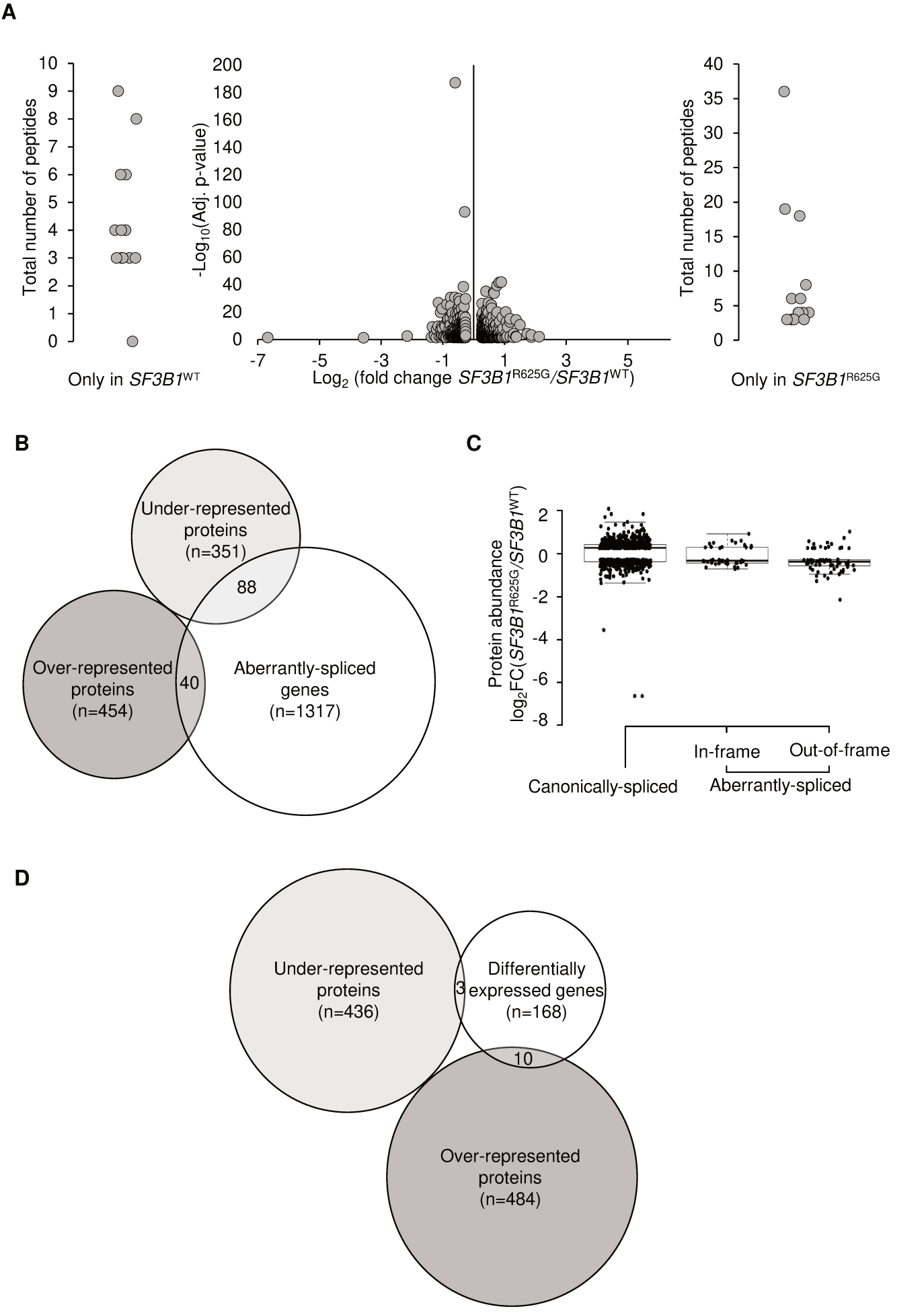
A
Total number of peptides
Only in SF3B1WT
-Log10(Adj. p-value)
Log2 (fold change SF3B1R625G/SF3B1WT)
Total number of peptides
Only in SF3B1R625G
B
Under-represented proteins (n=351)
88
Over-represented proteins (n=454)
40
Aberrantly-spliced genes (n=1317)
C
Protein abundance log2FC(SF3B1R625G/SF3B1WT)
In-frame
Out-of-frame
Canonically-spliced
Aberrantly-spliced
D
Under-represented proteins (n=436)
3
Differentially expressed genes (n=168)
10
Over-represented proteins (n=484)

A

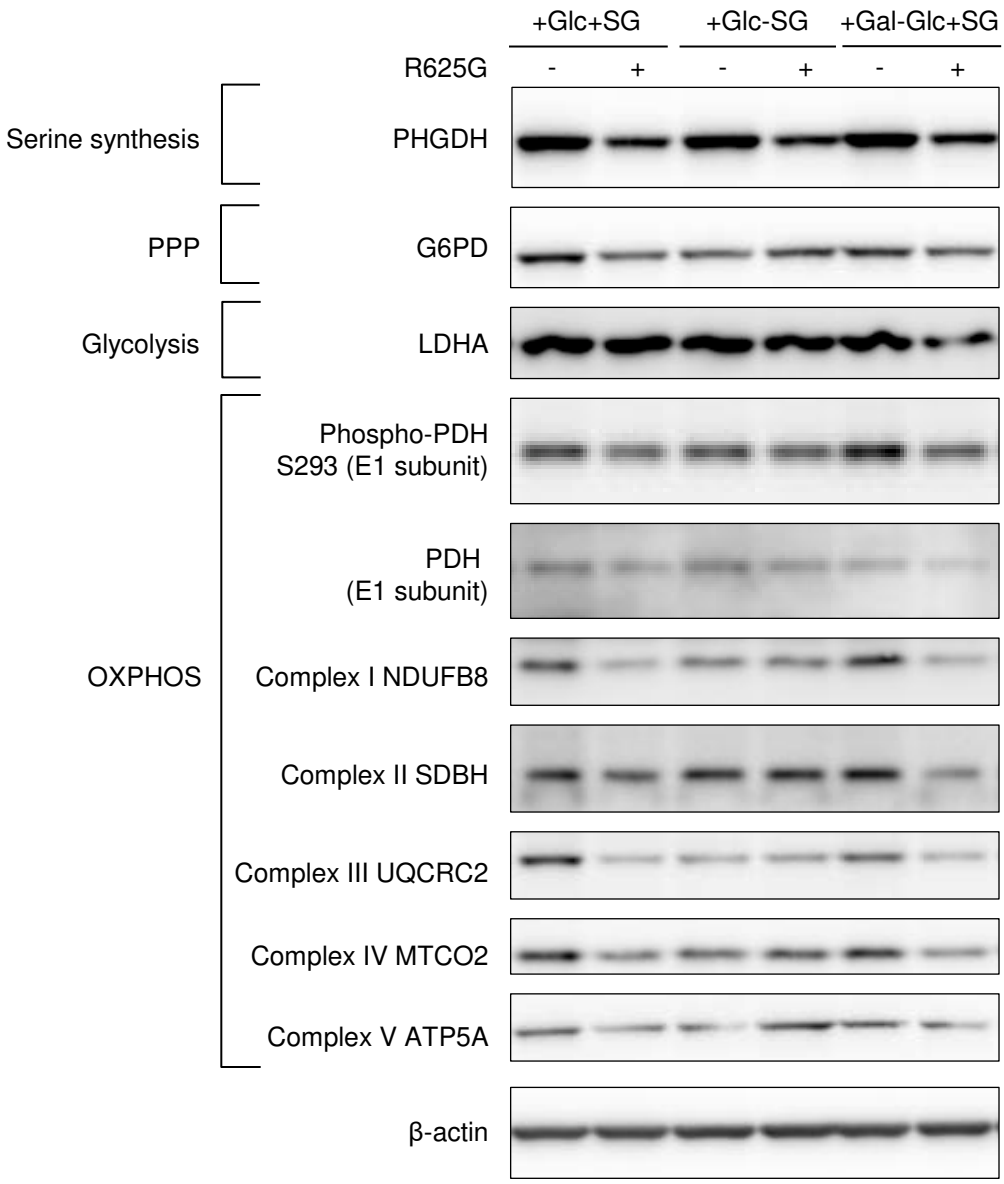
+Glc+SG
+Glc-SG
+Gal-Glc+SG
R625G
- + - + - +
Serine synthesis
PHGDH
PPP
G6PD
Glycolysis
LDHA
OXPHOS
Phospho-PDH S293 (E1 subunit)
PDH (E1 subunit)
Complex I NDUFB8
Complex II SDBH
Complex III UQCRC2
Complex IV MTCO2
Complex V ATP5A
β-actin

B

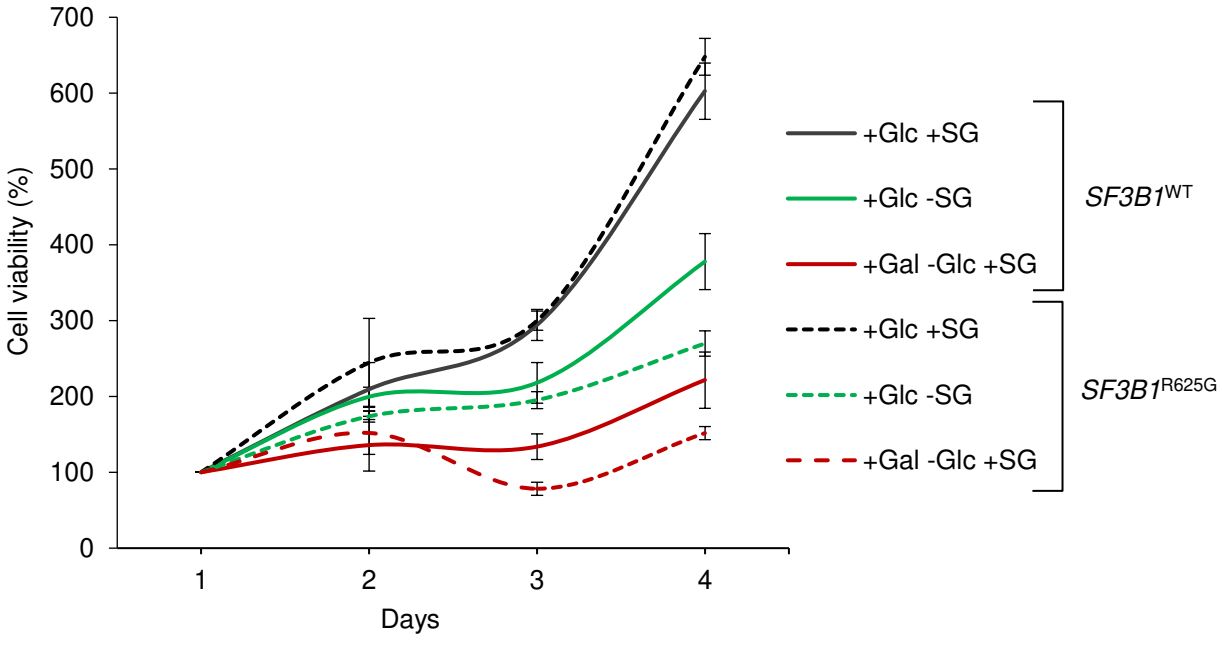
Cell viability (%)
700
600
500
400
300
200
100
0
1
2
3
4
Days
+Glc +SG
+Glc -SG
+Gal -Glc +SG
+Glc +SG
+Glc -SG
+Gal -Glc +SG
SF3B1WT
SF3B1R625G

A

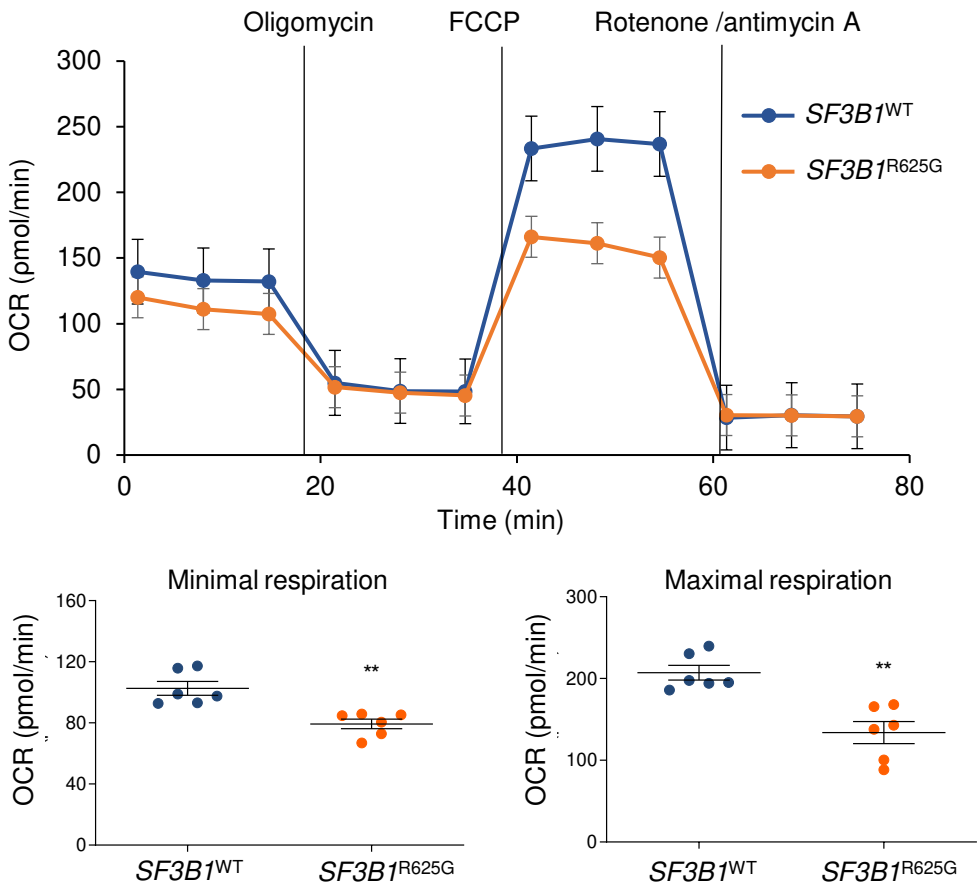
Oligomycin
FCCP
Rotenone /antimycin A
OCR (pmol/min)
Time (min)
SF3B1WT
SF3B1R625G
Minimal respiration
Maximal respiration
**
**

B

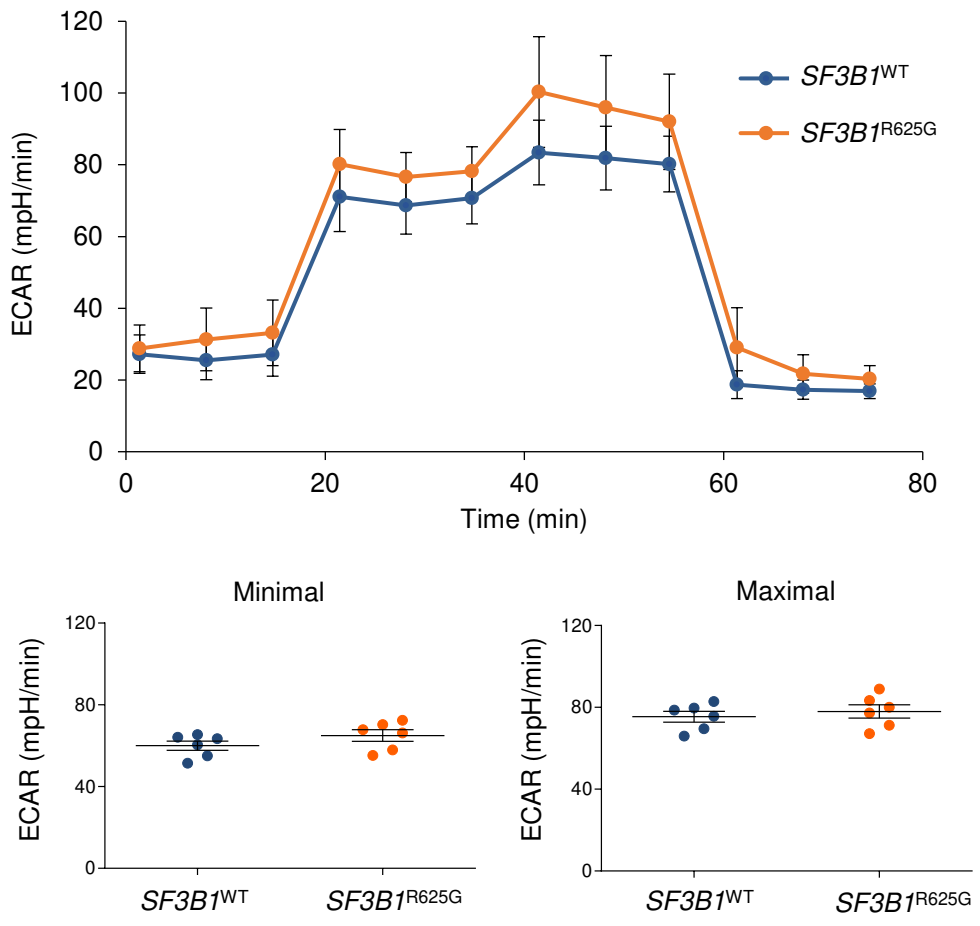
ECAR (mpH/min)
Time (min)
SF3B1WT
SF3B1R625G
Minimal
Maximal

A

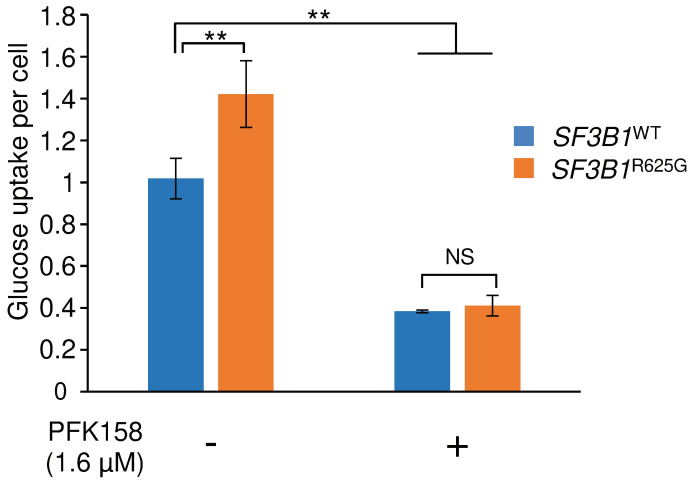
Glucose uptake per cell
1.8
1.6
1.4
1.2
1
0.8
0.6
0.4
0.2
0
**
**
NS
SF3B1WT
SF3B1R625G
PFK158
(1.6 µM)
-
+

B

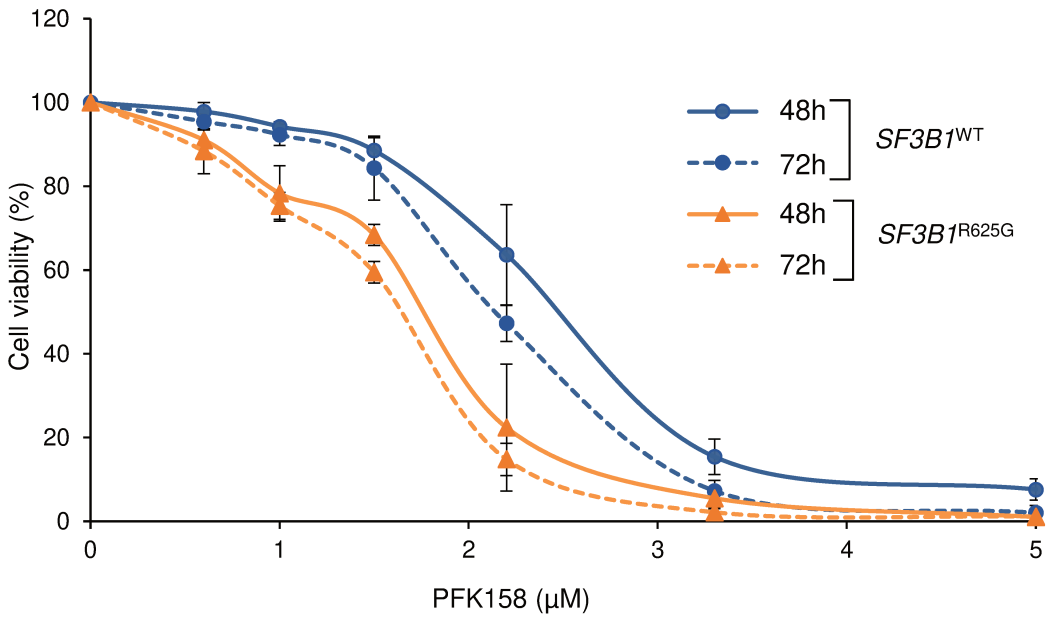
Cell viability (%)
120
100
80
60
40
20
0
0
1
2
3
4
5
PFK158 (µM)
48h
72h
SF3B1WT
48h
72h
SF3B1R625G

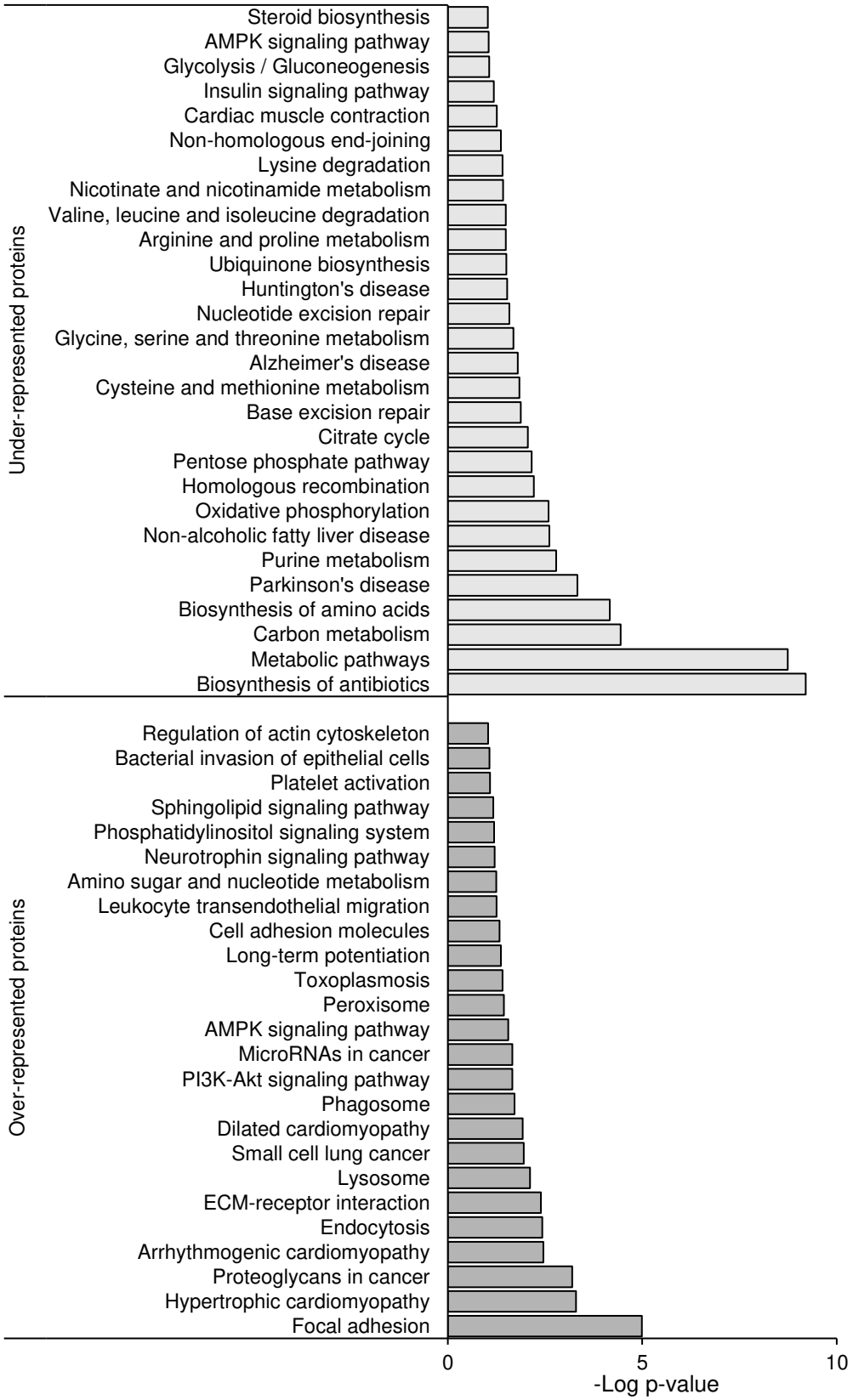

Supplementary Figure 1. Pathway enrichment of over-represented and under-represented proteins in *SF3B1*^{R625G} cells as compared to *SF3B1*^{WT} cells.

GO biological process enrichment analysis of the *SF3B1*^{R625G}-dysregulated proteins detected by quantitative LC-MS/MS (under-represented proteins in light grey and over-represented proteins in dark grey). Biological processes are represented against the minus log p-value. Only significantly dysregulated proteins were considered for the enrichment analysis ($log_2FC \geq |1.2|$ and p-value ≤ 0.05).

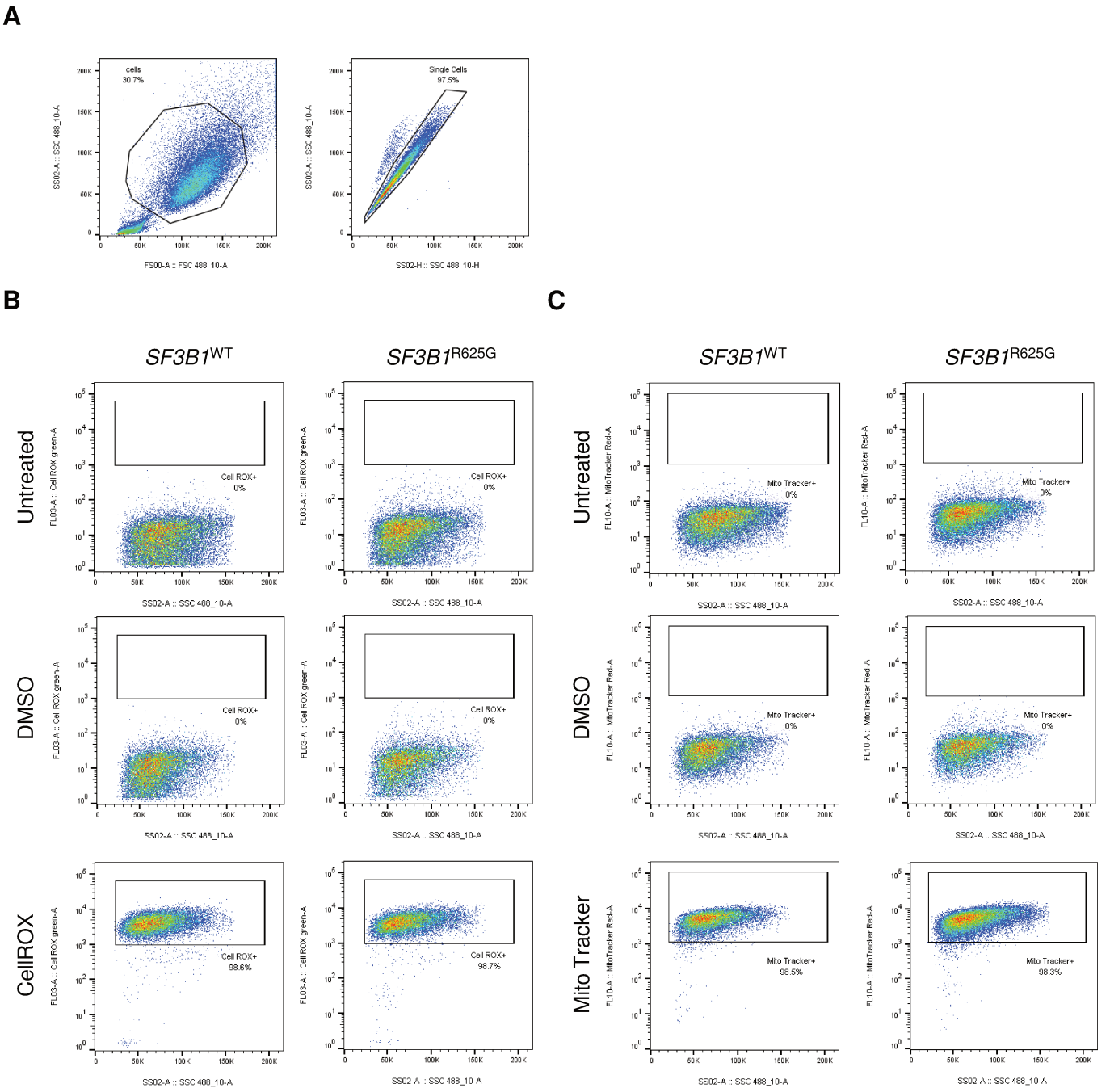

Supplementary Figure 2. *SF3B1*^{WT} and *SF3B1*^{R625G} cells display comparable ROS levels and equivalent mitochondrial content.

A) Gating strategy applied for staining of Mitotracker and CellROX. Cells were selected using morphology parameters, SSC vs FSC (left panel), and doublets of cells were excluded using SSC-A vs SSC-H parameters (right panel). **B)** *SF3B1*^{WT} and *SF3B1*^{R625G} cells stained for CellROX. **C)** *SF3B1*^{WT} and *SF3B1*^{R625G} cells stained for Mitotracker. The gating strategy described in (A) was applied to all samples. DMSO and untreated controls were included as negative controls. Gates for positive events for CellROX or Mitotracker staining were established using DMSO-treated samples as threshold. Data are represented as mean of triplicates.

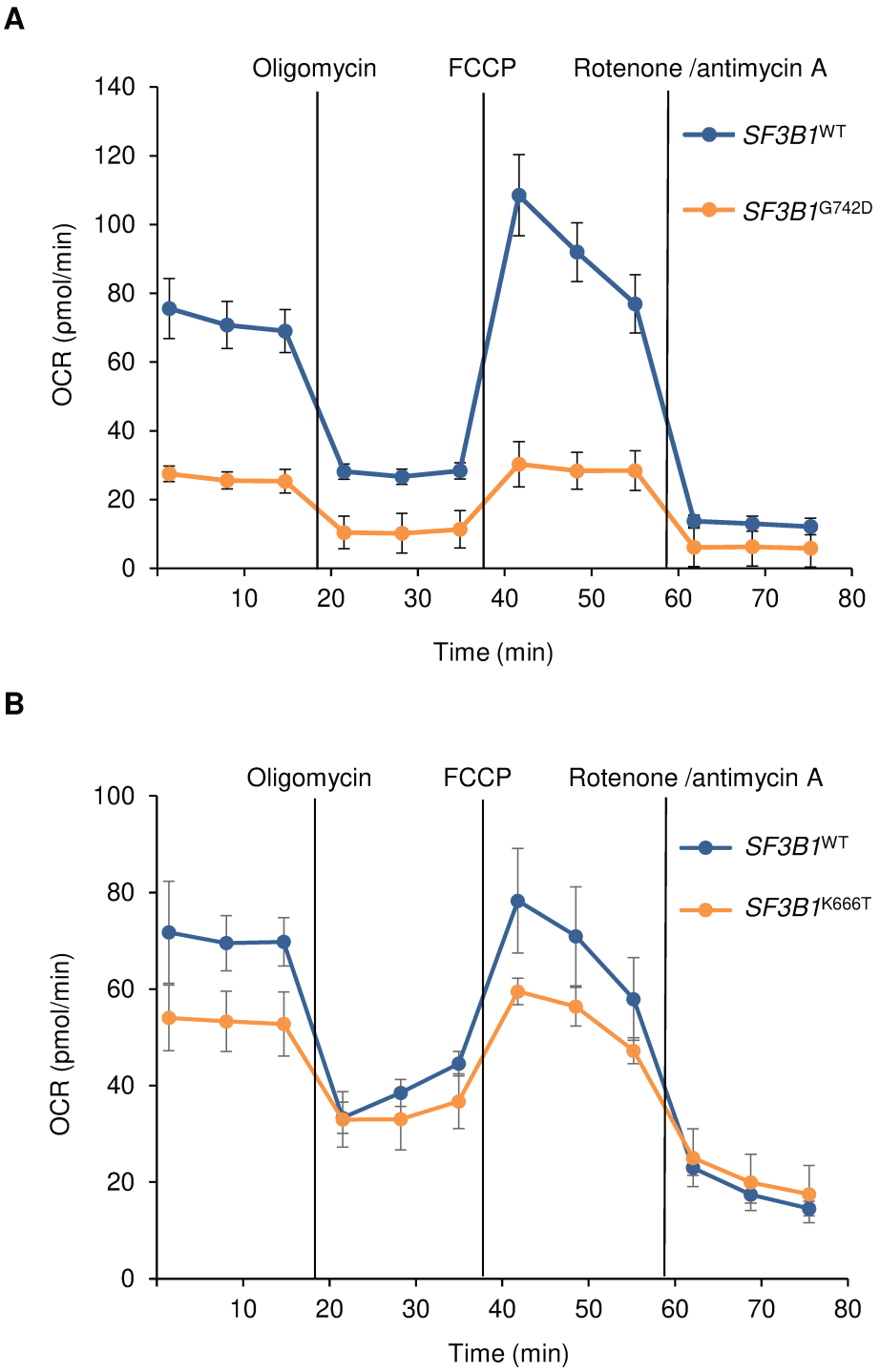

Supplementary Figure 3. *SF3B1*^{G742D} and *SF3B1*^{K666T} cells display a decreased mitochondrial respiration.

A) Oxygen consumption rate (OCR) of *SF3B1*^{WT} (blue) and *SF3B1*^{G742D} (orange) isogenic HAP1 cells as measured by Seahorse XF96 Analyzer. **B)** OCR in *SF3B1*^{WT} (blue) and *SF3B1*^{K666T} (orange) isogenic HEK293T cells as measured by Seahorse XF96 Analyzer.

A

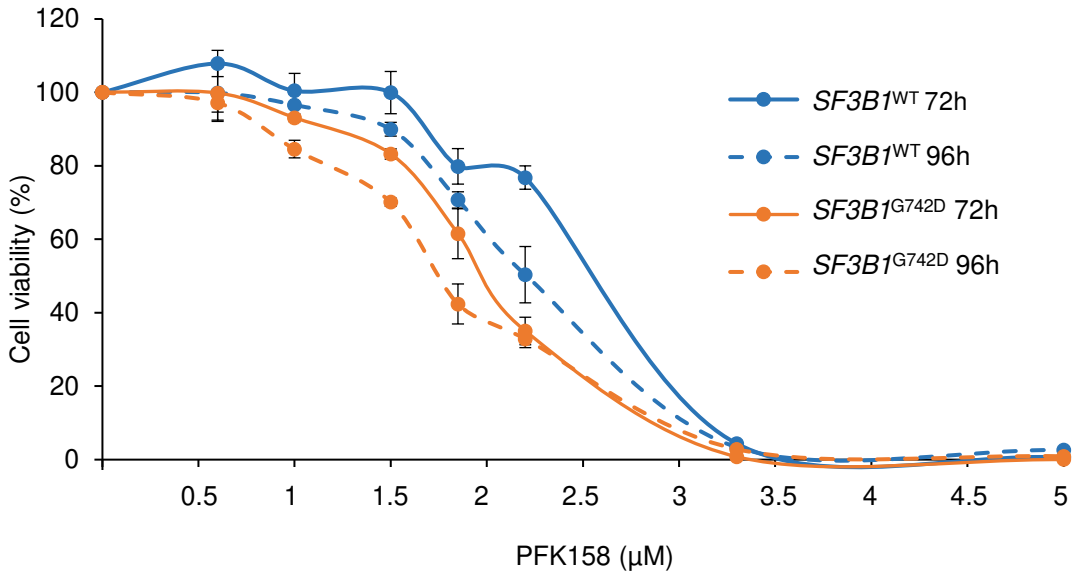

B

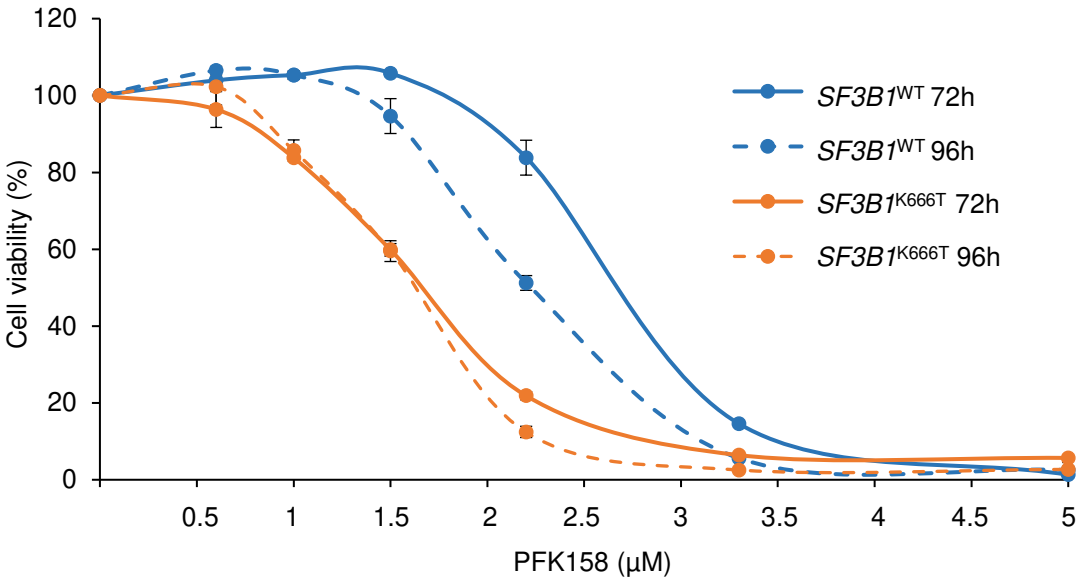

Supplementary Figure 3. *SF3B1*^{G742D} and *SF3B1*^{K666T} cells high sensitivity to glycolysis inhibition.

Cell viability upon treatment with PFK158 at 72 and 96 hours of *SF3B1*^{WT} (blue) and *SF3B1*^{G742D} (orange) isogenic HAP1 cells (**A**) and *SF3B1*^{WT} (blue) and *SF3B1*^{K666T} (orange) isogenic HEK293T cells (**B**). Data are represented as the mean of triplicates ± SD.

DISCUSSION

Nailing the hammer on the head

SF3B1 is recurrently mutated in UM (~23%) (Furney *et al.*, 2013; Harbour *et al.*, 2013; Martin *et al.*, 2013; Alsafadi *et al.*, 2016), with a prevalence of R625 hotspot mutations (Furney *et al.*, 2013; Harbour *et al.*, 2013; Martin *et al.*, 2013). *SF3B1* hotspot mutations in cancer target the HEAT repeats and have been suggested to induce conformational changes in the U2 snRNP complex thereby altering RNA recognition and affinity to other splicing factors (Alsafadi *et al.*, 2016, 2021; Z Liu *et al.*, 2020; Canbezdi *et al.*, 2021). Consequently, the binding to the BP is altered so that mutant SF3B1 recognizes and mediates the binding of U2 snRNP to a cryptic BP site. Hence, the underlying mechanism of *SF3B1*^{R625G} consists of a cryptic 3' ss usage, upstream of the canonical site (Darman *et al.*, 2015; Alsafadi *et al.*, 2016). Those mRNA transcripts that are sensitive to mutant SF3B1 (~0.5%) will consequently contain an additional fragment of the intron. Whether these aberrant transcripts share a common fate or trigger an oncogenic dysregulation remains a mystery that I aimed to decipher.

Of note, although we still ignore the global fate of the *SF3B1*^{mut}-induced aberrant transcripts, emerging studies have pinpointed the fate of concrete aberrant transcripts and some have been shown to play a role in oncogenesis. The vast majority of these reports showed that the studied *SF3B1*^{mut}-induced aberrant transcripts contain an intronic fragment and are degraded by NMD (Nonsense-Mediated mRNA Decay), leading to decreased mRNA levels (Lee *et al.*, 2018; Inoue *et al.*, 2019; Zhaoqi Liu *et al.*, 2020; Li *et al.*, 2021). Each of these aberrant transcripts has a differential functional impact towards promoting oncogenesis. For instance, decreased levels of *MAP3K7* result in a hyperactive NF-κb pathway (Lee *et al.*, 2018; Li *et al.*, 2021), BRD9 loss promotes melanogenesis (Inoue *et al.*, 2019) and *PPP2R5A* downregulation results in decreased apoptosis (Zhaoqi Liu *et al.*, 2020). In contrast, Wang *et al.* reported that mutant SF3B1 leads to the usage of a cryptic 3' ss located downstream of the canonical site. This is different from most studies, as the most common aberrant splicing event induced by mutant SF3B1 is the recognition of a cryptic 3' ss located upstream rather than downstream of the canonical site. The aberrant transcript of *DVL2* can no longer induce repression of the Notch signaling pathway so it stays activated (Pozzo *et al.*, 2020; Zhao *et al.*, 2021). *DVL2* mis-splicing by mutant SF3B1 also promotes the Wnt pathway in CLL cells (Wang *et al.*, 2016).

Altogether, these studies provide evidence of a direct link between aberrant splicing induced by mutant SF3B1 and tumor progression. At the same time, these studies report the fate of distinct aberrant transcripts in different types of cancer, which proves that while the aberrant splicing pattern induced by *SF3B1* is shared across tumors with different cellular origins, the downstream oncogenic role may be specific to the tissue and/or to the hotspot mutation. This demands further research on the oncogenic role of each *SF3B1* hotspot mutation. Given this and the lack of studies on the fate of *SF3B1*^{mut}-induced aberrant transcripts in UM, we conducted a molecular characterization of the consequences of R625G mutation, the most frequent *SF3B1* mutation in UM. The molecular characterization consisted of comprehending the impact of *SF3B1*^{R625G} at the levels of transcription, nascent protein synthesis, protein abundance, translation and metabolism.

After validation of the aberrant splicing pattern induced by *SF3B1*^{R625G} in our Mel202 isogenic model by RNA-sequencing, we proceeded with its molecular characterization (Figure 1A article). We first questioned whether *SF3B1*^{R625G} alters global gene expression by RNA-sequencing. Our data show that *SF3B1*^{R625G} induces a limited dysregulation of gene expression and such dysregulation is essentially independent of the splicing aberrations. This goes in line with previous studies that reported such a limited impact of aberrant splicing on mRNA expression levels (Shiozawa *et al.*, 2018; Dalton *et al.*, 2019).

Seeing such limited effect on mRNA expression levels, we assessed whether *SF3B1*^{R625G} affects the translatome. In fact, several studies have reported the role of splicing factors in the regulation of translation. The splicing factor from the family of serine/arginine rich (SR) proteins named SRSF1 or SF2/ASF interacts with translating ribosomes and promotes translation of certain mRNAs (Sanford *et al.*, 2004). Precisely, SRSF1 stimulates translation at the step of initiation by preventing dephosphorylation of 4E-BP in an mTOR-dependent manner. Dephosphorylated 4E-BP is inactivated thus it no longer inhibits cap-dependent translation, which promotes translation (Michlewski, Sanford and Cáceres, 2008). SRSF1 has been shown to regulate translation of mRNAs coding for proteins playing roles in cell cycle, RNA processing and mRNA translation (Maslon *et al.*, 2014). The splicing factor hnRNP C (heterogeneous nuclear ribonucleoprotein C) is recruited by the ribosomes and can promote translation of some mRNA transcripts while leaving translation efficiency unaltered (Aviner *et al.*, 2017).

These studies highlight the role of splicing factors as regulators of translation but none of them have assessed this role upon mutations. To this end, Palangat and colleagues

first found out that the splicing factor U2AF1 regulates mRNA translation. Then, they showed that upon S34F mutation of U2AF1, the translation of hundreds of mRNA is affected and for example, there is an increased production of chemokine interleukin, which promotes inflammation and tumorigenesis (Palangat *et al.*, 2019).

In our hands' analysis of nascent protein synthesis did not reveal any significant changes in the synthesis *de novo* of proteins in *SF3B1*^{R625G} cells as compared to *SF3B1*^{WT} cells (Figure 2A article).

We then wondered whether *SF3B1*^{R625G}-induced aberrant transcripts are efficiently translated into proteins. A great majority of studies chose to undertake polysome profiling to see the effect of mutant SF3B1 and its potential role in translation (Sanford *et al.*, 2004; Maslon *et al.*, 2014; Aviner *et al.*, 2017; Palangat *et al.*, 2019). Comparable polysome profiles between *SF3B1*^{WT} and *SF3B1*^{R625G} cells implied no alteration of translation efficiency by *SF3B1*^{R625G} (Figure 2B article), in line with our findings of no differences on nascent protein synthesis (Figure 2A article).

We then plotted the fractional distribution of *SF3B1*^{R625G}-aberrant transcripts as the logarithmic ratio of each aberrant transcript fold-change in polysomes to its fold-change in monosomes in *SF3B1*^{R625G} cells (Figure 2D article). We could distinguish two groups; **group A** containing 35% of aberrantly-spliced transcripts that are more translated than their canonically-spliced counterparts and **group B** formed by 65% of aberrantly-spliced transcripts that are less translated than their canonically-spliced counterparts (Figure 2D article). In conclusion, *SF3B1*^{R625G} alters translation in a target-specific manner. Strikingly, we found 35% of aberrantly-spliced transcripts that are more translated than their canonically spliced counterparts, were enriched in metabolic pathways.

We wanted to dig more into the effect of *SF3B1* R625G mutation on protein abundance. LC-MS/MS analysis showed 439 under-represented and 494 over-represented proteins in a significant manner in *SF3B1*^{R625G} cells as compared to *SF3B1*^{WT} cells (Figure 3A article). We then crossed the list of genes coding for these 933 significantly dysregulated proteins with the list of aberrantly-spliced genes and found that only 8.8% of the differentially spliced genes are associated with dysregulated protein levels (6.1% under-represented and 2.7% over-represented proteins) (Figure 3B article). To find a functional link, we performed gene enrichment analysis which showed a robust metabolic enrichment amongst the under-represented proteins (Supplementary Figure 1 and Supplementary Table 7 article).

Taking into account the observed dysregulated metabolic proteins in *SF3B1*^{R625G} cells as compared to *SF3B1*^{WT} cells, we aimed to examine the metabolic profile of these isogenic cell models. We first focused on PHGDH (Posphoglycerate Dehydrogenase), the enzyme catalyzing the first step of *de novo* synthesis of serine because it was under-represented in *SF3B1*^{R625G} cells, according to LC-MS/MS. Our goal was to check whether this under-representation sensitized *SF3B1*^{R625G} cells to serine and glycine deprivation. Serine and glycine dependency has been reported in some types of cancer and a combination of serine and glycine deprivation with PHGDH inhibition results in decreased tumor growth in a xenograft model of colorectal cancer (Reid *et al.*, 2018; Tajan *et al.*, 2021). In addition, Dalton *et al.* reported that *SF3B1*^{mut} promotes a dysregulation of metabolic targets such as PHGDH in acute myeloid leukemia and breast cancer cells, which results in increased serine dependency (Dalton *et al.*, 2019, 2020). We validated PHGDH underexpression in *SF3B1*^{R625G} cells by immunoblotting (Figure 4A article) and given the crucial role of PHGDH to provide carbon units from serine and glycine, we tested deprivation of serine and glycine for 4 days in *SF3B1*^{WT} and *SF3B1*^{R625G} cells. Upon 4 days of deprivation of serine and glycine, *SF3B1*^{R625G} cells showed a higher decreased viability as compared with wild-type counterpart, suggesting that *SF3B1*^{R625G} cells are more dependent on serine and glycine (Figure 4B article).

Then, we noticed an under-representation of PGD (6-phosphogluconate dehydrogenase) by LC-MS/MS. PGD is part of the pentose phosphate pathway (PPP) and catalyzes the formation of ribulose 5-phosphate that can be converted into ribose 5-phosphate and further used for nucleotide synthesis. In line with a PGD under-representation, we found a decreased expression for G6PD (Glucose-6-phosphate dehydrogenase). Altogether, these findings suggest a decreased rate of PPP in *SF3B1*^{R625G} cells. Provided that the PPP is one of the main sources of NADPH used to scavenge ROS levels (Dubreuil *et al.*, 2020), we checked the ROS levels in both cell lines. Our data show that the ROS levels remain unchanged (Supplementary Figures paper 2A and 2B article). Accordingly, the enzyme LDHA (lactate dehydrogenase A) which catalyzes the last step of glycolysis from pyruvate to lactate (Ooi and Gomperts, 2016), had comparable expression levels in *SF3B1*^{WT} and *SF3B1*^{R625G} cells (Figure 4A article).

We also checked the expression of PDH (Pyruvate Dehydrogenase) catalyzes the reaction to transform pyruvate to acetyl CoA which joins the citric acid cycle and OXPHOS (oxidative phosphorylation) to glycolysis, gluconeogenesis and lipid and amino acid metabolic pathways. There seems to be a decrease of total PDH in *SF3B1*^{R625G} cells

versus *SF3B1*^{WT} cells, thereby suggesting that the activity of PDH is hampered upon *SF3B1* mutations (Figure 4A article).

Of high interest, the core assembly factors of complex II of the mitochondrial electron transport chain *UQCC1* and *UQCC2* were mis-spliced by *SF3B1*^{R625G} and under-represented, as shown by LC-MS/MS. To see if this was linked with OXPHOS impairment in *SF3B1*^{R625G} cells, we analyzed the expression of mitochondrial complexes I-V by immunoblotting and found they were indeed underexpressed in *SF3B1*^{R625G} cells. Decreased expression of OXPHOS complexes I, III, IV and V was more intense upon serine and glycine deprivation in *SF3B1*^{WT} cells whereas it was stable in *SF3B1*^{R625G} cells (Figure 4B article). Given that *SF3B1*^{R625G} cells exhibit mitochondrial defects we decided to explore if *SF3B1*^{R625G} cells rely more on glycolysis or OXPHOS for energy obtention. To this end, we replaced glucose with galactose; galactose is a stereoisomer of glucose, but unlike glucose, the reaction rate to convert it into glucose-6-phosphate is slow. When replacing glucose for galactose for 3 days, *SF3B1*^{R625G} cells showed a decrease in viability much more significant than *SF3B1*^{WT} cells, indicating that *SF3B1*^{R625G} cells are more affected by the change in the source of energy and that they are more dependent on glycolysis.

To further understand this observed glycolysis dependency in *SF3B1*^{R625G} cells, we performed a seahorse analysis to assess the mitochondrial respiration by measuring the oxygen consumption rate (OCR) and extracellular acidification rate (ECAR) of *SF3B1*^{WT} and *SF3B1*^{R625G} cells. Both the minimal and maximal cellular OCR were significantly decreased in *SF3B1*^{R625G} cells as compared to *SF3B1*^{WT} cells (Figure 5A article), which is in line with the underexpression of UQCC1 and UQCC2 found by LC-MS/MS. These results were also confirmed with other isogenic cell models, namely *SF3B1*^{G742D}-HAP1 and *SF3B1*^{K666T}-HEK293T cell lines (Supplementary Figures 3A and 3B article). The decreased respiration is justified by the underexpression of OXPHOS complexes found in *SF3B1*^{R625G} cells (Figures 4A and 5A article). Notably, decreased OCR cannot be attributed to a decreased mitochondrial content because comparable levels were observed in *SF3B1*^{WT} and *SF3B1*^{R625G} cells (Supplementary Figures 2A and 2C article). Conclusively, *SF3B1*^{mut} triggers a decrease in mitochondrial respiration.

Finally, we interrogated whether *SF3B1*^{mut} cells favour glycolysis to compensate for their mitochondrial defects. In line with this, enrichment of aerobic glycolysis metabolites upon *SF3B1* mutations was recently described in in pancreatic ductal adenocarcinoma cells. In fact, *SF3B1*^{K700E} cells showed increased glucose consumption, lactate release and

increased ECAR, indicative of increased glycolysis (Yang *et al.*, 2021). Although we did not observed increased lactate release and ECAR, the existance of studies elucidating an involvement of mutant SF3B1 in different metabolic alterations according to the cancer type, calls for metabolic characterization.

Glucose uptake was significantly higher in *SF3B1*^{R625G} cells versus *SF3B1*^{WT}cells (Figure 6A article), suggesting an increased glycolytic rate to promote the obtention of glycolytic intermediates on early glycolysis. To decipher the therapeutic potential of this metabolic feature, we treated cells with PFK158, a PFKFB3 (6-phosphofructo-2-kinase/fructose-2,6-biphosphate 3) inhibitor. *SF3B1*^{R625G} cells were more sensitive to PFKFB3 inhibition than *SF3B1*^{WT} cells (Figure 6B article). The same effect was observed for *SF3B1*^{G742D} and *SF3B1*^{K666T} cells in comparison with *SF3B1*^{WT} counterparts (Supplementary Figures 4A and 4B article), confirming that the metabolic rewiring observed is specific to *SF3B1*^{mut}. Taken together, *SF3B1*^{mut} induces metabolic defects that in turn promote the usage of glycolysis thereby making *SF3B1*^{mut} cells more sensitive to glycolysis inhibition.

This is the first comprehensive molecular study of mutant SF3B1 in UM. We have demonstrated that mutant SF3B1 induces mis-splicing of metabolic targets that leads to underexpression of OXPHOS complexes and consequent decreased mitochondrial respiration. To compensate for their metabolic defects, cells harbouring mutations on *SF3B1* promote metabolic rewiring towards glycolysis and thus become more sensitive to glycolysis inhibition. The translational relevance of this study consists of offering a novel therapeutic opportunity to treat the metabolic defects in UM patients harbouring *SF3B1* mutations and ultimately reducing tumor growth.

General conclusion

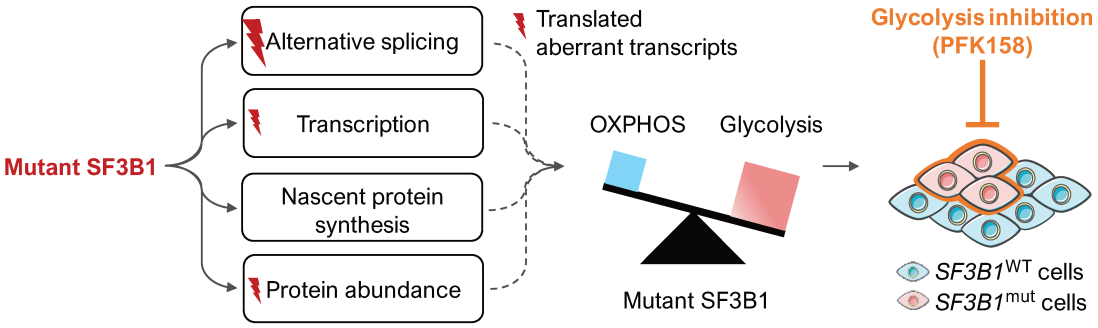

Figure 17. Graphical abstract of the manuscript titled [Glycolysis dependency as a hallmark of SF3B1-mutated cells in uveal melanoma. Mutant SF3B1 leads to the formation of aberrant transcripts on a subset of genes, with a restricted impact on transcription and poor oncogenic implication. Mutant SF3B1 does not affect nascent protein synthesis but results in an under-representation of metabolic proteins. Translated aberrant transcripts are in fact enriched in metabolism. Globally, these metabolic impairments favour an increased reliance on glycolysis thus sensitizing *SF3B1*^{mut} cells to glycolysis inhibition by PFK158, which targets the glycolytic target PFKFB3.

To be continued...

Two major potential therapeutic axes emerge from this study: **a)** correcting aberrant splicing and/or **b)** targeting the metabolic functional dysregulation.

A) Correcting aberrant splicing

To date, targeting aberrant splicing has shifted from inhibition towards modulation because inhibiting a vital process for cells results in cytotoxic side-effects that limit the therapeutic window (discussed in the review in chapter I). For instance, H3B-8800 is a small molecule that has been reported to selectively inhibit aberrant splicing induced by mutant SF3B1 by showing the preferential killing of *SF3B1*^{mut} cells than *SF3B1*^{WT} cells (Seiler *et al.*, 2018). H3B-8800 is currently being tested in clinical trials for patients with myelodysplastic syndromes, acute myeloid leukemia and chronic myelomonocytic leukemia (NCT02841540). Another interesting approach based on aberrant splicing consists of vaccine development to target the neoepitopes generated by *SF3B1*^{mut}-induced aberrant transcripts. A recent study already reported selective killing of cell lines with *SF3B1* mutations by CD8^{+} cells (Bigot *et al.*, 2021).

As previously summarized, Inoue *et al.* demonstrated the inclusion of a poison exon in *BRD9* by mutant SF3B1 that interrupts the reading frame resulting in the *BRD9* mRNA degradation. After full comprehension of aberrant splicing by *SF3B1*^{mut}, they corrected the mis-splicing by binding antisense oligonucleotides to mask the poison exon which was no longer included. They also tested this mis-splicing correction by intratumoral injection of the antisense oligonucleotides in xenografts and tumor growth was reduced (Inoue *et al.*, 2019). Convincingly, comprehension of the mechanisms underlying aberrant splicing is a must to develop therapies aimed at correcting these defects.

B) Targeting the functional metabolic dysregulation

Modulating or correcting splicing may not always be straightforward or sufficient, thus, aiming to target the functional impact of aberrant splicing is also a valid approach. Herein, I will focus on targeting defective metabolism resulting from *SF3B1*^{mut}-induced aberrant splicing because such an approach may be feasible for UM patients harbouring *SF3B1* R625G mutations.

First of all, I will describe previous studies showing a role of splicing factors in metabolism and I will detail future experiments to be conducted in order to fully characterize the metabolic profile of *SF3B1*^{WT} and *SF3B1*^{R625G} UM cells. Elucidating of all metabolic switches induced by mutant SF3B1 are crucial to spot druggable or targetable metabolic weaknesses.

Previous studies have linked mutations in splicing factors to impairment in cell metabolism. Sen *et al.* found that loss of expression of *SRSF3* led to impairment of hepatocyte maturation by altering crucial regulators of glucose and lipid homeostasis (Sen, Jumaa and Webster, 2013). Gökmen-Polar *et al.* reported that knockdown of *ESRP1* (epithelial splicing regulatory protein 1) in breast cancer cells leads to decreased expression of FASN (fatty acid synthase), SCD1 (stearoyl-CoA desaturase 1), and PHGDH (D-3-phosphoglycerate dehydrogenase) (Gökmen-Polar *et al.*, 2019). Mutations in *SF3B1* have also been linked to metabolic impairment. Dalton *et al.* showed that mutant SF3B1 reprograms mitochondrial metabolism in breast epithelial cells by downregulating proteins that are highly enriched in metabolic pathways. Metabolic reprogramming is a hallmark of cancer that can guide tumorigenesis by redirecting nutrient utilization. One notable signal was in the mitochondrial respiratory chain complex III of the ETC (electron transport chain), assembled by factors UQCC1 (ubiquinol-cytochrome C reductase

complex assembly factor 1) and UQCC2 (ubiquinol-cytochrome C reductase complex assembly factor 2). In fact, mutant SF3B1 mis-splices *UQCC1*, leading to a decrease in the levels of expression of mitochondrial complex III expression. It was also found that mutant SF3B1 represses the serine synthesis pathway in breast epithelial cells by mis-splicing of *PHGDH*, which encodes an enzyme involved in *de novo* synthesis of serine (Dalton *et al.*, 2019).

More recently, Yang *et al.* found that *SF3B1* mutations lead to *in vivo* tumor growth of PDAC. They performed a GSEA (gene set enrichment analysis) to establish the mechanism by which *SF3B1* mutations contribute to PDAC tumor growth and found that *SF3B1* mutations dysregulate glucose metabolism. They also found that in PDAC cells, *PPP2R5A* is aberrantly spliced in the context of SF3B1 mutations resulting in an induction of c-Myc activation and tumor growth. Finally, they tested a PPP2A activator, FTY720, and found that this treatment inhibits the colony formation and glycolysis pathway, and downregulates phosphorylated c-Myc in PDAC cells. When tested *in vivo*, FTY720 inhibits tumor growth in *SF3B1* mutant PDAC cells with no toxic effects (Yang *et al.*, 2021).

Our functional study of the metabolic characteristics in the isogenic UM cell model *SF3B1*^{R625G} as compared to *SF3B1*^{WT} Mel202 cells shows that *SF3B1*^{R625G} cells are more addicted to glucose and have a reduced rate of mitochondrial respiration as compared to *SF3B1*^{WT}. Taken together with the underexpression of UQCC1 and UQCC2 found by LC-MS/MS, this suggests that *SF3B1*^{R625G} cells go through a metabolic switch towards glycolysis to compensate for their mitochondrial defects. This phenomenon was described in 1925 by Warburg, when he observed that tumor cells uptake large amounts of glucose and convert it into lactate, even in the presence of oxygen (aerobic glycolysis), instead of oxidizing it for cellular respiration (Warburg, 1925). In fact, metabolic reprogramming is a hallmark of cancer that drives tumor growth and proliferation (Hanahan and Weinberg, 2011). We could speculate that *SF3B1*^{R625G} cells undergo metabolic reprogramming to meet the increased demand for nutrients including nucleotides, lipids, and amino acids to support tumor progression. More recently, it has been shown that suppressing aerobic glycolysis impaired cancer cell proliferation by decreasing the NAD^+/NADH ratio. NAD^+ is an electron acceptor used to synthesize oxidized molecules such as nucleotides, lipids and amino acids. Indeed, when cancer cells with suppressed aerobic glycolysis were given various treatments to synthesize NAD^+, the proliferation rates were restored (Luengo *et al.*, 2021). Therefore, demand for

NAD^+ may explain the preference of *SF3B1*^{R625G} cells for glycolysis. Future studies are warranted to investigate the glycolytic preference in *SF3B1*^{R625G} cells and whether activation in oncogenes and mutant tumor suppressors are associated with it.

Given that PHGDH was underexpressed in the LC-MS/MS data, we evaluated the vulnerability of *SF3B1*^{R625G} and *SF3B1*^{WT} to serine and glycine starvation and showed that *SF3B1*^{R625G} cells are more dependent of serine and glycine than *SF3B1*^{WT} cells. Notably, inhibition of PHGDH combined with a dietary restriction of SG results in reduced tumor growth in a xenograft model of colorectal cancer (Tajan *et al.*, 2021). Moreover, *SF3B1* hotspot mutations targeting codons K700, K666, and H662, have previously been described to induce the mis-splicing of *PHGDH*, leading to increase dependency on serine in acute myeloid leukemia and breast cancer cells. Furthermore, dietary restrictions of serine and glycine resulted in tumor growth repression *in vitro* and *in vivo* (Dalton *et al.*, 2019). In this way, certain subsets of breast cancer have been shown to be dependent on the serine synthesis pathway (Murphy *et al.*, 2018). Our results extend these findings to *SF3B1*^{R625G} hotspot mutation in UM cells.

Suppression of *PHGDH* in endothelial cells has been shown to disturb mitochondrial homeostasis and heme synthesis, which could explain the formation of ring sideroblasts, which are iron deposits in the mitochondria and a distinctive feature of MDS, driven by *SF3B1* mutations (Papaemmanuil *et al.*, 2011; Vandekeere *et al.*, 2018). Additional studies are needed to investigate whether the aberrant splicing of *PHGDH* affects the oncogenesis of UM harboring *SF3B1* mutations. Moreover, dietary restrictions could be a promising therapeutic approach.

In 1955, Harry Eagle described that tumor cells exhibited an increasing demand for glutamine in comparison with other amino acids (Eagle, 1955). In fact, glutamine deprivation has been observed to inhibit leukemia and lung cancer cell growth (Hassanein *et al.*, 2015; Polet *et al.*, 2016). Moreover, in breast cancer cells, glutamine depletion results in decreased cell proliferation and aberrant mitochondrial membrane potential (Gwangwa, Joubert and Visagie, 2019). Glutamine can be degraded in a process called glutaminolysis, in which the glutamine present in the cytoplasm is transported into the mitochondria, generating α-KG (alpha-ketoglutarate) that is fed into the TCA cycle supporting the OXPHOS pathway (Yoo *et al.*, 2020). However, our study suggests that *SF3B1*^{R625G} cells have defective mitochondria, therefore it would be interesting to study whether *SF3B1*^{R625G} cells utilize glutamine in another metabolic

pathway, such as for the synthesis of purine and pyrimidine nucleotides and asparagine, which occurs in the cytoplasm (Pavlova and Thompson, 2018). This finding may help us see if *SF3B1* mutations in UM cells lead to dependency on glutamine for survival, and if it is the case, further investigation will hopefully determine the mechanisms underlying glutamine addiction.

Another appealing approach is to assess the activation of mTOR pathway in *SF3B1*^{WT} and *SF3B1*^{R625G} cells. Activation of mTOR increases the expression of transporter proteins on the cell surface of cancer cells, resulting in a greater uptake of nutrients of the cell to support their proliferation rate (Advani, 2010). Moreover, a study showed that mTOR activation of pS6K increased the protein levels of survivin, an inhibitor of apoptosis, in prostate cancer cells supporting their survival (Vaira *et al.*, 2007). The activation of mTOR promotes metabolic reprograming by increasing glycolysis mediated by phosphorylated S6 and 4E-BP1 (Mirabilii, Ricciardi and Tafuri, 2020), and mTOR signaling can also control cell metabolism by increasing the expression of metabolic enzymes. As mentioned previously, *SF3B1*^{R625G} cells undergo a metabolic switch towards glycolysis to meet their energy demand while compensating for their defective mitochondria. Hence, a potential hyperactivation of mTOR pathway observed on *SF3B1*^{R625G} cells may explain the higher rate of glycolytic enzyme synthesis and their dependency on glycolysis.

Finally, *SF3B1*^{WT} and *SF3B1*^{R625G} cells could be challenged under hypoxic conditions to assess their response. As the tumor expands, it must find ways to sustain proliferation, which can be achieved by increasing the expression of glycolytic enzymes induced by HIF. This has been observed in human hepatocellular carcinoma cells (Iyer *et al.*, 1998) and in prostate epithelial cells, where mTOR enhances the translation of HIF, leading to an increased expression of glycolysis regulating enzymes (Majumder *et al.*, 2004). Further studies are warranted to investigate the expression of HIF in *SF3B1*^{WT} and *SF3B1*^{R625G} cells to determine if this accounts for the observed increase in glycolytic enzymes.

Overall, we provide a comprehensive metabolic characterization of mutant SF3B1 in UM. We show that mutant SF3B1 rewires the metabolism of UM cells as observed by the increased dependency on glycolysis to compensate for the decreased mitochondrial respiration. We also demonstrate that mutant SF3B1 promotes a dependency on glutamine and the activation of the mTOR pathway. Finally, we show that both mutated

and wild-type *SF3B1* UM cells can survive under hypoxic conditions through metabolic reprogramming towards glycolysis. Our study sheds light on the oncogenic consequences of *SF3B1* mutations which can offer new therapeutic perspectives for UM patients harboring *SF3B1* mutations.

Our observations are based on *in vitro* experiments, conducted under non-physiological nutrient conditions. It would be mandatory to assess *in vivo* if inhibition of glycolysis is a promising therapeutic approach. Furthermore, other metabolism pathways, such as fatty acids, need be studied to determine if energy can also be obtained from other pathways to compensate for the impaired mitochondria in *SF3B1*^{R625G} cells. Last but not least, it would be important to investigate whether metabolic reprogramming is a common feature in the oncogenic involvement of other splicing factors. Optimal validation should be performed in cellular isogenic models that are required for optimal validation, like the U2AF isogenic model developed by Palangat and collaborators (Palangat *et al.*, 2019).

REFERENCES

Aarntzen, E. H. J. G. *et al.* (2012) 'Skin-test infiltrating lymphocytes early predict clinical outcome of dendritic cell-based vaccination in metastatic melanoma', *Cancer Research*, 72(23), pp. 6102–6110. doi: 10.1158/0008-5472.CAN-12-2479.

Advani, S. H. (2010) 'Targeting mTOR pathway: A new concept in cancer therapy', *Indian J Med Paediatr Oncol*, 31(4), pp. 132–136.

Akyuz, M. *et al.* (2016) 'Laparoscopic management of liver metastases from uveal melanoma', *Surgical Endoscopy*, 30, pp. 2567–2571.

All-Ericsson, C. *et al.* (2004) 'c-kit-dependent growth of uveal melanoma cells: A potential therapeutic target?', *Investigative Ophthalmology and Visual Science*, 45(7), pp. 2075–2082. doi: 10.1167/iovs.03-1196.

Alsafadi, S. *et al.* (2016) 'Cancer-associated SF3B1 mutations affect alternative splicing by promoting alternative branchpoint usage', *Nature Communications*, 7(10615), pp. 1–12. doi: 10.1038/ncomms10615.

Alsafadi, S. *et al.* (2021) 'Genetic alterations of SUGP1 mimic mutant-SF3B1 splice pattern in lung adenocarcinoma and other cancers', *Oncogene*. Springer US, 40(1), pp. 85–96. doi: 10.1038/s41388-020-01507-5.

Alt, J. R. *et al.* (2000) 'Phosphorylation-dependent regulation of cyclin D1 nuclear export and cyclin D1-dependent cellular transformation', *Genes and Development*, 14(24), pp. 3102–3114. doi: 10.1101/gad.854900.

Alzahrani, A. S. (2019) 'PI3K/Akt/mTOR inhibitors in cancer: At the bench and bedside', *Seminars in Cancer Biology*. Elsevier, (April), pp. 0–1. doi: 10.1016/j.semcancer.2019.07.009.

An, M. and Henion, P. D. (2013) 'The zebrafish sf3b1-b460 mutant reveals differential requirements for the sf3b1 pre-mRNA processing gene during neural crest development', *Int J Dev Biol*, 56(4), pp. 223–237. doi: 10.1387/ijdb.113383ma.The.

Anczukow, O. and Krainer, A. R. (2016) 'Splicing-factor alterations in cancers', *Rna*, 22(9), pp. 1285–1301. doi: 10.1261/rna.057919.116.

Andersona, D. D., Quintero, C. M. and Stovera, P. J. (2011) 'Identification of a de novo thymidylate biosynthesis pathway in mammalian mitochondria', *PNAS*, 108(37), pp. 15163–15168. doi: 10.1073/pnas.1103623108.

Aronow, M. E., Topham, K. and Singh, A. D. (2018) 'Uveal Melanoma : 5-Year Update on Incidence , Treatment , and Survival (SEER 1973 – 2013)', pp. 145–151. doi: 10.1159/000480640.

Arsham, A. M. *et al.* (2002) 'Phosphatidylinositol 3-kinase/Akt signaling is neither required for hypoxic stabilization of HIF-1α nor sufficient for HIF-1-dependent target gene transcription', *Journal of Biological Chemistry*, 277(17), pp. 15162–15170. doi: 10.1074/jbc.M111162200.

Aviner, R. *et al.* (2017) 'Proteomic analysis of polyribosomes identifies splicing factors as potential regulators of translation during mitosis', *Nucleic Acids Research*, 45(10), pp. 5945–5957. doi: 10.1093/nar/gkx326.

Bakalian, S. *et al.* (2008) 'Molecular pathways mediating liver metastasis in patients with uveal melanoma', *Clinical Cancer Research*, 14(4), pp. 951–956. doi: 10.1158/1078-0432.CCR-06-2630.

Bao, X. R. *et al.* (2016) 'Mitochondrial dysfunction remodels one-carbon metabolism in human cells', *eLife*, 5, pp. 1–24. doi: 10.7554/eLife.10575.

Barash, Y. *et al.* (2010) 'Deciphering the splicing code', *Nature*, 465(7294), pp. 53–59. doi: 10.1038/nature09000.

Barker, C. A. and Salama, A. K. (2018) 'New NCCN guidelines for uveal melanoma and treatment of recurrent or progressive distant metastatic melanoma', *JNCCN Journal of the National Comprehensive Cancer Network*, 16(5), pp. 646–650. doi: 10.6004/jnccn.2018.0042.

Baughman, J. M. *et al.* (2017) 'NeuCode proteomics reveals Bap1 regulation of metabolism', *Cell Reports*, 16(2), pp. 583–595. doi: 10.1016/j.celrep.2016.05.096.NeuCode.

Bellacosa, A. (2001) 'Role of MED1 (MBD4) Gene in DNA Repair and Human Cancer', *Journal of Cellular Physiology*, 187, pp. 137–144. doi: 10.1002/jcp.1064.

De Berardinis, R. J. and Chandel, N. S. (2016) 'Fundamentals of cancer metabolism', *Science Advances*, 2(5). doi: 10.1126/sciadv.1600200.

Berget, S. M., Moore, C. and Sharp, P. A. (1977) 'Spliced segments at the 5' terminus of adenovirus 2 late mRNA', *PNAS*, 74(8), pp. 3171–3175. doi: 10.1073/pnas.74.8.3171.

Bergot, T. *et al.* (2020) 'Human cancer-associated mutations of SF3B1 lead to a splicing modification of its own RNA', *Cancers*, 12(3), pp. 1–16. doi: 10.3390/cancers12030652.

Bertrand, L. *et al.* (1999) 'Heart 6-phosphofructo-2-kinase activation by insulin results from Ser- 466 and Ser-483 phosphorylation and requires 3-phosphoinositide-dependent kinase-1, but not protein kinase B', *Journal of Biological Chemistry*, 274(43), pp. 30927–30933. doi: 10.1074/jbc.274.43.30927.

Bessonov, S. *et al.* (2010) 'Characterization of purified human Bact spliceosomal complexes reveals compositional and morphological changes during spliceosome activation and first step catalysis', *RNA*, 16(12), pp. 2384–2403. doi: 10.1261/rna.2456210.

Biankin, A. V *et al.* (2012) 'Pancreatic cancer genomes reveal aberrations in axon guidance pathway genes', *Nature*, 491(7424), pp. 399–405. doi: 10.1038/nature11547.

Bigot, J. *et al.* (2021) 'Splicing patterns in SF3B1 mutated uveal melanoma generate shared immunogenic tumor-specific neo-epitopes', *Cancer Discovery*, (2). doi: 10.1158/2159-8290.cd-20-0555.

Binkley, E. *et al.* (2020) 'A prospective trial of adjuvant therapy for high-risk uveal melanoma: Assessing 5-year survival outcomes', *British Journal of Ophthalmology*, 104(4), pp. 524–528. doi: 10.1136/bjophthalmol-2019-314461.

Birsoy, K. *et al.* (2014) 'Metabolic determinants of cancer cell sensitivity to glucose limitation and biguanides', *Nature*, 508(1), pp. 108–112. doi: 10.1038/nature13110.

Blum, E. S. *et al.* (2016) 'Clinical Management of Uveal and Conjunctival Melanoma', *Oncology*, 30(1), pp. 29–29.

Bol, K. F. *et al.* (2014) 'Long overall survival after dendritic cell vaccination in metastatic uveal Melanoma Patients', *American Journal of Ophthalmology*, 158(5), pp. 939-947.e5. doi: 10.1016/j.ajo.2014.07.014.

Boudrez, A. *et al.* (2002) 'Phosphorylation-dependent interaction between the splicing factors SAP155 and NIPP1', *Journal of Biological Chemistry*, 277(35), pp. 31834–31841. doi: 10.1074/jbc.M204427200.

Bouzier-Sore, A.-K. and Bolaños, J. P. (2015) 'Uncertainties in pentose-phosphate pathway flux assessment underestimate its contribution to neuronal glucose consumption: relevance for neurodegeneration and aging', *Frontiers Aging Neuroscience*, 19(7), p. 89.

Brand, M. D. and Nicholls, D. G. (2011) 'Assessing mitochondrial dysfunction in cells', *Biochemical Journal*, 435(2), pp. 297–312. doi: 10.1042/BJ20110162.

Brantley, M. A. and Harbour, J. W. (2000) 'Deregulation of the Rb and p53 Pathways in Uveal Melanoma', *Nature Cell Biology*, 157(6), pp. 1795–1801.

Brooks, A. N. *et al.* (2014) 'A pan-cancer analysis of transcriptome changes associated with somatic mutations in U2AF1 reveals commonly altered splicing events', *PLoS ONE*, 9(1). doi: 10.1371/journal.pone.0087361.

Burns, A. (1811) *Observations on the Surgical Anatomy of the Head and Neck. Illustrated by Cases and Engravings.*, *Edinburgh: Bryce & Co.*

Cáceres, J. F., Screaton, G. R. and Krainer, A. R. (1998) 'A specific subset of SR proteins shuttles continuously between the nucleus and the cytoplasm', *Genes and Development*, 12(1), pp. 55–66. doi: 10.1101/gad.12.1.55.

Canbezdi, C. *et al.* (2021) 'Functional and conformational impact of cancer-associated SF3B1 mutations depends on the position and the charge of amino acid substitution', *Computational and Structural Biotechnology Journal*. The Author(s), 19, pp. 1361–1370. doi: 10.1016/j.csbj.2021.02.012.

Cass, D. M. and Berglund, J. A. (2006) 'The SF3b155 N-Terminal Domain Is a Scaffold Important for Splicing', *Biochemistry*, 45(33), p. 10092.10101.

Cavalli, L. R., Varella-Garcia, M. and Liang, B. C. (1997) 'Diminished tumorigenic phenotype after depletion of mitochondrial DNA', *Cell Growth and Differentiation*, 8(11), pp. 1189–1198.

Chaneton, B. *et al.* (2012) 'Serine is a natural ligand and allosteric activator of pyruvate kinase M2', *Nature*, 491(7424), pp. 458–462. doi: 10.1038/nature11540.

Char, D. H., Char, D. H. and Kaleta-Michaels, S. (1992) 'Infiltrating lymphocytes and antigen expression in uveal melanoma', *Ophthalmic Research*, 24(1), pp. 20–26. doi: 10.1159/000267140.

Chen, L. *et al.* (2018) 'The Augmented R-Loop Is a Unifying Mechanism for Myelodysplastic Syndromes Induced by High-Risk Splicing Factor Mutations', *Molecular Cell*. Elsevier Inc., 69(3), pp. 412-425.e6. doi: 10.1016/j.molcel.2017.12.029.

Cho, S. *et al.* (2011) 'Interaction between the RNA binding domains of Ser-Arg splicing factor 1 and U1-70K snRNP protein determines early spliceosome assembly', *PNAS*, 108(20), pp. 8233–8238. doi: 10.1073/pnas.1017700108.

Chow, L. T. *et al.* (1977) 'An amazing sequence arrangement at the 5′ ends of adenovirus 2 messenger RNA', *Cell*, 12(1), pp. 1–8. doi: 10.1016/0092-8674(77)90180-5.

Christofk, H. R. *et al.* (2008) 'The M2 splice isoform of pyruvate kinase is important for cancer metabolism and tumour growth', *Nature*, 452(7184), pp. 230–233. doi: 10.1038/nature06734.

Chua, V. *et al.* (2017) 'Dysregulated GPCR Signaling and Therapeutic Options in Uveal Melanoma', *Molecular Cancer Research*, 15(5), pp. 501–506. doi: 10.1158/1541-7786.MCR-17-0007.

Cooper, B. H. and Schneidau, J. D. (2015) 'Mutational landscape determines sensitivity to PD-1 blockade in non–small cell lung cancer', *Science*, 348(6230), pp. 124–128. doi: 10.1126/science.aaa1348.

Coupland, S. E. *et al.* (1998) 'Expression patterns of cyclin D1 and related proteins regulating G1-S phase transition in uveal melanoma and retinoblastoma', *British Journal of Ophthalmology*, 82(8), pp. 961–970. doi: 10.1136/bjo.82.8.961.

Cretu, C. *et al.* (2016) 'Molecular Architecture of SF3b and Structural Consequences of Its Cancer-Related Mutations', *Molecular Cell*, 64(2), pp. 307–319. doi:

10.1016/j.molcel.2016.08.036.

Dalton, W. *et al.* (2020) 'The K666N mutation in SF3B1 is associated with increased progression of MDS and distinct RNA splicing', *Blood Advances*, 4(7), pp. 1192–1196. doi: 10.1182/bloodadvances.2019001127.

Dalton, W. B. *et al.* (2019) 'Hotspot SF3B1 mutations induce metabolic reprogramming and vulnerability to serine deprivation', *Journal of Clinical Investigation*, 8(130). doi: 10.1172/JCI125022.

Darman, R. B. *et al.* (2015) 'Cancer-Associated SF3B1 Hotspot Mutations Induce Cryptic 3' Splice Site Selection through Use of a Different Branch Point', *Cell Reports*, 13(5), pp. 1033–1045. doi: 10.1016/j.celrep.2015.09.053.

DeBoever, C. *et al.* (2015) 'Transcriptome Sequencing Reveals Potential Mechanism of Cryptic 3' Splice Site Selection in SF3B1-mutated Cancers', *PLoS Computational Biology*, 11(3), pp. 1–19. doi: 10.1371/journal.pcbi.1004105.

Depre, C. *et al.* (1993) 'Role of fructose 2,6-bisphosphate in the control of heart glycolysis', *Journal of Biological Chemistry*, 268(18), pp. 13274–13279. doi: 10.1016/s0021-9258(19)38648-x.

Desjardins, L. (1997) 'Randomized study on adjuvant therapy by DTIC in choroidal melanoma', *Melanoma Research*, 7(2), p. 166.

Diehl, J. A. *et al.* (1998) 'Glycogen synthase kinase-3B regulates cyclin D1 proteolysis and subcellular localization', *Genes and Development*, 12, pp. 3499–3511.

Diener-West, M. *et al.* (2005) 'Development of metastatic disease after enrollment in the COMS trials for treatment of choroidal melanoma: Collaborative Ocular Melanoma Study Group Report No. 26.', *Archives of Ophthalmology*, 123(122), pp. 1639–43.

Divakaruni, A. S. *et al.* (2014) *Analysis and interpretation of microplate-based oxygen consumption and pH data*. 1st edn, *Methods in Enzymology*. 1st edn. Elsevier Inc. doi: 10.1016/B978-0-12-801415-8.00016-3.

Dolatshad, H. *et al.* (2016) 'Cryptic splicing events in the iron transporter ABCB7 and other key target genes in SF3B1-mutant myelodysplastic syndromes', *Leukemia*, 30(12), pp. 2322–2331. doi: 10.1038/leu.2016.149.

Dubreuil, M. M. *et al.* (2020) 'Systematic Identification of Regulators of Oxidative Stress Reveals Non-canonical Roles for Peroxisomal Import and the Pentose Phosphate Pathway', *Cell Reports*, 30(5), pp. 1417-1433.e7. doi: 10.1016/j.celrep.2020.01.013.

Durante, M. A. *et al.* (2020) 'Single-cell analysis reveals new evolutionary complexity in uveal melanoma', *Nature Communications*, 11(1). doi: 10.1038/s41467-019-14256-1.

Dvinge, H. *et al.* (2016) 'RNA splicing factors as oncoproteins and tumor suppressors', *Nature reviews. Cancer*, 16(7), pp. 413–430. doi: 10.1038/nrc.2016.51.

Eagle, B. H. (1955) 'The minimum vitamin requirements of the L and HeLa cells in tissue culture, the production of specific vitamin deficiencies, and their cure', *the Journal of Experimental Medicine*, 102, pp. 595–600.

Esfahani, M. S. *et al.* (2019) 'Functional significance of U2AF1 S34F mutations in lung adenocarcinomas', *Nature Communications*, 10(1), pp. 1–13. doi: 10.1038/s41467-019-13392-y.

Fantin, V. R., St-Pierre, J. and Leder, P. (2006) 'Attenuation of LDH-A expression uncovers a link between glycolysis, mitochondrial physiology, and tumor maintenance', *Cancer Cell*, 9(6), pp. 425–434. doi: 10.1016/j.ccr.2006.04.023.

Fedele, C. G. *et al.* (2010) 'Inositol polyphosphate 4-phosphatase II regulates PI3K/Akt signaling and is lost in human basal-like breast cancers', *PNAS*, 107(51), pp. 22231–

22236. doi: 10.1073/pnas.1015245107.

Fei, D. L. *et al.* (2018) 'Impaired hematopoiesis and leukemia development in mice with a conditional knock-in allele of a mutant splicing factor gene U2af1', *PNAS*, 115(44), pp. E10437–E10446. doi: 10.1073/pnas.1812669115.

Francken, A. B. *et al.* (2006) 'Detection of metastatic disease in patients with uveal melanoma using positron emission tomography', *European Journal of Surgical Oncology*, 32(7), pp. 780–784. doi: 10.1016/j.ejso.2006.04.011.

Furney, S. J. *et al.* (2013) 'SF3B1 mutations are associated with alternative splicing in uveal melanoma', *Cancer Discovery*, 3(10), pp. 1122–1129. doi: 10.1158/2159-8290.CD-13-0330.

Gaude, E. and Frezza, C. (2016) 'Tissue-specific and convergent metabolic transformation of cancer correlates with metastatic potential and patient survival', *Nature Communications*, 7, pp. 1–9. doi: 10.1038/ncomms13041.

Gentien, D. *et al.* (2014) 'A common alternative splicing signature is associated with SF3B1 mutations in malignancies from different cell lineages', *Leukemia*, 28(6), pp. 1355–1357. doi: 10.1038/leu.2014.28.

Girard, C. *et al.* (2012) 'Post-transcriptional spliceosomes are retained in nuclear speckles until splicing completion', *Nature Communications*, 3. doi: 10.1038/ncomms1998.

Glancy, B. and Balaban, R. S. (2011) 'Protein composition and function of red and white skeletal muscle mitochondria', *American Journal of Physiology*, 300(6), pp. 1280–90.

Gökmen- Polar, Y. *et al.* (2019) 'Splicing factor ESRP1 controls ER - positive breast cancer by altering metabolic pathways', *EMBO reports*, 20(2), pp. 1–19. doi: 10.15252/embr.201846078.

Golas, M. M. *et al.* (2003) 'Molecular Architecture of the Multiprotein Splicing Factor SF3b', *Science*, 300(5621), pp. 980–984.

Gozani, O., Potashkin, J. and Reed, R. (1998) 'A Potential Role for U2AF-SAP 155 Interactions in Recruiting U2 snRNP to the Branch Site', *Molecular and Cellular Biology*, 18(8), pp. 4752–4760. doi: 10.1128/mcb.18.8.4752.

De Graaf, K. *et al.* (2006) 'The protein kinase DYRK1A phosphorylates the splicing factor SF3b1/SAP155 at Thr434, a novel in vivo phosphorylation site', *BMC Biochemistry*, 7, pp. 1–13. doi: 10.1186/1471-2091-7-7.

Graubert, T. A. *et al.* (2012) 'Recurrent mutations in the U2AF1 splicing factor in myelodysplastic syndromes.', *Nature genetics*, 44(1), pp. 53–57. doi: 10.1038/ng.1031.

Graveley, B. R. and Maniatis, T. (1998) 'Arginine/Serine-Rich Domains of SR Proteins Can Function as Activators of Pre-mRNA Splicing', *Molecular Cell*, 1, pp. 765–771.

Guenterberg, K. D. *et al.* (2011) 'A pilot study of bevacizumab and interferon-α2b in ocular melanoma', *American Journal of Clinical Oncology: Cancer Clinical Trials*, 34(1), pp. 87–91. doi: 10.1097/COC.0b013e3181d2ed67.

Gwangwa, M. V., Joubert, A. M. and Visagie, M. H. (2019) 'Effects of glutamine deprivation on oxidative stress and cell survival in breast cell lines', *Biological research*. BioMed Central, 52(1), p. 15. doi: 10.1186/s40659-019-0224-9.

Haferlach, T. *et al.* (2014) 'Landscape of genetic lesions in 944 patients with myelodysplastic syndromes', *Leukemia*, 28, pp. 241–247. doi: 10.1038/leu.2013.336.

Hall, S. L. and Padgett, R. A. (1994) 'Conserved sequences in a class of rare eukaryotic nuclear introns with non-consensus splice sites', *Journal of Molecular Biology*, 239(3), pp. 357–365.

Hall, S. L. and Padgett, R. A. (1996) 'Requirement of U12 snRNA for in vivo splicing of a minor class of eukaryotic nuclear pre-mRNA introns', *Science*, 271(5256), pp. 1716–8.

Han, A. *et al.* (2021) 'BAP1 mutant uveal melanoma is stratified by metabolic phenotypes with distinct vulnerability to metabolic inhibitors', *Oncogene*. Springer US, 40(3), pp. 618–632. doi: 10.1038/s41388-020-01554-y.

Hanahan, D. and Weinberg, R. (2011) 'Hallmarks of cancer: the next generation', *Cell*, 4(144), pp. 646–674. Available at: http://www.ncbi.nlm.nih.gov/pubmed/21376230.

Harbour, J. W. *et al.* (2013) 'Recurrent mutations at codon 625 of the splicing factor SF3B1 in uveal melanoma', *Nature Genetics*, 45(2), pp. 133–135. doi: 10.1038/ng.2523.

Hassanein, M. *et al.* (2015) 'Targeting SLC1A5-mediated glutamine dependence in non-small cell lung cancer', *International Journal of Cancer*, 137(7), pp. 1587–1597. doi: 10.1002/ijc.29535.Targeting.

Hay, N. (2016) 'Reprogramming glucose metabolism in cancer: Can it be exploited for cancer therapy?', *Nature Reviews Cancer*, 16(10), pp. 635–649. doi: 10.1038/nrc.2016.77.

Hebert, L. *et al.* (2017) 'Modulating BAP1 expression affects ROS homeostasis, cell motility and mitochondrial function', *Oncotarget*, 8(42), pp. 72513–72527. doi: 10.18632/oncotarget.19872.

Vander Heiden, M. G., Cantley, L. C. and Thompson, C. B. (2009) 'Understanding the Warburg Effect: The Metabolic Requirements of Cell Proliferation', *Science*, 324(5930), pp. 3828–3828. doi: 10.1007/978-3-540-29678-2_5605.

Helgadottir, H. and Höiom, V. (2016) 'The genetics of uveal melanoma: Current insights', *Application of Clinical Genetics*, 9, pp. 147–155. doi: 10.2147/TACG.S69210.

Heppt, M. V. *et al.* (2017) 'Immune checkpoint blockade for unresectable or metastatic uveal melanoma: A systematic review', *Cancer Treatment Reviews*. Elsevier Ltd, 60, pp. 44–52. doi: 10.1016/j.ctrv.2017.08.009.

Hofmann, U. B. *et al.* (2009) 'Overexpression of the KIT/SCF in uveal melanoma does not translate into clinical efficacy of imatinib mesylate', *Clinical Cancer Research*, 15(1), pp. 324–329. doi: 10.1158/1078-0432.CCR-08-2243.

Hollstein, M. *et al.* (1991) 'p53 mutations in human cancers', *Sciene*, 253(5015).

Homsi, J. *et al.* (2009) 'Phase 2 open-label study of weekly docosahexaenoic acid-paclitaxel in cutaneous and mucosal metastatic melanoma patients', *Melanoma Research*, 19(4), pp. 238–242. doi: 10.1097/CMR.0b013e32832a1e2f.

Ilagan, J. O. *et al.* (2015) 'U2AF1 mutations alter splice site recognition in hematological malignancies', *Genome Research*, 25(1), pp. 14–26. doi: 10.1101/gr.181016.114.

Imielinski, M. *et al.* (2012) 'Mapping the hallmarks of lung adenocarcinoma with massively parallel sequencing', *Cell*, 150(6), pp. 1107–1120. doi: 10.1016/j.cell.2012.08.029.Mapping.

Inoue, D. *et al.* (2019) 'Spliceosomal disruption of the non-canonical BAF complex in cancer', *Nature*. Springer US, 574(7778), pp. 432–436. doi: 10.1038/s41586-019-1646-9.

Ishida, C. *et al.* (2019) 'Metabolic Reprogramming by Dual AKT/ERK Inhibition Through Imipridones Elicits Unique Vulnerabilities in Glioblastoma', *Physiology & behavior*, 24(21), pp. 5392–5406. doi: 10.1158/1078-0432.CCR-18-1040.Metabolic.

Isono, K. *et al.* (2005) 'Mammalian Polycomb-mediated repression of Hox genes requires the essential spliceosomal protein Sf3b1', *Genes and Development*, 19(5), pp. 536–541. doi: 10.1101/gad.1284605.

Iyer, N. V. *et al.* (1998) 'Cellular and developmental control of O2 homeostasis by hypoxia- inducible factor 1α', *Genes and Development*, 12(2), pp. 149–162. doi: 10.1101/gad.12.2.149.

Jain, R. K., Munn, L. L. and Fukumura, D. (2002) 'Dissecting tumour pathophysiology using intravital microscopy', *Nature Reviews Cancer*, 2(4), pp. 266–276. doi: 10.1038/nrc778.

Johansson, P. A. *et al.* (2019) 'Prolonged stable disease in a uveal melanoma patient with germline MBD4 nonsense mutation treated with pembrolizumab and ipilimumab', *Immunogenetics*. Immunogenetics, 4, pp. 1–4. doi: 10.1007/s00251-019-01108-x.

Kappler, L. *et al.* (2016) 'Purity matters: A workflow for the valid high-resolution lipid profiling of mitochondria from cell culture samples', *Scientific Reports*. Nature Publishing Group, 6(January), pp. 1–10. doi: 10.1038/srep21107.

Khan, S. *et al.* (2020) 'Adjuvant crizotinib in high-risk uveal melanoma following definitive therapy', *Journal of Clinical Oncology*, p. 10075.

Khan, S. and Carvajal, R. D. (2020) 'Novel Approaches to the Systemic Management of Uveal Melanoma', *Current Oncology Reports*, 22(10). doi: 10.1007/s11912-020-00965-0.

Kholmukhamedov, A., Schwartz, J. M. and Lemasters, J. J. (2013) 'MitoTracker Probes and Mitochondrial Membrane Potential Andaleb', *Shock*, 39(6), p. 543. doi: 10.1097/01.shk.0000430660.63077.7f.

Kim, E. *et al.* (2016) 'SRSF2 Mutations Contribute to Myelodysplasia Through Mutant-Specific Effects on Exon Recognition', *Cancer Cell*, 27(5), pp. 617–630. doi: 10.1016/j.ccell.2015.04.006.

Kim, J. W. *et al.* (2006) 'HIF-1-mediated expression of pyruvate dehydrogenase kinase: A metabolic switch required for cellular adaptation to hypoxia', *Cell Metabolism*, 3(3), pp. 177–185. doi: 10.1016/j.cmet.2006.02.002.

Kitamura, K. *et al.* (1988) 'Phosphorylation of myocardial fructose-6-phosphate,2-kinase:fructose-2,6-bisphosphatase by cAMP-dependent protein kinase and protein kinase C', *Journal of Biological Chemistry*, 263(32), pp. 16796–16801. doi: 10.1016/s0021-9258(18)37461-1.

Kong, Y., Krauthammer, M. and Halaban, R. (2014) 'Rare SF3B1 R625 mutations in cutaneous melanoma Yong', *Melanoma Research*, 24(4), pp. 332–334. doi: 10.1097/CMR.0000000000000071.Rare.

Kruiswijk, F., Labuschagne, C. F. and Vousden, K. H. (2015) 'P53 in survival, death and metabolic health: A lifeguard with a licence to kill', *Nature Reviews Molecular Cell Biology*, 16(7), pp. 393–405. doi: 10.1038/nrm4007.

Kujala, E., Mäkitie, T. and Kivelä, T. (2003) 'Very long-term prognosis of patients with malignant uveal melanoma', *Investigate ophtalmology & visual science*, 44(11), pp. 4651–9. doi: 10.1167/iovs.03-0538.

Lamond, A. I. and Spector, D. L. (2003) 'Nuclear speckles: a model for nuclear organelles', *Nature Reviews Molecular Cell Biology*, 4, pp. 605. – 612.

Lane, A., Egan, K. and Harmon, D. (2009) 'Adjuvant interferon therapy for patients with uveal melanoma at high risk of metastasis', *Ophtalmology*, 116, pp. 2206–2212.

Lane, A. M., Kim, I. K. and Gragoudas, E. S. (2018) 'Survival rates in patients after treatment for metastasis from uveal melanoma', *JAMA Ophthalmology*, 136(9), pp. 981–986. doi: 10.1001/jamaophthalmol.2018.2466.

Larman, T. C. *et al.* (2012) 'Spectrum of somatic mitochondrial mutations in five

cancers', *PNAS*, 109(35), pp. 14087–14091. doi: 10.1073/pnas.1211502109.

Larsen, S. *et al.* (2012) 'Biomarkers of mitochondrial content in skeletal muscle of healthy young human subjects', *Journal of Physiology*, 590(14), pp. 3349–3360. doi: 10.1113/jphysiol.2012.230185.

Lee, S. C. *et al.* (2018) 'Synthetic Lethal and Convergent Biological Effects of Cancer-Associated Spliceosomal Gene Mutations', *Cancer Cell*, 34(2), pp. 225–241. doi: 10.1016/j.ccell.2018.07.003.Synthetic.

Lerner, E. A. *et al.* (1981) 'Monoclonal antibodies to nucleic acid-containing cellular constituents: probes for molecular biology and autoimmune disease', *PNAS*, 78(5), pp. 2737–41.

Levine, A. J. and Puzio-Kuter, A. M. (2010) 'The control of the metabolic switch in cancers by oncogenes and tumor suppressor genes', *Science*, 330(6009), pp. 1340–1344. doi: 10.1126/science.1193494.

Li, A. M. and Ye, J. (2020) 'The PHGDH enigma: Do cancer cells only need serine or also a redox modulator?', *Cancer Letters*. Elsevier, 476(January), pp. 97–105. doi: 10.1016/j.canlet.2020.01.036.

Li, M. *et al.* (2017) 'STAT3 regulates glycolysis via targeting hexokinase 2 in hepatocellular carcinoma cells', *Oncotarget*, 8(15), pp. 24777–24784.

Li, Z. *et al.* (2021) 'Characterization of the aberrant splicing of MAP3K7 induced by cancer-associated SF3B1 mutation', *The Journal of Biochemistry*, mvab023.

Liu, H.-X. *et al.* (2000) 'Exonic Splicing Enhancer Motif Recognized by Human SC35 under Splicing Conditions', *Molecular and Cellular Biology*, 20(3), pp. 1063–1071. doi: 10.1128/mcb.20.3.1063-1071.2000.

Liu, Zhaoqi *et al.* (2020) 'Mutations in the RNA splicing factor SF3B1 promote tumorigenesis through MYC stabilization', *Cancer Discovery*, 10(6), pp. 806–821. doi: 10.1158/2159-8290.CD-19-1330.

Liu, Z *et al.* (2020) 'Pan-cancer analysis identifies mutations in SUGP1 that recapitulate mutant SF3B1 splicing dysregulation', *PNAS*, 117(19), pp. 10305–10312. doi: 10.1073/pnas.1922622117.

Locasale, J. W. *et al.* (2011) 'Phosphoglycerate dehydrogenase diverts glycolytic flux and contributes to oncogenesis', *Nature Genetics*, 43(9), pp. 869–874. doi: 10.1038/ng.890.

Lucignani, G. *et al.* (1992) 'MRI, Antibody-Guided Scintigraphy, and Glucose Metabolism in Uveal Melanoma', *J Comput Assist Tomogr*, 16.

Luengo, A. *et al.* (2021) 'Increased demand for NAD+ relative to ATP drives aerobic glycolysis', *Molecular Cell*. Elsevier Inc., 81(4), pp. 691-707.e6. doi: 10.1016/j.molcel.2020.12.012.

Lv, X. *et al.* (2017) 'The role of hypoxia-inducible factors in tumor angiogenesis and cell metabolism', *Genes and Diseases*. Elsevier Ltd, 4(1), pp. 19–24. doi: 10.1016/j.gendis.2016.11.003.

Madan, V. *et al.* (2015) 'Aberrant splicing of U12-type introns is the hallmark of ZRSR2 mutant myelodysplastic syndrome', *Nature Communications*, 6(6042). doi: 10.1038/ncomms7042.

Mahendraraj, K. *et al.* (2016) 'Trends in incidence, survival, and management of uveal melanoma: A population-based study of 7,516 patients from the surveillance, epidemiology, and end results database (1973–2012)', *Clinical Ophthalmology*, 10, pp. 2113–2119. doi: 10.2147/OPTH.S113623.

Majumder, P. K. *et al.* (2004) 'mTOR inhibition reverses Akt-dependent prostate intraepithelial neoplasia through regulation of apoptotic and HIF-1-dependent pathways', *Nature medicine*, 10, pp. 594–601.

Mallikarjuna, K. *et al.* (2007) 'Expression of Epidermal Growth Factor Receptor, Ezrin, Hepatocyte Growth Factor, and c-Met in Uveal Melanoma: An Immunohistochemical Study', *Current Eye Research*, pp. 281–290.

Mariani, P. *et al.* (2016) 'Radiofrequency ablation and surgical resection of liver metastases from uveal melanoma', *European Journal of Surgical Oncology*. Elsevier Ltd, 42(5), pp. 706–712. doi: 10.1016/j.ejso.2016.02.019.

Martin, M. *et al.* (2013) 'Exome sequencing identifies recurrent somatic mutations in EIF1AX and SF3B1 in uveal melanoma with disomy 3', *Nature Genetics*, 45(8), pp. 933–936. doi: 10.1038/ng.2674.

Maslon, M. M. *et al.* (2014) 'The translational landscape of the splicing factor SRSF1 and its role in mitosis', *eLife*, 2014(3), pp. 1–27. doi: 10.7554/eLife.02028.

Matera, A. G., Terns, R. M. and Terns, M. P. (2007) 'Non-coding RNAs: Lessons from the small nuclear and small nucleolar RNAs', *Nature Reviews Molecular Cell Biology*, 8(3), pp. 209–220. doi: 10.1038/nrm2124.

Mathis, T. *et al.* (2018) 'Management of uveal melanomas, guidelines for oncologists', *Bulletin du Cancer*. Société Française du Cancer, 105(10), pp. 967–980. doi: 10.1016/j.bulcan.2018.07.011.

McLaughlin, K. L. *et al.* (2020) 'Novel approach to quantify mitochondrial content and intrinsic bioenergetic efficiency across organs', *Scientific Reports*. Nature Publishing Group UK, 10(1), pp. 1–15. doi: 10.1038/s41598-020-74718-1.

Meggendorfer, M. *et al.* (2012) 'SRSF2 mutations in 275 cases with chronic myelomonocytic leukemia (CMML)', *Blood*, 120(15), pp. 3080–3088. doi: 10.1182/blood-2012-01-404863.

Michlewski, G., Sanford, J. R. and Cáceres, J. F. (2008) 'The Splicing Factor SF2/ASF Regulates Translation Initiation by Enhancing Phosphorylation of 4E-BP1', *Molecular Cell*, 30(2), pp. 179–189. doi: 10.1016/j.molcel.2008.03.013.

Mirabilii, S., Ricciardi, M. R. and Tafuri, A. (2020) 'mTOR Regulation of Metabolism in Hematologic Malignancies', *Cells*, 9(2), pp. 1–17. doi: 10.3390/cells9020404.

Modorati, G. *et al.* (1996) 'Glucose metabolism and pathological findings in uveal melaoma: Preliminary results', *Nuclear Medicine Communications*, 17, pp. 1052–1056.

Moench, R. *et al.* (2016) 'Exclusive inhibition of PI3K/Akt/mTOR signaling is not sufficient to prevent PDGF-mediated effects on glycolysis and proliferation in colorectal cancer', *Oncotarget*, 7(42), pp. 68749–68767. doi: 10.18632/ONCOTARGET.11899.

Montzka, K. A. and Steitz, J. A. (1988) 'Additional low-abundance human small nuclear ribonucleoproteins: U11, U12, etc.', *PNAS*, 85(23), pp. 8885–8889.

Morton, J. J. and Blumenthal, T. (2011) 'RNA processing in C. elegans', *Methods in Cell Biology*, 106, pp. 187–217.

Mupo, A. *et al.* (2017) 'Hemopoietic-specific Sf3b1-K700E knock-in mice display the splicing defect seen in human MDS but develop anemia without ring sideroblasts', *Leukemia*, 31(3), pp. 720–727. doi: 10.1038/leu.2016.251.

Murphy, J. P. *et al.* (2018) 'The NAD+ Salvage Pathway Supports PHGDH-Driven Serine Biosynthesis', *Cell Reports*, 24(9), pp. 2381–2391. doi: 10.1016/j.celrep.2018.07.086.The.

Muto, T. *et al.* (2013) 'Concurrent loss of *Ezh2* and *Tet2* cooperates in the pathogenesis

of myelodysplastic disorders', *The Journal of Experimental Medicine*, 210(12), pp. 2627–2639. doi: 10.1084/jem.20131144.

Nguyen, H. D. *et al.* (2019) 'Spliceosome Mutations Induce R loop-Associated Sensitivity to ATR Inhibition in Myelodysplastic Syndrome', *Cancer Research*, 78(18), pp. 5363–5374. doi: 10.1158/0008-5472.CAN-17-3970.Spliceosome.

Nguyen, T. H. D. *et al.* (2016) 'The architecture of the spliceosomal U4/U6.U5 tri-snRNP', *Nature*, 523(7558), pp. 47–52.

Obeng, E. A. *et al.* (2016) 'Physiologic Expression of Sf3b1K700E Causes Impaired Erythropoiesis, Aberrant Splicing, and Sensitivity to Therapeutic Spliceosome Modulation', *Cancer Cell*. Elsevier Inc., 30(3), pp. 404–417. doi: 10.1016/j.ccell.2016.08.006.

Okeyo-Owuor, T. *et al.* (2015) 'U2AF1 mutations alter sequence specificity of pre-mRNA binding and splicing', *Leukemia*, 29(4), pp. 909–917. doi: 10.1038/leu.2014.303.

Ooi, A. T. and Gomperts, B. N. (2016) 'Molecular Pathways: Targeting Cellular Energy Metabolism in Cancer via Inhibition of SLC2A1 and LDHA', *Clinical Cancer Research*, 21(11), pp. 2440–2444. doi: 10.1158/1078-0432.CCR-14-1209.

Palangat, M. *et al.* (2019) 'The splicing factor U2AF1 contributes to cancer progression through a noncanonical role in translation regulation', *Genes and Development*, 33(9–10), pp. 482–497. doi: 10.1101/gad.319590.118.

Pan, Q. *et al.* (2008) 'Deep surveying of alternative splicing complexity in the human transcriptome by high-throughput sequencing', *Nature Genetics*, 40(12), pp. 1413–1415. doi: 10.1038/ng.259.

Pan, S. *et al.* (2020) 'Serine, glycine and one- carbon metabolism in cancer', *International Journal of Oncology*, 58(2), pp. 158–170. doi: 10.3892/ijo.2020.5158.

Papaemmanuil, E. *et al.* (2011) 'Somatic *SF3B1* Mutation in Myelodysplasia with Ring Sideroblasts', *New England Journal of Medicine*, 365(15), pp. 1384–1395. doi: 10.1056/NEJMoa1103283.

Papastefanou, V. P. *et al.* (2014) 'Metabolic activity of primary uveal melanoma on PET/CT scan and its relationship with monosomy 3 and other prognostic factors', *British Journal of Ophthalmology*, 98(12), pp. 1659–1665. doi: 10.1136/bjophthalmol-2014-305304.

Park, S. M. *et al.* (2017) 'U2AF35(S34F) Promotes Transformation by Directing Aberrant ATG7 Pre-mRNA 3' End Formation', *Molecular Cell*, 62(4), pp. 479–490. doi: 10.1016/j.molcel.2016.04.011.U2AF35(S34F).

Pasteur, L. (1857) 'Mémoire sur la fermentation alcoolique', *CR Acad Sci*, 45, pp. 1032–1036.

Patel, S. P. *et al.* (2011) 'A phase II study of gefitinib in patients with metastatic melanoma', *Melanoma Research*, 21(4), pp. 357–363. doi: 10.1097/CMR.0b013e3283471073.

Pavlova, N. N. and Thompson, C. B. (2018) 'Emerging metabolic hallmarks of cancer', *Physiology & behavior*, 176(1), pp. 139–148. doi: 10.1016/j.cmet.2015.12.006.THE.

Pfeiffer, T., Schuster, S. and Bonhoeffer, S. (2001) 'Cooperation and competition in the evolution of ATP-producing pathways', *Science*, 292(5516), pp. 504–507. doi: 10.1126/science.1058079.

Piperno-Neumann, S. *et al.* (2017) 'A randomized multicenter phase 3 trial of adjuvant fotemustine versus surveillance in high risk uveal melanoma (UM) patients (FOTEADJ)', *Journal of Clinical Oncology*.

Polak, M. E. *et al.* (2007) 'Presence and phenotype of dendritic cells in uveal melanoma', *British Journal of Ophthalmology*, 91(7), pp. 971–976. doi: 10.1136/bjo.2006.110908.

Polet, F. *et al.* (2016) 'Reducing the serine availability complements the inhibition of the glutamine metabolism to block leukemia cell growth', *Oncotarget*, 7(2), pp. 1765–1776. doi: 10.18632/oncotarget.6426.

Poli, V. and Camporeale, A. (2015) 'STAT3-Mediated Metabolic Reprograming in Cellular Transformation and Implications for Drug Resistance', *Frontiers in Oncology*, 8(5).

Possemato, R. *et al.* (2012) 'Functional genomics reveals serine synthesis is essential in PHGDH-amplified breast cancer', *Nature*, 476(7360), pp. 346–350. doi: 10.1038/nature10350.Functional.

Pozzo, F. *et al.* (2020) SF3B1-*mutated chronic lymphocytic leukemia shows evidence of NOTCH1 pathway activation including CD20 downregulation*, *Haematologica*. doi: 10.3324/haematol.2020.261891.

Quesada, V. *et al.* (2011) 'Exome sequencing identifies recurrent mutations of the splicing factor SF3B1 gene in chronic lymphocytic leukemia', *Nature Genetics*, 44(1), pp. 47–52. doi: 10.1038/ng.1032.

Quesada, V., Ramsay, A. J. and Lopez-Otin, C. (2012) 'Chronic Lymphocytic Leukemia with SF3B1 Mutation', *New England Journal of Medicine*, 366(26).

Van Raamsdonk, C. D. *et al.* (2009) 'Frequent somatic mutations of GNAQ in uveal melanoma and blue naevi', *Nature*, 457(29), pp. 599–602. doi: 10.1038/nature07586.

Ramón y Cajal, S. (1910) 'El nucleo de las celulas piramidales del cerebro humano y de algunos mamiferos', *Trab Lab Invest Biol*, 8, pp. 27–62.

Reid, M. A. *et al.* (2018) 'Serine synthesis through PHGDH coordinates nucleotide levels by maintaining central carbon metabolism', *Nature Communications*. Springer US, 9(1), pp. 1–11. doi: 10.1038/s41467-018-07868-6.

Reina-Campos, M., Diaz-Meco, M. T. and Moscat, J. (2020) 'The complexity of the serine glycine one-carbon pathway in cancer', *Journal of Cell Biology*, 219(1). doi: https://doi.org/10.1083/jcb.201907022.

Richtig, E., Langmann, G. and Schlemmer, G. (2006) 'Safety and efficacy of interferon alfa-2b in the adjuvant treatment of uveal melanoma', *Ophthalmologe*, 103, pp. 506–511.

Rietschel, P. *et al.* (2005) 'Variates of survival in metastatic uveal melanoma', *Journal of Clinical Oncology*, 23(31), pp. 8076–8080. doi: 10.1200/JCO.2005.02.6534.

Riganti, C. *et al.* (2012) 'The pentose phosphate pathway: An antioxidant defense and a crossroad in tumor cell fate', *Free Radical Biology and Medicine*. Elsevier, 53(3), pp. 421–436. doi: 10.1016/j.freeradbiomed.2012.05.006.

Rivoire, M. *et al.* (2005) 'Treatment of Liver Metastases From Uveal Melanoma', *Annals of Surgical Oncology*, 12, pp. 422–428.

Robertson, A. G. *et al.* (2018) 'Integrative Analysis Identifies Four Molecular and Clinical Subsets in Uveal Melanoma', *Cancer Cell*, 32(2), pp. 204–220. doi: 10.1016/j.ccell.2017.07.003.

Rodrigues, M. *et al.* (2018) 'Outlier response to anti-PD1 in uveal melanoma reveals germline MBD4 mutations in hypermutated tumors', *Nature Communications*. Springer US, 9(1866), pp. 1–6. doi: 10.1038/s41467-018-04322-5.

Rodriguez-Vidal, C. *et al.* (2020) 'Treatment of metastatic uveal melanoma: Systematic

review', *Cancers*, 12(9), pp. 1–22. doi: 10.3390/cancers12092557.

Saez, B., Walter, M. J. and Graubert, T. A. (2017) 'Splicing factor gene mutations in hematologic malignancies', *Blood*, 129(10), pp. 1260–1269.

Sahtoe, D. D. *et al.* (2016) 'BAP1/ASXL1 recruitment and activation for H2A deubiquitination', *Nature Communications*, 7(10292), pp. 1–13. doi: 10.1038/ncomms10292.

Samanta, D. *et al.* (2016) 'PHGDH expression is required for mitochondrial redox homeostasis, breast cancer stem cell maintenance, and lung metastasis', *Cancer Research*, 76(15), pp. 4430–4442. doi: 10.1158/0008-5472.CAN-16-0530.

Sanford, J. R. *et al.* (2004) 'A novel role for shuttling SR proteins in mRNA translation.Genes&development.pdf', *Genes and Development*, 18, pp. 755–768. doi: 10.1101/gad.286404.nucleocytoplasmic.

Sato, T. *et al.* (2020) 'A randomized phase II study of adjuvant sunitinib or valproic acid in high-risk patients with uveal melanoma', *Journal of Clinical Oncology*.

Schaal, T. D. and Maniatis, T. (1999) 'Multiple Distinct Splicing Enhancers in the Protein-Coding Sequences of a Constitutively Spliced Pre-mRNA', *Molecular and Cellular Biology*, 19(1), pp. 261–273. doi: 10.1128/mcb.19.1.261.

Scheuerman, J. *et al.* (2010) 'Histone H2A deubiquitinase activity of the Polycomb repressive complex PR-DUB', *Nature*, 465(7295), pp. 243–247. doi: 10.1038/nature08966.

Schmittel, A. *et al.* (2006) 'A randomized phase II trial of gemcitabine plus treosulfan versus treosulfan alone in patients with metastatic uveal melanoma', *Annals of Oncology*, 17(12), pp. 1826–1829. doi: 10.1093/annonc/mdl309.

Seghezzi, W. *et al.* (1998) 'Cyclin E Associates with Components of the Pre-mRNA Splicing Machinery in Mammalian Cells', *Molecular and Cellular Biology*, 18(8), pp. 4526–4536. doi: 10.1128/mcb.18.8.4526.

Seiler, M. *et al.* (2018) 'H3B-8800, an orally available small-molecule splicing modulator, induces lethality in spliceosome-mutant cancers', *Nature Medicine*, 24(4), pp. 497–504. doi: 10.1038/nm.4493.

Sen, S., Jumaa, H. and Webster, N. J. G. (2013) 'Splicing factor SRSF3 is crucial for hepatocyte differentiation and metabolic function', *Nature Communications*, 4(1336). doi: 10.1038/ncomms2342.

Serrat, X. *et al.* (2019) 'Modeling of SF3B1 cancer-related missense mutations in C. elegans uncovers targets for synthetic lethal interactions', *bioRxiv*, pp. 1–44.

Servois, V. *et al.* (2019) 'Iterative treatment with surgery and radiofrequency ablation of uveal melanoma liver metastasis: Retrospective analysis of a series of very long-term survivors', *European Journal of Surgical Oncology*, 45(9), pp. 1717–1722. doi: 10.1016/j.ejso.2019.06.036.

Seyfried, T. N. (2015) 'Cancer as a mitochondrial metabolic disease', *Frontiers in Cell and Developmental Biology*, 3(JUL), pp. 1–12. doi: 10.3389/fcell.2015.00043.

Shiozawa, Y. *et al.* (2018) 'Aberrant splicing and defective mRNA production induced by somatic spliceosome mutations in myelodysplasia', *Nature Communications*. Springer US, 9(1). doi: 10.1038/s41467-018-06063-x.

Shirai, C. L. *et al.* (2015) 'Mutant U2AF1 Expression Alters Hematopoiesis and Pre-mRNA Splicing In Vivo', *Cancer Cell*, 27(5), pp. 631–643. doi: 10.1016/j.ccell.2015.04.008.Mutant.

Singh, A. D., Turell, M. E. and Topham, A. K. (2011) 'Uveal melanoma: Trends in

incidence, treatment, and survival', *Ophthalmology*. Elsevier Inc., 118(9), pp. 1881–1885. doi: 10.1016/j.ophtha.2011.01.040.

Smith, M. A. *et al.* (2019) 'U2AF1 mutations induce oncogenic IRAK4 isoforms and activate innate immune pathways in myeloid malignancies', *Nature cell biology*, 21(5), pp. 640–650. doi: 10.1038/s41556-019-0314-5.U2AF1.

Spadaccini, R. *et al.* (2006) 'Biochemical and NMR analyses of an SF3b155-p14-U2AF-RNA interaction network involved in branch point definition during pre-mRNA splicing', *RNA*, 12(3), pp. 410–425. doi: 10.1261/rna.2271406.

Spagnolo, F. *et al.* (2013) 'Treatment of metastatic uveal melanoma with intravenous fotemustine', *Melanoma Research*, 23(3), pp. 196–198. doi: 10.1097/CMR.0b013e3283610586.

Spector, D. L. and Lamond, A. I. (2011) 'Nuclear speckles', *Cold Spring Harbor Perspectives in Biology*, 3(2), pp. 1–12. doi: 10.1101/cshperspect.a000646.

Spraul, C. W., Lang, G. E. and Lang, G. K. (2001) 'Value of Positron Emission Tomography Tumors', *Ophthalmologica*, 215, pp. 163–168.

Stephens, P. J. *et al.* (2012) 'The landscape of cancer genes and mutational processes in breast cancer', *Nature*, 486(7403), pp. 400–404. doi: 10.1038/nature11017.

Steuhl, K. P. *et al.* (1993) 'Significance, Specificity, and Ultrastructural Localization of HMB-45 Antigen in Pigmented Ocular Tumors', *Ophthalmology*, 100(2), pp. 208–215. doi: 10.1016/S0161-6420(93)31668-4.

Stine, Z. E. *et al.* (2015) *MYC, Metabolism, and Cancer*, *Cancer discovery*. doi: 10.1158/2159-8290.CD-15-0507.MYC.

Sussman, T. A., Funchain, P. and Singh, A. (2020) 'Clinical Trials in Metastatic Uveal Melanoma: Current Status', *Ocular Oncology and Pathology*, 6(6), pp. 381–387. doi: 10.1159/000508383.

Tacke, R., Chen, Y. and Manley, J. L. (1997) 'Sequence-specific RNA binding by an SR protein requires rs domain phosphorylation: Creation of an SRp40-specific splicing enhancer', *PNAS*, 94(4), pp. 1148–1153. doi: 10.1073/pnas.94.4.1148.

Tajan, M. *et al.* (2021) 'Serine synthesis pathway inhibition cooperates with dietary serine and glycine limitation for cancer therapy', *Nature Communications*, 12(1), pp. 1–16. doi: 10.1038/s41467-020-20223-y.

Tarn, W. Y. and Steitz, J. A. (1996) 'Highly diverged U4 and U6 small nuclear RNAs required for splicing rare AT-AC introns', *Science*, 273(5283), pp. 1824–32.

Teh, J. L. F. *et al.* (2020) 'Metabolic adaptations to MEK and CDK4/6 cotargeting in uveal melanoma', *Molecular Cancer Therapeutics*, 19(8), pp. 1719–1726. doi: 10.1158/1535-7163.MCT-19-1016.

Thickman, K. R. *et al.* (2006) 'Multiple U2AF65 Binding Sites within SF3b155: Thermodynamic and Spectroscopic Characterization of Protein–Protein Interactions among pre-mRNA Splicing Factors', *Journal of Molecular Biology*, 356(3), pp. 664–683.

Tourasse, N. J., Millet, J. R. M. and Dupuy, D. (2017) 'Quantitative RNA-seq meta-analysis of alternative exon usage in C. elegans', *Genome Research*, 27(12), pp. 2120–2128. doi: 10.1101/gr.224626.117.

Tronchère, H., Wang, J. and Fu, X. D. (1997) 'A protein related to splicing factor U2AF35 that interacts with U2AF65 and SR proteins in splicing of pre-mRNA', *Nature*, 388(6640), pp. 397–400.

Vaira, V. *et al.* (2007) 'Regulation of survivin expression by IGF-1/mTOR signaling', *Oncogene*, 26(19), pp. 2678–2684. doi: 10.1038/sj.onc.1210094.

Vandekeere, S. *et al.* (2018) 'Serine Synthesis via PHGDH Is Essential for Heme Production in Endothelial Cells', *Cell Metabolism*, 28(4), pp. 573-587.e13. doi: 10.1016/j.cmet.2018.06.009.

Viale, A., Corti, D. and Draetta, G. F. (2015) 'Tumors and mitochondrial respiration: a neglected connection', *Cancer research*, 75(18), pp. 3685–3686. doi: 10.1158/0008-5472.CAN-15-0491.

Vivet-Noguer, R. *et al.* (2019) 'Emerging Therapeutic Opportunities Based on Current Knowledge of Uveal Melanoma Biology', *Cancers*, 11(7), p. 1019. doi: 10.3390/cancers11071019.

De Vries, T. J. *et al.* (1998) 'High expression of immunotherapy candidate proteins gp100, MART-1, tyrosinase and TRP-1 in uveal melanoma', *British Journal of Cancer*, 78(9), pp. 1156–1161. doi: 10.1038/bjc.1998.646.

De Waard-Siebinga, I. *et al.* (1996) 'HLA expression and tumor-infiltrating immune cells in uveal melanoma', *Graefe's Archive for Clinical and Experimental Ophthalmology*, 234(1), pp. 34–42. doi: 10.1007/BF00186516.

Wahl, M. C., Will, C. L. and Lührmann, R. (2009) 'The Spliceosome: Design Principles of a Dynamic RNP Machine', *Cell*, 136(4), pp. 701–718. doi: 10.1016/j.cell.2009.02.009.

Walker, T. M. *et al.* (2002) 'Expression of Angiogenic Factors Cyr61 and Tissue Factor in Uveal Melanoma', *Archives of Ophthalmology*, 120, pp. 1719–1725.

Wallace, D. C. (2012) 'Mitochondria and cancer', *Nature Reviews Cancer*, 12(10), pp. 685–698. doi: 10.1038/nrc3365.

van der Walt, G. and Louw, R. (2020) 'Novel mitochondrial and cytosolic purification pipeline for compartment-specific metabolomics in mammalian disease model tissues', *Metabolomics*. Springer US, 16(7), pp. 1–15. doi: 10.1007/s11306-020-01697-9.

Wan, R., Yan, C., Bai, R., Huang, G., *et al.* (2016) 'Structure of a yeast activated spliceosome at 3.5 Å resolution', *Science*, 353(6302), pp. 904–911.

Wan, R., Yan, C., Bai, R., Wang, L., *et al.* (2016) 'The 3.8 Å structure of the U4/U6.U5 tri-snRNP: Insights into spliceosome assembly and catalysis', *Science*, 351(6272), pp. 466–475.

Wang, C. *et al.* (1998) 'Phosphorylation of spliceosomal protein SAP 155 coupled with splicing catalysis', *Genes and Development*, 12(10), pp. 1409–1414. doi: 10.1101/gad.12.10.1409.

Wang, L. *et al.* (2011) 'SF3B1 and Other Novel Cancer Genes in Chronic Lymphocytic Leukemia', *New England Journal of Medicine*, 365(26), pp. 2497–2506. doi: 10.1056/NEJMoa1109016.

Wang, L. *et al.* (2016) 'Transcriptomic Characterization of SF3B1 Mutation Reveals Its Pleiotropic Effects in Chronic Lymphocytic Leukemia', *Cancer Cell*. Elsevier Inc., 30(5), pp. 750–763. doi: 10.1016/j.ccell.2016.10.005.

Wang, Z. *et al.* (2013) 'Charged Particle Radiation Therapy for Uveal Melanoma: A Systematic Review and Meta-Analysis', *International Journal of Radiation Oncology Biology Physics*, 86(1), pp. 18–26.

Warburg, O. (1925) 'The metabolism of carcinoma cells 1', *The Journal of Cancer Research*, 9(1), pp. 148–163. doi: 10.1158/jcr.1925.148.

Wardrop, J. (1809) *Observations on fungus hæmatodes or soft cancer, in several of the most important organs of the human body; containing also a comparative view of the structure of fungus hæmatodes and cancer. With cases and dissections.* Edinburgh: George Ramsay.

Weinberg, F. *et al.* (2010) 'Mitochondrial metabolism and ROS generation are essential for Kras-mediated tumorigenicity', *PNAS*, 107(19), pp. 8788–8793. doi: 10.1073/pnas.1003428107.

Weinberg, S. C. and Chandel, N. S. (2015) 'Targeting mitochondria metabolism for cancer therapy', *Nature Chemical Biology*, 11(1), pp. 9–15. doi: 10.1038/nchembio.1712.Targeting.

Weinhouse, S. (1976) 'The Warburg Hypothesis Fifty Years Later', *Z. Krebsforsch*, 87, pp. 115–126.

Will, C. L. *et al.* (1999) 'Identification of Both Shared and Distinct Proteins in the Major and Minor Spliceosomes', *Science*, 284(5422), pp. 2003–2005.

Will, C. L. *et al.* (2001) 'A novel U2 and U11/U12 snRNP protein that associates with the pre-mRNA branch site', *EMBO Journal*, 20(16), pp. 436–4546.

Will, C. L. *et al.* (2002) 'Characterization of novel SF3b and 17S U2 snRNP proteins, including a human Prp5p homologue and an SF3b DEAD-box protein', *EMBO Journal*, 21(18), pp. 4978–4988. doi: 10.1093/emboj/cdf480.

Wu, S. *et al.* (1999) 'Functional recognition 3' splice site AG by the splicing factor U2AF35', *Nature*, 402(6763), pp. 832–835. doi: 10.1038/45590.

Yan, C. *et al.* (2015) 'Structure of a yeast spliceosome at 3.6-angstrom resolution', *Science*, 349(6253), pp. 1182–91.

Yang, D. Q. *et al.* (2016) 'Measuring relative utilization of aerobic glycolysis in breast cancer cells by positional isotopic discrimination', *FEBS Letters*, 590(18), pp. 3179–3187. doi: 10.1002/1873-3468.12360.

Yang, J. *et al.* (2018) 'Treatment of uveal melanoma: where are we now?', *Therapeutic advances in medical oncology*, 10, pp. 1–17. doi: 10.1177/1758834018757175.

Yang, J. Y. *et al.* (2021) 'SF3B1 mutation in pancreatic cancer contributes to aerobic glycolysis and tumor growth through a PP2A–c-Myc axis', *Molecular Oncology*, pp. 1–15. doi: 10.1002/1878-0261.12970.

Ye, J. *et al.* (2012) 'Pyruvate kinase M2 promotes de novo serine synthesis to sustain mTORC1 activity and cell proliferation', *PNAS*, 109(18), pp. 6904–6909. doi: 10.1073/pnas.1204176109.

Yin, S. *et al.* (2019) 'A murine model of chronic lymphocytic leukemia based on B cell-restricted expression of Sf3b1 mutation and Atm deletion Shanye', *Cancer Cell*, 35(2), pp. 283–296. doi: 10.1016/j.ccell.2018.12.013.A.

Yip, B. H. *et al.* (2017) 'The U2AF1S34F mutation induces lineage-specific splicing alterations in myelodysplastic syndromes', *Journal of Clinical Investigation*, 127(6), pp. 2206–2221. doi: 10.1172/JCI91363.

Yoo, H. C. *et al.* (2020) 'Glutamine reliance in cell metabolism', *Experimental and Molecular Medicine*. Springer US, 52(9), pp. 1496–1516. doi: 10.1038/s12276-020-00504-8.

Yoshida, K. *et al.* (2011) 'Frequent pathway mutations of splicing machinery in myelodysplasia', *Nature*, 478(7367), pp. 64–69. doi: 10.1038/nature10496.

Yoshimi, A. and Abdel-Wahab, O. (2017) 'Molecular pathways: Understanding and targeting mutant spliceosomal proteins', *Clinical Cancer Research*, 23(2), pp. 336–341. doi: 10.1158/1078-0432.CCR-16-0131.

Yoshino, H. *et al.* (2018) 'PHGDH as a key enzyme for serine biosynthesis in HIF2α-targeting therapy for renal cell carcinoma', *Cancer Research*, 77(22), pp. 6321–6329. doi: 10.1158/0008-5472.CAN-17-1589.PHGDH.

Yu, C. *et al.* (2019) 'Combination of immunotherapy with targeted therapy: Theory and practice in metastatic melanoma', *Frontiers in Immunology*, 10(990). doi: 10.3389/fimmu.2019.00990.

Zaal, E. A. *et al.* (2017) 'Bortezomib resistance in multiple myeloma is associated with increased serine synthesis', *Cancer & Metabolism*. Cancer & Metabolism, 5(1), pp. 1–12. doi: 10.1186/s40170-017-0169-9.

Zamore, P. D., Patton, J. G. and Green, M. R. (1992) 'Cloning and domain structure of the mammalian splicing factor U2AF', *Nature*, 355, pp. 609–713.

Zeng, L. *et al.* (2016) 'Wortmannin influences hypoxia-inducible factor-1 alpha expression and glycolysis in esophageal carcinoma cells', *World Journal of Gastroenterology*, 22(20), pp. 4868–4880. doi: 10.3748/wjg.v22.i20.4868.

Zhang, J. *et al.* (2019) 'Disease-Causing Mutations in SF3B1 Alter Splicing by Disrupting Interaction with SUGP1', *Molecular ce*, 76(1), pp. 82–95. doi: 10.1016/j.molcel.2019.07.017.Disease-Causing.

Zhang, W. C. *et al.* (2012) 'Glycine decarboxylase activity drives non-small cell lung cancer tumor-initiating cells and tumorigenesis', *Cell*. Elsevier Inc., 148(1–2), pp. 259–272. doi: 10.1016/j.cell.2011.11.050.

Zhang, X. *et al.* (2018) 'Structure of the human activated spliceosome in three conformational states', *Cell Research*, 28(3), pp. 307–322. doi: 10.1038/cr.2018.14.

Zhao, B. *et al.* (2021) 'Characterization of the aberrant splicing of DVL2 induced by cancer-associated SF3B1 mutation', *Biochemical and Biophysical Research Communications*. Elsevier Ltd, 546, pp. 21–28. doi: 10.1016/j.bbrc.2021.01.084.

Zhao, R. Z. *et al.* (2019) 'Mitochondrial electron transport chain, ROS generation and uncoupling (Review)', *International Journal of Molecular Medicine*, 44(1), pp. 3–15. doi: 10.3892/ijmm.2019.4188.

Zhou, Q. *et al.* (2015) 'A chemical genetics approach for the functional assessment of novel cancer genes', *Cancer Research*, 75(10), pp. 1949–1958. doi: 10.1158/0008-5472.CAN-14-2930.

Zhu, X., Liao, Y. and Tang, L. (2020) 'Targeting BRD9 for Cancer Treatment : A New Strategy', pp. 13191–13200.

ANNEXES

Annex 1 – Preclinical evaluation of drug combinations identifies co-inhibition of Bcl-2/XL/W and MDM2 as a potential therapy in uveal melanoma [attachment]

Decaudin, D.; Frisch Dit Leitz, E.; Nemati, F.; Tarin, M.; Naguez, A.; Zerara, M.; Marande, B.; **Vivet-Noguer, R.**; Halilovic, E.; Fabre, C.; Jochemsen, A.; Roman-Roman, S.; Alsafadi, S. European Journal of Cancer. 2020; 126: p. 93-103. DOI: https://doi.org/10.1016/j.ejca.2019.12.012.

European Journal of Cancer 126 (2020) 93–103

Available online at www.sciencedirect.com

ScienceDirect

journal homepage: www.ejcancer.com

Original Research

Preclinical evaluation of drug combinations identifies co-inhibition of Bcl-2/XL/W and MDM2 as a potential therapy in uveal melanoma

Didier Decaudin [a,b,1], Estelle Frisch Dit Leitz [c,1], Fariba Nemati [a,1], Malcy Tarin [c], Adnan Naguez [a], Mohamed Zerara [a], Benjamin Marande [c], Raquel Vivet-Noguer [c], Ensar Halilovic [d], Claire Fabre [d], Aart Jochemsen [e], Sergio Roman-Roman [c], Samar Alsafadi [c,*]

[a] *Laboratory of Preclinical Investigation, Department of Translational Research, Institut Curie, PSL University, Paris, France*
[b] *Department of Medical Oncology, Institut Curie, Paris, France*
[c] *Uveal Melanoma Translational Group, Department of Translational Research, Institut Curie, PSL Research University, Paris, France*
[d] *Novartis Institutes for Biomedical Research, Cambridge, MA, USA*
[e] *Department of Cell and Chemical Biology, Leiden University Medical Center, Leiden, the Netherlands*

Received 29 November 2019; accepted 6 December 2019
Available online 9 January 2020

KEYWORDS
Uveal melanoma;
Bcl-2/XL/W;
MDM2;
Drug synergism;
Drug screening;
Patient-derived xenografts

Abstract ***Introduction:*** Uveal melanoma (UM) is a rare and malignant intraocular tumour with a dismal prognosis. Despite a good control of the primary tumour by radiation or surgery, up to 50% of patients subsequently develop metastasis for which no efficient treatment is yet available.

Methodology: To identify therapeutic opportunities, we performed an *in vitro* screen of 30 combinations of different inhibitors of pathways that are dysregulated in UM. Effects of drug combinations on viability, cell cycle and apoptosis were assessed in eight UM cell lines. The best synergistic combinations were further evaluated in six UM patient-derived xenografts (PDXs).

Results: We demonstrated that the Bcl-2/X_L/W inhibitor (ABT263) sensitised the UM cell lines to other inhibitors, mainly to mammalian target of rapamycin (mTOR), mitogen-activated protein kinase kinase (MEK) and murine double minute 2 (MDM2) inhibitors. mTOR (RAD001) and MEK1/2 (trametinib) inhibitors were efficient as single agents, but their combinations with ABT263 displayed no synergism in UM PDXs. In contrast, the combination of

* *Corresponding author*:
E-mail address: samar.alsafadi@curie.fr, samaralsafadi@yahoo.com (S. Alsafadi).
[1] Joint first co-author.

https://doi.org/10.1016/j.ejca.2019.12.012

ABT263 with MDM2 inhibitor (HDM201) showed a trend for a synergistic effect.
Conclusion: We showed that inhibition of Bcl-2/X_L/W sensitised the UM cell lines to other treatments encouraging investigation of the underlying mechanisms. Furthermore, our findings highlighted Bcl-2/X_L/W and MDM2 co-inhibition as a promising strategy in UM.

1. Introduction

Uveal melanoma (UM) is a rare tumour deriving from melanocytes in the uveal tract. Considered to be the most common primary malignant intraocular tumour in adults, UM affects five individuals per million per year [1]. Despite a good control of the localised tumour by radiotherapy or surgery, up to 50% of UM patients develop metastases mainly in the liver. Once the disease has spread, the prognosis is poor with median survival of 9 months, and the treatment is challenging with absence of efficient therapeutic strategies [2,3].

In contrast to cutaneous melanoma, UM has a low mutational burden with two events per tumour beside few genomic alterations (losses of chromosome 1p, 3, 6q and 8p and gain of 8q) [4]. The first and most recurrent event in UM is the activation of Gαq signalling induced by mutations of *GNAQ/11* [5]. These mutations lead to activation in downstream effectors including protein kinase C (PKC), mitogen-activated protein kinases (MAPK) and yes-associated protein (YAP), implying a strong rational for therapeutic targeting of the related pathways in UM [6–9]. The second event consists of mutually exclusive mutations in the *BAP1*, *SF3B1 and EIF1AX* genes involved in processes of chromatin remodelling, splicing and translation, respectively.

Previous studies have shown that UM cell lines and patient-derived xenografts (PDXs) are susceptible to inhibition of single pathways such as PKC or mitogen-activated protein kinase kinase (MEK) [8,10,11]. However, clinical trials relying on monotherapeutic strategies have not resulted in any significant benefit in terms of overall survival of UM patients [12–14]. Such findings emphasised the need for combined strategies to improve clinical outcomes. We and others have previously shown that co-inhibition of targets such as PKC and murine double minute 2 (MDM2)/MDM4 or mammalian target of rapamycin (mTOR), and phosphoinositide 3-kinase (PI3K) synergistically improved the response in preclinical models [15–21].

Here, to identify further therapeutic opportunities in UM, we performed an *in vitro* screen of 30 combinations of different inhibitors of pathways dysregulated in UM. Cell viabilities under treatment with single or combined agents in eight UM cell lines were considered to calculate the synergy score for each drug combination. The eight best-ranked combinations were further evaluated for apoptosis, cell cycle profiles and related pathway engagement. Our data showed that the Bcl-2/X_L/W inhibitor (ABT263) displayed a highly synergistic potential in UM cell lines, mainly with mTOR, MEK and MDM2 inhibitors. These ABT263-based combinations were selected for assessment in six UM PDXs. mTOR (RAD001) and MEK (trametinib) inhibitors showed good efficacy in UM PDXs as single agents, but their combinations with ABT263 showed no clear benefit. In contrast, the combination of ABT263 with MDM2 inhibitor (HDM201) showed a trend for a synergistic effect encouraging further investigation of Bcl-2/X_L/W and MDM2 co-inhibition.

2. Materials and methods

2.1. Cell culture

MP38, MP46, MP65, MM28 and MM66 were established in our laboratory [11]. OMM1, OMM2.3 and OMM2.5 were kindly provided by P.A. van der Velden (Leiden University Medical Center, The Netherlands). The main characteristics of the used cell lines are reported in Supplementary Table S1. The immortalised hTERT RPE1 cell line was purchased from the ATCC. Cells were cultured in RPMI-1640 supplemented with 10% foetal bovine serum (FBS) (OMM1, OMM2.3, OMM2.5, RPE1) or 20% FBS (MP38, MP46, MP65, MM28, MM66). All cells were maintained at 37°C in a humidified atmosphere with 5% CO2 and were tested and certified as mycoplasma free.

2.2. Compounds

All drugs and inhibitors (Supplementary Table S2) were purchased from SelleckChem except HDM201 generously provided by Novartis Institutes for Biomedical Research. For the *in vitro* study, all drugs were dissolved in dimethyl sulfoxide (DMSO) at 10 mM and stored at −20°C. For the *in vivo* study, drug preparations are detailed in the Supplementary Table S3.

2.3. Drug combination cell viability screen

Cells were plated in 96-well plates at appropriate concentration. Twenty-four hours later, drugs were added as single agents or in combinations. Serial 1:3 dilutions were prepared starting from the maximal concentration for each

drug (Supplementary Table S2), resulting in six different concentrations (Supplementary Fig. S1). Cell viability was assessed after 5 days of treatment using MTT (3-(4,5-dimethylthiazol-2-yl)-2,5-diphenyltetrazolium bromide) assay (Sigma). Three technical replicates and three independent biological replicates were performed for each treatment and for each cell model. As detailed in a previous paper, Bliss independence model was used to determine the combination synergistic potential [15].

2.4. Caspase-3/7 activity assay and cell cycle analysis

Cells were treated with combinations at synergistic doses defined according to the screening. A fluorescence-based assay was used to determine the activity of caspases-3 and caspase-7 (Apo-One Homogeneous Caspase-3/7 Assay, Promega). The assay was performed according to the manufacturer's recommendations.

For cell cycle profiling, cells were collected, washed twice with phosphate buffered saline (PBS) and fixed with cold ethanol. Afterwards, cells were pelleted and resuspended in PBS containing 50 µg/ml propidium iodide (Sigma Aldrich) and 2.5U/mL RNAse I (ThermoFisher). Samples were analysed using FACScalibur (Becton Dickinson) and CellQuest software (Becton Dickinson).

2.5. Immunoblot analyses

Protein extracts, separated by SDS-PAGE and transferred onto polyvinylidene difluoride (PVDF) membranes, were probed with antibodies against p21 (#2947), pS6 (#2215), S6 (#2317), poly ADP-ribose polymerase (PARP, #9542),

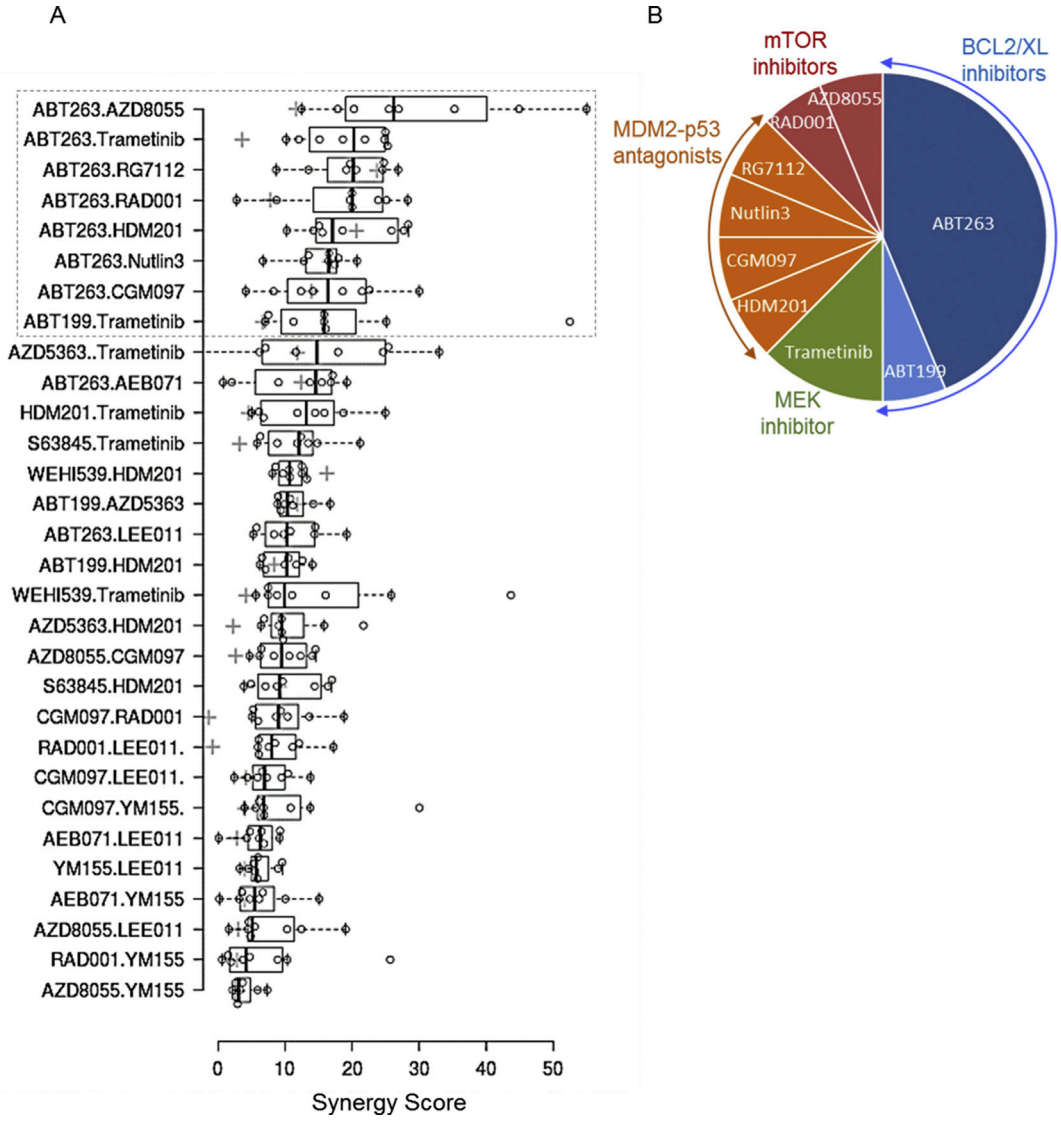

Fig. 1. **Ranking of drug combinations tested *in vitro* according to synergy scores**. (A) The screening of drug combinations was done in eight uveal melanoma cell lines and in RPE1 (retinal pigment epithelial cells). The best-ranked eight combinations in uveal melanoma cell lines are indicated. Each circle represents the synergy score in one cell line. The light grey plus (+) represents the synergy score in RPE1. (B) Representation of compound and targeted pathway enrichment in the best-ranked eight combinations.

pERK (#9101), extracellular signal-regulated kinase (ERK) (#9102) and actin (#3700), all purchased from Cell Signaling Technology (Beverly, MA). Immunolabelled proteins were detected using Odyssey secondary antibodies coupled to a 700 or 800 nm and the Odyssey Infrared Imaging System (Li-cor). Actin immunoblotting was used to quantify and normalise results.

2.6. Uveal melanoma PDX models and in vivo treatments

We used PDXs derived from liver metastatic tumour samples (MM26, MM66, MM224, MM252, MM267, MM300 and MM309), and one established from a cutaneous metastasis (MM33). The main molecular features of these models are presented in the Supplementary Table S4. The experimental protocol of the *in vivo* study is detailed in the supplementary methods [10,30].

3. Results

3.1. Identification of synergistic combinations in a panel of uveal melanoma cell lines

We performed a screen of 30 dual drug combinations in a panel of eight UM cell lines harbouring the most frequent genetic features of the metastatic disease with *GNAQ* or *GNA11* mutations associated or not with BAP1 deficiency. The assessed cell lines were derived either from metastases or from primary tumours lacking BAP1 expression, a feature correlated with poor prognosis (Supplementary Table S1). Immortalised RPE1 cell line was included as a control cell line with no mutations affecting the targeted pathways. The tested compounds were selected based on the current knowledge of pathways dysregulated in UM for which specific inhibitors are available (Supplementary Table S2). All combinations were assessed for synergy based on cell viability and according to the Bliss independence model. Fig. 1A shows the ranking of the tested combinations according to their median Best Excess Over Bliss values in UM cell lines.

The best-ranked eight combinations were enriched by Bcl-2/X_L/W inhibitor ABT263 (Fig. 1B). ABT263 exhibited low efficacy as a single agent but synergised with most tested compounds in UM cell lines. The synergistic effect decreased when replacing ABT263 by selective inhibitors of Bcl-2 (ABT199), Bcl-X_L (WEHI539) or MCL1 (S63845). This finding suggests that simultaneous inhibition of different BCL-2 family members is needed to promote the synergism. MDM2 inhibitors were the second best represented compounds in the top-ranked eight combinations. Thus, the results of our drug screening suggest that the Bcl-2/X_L/W inhibitor ABT263 sensitises the UM cells to inhibitors of several pathways including MDM2, mTOR and MEK inhibitors.

3.2. Assessment of apoptosis and cell cycle under treatment with the best synergistic drug combinations

Since the synergy was evaluated based on cell viability reduction rather than cell death induction, we investigated the effects of the best-ranked eight combinations on apoptosis induction and cell cycle in the OMM1 cells.

We evaluated apoptosis based on caspase 3/7 activity at 72 h of treatment. Fig. 2 shows that the Bcl-2/X_L/W and Bcl-2 inhibitors, ABT263 and ABT199, induced caspase 3/7 activation as single agents. The other tested single agents did not affect caspase 3/7 activation. Interestingly, the eight drug combinations displayed a considerable synergistic potential in terms of caspase 3/7 activation as compared with single agents implying an added value of combining these agents.

Additionally, we characterised the effect of the selected drug combinations on cell cycle. As shown in Supplementary Fig. S2, the sub-G1 profiles confirmed an increased induction of cell death under treatment with ABT263 and MDM2 inhibitors including CGM097, Nutlin3, HDM201 and RG112 (32–40% in combined treatments versus 21% in ABT263 and 8–10% in MDM2 inhibitors) along with a decrease in the proportion of proliferating cells in S phase. On the other hand, single-agent treatments did not induce any significant changes in cell cycle.

We further analysed the expression of proteins engaged in the related pathways in treated OMM1 cells. As shown in Fig. 3A and B, we observed increased levels of PARP

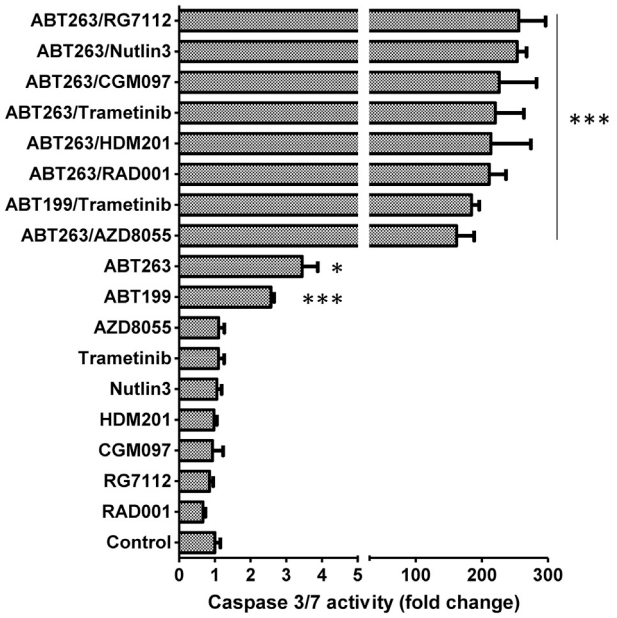

Fig. 2. **Apoptosis induction in OMM1 cells treated with eight best-ranked combinations**. Quantification of apoptosis induction after treatment with the eight best-ranked combinations. A fluorescence-based assay was used to determine the activity of caspase-3 and caspase-7, indicators of apoptosis induction.

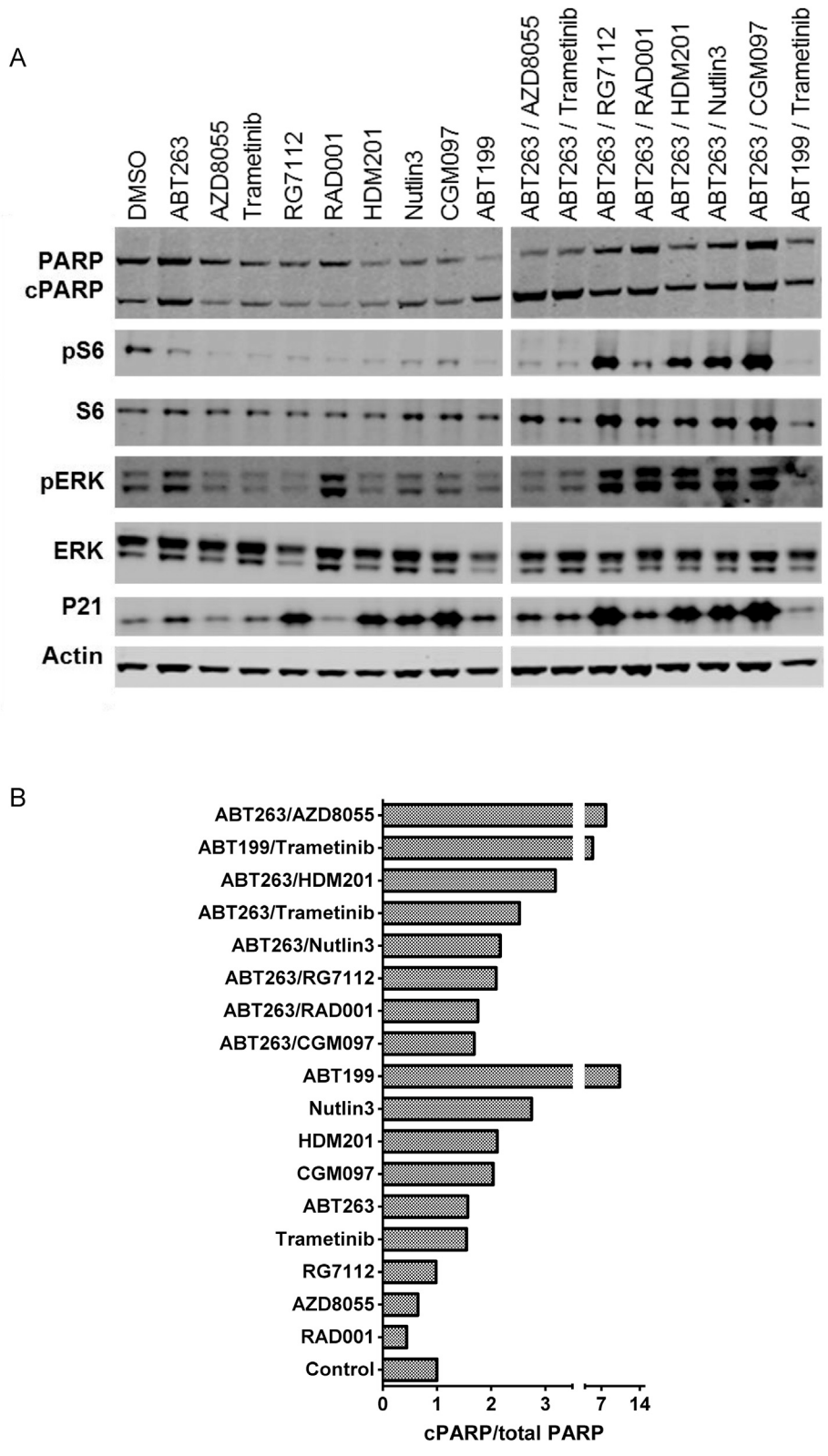

Fig. 3. **Immunoblot analysis for cleaved PARP and key signalling pathways in uveal melanoma**. (A) Western blots of OMM1 cells treated with the best-ranked drug combinations for 5 days. Cell lysates were analysed with the indicated antibodies. (B) Ratio of PARP cleavage product to total PARP as evaluated by Western blot intensities.

cleavage under combined treatments with ABT263 and HDM201/trametinib/AZD8055 as compared with single treatments. p21 was mainly induced following treatment with different MDM2 inhibitors, consistent with the activation of p53 pathway (Fig. 3A). MEK/ERK pathway was inhibited in treatments targeting MEK and MDM2 (Fig. 3A). Intriguingly, we observed a negative feedback regulation of ERK phosphorylation and S6 expression under combinations of ABT263 and MDM2 inhibitors.

Overall, our results show that the Bcl-2/X_L/W inhibitor ABT263 displays a highly synergistic potential with several agents in UM cell lines. MDM2, mTOR and MEK inhibitors were then selected as potential candidates to be combined with ABT263 for a further *in vivo* evaluation.

3.3. In vivo evaluation of ABT263-based combinations in UM PDXs

Based on these *in vitro* findings, three ABT263-based combinations were further assessed in six UM PDXs. These models were all established from liver metastases except for MM33 that was obtained from a cutaneous metastasis. Supplementary Table S4 recapitulates the histology and *GNAQ/GNA11*, *BAP1* and *SF3B1* statuses of these models. The list of tested drugs, doses and the schedule of administration are provided in Supplementary Table S3. We tested the Bcl-2/X_L/W inhibitor ABT263, alone or combined with the MDM2 inhibitor HDM201, the mTOR inhibitor RAD001 and with the MEK1/2 inhibitor trametinib. For each model, three mice were treated per group. Two of the drugs were administered in two different schedules to evaluate their efficacy while minimising the toxic effects: HDM201 was administered twice a week, every week (HDM-1) or every two weeks (HDM-2), while RAD001 was administered 5 days per week (RAD-1) or twice a week, every week (RAD-2) or every 4 weeks (RAD-3).

Single-agent ABT263 did not induce significant tumour regression in the tested models (Figs. 4–6 and Supplementary Figs. S3–S5). In contrast, HDM201 alone induced a slight but not dose-dependent antitumour efficacy with an overall response rate (ORR) lower than −0.5 of 35% and 43% in the continuous and discontinuous schedules of administration, respectively (Fig. 4A). Interestingly, we observed a slight synergistic effect of the combination of ABT263 + HDM-1 (continuous schedule of administration), but not HDM-2 (discontinuous schedule), with an ORR lower than

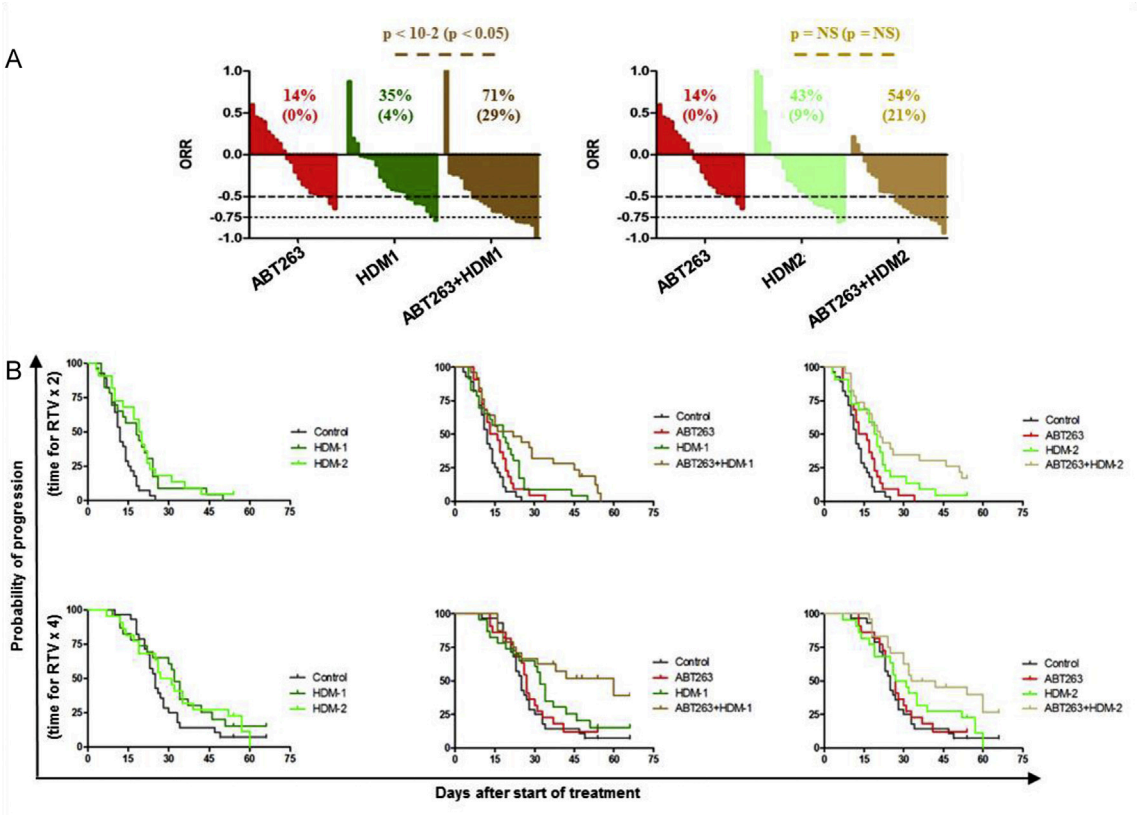

Fig. 4. ***In vivo* efficacy of ABT263 ± HDM201 in six uveal melanoma patient-derived xenografts**. (A) Overall response rate (ORR); the percentage in brackets correspond to an ORR lower than −0.75. (B) Probability of progression after each tested treatment; the methodology is detailed in the Materials & Methods section; the time to reach relative tumour volume (RTV) x 2 and RTV x 4 for each treated mouse has been calculated.

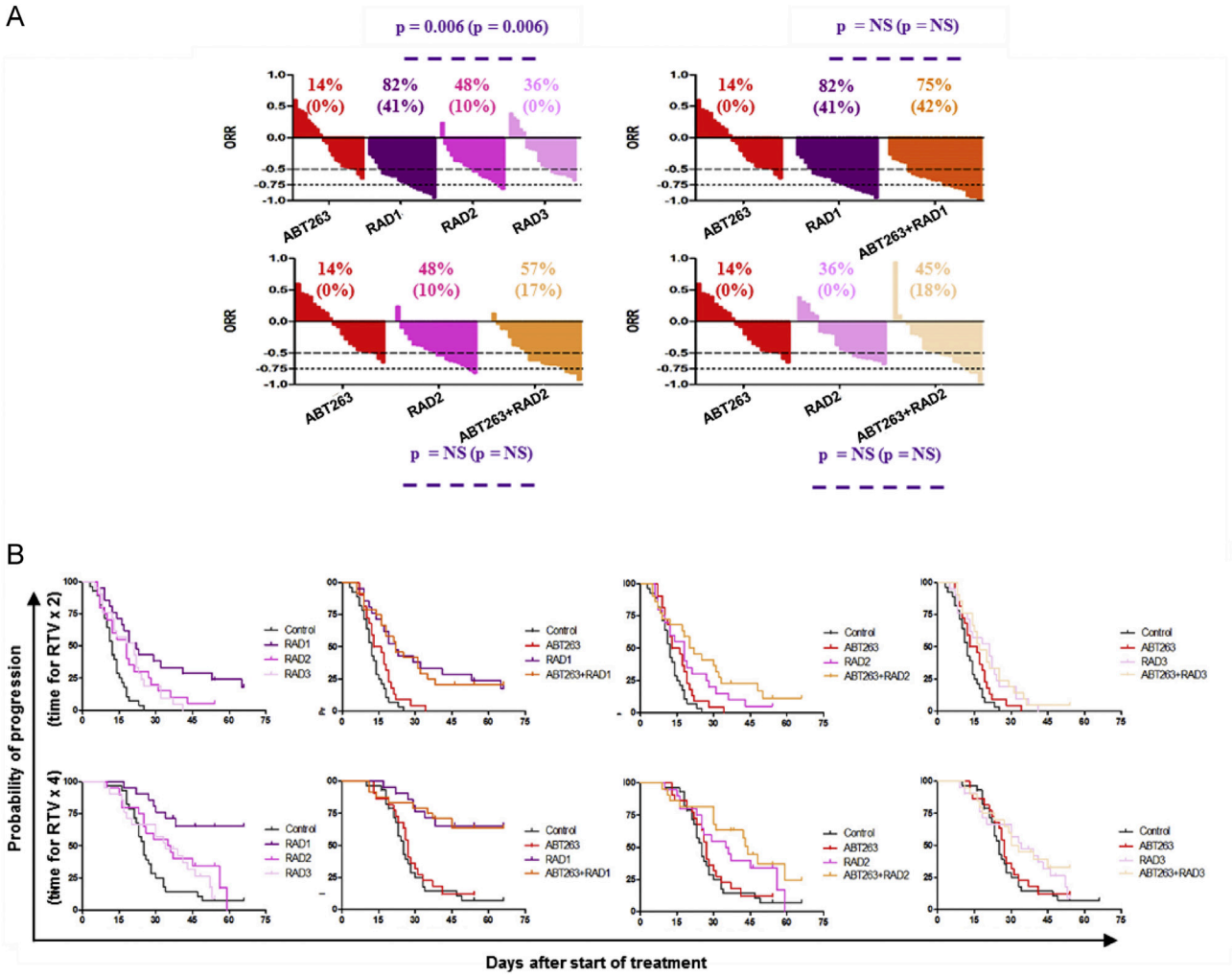

Fig. 5. ***In vivo*** **efficacy of ABT263 ± RAD001 in six uveal melanoma patient-derived xenografts**. (A) Overall response rate (ORR); the percentage in brackets correspond to an ORR lower than −0.75. (B) Probability of progression after each tested treatment; the methodology is detailed in the Materials & Methods section; the time to reach RTV x 2 and RTV x 4 for each treated mouse has been calculated.

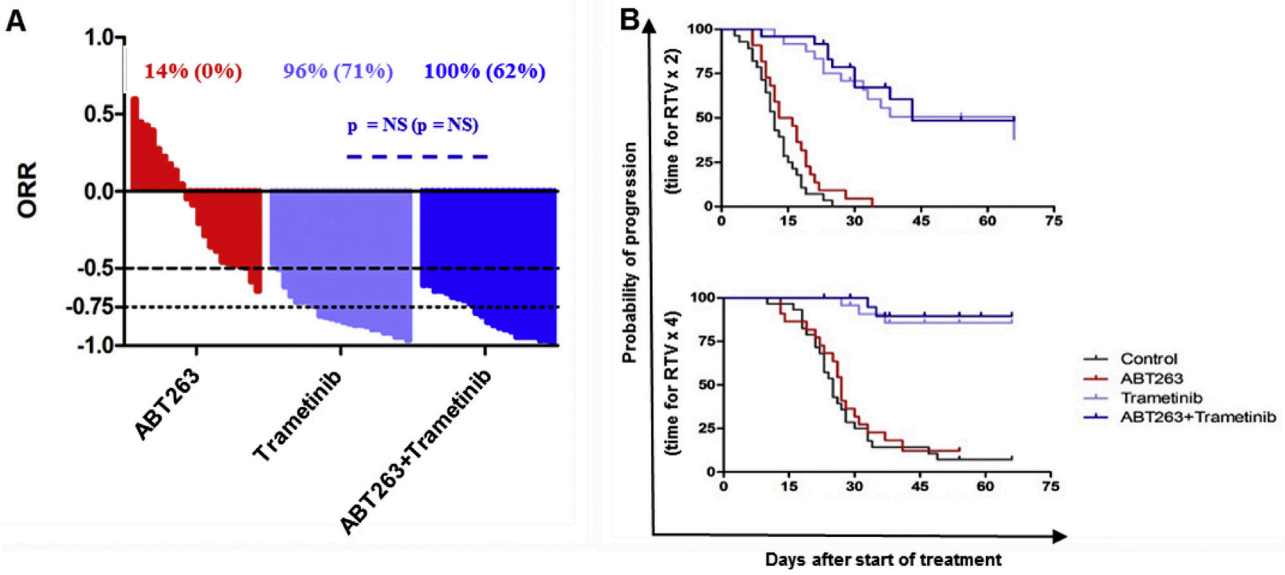

Fig. 6. ***In vivo*** **efficacy of ABT263 ± trametinib in six uveal melanoma patient-derived xenografts**. (A) Overall response rate (ORR); the percentage in brackets correspond to an ORR lower than −0.75. (B) Probability of progression after each tested treatment; the methodology is detailed in the Materials & Methods section; the time to reach RTV x 2 and RTV x 4 for each treated mouse has been calculated.

−0.5 of 35% and 71% after HDM-1 alone and ABT263 + HDM-1, respectively (Fig. 4A). Yet, we did not observe any significant impact on the probability of tumour progression (Fig. 4B). Individual curves are displayed in Supplementary Fig. S3.

Concerning the single-agent treatments, trametinib and full-dose RAD001 (RAD-1, 5 days/week) showed the best antitumour response. The antitumour effect of full-dose RAD001 was significantly higher ($p = 0.006$) than RAD001 administered with the other two schedules, showing a high dose-dependent antitumour efficacy (Fig. 5A). We did not observe any additive effect for ABT263 + RAD001, regardless of RAD001 administration schedule (Fig. 5B). Individual curves are displayed in Supplementary Fig. S4.

Despite a significant antitumour activity of trametinib alone with an ORR lower than −0.5 of 96% (Fig. 6A), its combination with ABT263 did not show any additive effect (Fig. 6B). Individual curves are displayed in Supplementary Fig. S5.

Analysis of protein expression of residual tumours in treated MM300 PDXs confirmed S6 or ERK dephosphorylation by RAD001 and trametinib (Fig. 7A and B). ABT263 + HDM-1 (continuous schedule of administration), but not HDM-2 (discontinuous schedule), showed significant increase of p21, indicator of p53 activation. Intriguingly, no significant PARP cleavage was detected. The absence of this indicator of apoptosis can be explained by the heterogeneity of cell exposure to treatments *in vivo* or by the fact that residual tumours represent cells resisting upon treatment.

We then investigated whether ABT199, a highly selective inhibitor of Bcl-2 with limited clinical toxicity, is as efficacious as ABT263 in combination with HDM201

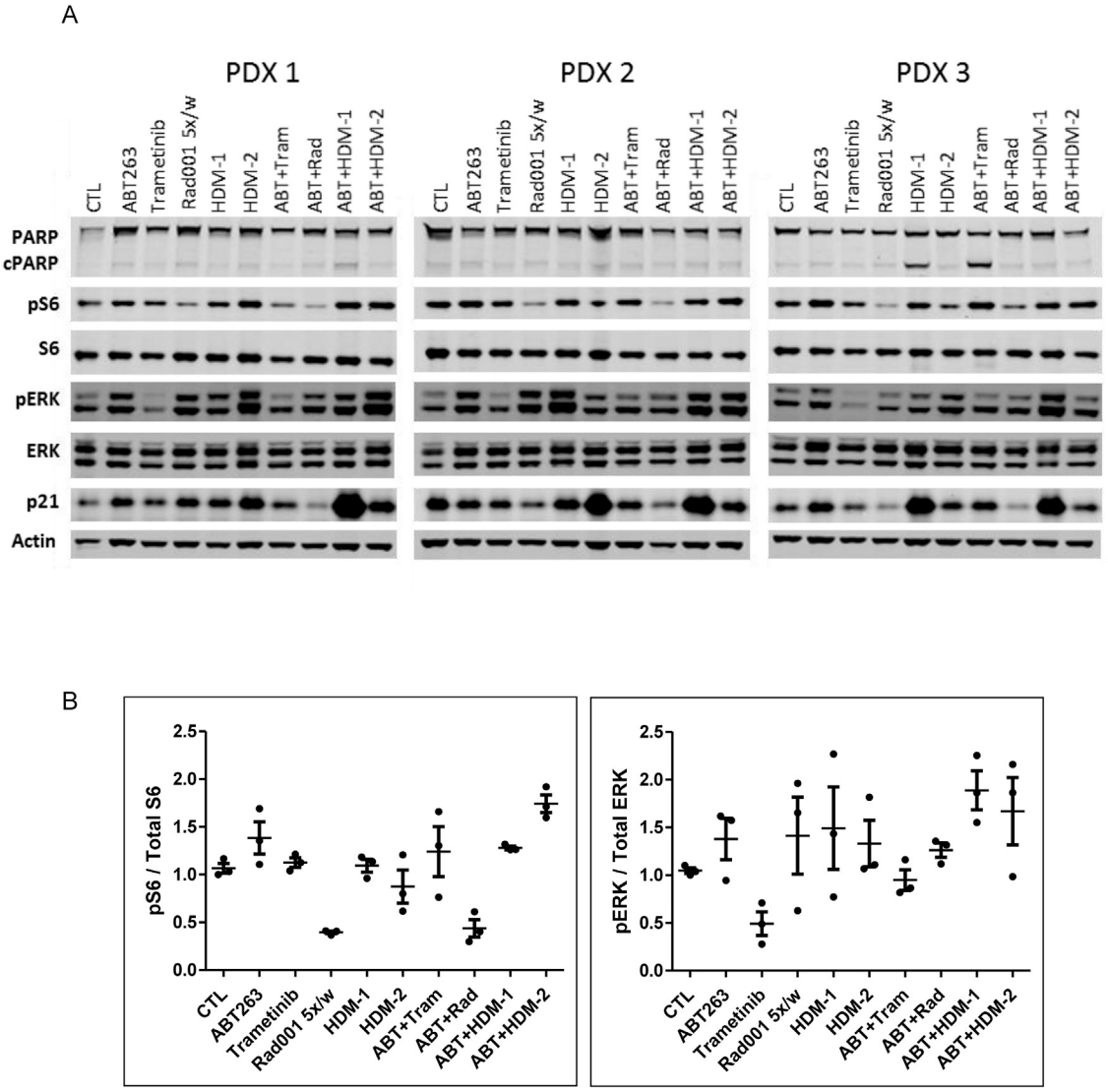

Fig. 7. **Protein expression levels after combination treatment *in vivo***. (A) Immunoblot analysis of key signalling pathways in three different mice of MM300 PDX model after treatment with ABT263 combined with HDM201, RAD001 or trametinib. (B) Ratios of blot intensities of pS6 to total S6 and pERK to total ERK as determined by ImageJ. ERK, extracellular signal-regulated kinase.

under the continuous schedule of treatment in two UM PDX models. In contrast to ABT263, ABT199 did not provide any significant increase of HDM201 antitumour effect (Supplementary Fig. S6).

Thus, based on our *in vivo* findings, trametinib and RAD001 showed good efficacy as single agents, but their tested combinations provided no significant antitumor benefit. Interestingly, the combination of ABT263 with HDM201 showed a trend of synergistic effect that was not observed when replacing ABT263 by the Bcl-2 selective inhibitor ABT199.

4. Discussion

UM is a rare tumour of which metastatic lesions remain a main therapeutic challenge in the absence of efficient treatments. The identification of the UM major driver events has oriented the preclinical and clinical trials towards inhibitors of the pathways dysregulated by these events. Nevertheless, single pathway inhibition has not improved patient outcomes so far, arguing for the need of combinatorial approaches.

Our screening of 30 combinations in eight UM cell lines identified the Bcl-2/X_L/W inhibitor ABT263 as the molecule with the highest synergistic potential followed by the MDM2 (RG7112, HDM201, Nutlin3, CGM097) and mTOR (AZD8055, RAD001) inhibitors. Our findings demonstrated that apoptosis was increased following treatment with these combinations as compared with single-agent treatments. The cell cycle profiles confirmed an increased induction of apoptosis in cells treated with ABT263 and MDM2 inhibitors along with a decrease in the proliferation rate. While single-agent ABT263 exhibited low efficacy in UM cell lines, it enhanced considerably the effect of the other compounds. These findings are consistent with previous studies reporting a high synergistic potential of Bcl-2/X_L/W inhibition when combined with cytotoxic agents in different types of cancer [22–27].

Based on the observed synergism between the Bcl-2/X_L/W inhibitor and MDM2, mTOR and MEK inhibitors (HDM201, RAD001 and trametinib, respectively), these combinations were further evaluated in metastatic UM PDXs. As in cell lines, single-agent ABT263 presented a modest effect on the tumour volume, while the other inhibitors (HDM201, RAD001 and trametinib) decreased considerably the tumour volume as monotherapies. The tested combinations did not show any synergistic effect in terms of progression probability except for the combination of ABT263 with HDM201. BCL2 and MDM2 are both reported to be highly expressed in UM arguing a further therapeutic interest of this co-inhibition [4,28,29]. Chapeau et al. conducted a large-scale transposon-based insertional mutagenesis screen to investigate the resistance to HDM201 in mice [26]. Among the most frequent alterations conferring resistance, they observed transposon-mediated gain-of-function alterations in Bcl-X_L and confirmed its overexpression in HDM201-resistant tumours. Furthermore, they demonstrated a significant synergy of MDM2 and Bcl-X_L co-inhibition in p53 wild-type cell lines [26]. Interestingly, our data are in line with these recent findings implying that synergism is due to Bcl-2/X_L/W inhibition rather than specific inhibition of Bcl-2 (ABT199), Bcl-X_L (WEHI539) or MCL1 (S63845).

5. Conclusion

Overall, our study highlights the potential of Bcl-2/X_L/W inhibition to enhance the activity of MDM2 inhibition in UM. Further characterisation of the underlying mechanisms to determine why and how such drug combinations synergise to induce apoptosis in UM cells would improve the current therapeutic strategies.

Conflicts of interest statement

E.H. and C.F. are employees at Novartis. The other authors declare no conflict of interest.

Acknowledgements

This study is supported by the European Union's Horizon 2020 research and innovation programme (UM Cure 2020 project, grant agreement no. 667787) and SIRIC Curie (Grant INCa-DGOS-Inserm_12554). The authors acknowledge Emilie Vinolo (seeding science SPRL, Limelette, Belgium) for her editorial support, as well as the other members of the UM Cure 2020 Consortium: Viviana Anelli, Marina Mione (Università degli Studi di Trento, Centre for Integrative Biology, Trento, Italy), Niels J. Brouwer, Rogier Nell, Pieter van der Velden, Annemijn Wierenga, Ellen Kapiteijn (Department of Medical Oncology, Leiden University Medical Center, Leiden, The Netherlands), Erica Cirri, Antoine Prestat, Jennifer Sengenes (PEP-Therapy SAS, Paris, France), Sophie Piperno-Neumann, Manuel Rodrigues (Department of Medical Oncology, Institut Curie, PSL Research University, Paris, France) Laurence Desjardins, Nathalie Cassoux (Department of Ocular Oncology, Institut Curie, PSL Research University, Paris, France), Raymond Barnhill (Department of Translational Research, Institut Curie, PSL Research University, Paris, France), Martyna Elas, Bozena Romanowska-Dixon (Jagiellonian University Medical College, Krakow, Poland), Martine J. Jager (Department of Ophtalmology, Leiden University Medical Center, Leiden, The Netherlands), Kseniya Glinkina (Department of Cell and Chemical Biology, Leiden

University Medical Center, Leiden, The Netherlands), Arwin Groenewoud, Ewa Snaar-Jagalska (Universiteit Leiden, Leiden, The Netherlands), Richard Marais, Pauline Hascoet, Valeria Pavet Rodrigues (Molecular Oncology Group, Cancer Research UK Manchester Institute, University of Manchester, Manchester, UK), Liesbeth Houkes, Dianne van den Heuvel (PamGene Internationa BV, BJ's-Hertogenbosch, The Netherlands), Sarah E. Coupland, Helen Kalirai, Matthew Traynor (Department of Molecular and Clinical Cancer Medicine, University of Liverpool, Liverpool, UK), Ana Lalanne, Olivier Lantz (INSERM U932 and Laboratory of Clinical Immunology, Institut Curie, PSL Research University, Paris, France), Pascale Mariani (Department of ophthalmologic surgery, Institut Curie, PSL Research University, Paris, France), Marc-Henri Stern, Lenha Mobuchon (Department of Genetics, Institut Curie, PSL Research University, Paris, France), André Valente, Guilherme Neri Pires, Constança Roquette (Champalimaud Foundation, Lisbon, Portugal), Bettina Ryll, Andrew Evans, Iain Galloway and Dick Plomp (Melanoma Patient Network Europe, Uppsala, Sweden).

The authors wish to thank the Animal Platform CRP2-UMS 3612 CNRS-US25 Inserm-IRD (Faculty of Pharmacy, Paris Descartes University, Paris), and the Animal Platform of Institut Curie. They also thank Justine Fleury and Steven Birot de la Pommeraye for their technical assistance (Laboratory of preclinical investigation, Institut Curie).

Appendix A. Supplementary data

Supplementary data to this article can be found online at https://doi.org/10.1016/j.ejca.2019.12.012.

References

[1] Mahendraraj K, Lau CSM, Lee I, Chamberlain RS. Trends in incidence, survival, and management of uveal melanoma: a population-based study of 7,516 patients from the surveillance, epidemiology, and end results database (1973–2012). Clin Ophthalmol 2016. https://doi.org/10.2147/OPTH.S113623.

[2] Singh M, Durairaj P, Yeung J. Uveal melanoma: a review of the literature. Oncol Ther 2018;6:87–104. https://doi.org/10.1007/s40487-018-0056-8.

[3] Vivet-Noguer R, Tarin M, Roman-Roman S, Alsafadi S. Emerging therapeutic opportunities based on current knowledge of uveal melanoma biology. Cancers 2019. https://doi.org/10.3390/cancers11071019.

[4] Helgadottir H, Höiom V. The genetics of uveal melanoma: current insights. Appl Clin Genet 2016. https://doi.org/10.2147/TACG.S69210.

[5] Van Raamsdonk CD, Griewank KG, Crosby MB, Garrido MC, Vemula S, Wiesner T, et al. Mutations in GNA11 in uveal melanoma. N Engl J Med 2010. https://doi.org/10.1056/nejmoa1000584.

[6] Feng X, Degese MS, Iglesias-Bartolome R, Vaque JP, Molinolo AA, Rodrigues M, et al. Hippo-independent activation of YAP by the GNAQ uveal melanoma oncogene through a trio-regulated rho GTPase signaling circuitry. Cancer Cell 2014. https://doi.org/10.1016/j.ccr.2014.04.016.

[7] Yu FX, Zhao B, Guan KL. Hippo pathway in organ size control, tissue homeostasis, and cancer. Cell 2015. https://doi.org/10.1016/j.cell.2015.10.044.

[8] Wu X, Zhu M, Fletcher JA, Giobbie-Hurder A, Hodi FS. The protein kinase C inhibitor enzastaurin exhibits antitumor activity against uveal melanoma. PLoS One 2012. https://doi.org/10.1371/journal.pone.0029622.

[9] Feng X, Arang N, Rigiracciolo DC, Lee JS, Yeerna H, Wang Z, et al. A Platform of synthetic lethal gene interaction networks reveals that the GNAQ uveal melanoma oncogene controls the hippo pathway through FAK. Cancer Cell 2019. https://doi.org/10.1016/j.ccell.2019.01.009.

[10] Decaudin D, Botty R El, Diallo B, Massonnet G, Fleury J, Naguez A, et al. Selumetinib-based therapy in uveal melanoma patient-derived xenografts. Oncotarget 2018. https://doi.org/10.18632/oncotarget.24670.

[11] Amirouchene-Angelozzi N, Nemati F, Gentien D, Nicolas A, Dumont A, Carita G, et al. Establishment of novel cell lines recapitulating the genetic landscape of uveal melanoma and preclinical validation of mTOR as a therapeutic target. Mol Oncol 2014. https://doi.org/10.1016/j.molonc.2014.06.004.

[12] Carvajal RD, Sosman JA, Quevedo JF, Milhem MM, Joshua AM, Kudchadkar RR, et al. Effect of selumetinib vs chemotherapy on progression-free survival in uveal melanoma: a randomized clinical trial. JAMA, J Am Med Assoc 2014. https://doi.org/10.1001/jama.2014.6096.

[13] Piperno-Neumann S, Kapiteijn E, Larkin JMG, Carvajal RD, Luke JJ, Seifert H, et al. Phase I dose-escalation study of the protein kinase C (PKC) inhibitor AEB071 in patients with metastatic uveal melanoma. J Clin Oncol 2019. https://doi.org/10.1200/jco.2014.32.15_suppl.9030.

[14] Yang J, Manson DK, Marr BP, Carvajal RD. Treatment of uveal melanoma: where are we now? Ther Adv Med Oncol 2018. https://doi.org/10.1177/1758834018757175.

[15] Amirouchene-Angelozzi N, Frisch-Dit-Leitz E, Carita G, Dahmani A, Raymondie C, Liot G, et al. The mTOR inhibitor Everolimus synergizes with the PI3K inhibitor GDC0941 to enhance anti-tumor efficacy in uveal melanoma. Oncotarget 2016. https://doi.org/10.18632/oncotarget.8054.

[16] Carita G, Frisch-Dit-Leitz E, Dahmani A, Raymondie C, Cassoux N, Piperno-Neumann S, et al. Dual inhibition of protein kinase C and p53-MDM2 or PKC and mTORC1 are novel efficient therapeutic approaches for uveal melanoma. Eur J Cancer 2016. https://doi.org/10.1016/s0959-8049(16)32672-7.

[17] Chen X, Wu Q, Tan L, Porter D, Jager MJ, Emery C, et al. Combined PKC and MEK inhibition in uveal melanoma with GNAQ and GNA11 mutations. Oncogene 2014. https://doi.org/10.1038/onc.2013.418.

[18] Khalili JS, Yu X, Wang J, Hayes BC, Davies MA, Lizee G, et al. Combination small molecule MEK and PI3K inhibition enhances uveal melanoma cell death in a mutant GNAQ- and GNA11-dependent manner. Clin Cancer Res 2012. https://doi.org/10.1158/1078-0432.CCR-11-3227.

[19] Musi E, Ambrosini G, de Stanchina E, Schwartz GK. The phosphoinositide 3-kinase α selective inhibitor BYL719 enhances the effect of the protein kinase C inhibitor AEB071 in GNAQ/GNA11-Mutant uveal melanoma cells. Mol Cancer Ther 2014. https://doi.org/10.1158/1535-7163.mct-13-0550.

[20] Heijkants R, Willekens K, Schoonderwoerd M, Teunisse A, Nieveen M, Radaelli E, et al. Combined inhibition of CDK and HDAC as a promising therapeutic strategy for both cutaneous and uveal metastatic melanoma. Oncotarget 2018. https://doi.org/10.18632/oncotarget.23485.

[21] Heijkants RC, Nieveen M, Hart KCT, Teunisse AFAS, Jochemsen AG. Targeting MDMX and PKCδ to improve current

uveal melanoma therapeutic strategies. Oncogenesis 2018. https://doi.org/10.1038/s41389-018-0041-y.

[22] Chen Q, Song S, Wei S, Liu B, Honjo S, Scott A, et al. ABT-263 induces apoptosis and synergizes with chemotherapy by targeting stemness pathways in esophageal cancer. Oncotarget 2015. https://doi.org/10.18632/oncotarget.4540.

[23] Chen J, Jin S, Abraham V, Huang X, Liu B, Mitten MJ, et al. The Bcl-2/Bcl-XL/Bcl-w inhibitor, navitoclax, enhances the activity of chemotherapeutic agents in vitro and in vivo. Mol Cancer Ther 2011. https://doi.org/10.1158/1535-7163.mct-11-0415.

[24] Némati F, De Montrion C, Lang G, Kraus-Berthier L, Carita G, Sastre-Garau X, et al. Targeting Bcl-2/Bcl-X L induces antitumor activity in uveal melanoma patient-derived xenografts. PLoS One 2014. https://doi.org/10.1371/journal.pone.0080836.

[25] Airiau K, Prouzet-Mauléon V, Rousseau B, Pigneux A, Jeanneteau M, Giraudon M, et al. Synergistic cooperation between ABT-263 and MEK1/2 inhibitor: effect on apoptosis and proliferation of acute myeloid leukemia cells. Oncotarget 2016. https://doi.org/10.18632/oncotarget.6417.

[26] Chapeau EA, Gembarska A, Durand EY, Mandon E, Estadieu C, Romanet V, et al. Resistance mechanisms to TP53-MDM2 inhibition identified by in vivo piggyBac transposon mutagenesis screen in an Arf −/− mouse model. Proc Natl Acad Sci 2017. https://doi.org/10.1073/pnas.1620262114.

[27] Duan Z, Chinn D, Tu MJ, Zhang QY, Huynh J, Chen J, et al. Novel synergistic combination of mitotic arrest and promotion of apoptosis for treatment of pancreatic adenocarcinoma. Transl Oncol 2019. https://doi.org/10.1016/j.tranon.2019.01.009.

[28] Coupland SE, Bechrakis N, Schüler A, Anagnostopoulos I, Hummel M, Bornfeld N, et al. Expression patterns of cyclin D1 and related proteins regulating G1-S phase transition in uveal melanoma and retinoblastoma. Br J Ophthalmol 1998. https://doi.org/10.1136/bjo.82.8.961.

[29] Brantley MA, Harbour JW. Deregulation of the Rb and p53 pathways in uveal melanoma. Am J Pathol 2000. https://doi.org/10.1016/s0002-9440(10)64817-1.

[30] Gao H, Korn JM, Ferretti S, Monahan JE, Wang Y, Singh M, et al. High-throughput screening using patient-derived tumor xenografts to predict clinical trial drug response. Nat Med 2015. https://doi.org/10.1038/nm.3954.

Annex 2 – Supplementary tables of the manuscript “Glycolysis dependency as a hallmark of SF3B1-mutated cells in uveal melanoma” [attachment available in digital format]

Annex 3 – Résumé de la thèse (thesis summary in French)

Les défauts d'épissage apparaissent comme une caractéristique du cancer et sont principalement causés par des mutations de gènes codant pour des facteurs d'épissage (FE). Des mutations au niveau de *SF3B1* (sous-unité 1A du facteur d'épissage 3B) ont été initialement rapportées dans les syndromes myélodysplasiques (SMD) et la leucémie lymphoïde chronique (LLC), ainsi que des altérations des FE U2AF1, SRSF2 et ZRSR2. Des mutations de *SF3B1* ont ensuite également été montrées dans des tumeurs solides, notamment dans le mélanome uvéal (UM), une tumeur rare avec une charge mutationnelle faible. Ces FEs sont tous impliqués dans la reconnaissance du site d'épissage 3' (3'ss), une étape précoce de l'épissage de l'ARNm. Les mutations dans les gènes codant pour les FEs sont mutuellement exclusives et conduisent à différentes aberrations d'épissage. Étant donné les interactions étroites entre ces FEs au cours de la reconnaissance du 3'ss et la récurrence de leurs mutations mutuellement exclusives dans le cancer, nous supposons que les mutations au niveau des FEs mutants donnent lieu a un mécanisme oncogène commun. Les preuves croissantes d'altérations de la machinerie d'épissage dans le cancer soulignent l'intérêt thérapeutique de cibler les défauts d'épissage.

La réaction d'épissage est catalysée par le spliceosome, un complexe formé de petites ribonucléoprotéines (snRNP) et de FEs. Les introns contiennent les séquences consensus connues sous le nom de 5' splice site (5'ss), branchpoint (BP) et 3'ss qui guident la machinerie d'épissage. SF3B1 sert de médiateur pour la liaison de la snRNP U2 au BP, une interaction qui doit être renforcée par d'autres composants comme U2AF35/65. L'assemblage du complexe permet à d'autres étapes d'avoir lieu, menant à l'excision de l'intron et à la ligature des exons.

SF3B1 est le gène d'épissage le plus fréquemment muté dans le cancer (28% dans les SMD, 15% dans les LLC et 23% dans les UM). Les mutations hotspot de *SF3B1* ciblent les codons R625, K666 et K700 dans les répétitions HEAT situées dans le domaine C-terminal. Les mutations K700 sont plus récurrentes dans les hémopathies malignes alors que les mutations R625 et K666 prédominent dans l'UM. Précisément, les mutations de *SF3B1* conduisent à la reconnaissance d'un 3'ss cryptique, et par conséquent à des jonctions d'épissage aberrantes dans un ensemble spécifique de transcrits. Ces aberrations d'épissage ont été caractérisées par notre groupe et

d'autres équipes au cours des dernières années. Ces études ont montré que la protéine SF3B1 mutante favorise la reconnaissance d'un BP cryptique situé en amont du site canonique. La liaison à un BP cryptique conduit à la rétention partielle de l'intron dans le produit final de l'ARNm. L'impact fonctionnel des variants aberrants qui en résultent reste à étudier afin d'élucider le mécanisme oncogène de la forme mutante de SF3B1. Dans ce contexte, ma thèse vise à caractériser davantage le devenir de ces variants aberrants. Leur caractérisation fonctionnelle permettra d'éclairer le rôle oncogène de *SF3B1* muté. Dans cette optique, des études récentes ont étudié l'impact en aval de certains variants aberrants induits par la mutation de SF3B1.

Différents groupes de recherche, dont le nôtre, ont caractérisé les défauts d'épissage induits par la mutation de *SF3B1* et le mécanisme sous-jacent. Cependant, nous savons peu de choses sur l'impact fonctionnel et oncogénique de ces défauts d'épissage et leur contribution à la transformation maligne. À la lumière de cette préoccupation, l'objectif principal de ma thèse a été de caractériser le rôle oncogène des variants épissés de façon aberrante dans l'UM.

Sur un modèle cellulaire isogénique de *SF3B1* muté généré par CRISPR-Degron, nous avons effectué une étude intégrale du transcriptome, de la synthèse des protéines naissantes, de l'abondance des protéines et de la traduction par RNA-Seq, Click IT, LC-MS/MS et profilage du polysome, respectivement. Suite aux résultats obtenus, nous avons caractérisé le profil métabolique des modèles cellulaires isogéniques. Nos résultats sur ce modèle montrent que la forme mutante de SF3B1 n'a pas d'impact global sur les niveaux d'expression des ARN ou des protéines, mais plutôt un impact spécifique à chaque cible. Environ 35% des transcrits épissés de manière aberrante sont traduits en protéines. Nous avons également constaté que la forme SF3B1 mutante entraîne la régulation négative des protéines métaboliques, ce qui conduit à une diminution de la capacité de respiration mitochondriale. Pour compenser ces défauts mitochondriaux, la forme SF3B1 mutante favorise la glycolyse, ce qui rend les cellules mutées par *SF3B1* plus sensibles à l'inhibition de la glycolyse.

Dans l'ensemble, nous apportons la preuve de l'implication oncogénique de la forme SF3B1 mutante dans le mélanome uvéal par l'induction d'un changement métabolique vers la glycolyse. Cette vulnérabilité aux inhibiteurs de la glycolyse offre une stratégie thérapeutique potentielle.

RÉSUMÉ

SF3B1 est le gène d'épissage le plus fréquemment muté dans le cancer. Les mutations de *SF3B1* sont des mutations de changement de fonction conduisant à une reconnaissance altérée du site d'épissage 3'. Les défauts d'épissage qui en résultent consistent en une rétention partielle de l'intron dans le produit ARNm. L'impact fonctionnel de ces transcrits aberrants reste à élucider pour déterminer le mécanisme oncogène du SF3B1 muté.

Sur un modèle cellulaire isogénique du SF3B1 muté généré par CRISPR-Degron, nous avons effectué une étude intégrale du transcriptome, de la synthèse des protéines naissantes, de l'abondance des protéines et de la traduction par RNA-Seq, Click IT, LC-MS/MS et profilage du polysome, respectivement. Suite aux résultats obtenus, nous avons caractérisé le profil métabolique des modèles cellulaires isogéniques.

Nos résultats sur ce model montrent que la forme mutante de SF3B1 n'a pas d'impact global sur les niveaux d'expression des ARN ou des protéines, mais plutôt un impact spécifique à chaque cible. Environ 35% des transcrits épissés de manière aberrante sont traduits en protéines. Nous avons également constaté que la forme SF3B1 mutante entraîne la régulation négative des protéines métaboliques, ce qui conduit à une diminution de la capacité de respiration mitochondriale. Pour compenser ces défauts mitochondriaux, *SF3B1*^{mut} favorise la glycolyse, ce qui rend les cellules SF3B1mut plus sensibles à l'inhibition de la glycolyse.

Dans l'ensemble, nous apportons la preuve de l'implication oncogénique de la forme SF3B1 mutante dans le mélanome uvéal par l'induction d'un changement métabolique vers la glycolyse. Cette vulnérabilité aux inhibiteurs de la glycolyse offre une stratégie thérapeutique potentielle.

MOTS CLÉS

SF3B1 ; épissage ; mélanome de l'uvée ; oncogenèse ; métabolisme ; respiration mitochondriale ; inhibiteurs de la glycolyse

ABSTRACT

SF3B1 is the most frequently mutated splicing gene in cancer. *SF3B1* mutations are change-of-function missense mutations which lead to the recognition of a cryptic 3' splice site. The resulting splicing aberrations consist of partial intron retention in the mRNA product, thereby leading to the formation of aberrant transcripts in a set of genes. The functional impact of the aberrant mRNA transcripts remains to be investigated in order to elucidate the oncogenic impact of *SF3B1* mutations.

Based on an *SF3B1* isogenic cell model developed by CRISPR-Degron, we performed a comprehensive molecular study of the transcriptome, synthesis of proteins *de novo*, protein abundance and translation by RNA-Seq, Click IT, LC-MS/M/S and Polysome Profiling, respectively. Based on the resulting data, we proceeded to examine the metabolic profile of the *SF3B1* isogenic cell models.

Our results show that mutant SF3B1 does not have a global impact on the RNA nor on protein expression levels, but rather a target-specific impact. Around 35% of the aberrant splicing variants are translated into proteins. We also found that mutant SF3B1 leads to the downregulation of metabolic proteins which in turn leads to a decreased mitochondrial respiration capacity. We revealed that $SF3B1^{mut}$ promotes glycolysis to compensate for their mitochondrial defects, which makes $SF3B1^{mut}$ cells more sensitive to glycolysis inhibition.

Here, we provide evidence of the oncogenic role of mutant SF3B1 in uveal melanoma through a metabolic switch towards glycolysis, thus sensitizing cells to glycolysis inhibitors. Overall, our findings elucidate a promising therapeutic strategy for uveal melanoma patients harbouring SF3B1 mutations.

KEYWORDS

SF3B1 ; splicing ; uveal melanoma ; oncogenesis, metabolism, mitochondrial respiration, glycolysis inhibitors